Studies on Methylaluminoxane Catalyst Activators

Chrysoula Pateraki

PhD Thesis

University of East Anglia

School of Chemistry

September 2014

Statement of Original Work

The work presented in this thesis has been conducted by the author, Chrysoula Pateraki, and is, to the best of her knowledge, original, except where references have been made to other people's work. The corresponding references have been detailed in each chapter.

Abstract

The first part of this PhD was devoted to the structural characterization of methylaluminoxane (MAO). Initially the work focused upon MAO formation by studying the hydrolysis reaction of trimethylaluminium (TMA), with a greater interest in the initial reaction steps of TMA with H_2O. This was attempted by using ^1H VT NMR spectroscopy and by combining infrared spectroscopy with the matrix isolation technique. Low temperature NMR experiments successfully led to the identification of the $AlMe_3 \cdot H_2O$ adduct as the first intermediate, followed by formation of Me_2AlOH, when THF was employed as a solvent.

Another approach focused on the characterization of MAO by developing a fast and reliable method for quantification of the TMA content of commercial MAO solutions via ^1H-NMR spectroscopy with addition of donors. This research also showed that MAO contains a small amount of certain structures, which upon addition of THF or pyridine can lead to the formation of cationic species $[AlMe_2L_2]^+$.

The second part of this work was devoted to the enhancement of MAO's catalytic efficiency by kinetic studies on 1-hexene. The primary aim was to produce MAO soluble in aliphatic hydrocarbons by addition of branched or long chain aluminium trialkyls, which proved to be effective solubilizing agents, and by modification of MAO with long chain silanols. Addition of silanols led to polymers with lower $\overline{M_n}$. Differences in productivity, polymer molecular weight and number of active species were shown to be primarily a linear function of the TMA concentration.

An important part of this PhD was the development of a synthetic route towards ethyl-iso-butylaluminoxane (EBAO) and use in 1-hexene polymerization. This is the first study where EBAO is successfully used as a soluble component in 1-hexene polymerization in heptane and leads to comparable or even higher productivities and higher number average molecular weights compared to the MAO catalytic systems.

Table of Contents

Acknowledgements

I would like to express my sincere gratitude to my supervisor, Prof. Manfred Bochmann, for his continuous support and patience. I would also like to thank Dr. Simon Lancaster for his assistance, learning opportunities that he provided and the time he sacrificed for our regular meetings, as well as Dr. Jas Jayasooriya for his guidance and encouragement.

The completion of my work may not have been accomplished without the support of my colleagues and collaboration partners of the EU consortium. I would especially like to thank the post-doctoral researcher Dr. Fabio Ghiotto who patiently helped me to learn how to work in an advanced chemistry lab, of which I had no prior experience; Dr. Chiranjib Banerjee for his advice when I first started working in the lab, his generosity and true friendship, and Dr. Dragos Rosca for his sharing of knowledge and X-ray crystallographic analysis. Dr. Joseph Wright has also been an extremely valuable point of contact for almost every instrumental problem that I had to solve.

I would also like to extend my deepest thanks to my partner, James Tonkin, for his constant moral support, care, chemistry discussions and patience.

Finally, I would like to express my true appreciation to my mother and grandmother, because without them I wouldn't have achieved my goals and be standing as the person I am today. My aunt, Dr. Nikolitsa Giannopoulou, has also been a great inspiration for me.

Abbreviations

$[C]_T$	catalyst concentration
$[C^*]$	mol fraction of the catalyst involved in polymer chain growth at any time
[M]	monomer concentration
$[M]_0$	initial monomer concentration
$\overline{M_n}$	number average molecular weight
$\overline{M_w}$	weight average molecular weight
% v/v	volume percent
[Zr]	zirconocene
$< n >$	number-average degree of polymerization
°C	degrees Celsius
a. sym. def.	asymmetric deformation
a. sym. stretch	asymmetric stretching
A_d	dimer absorbance
Al	aluminium
A_m	monomer absorbance
A_x	integrated signal area
B	bridging
Benz[e]Ind	benzindenyl
Br	bromine
br	broad
cm^{-1}	reciprocal centimeter
cm^3	cubic centimeter
Cp	cyclopentadienyl
DBP	2,6-di-*tert*-butylphenol
DMM	dimethoxymethane

DTGS	deuterated triglycine sulphate
d-TMA	dimeric trimethylaluminium
e.g.	*exempli gratia*
EPR	electron paramagnetic resonance
ESR	electron spin resonance
Et	ethyl
et al.	et alia
EU	European Union
F	fluorine
f.c.c.	face-centred cube
FF	1,2-difluorobenzene
Flu	fluorenyl
g	grams
GC	gas chromatography
GPC	gel permeation chromatography
h	hour
H	hydrogen
HPLC	high performance liquid chromatography
Hz	Hertz
i-Bu	*iso*-butyl
Ind	indenyl
^{i}Pr	*iso*-propyl
IR	infrared
i-TMA	intermediate trimethylaluminium
J	coupling constant
K	Kelvin
k	chain propagation rate constant

k_i	rate constant of initiation
k_p	rate constant of propagation
k_p^{app}	apparent propagation rate constant
k_s	a spectrometer constant
k_t	rate constant of termination
L	ligand
L_2	bidentate ligand
M	metal or molar
m	medium or multiplet
MAO	methylaluminoxane
MBAO	isobutylmethylaluminoxane
mbar	millibar
Me	methyl
min	minutes
mL	millilitre
mm	millimetres
MMAO	modified methylaluminoxane
mmol	millimoles
mol	moles
mp	melting point
m-TMA	monomeric trimethylaluminium
MWD	molecular weight distribution
N	nitrogen
NMR	nuclear magnetic resonance
N_x	number of nuclei
O	oxygen

Oct	octyl
PDI	polydispersity index
Ph	phenyl
ppm	parts per million
P_x	purity of compound X
Py	pyridine
R	alkyl group
rac	racemic
s	strong or seconds or singlet
SANS	small-angle neutron scattering
sh	shoulder
Si	silicon
sym def.	symmetric deformation
Sym. stretch	symmetric stretching
T	terminal
t	reaction time
^{t}Bu	tertiary butyl
T_{dep}	deposition temperature
TEA	triethylaluminium
TEMPO	2,2,6,6-tetramethylpiperidine-n-oxyl
THF	tetrahydrofuran
TIBA	triisobutylaluminium
TIBAO	tetraisobutylaluminoxane
TIOAO	tetraisooctylaluminoxane
TMA	trimethylaluminium
TOA	trioctylaluminium
vs	very strong

VT	variable temperature
UV-vis	ultraviolet-visible spectroscopy
vw	very weak
w	weak
wt%	weight per cent
Zr	zirconium
δ	chemical shift
μ	bridging
μmol	micromoles
μL	microlitre
ν	vibrational mode

Chapter 1

Introduction

1.1 Homogeneous Ziegler-Natta Catalysts and the Discovery of Methylaluminoxane (MAO)

Although the first homogeneous Ziegler-Natta catalyst, Cp_2TiCl_2, had been discovered in 1957 by Breslow and Natta,[1-2] considerable attention was only given to olefin polymerization by homogeneous Ziegler-Natta catalysts after the discovery and use of MAO as an activator. In 1980, Sinn and Kaminsky[3-4] discovered that addition of water to a Cp_2ZrMe_2/TMA system creates a highly active catalytic system for ethylene polymerization. This led them to the hypothesis that a new compound was formed by the partial hydrolysis of TMA, an oligomeric aluminoxane containing the structure $[–O–Al(Me)–]_n$, which was responsible for the surprisingly high activity of the system.

After the establishment of high polymerization activities of MAO (cocatalyst) and group 4B transition metallocene (the main component of the homogeneous Ziegler-Natta catalyst systems) systems, many scientific groups across the globe focused their interest on the olefin polymerization by single-site Ziegler-Natta catalysts in combination with an alkylaluminoxane. This led to the synthesis of different metallocenes with specific stereochemistry, e.g. the discovery of *ansa*-metallocenes which started with the synthesis of the famous Brintzinger catalysts, $Et(Ind)_2ZrCl_2$ and $Et(H_4Ind)_2ZrCl_2$,[5] and to the conclusion that stereochemical control of the final polymer can be achieved by tailoring the ligand symmetry of the stereorigid metallocene.[6-7]

MAO was superior to any other alkylaluminoxanes used as cocatalysts, and was soon declared as the most important cocatalyst for the Group 4B metallocenes.[7] However, the large excess of MAO needed to activate the catalyst in solution-phase (typically Al/transition-metal ratios of the order of 10^3-10^4/1),[8-10] the limited shelf-life of MAO and the differences in catalytic behaviour of MAO synthesized under different methods (all the different synthetic routes are discussed in detail in Chapter 2, Section 2.1.1) or slightly different conditions, also attracted huge interest in the scientific community, leading to numerous studies in order to

elucidate the structural characteristics of MAO and improve its activity, solubility and stability.[8-24]

One major drawback when solution-based technologies are employed, is that MAO is insoluble in aliphatic hydrocarbons, which are the preferred solvents in industrial polymerization processes.[25-26] For this reason, additives like long or branched chain alkylaluminiums have been added to MAO in order to improve its solubility. More details about this can be found in Chapter 5, Section 5.1.1. Chapter 5 also includes a study on 1-hexene polymerization after addition of Al(*i*-Bu)$_3$ or Al(Oct)$_3$ in heptane, but it is mostly devoted to the modification of MAO by long chain silanols and evaluating the catalytic performance of the modified MAO catalyst system in 1-hexene polymerizations in toluene and heptane. The aim of this work was to produce an MAO soluble in aliphatic hydrocarbons with enhanced catalytic activity.

Additionally, aluminoxanes with higher alkyl groups have been synthesized and used in olefin polymerization, but are usually inferior to MAO.[27-32] Chapter 6 is devoted to a study for the synthesis of ethyl-*iso*-butyl-aluminoxane and its performance in 1-hexene polymerization in heptane compared to an MAO catalyst system.

1.2 Characterization and Structure of MAO

Unfortunately, despite all the efforts the precise structure of MAO still remains unknown. However, there are many studies that have shed light on the constitution of MAO and helped towards a better understanding of its characteristics and the chemistry involved.

MAO solutions consist of two parts: a mixture of different MAO oligomers in equilibria, which are usually presented with the chemical formula $[-Al(CH_3)O-]_n$ or as $[Al(CH_3)_{1.4-1.5}O_{0.75-0.80}]_n$, and residual TMA, which interacts with MAO and adds another obstacle to the structural investigations of MAO.[18,23-24,33-36] TMA can be either 'free' or 'bound', but more details about the presence and nature of TMA in MAO can be found on Chapter 4, Sector 4.1.1. Chapter 4 focuses on developing methods for TMA determination in commercial MAO solutions because it is crucial to accurately determine the TMA content of MAO, which plays a major role in the properties and catalytic behaviour of the MAO.

The second chemical formula, $[Al(CH_3)_{1.4–1.5}O_{0.75–0.80}]_n$, was introduced by Imhoff *et al.* who used a ^1H NMR method to determine the TMA content. They managed to measure the number of methyl groups per aluminium in MAO by combining an independent method for measuring the aluminium content and calculating the amount of methane evolved by NMR.[36] In another study, Imhoff and co-workers proposed a Me/Al ratio between 1.4–1.5[37] (when steps have been taken to remove or correct for residual TMA), while Sinn and his co-workers[38-39] reported a ratio close to 1.5.

Several different models have been proposed for the structure of the MAO oligomers over the years. Initially, Kaminsky[4] assumed cyclic structures for the MAO oligomers (Figure 1.1). However, the Al atoms in these structures have a coordination number of three which is not common for Al compounds without sterically bulky ligands. It would have been expected that the Al atoms in MAO structures would form bridges with O (or Me groups) in order to maximize their coordination number. Giannetti and his co-workers[40] claimed a linear structure (Figure 1.1) without ruling out the possibility of a cyclic one.

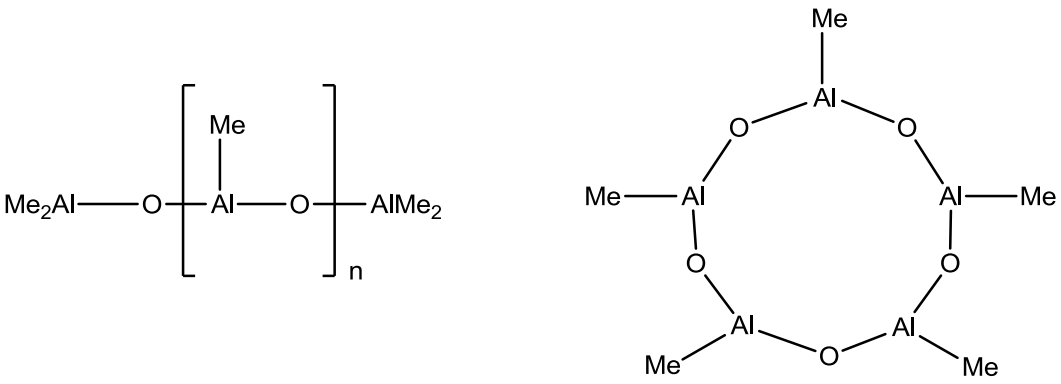

Figure 1.1: A linear MAO structure on the left and a cyclic MAO structure on the right

Atwood and co-workers successfully isolated and characterized the $[Al_7O_6Me_{16}]^-$ anion (Figure 1.2) via X-ray, and proposed a structure that consists of an Al_6O_6 cage capped by a seventh Al atom which is bonded to three alternate oxygen atoms in the ring. Two terminal methyl groups are attached to each of the six Al atoms of the cage, but the seventh Al is bonded only to one methyl group. Each Al atom is four-coordinate, while each O atom is three-coordinate. The O atoms that are not bonded to the seventh Al atom, bridge two Al atoms each and have one Me group attached each.[39]

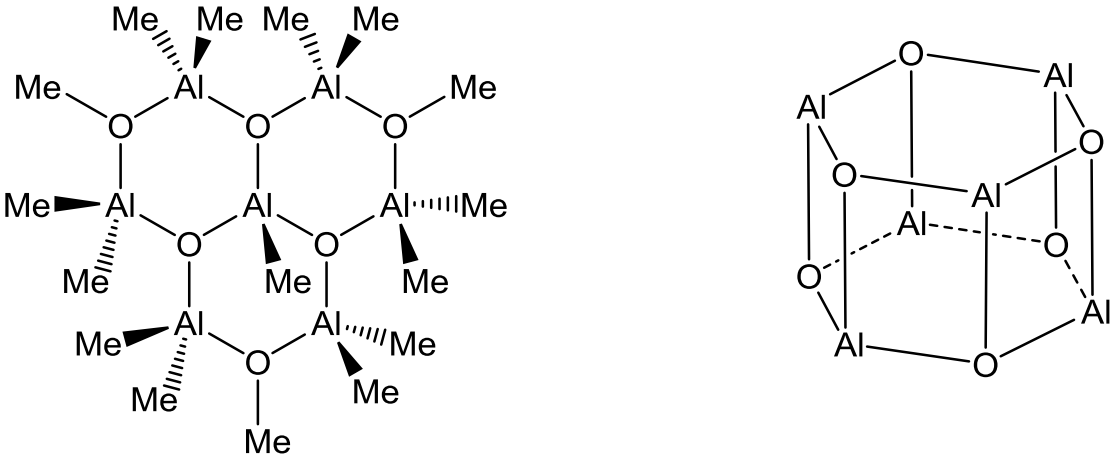

Figure 1.2: The $[Al_7O_6Me_{16}]^-$ anion isolated and characterized by Atwood *et al.*[39] on the left and the $[^tBuAl(\mu_3\text{-}O)]_6$ cluster synthesized and characterized by Barron *et al.*[41-42] (the ^{t}Bu groups were omitted for clarity).

Barron *et al.*[41-42] synthesized a number of *tert*-butyl aluminoxane clusters, such as $[^tBuAl(\mu_3\text{-}O)]_6$ or $[^tBuAl(\mu_3\text{-}O)]_8$ (Figure 1.2), and determined their structure by X-ray crystallography, showing that they have three-dimensional cage structures with four-coordinate Al centres and O atoms bridging three Al atoms. Based on the known chemistry of aluminium[43-44] they supported that MAO also has three-dimensional cage structures. However, the above structural models of MAO do not include the residual TMA that coexists in MAO solutions, and its presence has been proven crucial in terms of structural characterization and catalytic properties.[45]

Theoretical and computational studies[4] also support MAO cage structures, similar to Barron's *tert*-butyl aluminoxane structures, and $(AlOMe)_{12}$ or $(AlOMe)_9$ [23,47] have been proposed as the most stable MAO cages (Figure 1.3). Linnolahti and his co-workers[24,48] also introduced the concept of nanotubular MAO structures, with ($Al_{16}O_{12}Me_{24}$) being in good agreement with experimental evidence and being able to activate single-site metallocene catalysts.

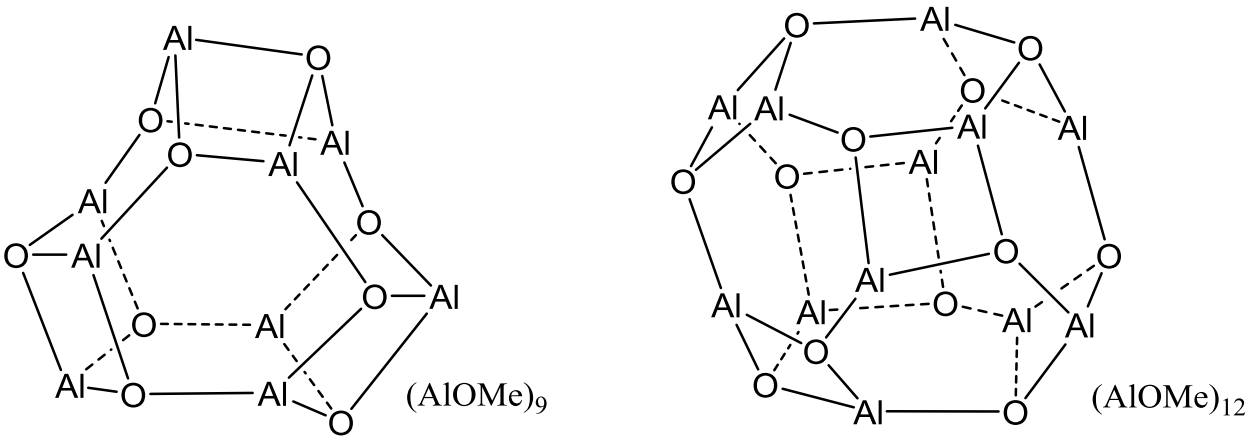

Figure 1.3: An example of an $(AlOMe)_{12}$ and an $(AlOMe)_9$ MAO cage structure[23,47]

Multinuclear NMR spectroscopy, and especially ^{27}Al and ^{17}O NMR have supported the three dimensional MAO cage structures with four-coordinate Al atoms and three-coordinate O atoms.[49-50] Babushkin and co-workers[49] reported an ^{27}Al resonance at δ 149–153 which they attributed to residual TMA, and a broad resonance at δ ~ 60 which is attributed to MAO and is within the range reported for the *tert*-butyl aluminoxane clusters with cage structure. The ^{17}O resonance of MAO (δ 67 at 50 °C) is also in agreement with a three-coordinate oxo ligand. The existence of four-coordinate Al centres in MAO is also supported by ESR spin probe measurements.[30]

Another important parameter that many researchers have attempted to determine is the molecular weight of MAO. The main method used is cryoscopy. Sinn[38-39] and his co-workers reported molecular weights between 1000–1200 g/mol using benzene or TMA as solvent, while Imhoff *et al.*[37] reported lower molecular weights in the range of 700–1100 g/mol using dioxane (after correcting the values according to the TMA content). However, different studies have reported different molecular weights covering a wide range between 400–3000 g/mol.[38-39,51-52]

Other means of determining the molecular weight of MAO are gel permeation chromatography (GPC) and mass spectrometry.[4,40,53] However, the results derived from these methods proved to be unreliable. Recently, small-angle neutron scattering (SANS) measurements report an average molecular weight of 1800 ± 100 g/mol, with approximately 30 Al atoms in an MAO polymer and approximately one TMA molecule per MAO polymer. However, NMR diffusion coefficient measurements report a higher Al number (50–60 Al atoms per MAO polymer).[45]

1.3 Polymerization Mechanisms

When a metallocene is used in olefin polymerization as a catalyst, it needs to be activated by a cocatalyst which acts as a Lewis acid. In the case of MAO, it was initially assumed that three-coordinate Al atoms present on the MAO structure were responsible for the Lewis acidity of MAO and consequently its ability to act as an activating agent by extracting a ligand from the metallocene and creating a coordination site for the olefin.[4,54]

However, when further studies revealed the existence of four-coordinate Al sites on MAO, as described earlier, Barron and his co-workers introduced the concept of the 'latent Lewis acidity' of MAO to interpret its cocatalytic activity, where cages with saturated Al sites that are not Lewis acidic themselves, can open via heteroleptic bond cleavage to create a Lewis acidic site. This cage opening becomes possible due to the ring strain present in the cage.[55-56]

Barron[56] isolated $[(^t\text{Bu})_2\text{Al}\{\text{OAl}(^t\text{Bu})_2\}]_2$ which has two three-coordinate Al centers and $[(^t\text{Bu})\text{AlO}]_n$ where n = 6, 7 and 9, as it was described earlier, and observed their reaction with Cp_2ZrMe_2. $[(^t\text{Bu})_2\text{Al}\{\text{OAl}(^t\text{Bu})_2\}]_2$ did not react with the zirconocene, while the four-coordinate Al cages activated the catalyst successfully.

It is generally accepted that activation of a metallocene with two chloride ligands starts with methylation and continues with methyl abstraction to give the cationic active species. The first step is the monomethylation of the dichlorometallocene (Scheme 1.1).[6,25,57] Cam and Giannini[58] supported the idea that the methylating agent is the remaining TMA on the MAO, by studying the reaction of MAO with Cp_2ZrCl_2 at different Al/Zr ratios (=1, 5, 7 and 15) by ^{1}H NMR spectroscopy. They claimed that methylation did not occur when MAO without the presence of TMA was used. Resconi *et al.*[59] suggested that TMA itself within the MAO solution was the actual cocatalyst, responsible for the generation of the cationic species in propylene polymerization with $C_2H_4(Ind)_2ZrCl_2$.

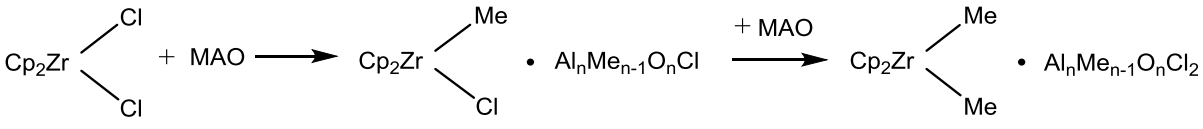

Scheme 1.1: Methylation of Cp_2ZrCl_2 by MAO

However, Tritto *et al.* claimed that MAO is a better alkylating agent than TMA, based on studies of the reaction of MAO and TMA with $Cp_2TiMeCl$ by NMR.[60] Deffieux and co-workers[61-65] who studied the reaction of zirconocene dichloride catalysts with MAO or TMA by UV/Visible spectroscopy supported that the catalyst is first monomethylated by MAO at low Al/Zr ratios. Addition of TMA itself can also lead to complete monomethylation, but the presence of free TMA is not indispensable since TMA-depleted or TMA-free MAO also has the ability to monomethylate the zirconocene dichloride species.[65]

Undoubtedly, the role of remaining TMA in MAO in the activation process of a metallocene is controversial. Additionally, some researchers like Sivaram *et al*. claim that higher productivity is achieved with addition of TMA to an MAO/Cp_2ZrCl_2 system for ethylene polymerization under certain conditions.[66] However, the system containing only MAO with an Al/Zr ratio of 1000 was compared with the system where TMA was added; the latter system had a higher Al/Zr ratio (= 1676). Sivaram did not observe an essential decrease of the MW of the polymer after addition of TMA, which other studies have reported.[66] On the other hand, Giannetti and his co-workers[40] reported a decrease of the productivity and MW of the final polymer upon addition of increasing amounts of TMA to an MAO/$(Ind)_2Zr(CH_3)_2$ or $Cp_2Zr(CH_2C_6H_5)_2$ system in ethylene polymerization. This agrees with our observations where it was proven that catalyst productivity and $\overline{M_n}$ of the polymer are decreasing with increasing amounts of TMA in 1-hexene polymerization (catalyst system: MAO/*rac*-Me_2Si(2-Me-Benz[e]Ind)$_2ZrCl_2$).[67-68]

The monomethylated metallocene species can undergo further methylation of the second chloride ligand (Scheme 1.1), under the presence of excess MAO. In the case of Cp_2ZrMe_2 at low Al/Zr ratios (<100) the methylated zirconocene species will interact with MAO to give a weak complex (I) or/and proceed to the formation of the homobinuclear species II (see Scheme 1.4 for species I and II).[69]

It is believed that at higher Al/Zr ratios species I and II start to disappear, while new species (III and IV, see Scheme 1.4) appear. Species III were identified by ^1H and ^{13}C NMR as the heterobinuclear ion-pair $[Cp_2Zr(\mu\text{-}Me_2)AlMe_2]^+[Me\text{-}MAO]^-$. An upfield shift (5.53 → 5.44 ppm) of the ^1H NMR resonance of the bridging Me group of species III when the [Zr] was decreased from 50 mM to 0.5 mM indicated that species III coexist in two forms according to the equilibrium (Scheme 1.2):

Scheme 1.2: Equilibrium of the two different species of III

where the IIIa form is the 'contact' ion-pair and IIIb is the solvent-separated ion-pair. It was suggested that at high Al/Zr ratios only the highly Lewis acidic sites of MAO form anions. These anions are easily dissociated to the IIIb species. At lower Al/Zr ratios this dissociation will not be so fast, because the Lewis acidic sites are weaker.[16]

Tritto and his co-workers[15] managed to verify the formation of monomeric $[Cp_2Zr(^{13}CH_3)]^+[Me{\cdot}MAO]^-$, dimeric $[Cp_2Zr(^{13}CH_3)]_2(\mu\text{-}^{13}CH_3)^+[Me{\cdot}MAO]^-$ and $[Cp_2Zr(\mu\text{-}Me)_2AlMe_2]^+ [Me{\cdot}MAO]^-$ by ^1H and ^{13}C NMR, after comparison with the reaction products of Cp_2ZrMe^+ with Cp_2ZrMe_2 or TMA which were studied by Bochmann[70] (the cationic species Cp_2ZrMe^+ were generated by reaction of Cp_2ZrMe_2 with $B(C_6F_5)_3$.

Species IV possibly have an unsymmetrical Me bridge, as it was shown by Babushkin and co-workers,[16] although other studies had claimed that the bridge was an O atom, bound to an Al.[40,71-72] The existence of the Me bridge was supported by the broadening of the ^1H and ^{13}C NMR signals attributed to this, and by the agreement of the ^{13}C NMR spectrum of a structurally similar compound, $Cp_2ZrMe(\mu\text{-}Me)Al(C_6F_5)_3$. Species IV probably represent a dormant state, due to the tight ion-pair binding.[73]

The unsaturated active species could be generated by dissociation of species IV or dissociation of species III (Scheme 1.3).[16]

Scheme 1.3: Generation of the active species by dissociation of species III

However, on a later study, Talsi and his co-workers claimed that the actual active species precursor is the ion pair III, supported by comparing the catalytic activities of L_2ZrCl_2/MAO systems depending on the ratio of IV/III (absence of species IV was observed in some cases; the system was catalytically active due to the presence of species III).[74]

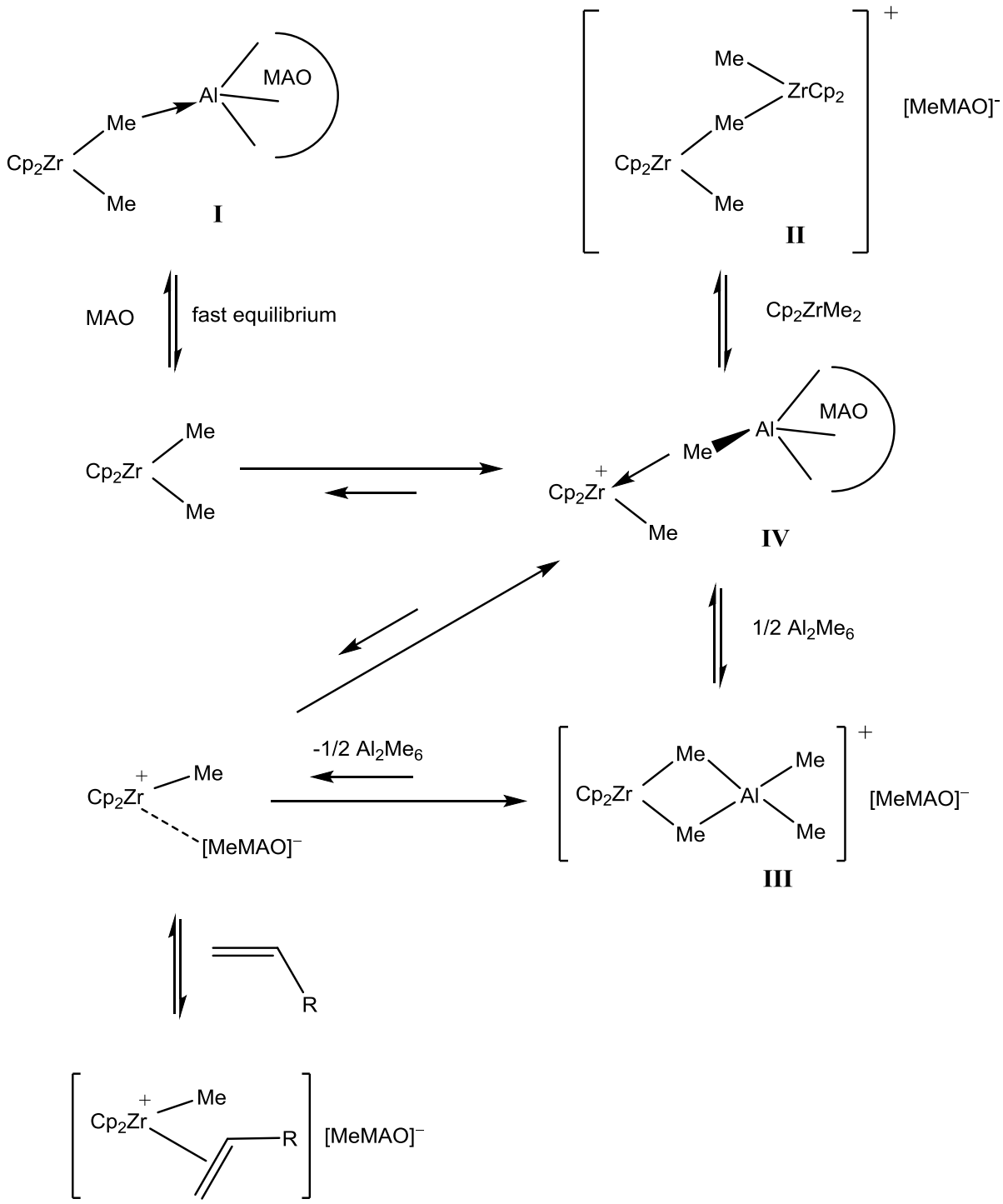

Scheme 1.4: Activation of Cp_2ZrMe_2 by MAO

It is stated that the ratio of IV/III is very high at low Al/Zr ratios, while at high Al/Zr ratios (>500) the ratio of IV/III is between 1–4, depending on the amount of TMA present. This is explained by the possible decrease in the average dissociation tendency of IV as more and more Lewis acidic sites on MAO become occupied.[16] Talsi and co-workers[69] supported that the relative concentration of species III increased with increasing the Al/Zr ratio (they used various metallocenes of the general formula L_2ZrCl_2 and L_2TiCl_2 in their investigations)

1.4 Deactivation Processes, Stabilization of Ion-Pairs in Solution and Chain Transfer Reactions

In the presence of MAO, the metallocenium alkyl species might undergo a-hydrogen abstraction (Scheme 1.5) which leads to the formation of Zr–CH_2–Al or Zr–CH_2–Zr species, liberating CH_4. This is the most common deactivation process of MAO catalyst systems. The rate of formation of the inactive Zr–CH_2–Al species depends on the zirconocene structure, the polymerization temperature, the Al/Zr ratio and concentration. However, when excess MAO is present these inactive species can be reactivated (Scheme 1.6).[75]

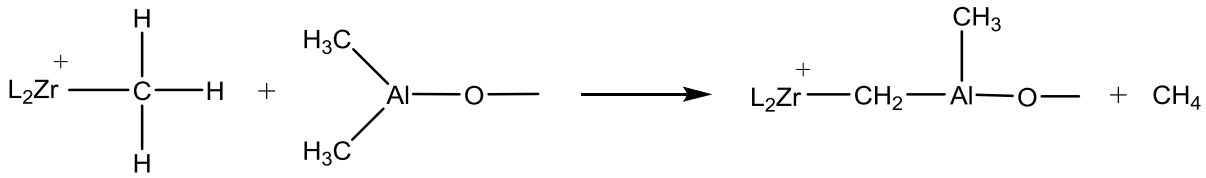

Scheme 1.5: Formation of inactive Zr–CH_2–Al species

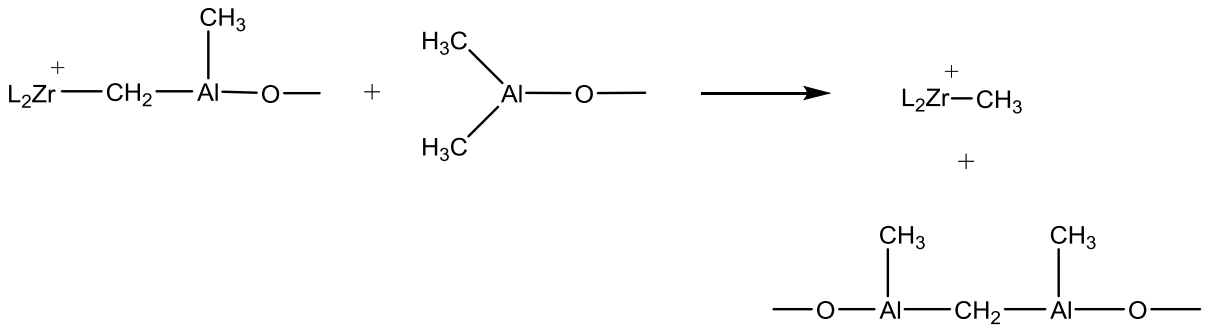

Scheme 1.6: Reactivation of the inactive Zr–CH_2–Al species

When Mülhaupt and his co-workers studied the kinetics of propylene oligomerization using Cp_2ZrCl_2/MAO as the catalyst system, they suggested another type of deactivation process which included a reversible second order decay of the active cationic Zr sites, caused probably due to zirconocene dimerization, and an irreversible deactivation of the active and dormant Zr sites (see Scheme 1.7).[76-77]

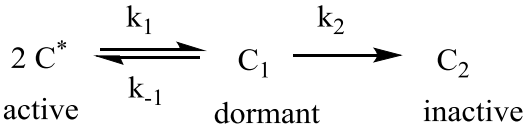

Scheme 1.7: Irreversible deactivation of the active and dormant Zr sites

The reversible or irreversible deactivation of the cationic metallocenium species might be prevented up to a certain degree by coordination of the anion, $X–MAO^-$. Many studies have investigated the interaction of methylaluminoxane with a metallocene, via ^1H and ^{13}C NMR spectroscopy[14-15,58,78-79] and UV-visible spectroscopy,[40,61] and attempted to relate the coordination of the anion with the cationic species formed to the reactivity of the catalyst system. In general, it was found that the weaker the coordination of the anion, the higher the reactivity of a given cation.[75,80-81] Association of the anion with the cationic species is necessary in order to avoid deactivation or decomposition of the active species. However, there is a fine line between stabilizing the ion-pair and compromising the reactivity of the cation because the Lewis basicity of the coordinative anion can suppress the catalytic activity of the system. 'Engineering' of the ion-pair to achieve higher catalytic activities can be achieved by careful choice of the ligand subtituents of the metallocene.[75]

Brintzinger and co-workers[82] studied the reaction of *rac*-$Me_2Si(Ind)_2ZrCl_2$ with MAO, and discovered that two types on anions, Me-MAO_A^- and Me-MAO_B^-, with different coordinative strength are generated along with the cationic species, $[Me_2Si(Ind)_2Zr]^+$. The Me-MAO_B^- anion forms a more strongly bound contact pair, $[Me_2Si(Ind)_2Zr^+$... Me-$MAO_B^-]$, which can be converted to a less strongly coordinative ion pair, $[Me_2Si(Ind)_2Zr^+$... Me-$MAO_A^-]$, when excess MAO is present. The latter species are the ones that are capable of generating species III upon reaction with TMA. When these authors[83] studied another catalyst system, $(MeC_5H_4)_2ZrCl_2$/MAO, they were led to similar conclusions.

Termination of the polymeryl chain in MAO based catalyst systems and subsequently control of the molecular weight and molecular weight distribution of the polymer may occur due to chain transfer reactions to Al, in addition to other common termination mechanisms in homogeneous Ziegler-Natta polymerizations (β-H elimination, β-Me transfer, chain transfer to the monomer). Many factors may determine whether a chain transfer reaction to Al will occur, and to what extent, such us the monomer employed, the polymerization temperature, the type of the ligands and the transition metal of the metallocene.[25] In some systems, like in the copolymerization of ethylene-allylbenzene with Cp_2ZrCl_2/MAO or $Et(Ind)_2$-$ZrCl_2$/MAO it is the main chain termination reaction,[84-86] or in the polymerization of ethylene with Cp_2ZrMe_2/MAO at very low Al/Zr ratios,[79] while in other systems it does not occur at all like in ethylene polymerization with a dichloride tantalum catalyst and MAO.[87-88]

1.5 MAO-ROBOTS project

Against this background of uncertainly about MAO and sometimes contradictory reports, a more in-depth study of the structure and function of MAO seemed highly timely. This thesis is part of the work carried out within an EU-funded industry-university consortium with just this aim.

The work was conducted under the Framework 7 activity NMP-2009-1.2-2, grant 246274: 'Methylaluminoxane (MAO) activators in the molecular polyolefin factory'.

References

1. D. S. Breslow, N. R. Newburg, *J. Am. Chem. Soc*., **1957**, *79*, 5072.
2. G. Natta, P. Pino, G. Mazzanti, R. Lanzo, *Chim. Ind.* (Milan), **1957**, *39*, 1032.
3. H. Sinn, W. Kaminsky, H. J. Volmer, R. Woldt, *Angew. Chem*., **1980**, *92*, 396.
4. H. Sinn, W. Kaminsky, *Adv. Organomet. Chem*., **1980**, *18*, 99.
5. F. R. W. P. Wild, M. Wasincionek, G. Huttner, H. H. Brintzinger, *J. Organomet. Chem.*, **1985**, *288*, 63.
6. J. Huang, G. L. Rempel, *Prog. Polym. Sci*., **1995**, *20*, 459.
7. W. Kaminsky, *Macromolecules*, **2012**, *45*, 3289.

8. R. Kleinschmidt, Y. Van der Leek, M. Reffke, G. Fink, *J. Mol. Catal. A: Chem*., **1999**, *148*, 29.
9. S. Jüngling, R. J. Mülhaupt, *Organomet. Chem*., **1995**, *497*, 27.
10. S. S. Reddy, K. Radhakrishnan, S. Sivaram, *Polym. Bull*., **1996**, *36*, 165.
11. I. Tritto, M. C. Sacchi, P. Locatelli, S. X. Li, *Macromol. Chem. Phys*., **1996**, *197*, 1537.
12. I. Tritto, C. Mealares, M. C. Sacchi, P. Locatelli, *Macromol. Chem. Phys*., **1997**, *198*, 3963.
13. G. M. Smith, D. B. Malpass, S. N. Bernstein, P. D. Jones, D. J. Monfiston, J. Rogers, B. M. Su, S. W. Palmaka, C. F. Tirendi, C. C. Crapo, D. L. Deavenport, J. T. Hodges, R. H. Ngo, C. W. Post, C. S. Rabbitt, Proc. Polyolefins X – 10th Internat. Conf. Polyolefins 1997, 49.
14. I. Tritto, S. X. Li, M. C. Sacchi, P. Locatelli, G. Zannoni, *Macromolecules*, **1995**, *28*, 5358.
15. I. Tritto, R. Donetti, M. C. Sacchi, P. Locatelli, G. Zannoni, *Macromolecules*, **1997**, *30*, 1247
16. D. E. Babushkin, N. V. Semikolenova, V. A. Zakharov, E. P. Talsi, *Macromol. Chem. Phys*., **2000**, *201*, 558.
17. S. Pasynkiewicz, *Polyhedron*, **1990**, *9*, 429.
18. V. N. Panchenko, V. A. Zakharov, I. G. Danilova, E. A. Paukshtis, I. I. Zakharov, V. G. Gonchatov, A. P. Sunkey, *J. Mol. Catal. A: Chem*., **2001**, *174*, 107.
19. E. P. Talsi, N. V. Semikolenova, V. N. Panchenko, A. P. Sobolev, D. E. Babushkin, A. A. Shubin, V. A. Zakharov, *J. Mol. Catal. A: Chem*., **1999**, *139*, 131.
20. E. Zurek, T. Ziegler, *Prog. Polym. Sci*., **2004**, *29*, 107.
21. E. Zurek, T. Ziegler, *Inorg. Chem*., **2001**, *40*, 3279.
22. R. Glaser, X. Sun, *J. Am. Chem. Soc*., **2011**, *133*, 13323.
23. M. Ystenes, J. L. Eilertsen, J. K. Liu, M. Ott, E. Rytter, J. A. Stovneng, *J. Polym. Sci., Part A: Polym. Chem.*, **2000**, *38*, 3106.
24. M. Linnolahti, J. R. Severn, T. A. Pakkanen, *Angew. Chem. Int. Ed*., **2008**, *47*, 9279.
25. J.-N. Pédeutour, K. Radhakrishnan, H. Cramail, A. Deffieux, *Macromol. Rapid Commun.*, **2001**, *22*, 1095.
26. J. R. Severn, J. C. Chadwick, R. Duchateau, N. Friederichs, *Chem. Rev*., **2005**, *105*, 4073.

27. Q. Wang, J. Hong, Z. Fan, R. Tao, *J. Polym. Sci., Part A: Polym. Chem.*, **2003**, *41*, 998.
28. Q. Wang, J. Weng, Z. Fan, L. Feng, *Eur. Polym. J.*, **2000**, *36*, 1265.
29. Q. Wang, J. Weng, Z. Fan, L. Feng, *Macromol. Rapid Commun*., **1997**, *18*, 1101.
30. Q. Wang, Y. Zhao, L. Song, Z. Fan, L. Feng, *Macromol. Chem. Phys*., **2001**, *202*, 448.
31. Q. Wang, L. Song, Y. Zhao, L. Feng, *Macromol. Rapid Commun*., **2001**, *22*, 1030.
32. H. Yang, Q. Wang, Z. Fan, W. Lou, L. Feng, *Eur. Polym. J*., **2003**, *39*, 275.
33. J. R. Severn, In Tailor-Made Polymers, Via Immobilization of Alpha-Olefin Polymerization Catalysts, Wiley-VCH: Weinheim, Germany, 2008, p95.
34. I. I. Zakharov, V. A. Zakharov, A. G. Potapov, G. M. Zhidomirov, *Macromol. Theory Simul.*, **1999**, *8*, 272.
35. E. W. Hansen, R. Blom, P. O. Kvernberg, *Macromol. Chem. Phys*., **2001**, *202*, 2880.
36. D. W. Imhoff, L. S. Simeral, S. A. Sangokoya, J. H. Peel, *Organometallics*, **1998**, *17*, 1941.
37. D. W. Imhoff, L. S. Simeral, D. R. Blevis, W. R. Beard, *Symposium Series*, **2000**, *749*, 177.
38. H. Sinn, *Macromol. Symp*., **1995**, *97*, 27.
39. H. Sinn, I. Schimmel, M. Ott, H. von Thienen, A. Harder, W. Hagendorf, B. Heitmann, E. Haupt, In Metalorganic Catalysts for Synthesis and Polymerization, W. Kaminsky, Springer Ed., Berlin, 1999, p 105.
40. E. Giannetti, G. M. Nicoletti, R. Mazzocchi, *J. Polym. Sci.: Polym. Chem. Ed*., **1985**, *23*, 2117.
41. C. J. Harlan, M. R. Mason, A. R. Barron, *Organometallics*, **1994**, *13*, 2957.
42. M. R, Mason, J. M. Smith, S. G. Bott, A. R. Barron, *J. Am. Chem. Soc*., **1993**, *115*, 4971.
43. A. R. Barron, *Comments Inorg. Chem*., **1993**, *14*, 123.
44. M. Veith, *Chem. Rev*., **1990**, *90*, 3.
45. F. Ghiotto, C. Pateraki, J. Tanskanen, J. R. Severn, N. Luehmann, A. Kusmin, J. Stellbrink, M. Linnolahti, M. Bochmann, *Organometallics*, **2013**, *32*, 3354.
46. J. L. Atwood, D. C. Hrncir, R. D. Priester, R. D. Rogers, *Organometallics*, **1983**, *2*, 985.
47. E. Zurek, T. K. Woo, T.K. Firman, T. Ziegler, *Inorg. Chem*., **2001**, *40*, 361.
48. M. Linnolahti, J. R. Severn, T. A. Pakkanen, *Angew. Chem. Int. Ed.*, **2006**, *45*, 331.

49. D. E. Babushkin, N. V. Semikolenova, V. N. Panchenko, A. P. Sobolev, V. A. Zakharov, E. P. Talsi, *Macromol. Chem. Phys*. **1997**, *198*, 3845.
50. T. Sugano, K. Matsubara, T. Fujita, T. Takahashi, *J. Mol. Catal*., **1993**, *82*, 93.
51. K. von Lacroix, B. Heitmann, H. Sinn, *Macromol. Symp*., **1995**, *97*, 137.
52. M. Floor, G. M. Smith, D. B. Malpass, Proceedings of Metallocenes Europe '87, Schotland Business Research: Skillman, 1997, p 33.
53. D. Cam, E. Albizzati, P. Cinquina, *Macromol. Chem. Phys*., **1990**, *191*, 1641.
54. W, Kaminsky, H. Sinn, Proc. IUPAC, IUPAC, *Macromol. Symp*., **1982**, *28*, 247.
55. C. J. Harlan, S. G. Bott, A. R. Barron, *J. Am. Chem. Soc*., **1995**, *117*, 6465.
56. A. R. Barron, *Macromol. Symp*., **1995**, *97*, 15.
57. M. Bochmann, *Organometallics*, **2010**, *29*, 4711.
58. D. Cam, U. Giannini, *Makromol. Chem*., **1992**, *193*, 1049.
59. L. Resconi, S. Bossi, L. Abis, *Macromolecules*, **1990**, *23*, 4489.
60. I. Tritto, M. C. Sacchi, S. Li, *Macromol. Rapid Commun*., **1994**, *15*, 217.
61. Coevoet, H. Cramail, A. Deffieux, *Macromol. Chem. Phys*., **1998**, *199*, 1451.
62. D. Coevoet, H. Cramail, A. Deffieux, *Macromol. Chem. Phys*., **1998**, *199*, 1459.
63. D. Coevoet, H. Cramail, A. Deffieux, *Macromol. Chem. Phys*. **1999**, *200*, 1208.
64. J. N. Pédeutour, H. Cramail, D. Coevoet, A. Deffieux, *Macromol. Chem. Phys*., **1999**, *200*, 1215.
65. J. N. Pédeutour, H. Cramail, A. Deffieux, *J. Mol. Catal. A: Chem*., **2001**, *174*, 81.
66. S. Reddy, G. Shashidhar, S. Sivaram, *Macromolecules*, **1993**, *26*, 1180.
67. F. Ghiotto, C. Pateraki, J. R. Severn, N. Friederichs, M. Bochmann, *Dalton Transactions*, **2013**, *42*, 9040.
68. Chapter 5, Section 5.2.3.3.
69. E. P.Talsi, K. P. Bryliakov, N. V. Semikolenova, V. A. Zakharov, M. Bochmann, *Kinet. Catal*., **2007**, *48*, 490.
70. M. Bochmann, S. J. Lancaster, *Angew. Chem. Int. Ed. Engl*., **1994**, *33*, 1634.
71. W. Kaminsky, *Macromol. Chem. Phys*., **1996**, *197*, 3907.
72. A. R. Siedle, W. M. Lamanna, R. A. Newmark, J. N. Schoepfer, *J. Mol. Catal. A: Chem*., **1998**, *128*, 257.
73. M. Bochmann, M. J. Sarsfield, *Organometallics*, **1998**, *17*, 5908.
74. K. P. Bryliakov, N. V. Semikolenova, D. V. Yudaev, V. A. Zakharov, H. H. Brintzinger, M. Ystenes, E. Rytter, E. P. Talsi, *J. Organomet. Chem*., **2003**, *683*, 92.
75. E. Y. X. Chen, *Chem. Rev*., **2000**, *100*, 1391.

76. D. Fisher, S. Jüngling, R. Mülhaupt, *Makromol. Chem. Macromol. Symp*., **1993**, *66*, 191.
77. D. Fisher, R. Mülhaupt, *J. Organomet. Chem*., **1991**, *417*, C7-C11.
78. I. Tritto, S. X. Li, M. C. Sacchi, G. Zannoni, *Macromolecules*, **1993**, *26*, 7111.
79. I. Tritto, R. Donnetti, M. C. Sacchi, P. Locatelli, G. Zannoni, *Macromolecules*, **1999**, *32*, 264.
80. Y. X. Chen, C. L. Stern, S. Yang, T. J. Marks, *J. Am. Chem. Soc*., **1996**, *118*, 12451.
81. Y. X. Chen, M. V. Metz, L. Li, C. L. Stern, T. J. Marks, *J. Am. Chem. Soc*., **1998**, *120*, 6287.
82. U. Wieser, F. Schaper, H. H. Brintzinger, *Macromol. Symp*., **2006**, *236*, 63.
83. D. E. Babushkin, C. Naundorf, H. H. Brintzinger, *Dalton Trans*., **2006**, 4539.
84. L. Mogstad, R. M. Waymouth, *Macromolecules*, **1992**, *25*, 2282.
85. D. J. Byun, D. K. Shin, S. Y. Kim, *Macromol. Rapid Commun*., **1999**, *20*, 419.
86. D. J. Byun, S. Y. Kim, *Macromolecules*, **2000**, *33*, 1921.
87. K. Mashima, S. Fujikawa, A. Nakamura, *J. Am. Chem. Soc*., **1993**, *115*, 10990.
88. K. Mashima, S. Fujikawa, Y. Tanaka, H. Urata, T. Oshiki, E. Tanaka, A. Nakamura, *Organometallics*, **1995**, *14*, 2633.

.

Chapter 2

Studies on the Initial Reaction Steps of the Hydrolysis of TMA by ^{1}H VT NMR

2.1 Introduction

2.1.1 Synthesis of MAO

Methylaluminoxane (MAO) is primarily synthesized by the controlled and partial hydrolysis of TMA. However, the final product of the hydrolysis reaction might differ significantly and exhibit different catalytic performance when used as a co-catalyst in olefin polymerization, depending on the conditions of the reaction: the solvent, the concentration of the reactants, the temperature and the method of introducing water into the system.

The method of introducing water into the system has been the main focus of many research groups over recent decades, and many different methods have been developed, which are assorted in two basic categories: direct and indirect hydrolytic methods. Direct hydrolysis of TMA has been performed by using different water sources or carriers in an attempt to control the reaction, avoiding high exothermic runaway reactions that are likely to occur otherwise.[1-4]

A common water carrier that has been successfully employed is an inert gas, such as nitrogen, that is saturated with water vapour.[5-6] Condensation of water vapour into a benzene solution of the required trialkylaluminium (TMA in the case of MAO),[7] or water adsorbed into molecular sieves[8] have been used as water sources too. Finally, a common way of reacting water in a controlled way with TMA is by using the surface water of deeply cooled ice in a toluene solution of TMA at low temperatures.[9] Of course other means like temperature, concentration or mixing, play an important role in the final structural characteristics and properties of the synthesized MAO.

Indirect hydrolysis introduces chemically bonded water in the form of hydrated salts, and provides a better way of controlling the reaction. The most commonly used salt hydrates are $CuSO_4.5H_2O$ and $Al_2(SO_4)_3.18H_2O$.[1,4] Synthesis of MAO with $CuSO_4.5H_2O$ would

include addition of a TMA in toluene solution to a toluene solution that contains fine $CuSO_4.5H_2O$ (typical Al/H_2O = 1/1.1 n/n) at −20 °C. The mixture is kept stirring at −20 °C for 24 hours, and then the temperature is slowly raised to 20 °C.[10] Addition of TMA when $Al_2(SO_4)_3.18H_2O$ is used, usually takes place at a higher temperature (e.g. at 20 °C or 70 °C).[11]

One of the main disadvantages when hydrated salts are used is the presence of inorganic salts in the final product which might affect its properties. Additionally, the yield of the reaction is relatively low (about 40% of the initial Al is lost as insoluble material).[1,3]

Since the reaction of water with TMA is not a simple procedure (it requires deep thought in selecting the best way to introduce water into the system and control how the reaction proceeds by choosing the appropriate conditions for the method), many researchers focused on developing non-hydrolytic routes where milder conditions are used to produce MAO.

When a non-hydrolytic method is employed, water is completely absent, and an oxygen containing compound is used instead. These compounds can be organic compounds containing carbonyl groups such as CO_2, benzophenone or benzoic acid,[12-13] or compounds like Me_2SnO[14], phenylboronic acid[15] and trialkylboroxine[16]. Treatment of TMA with compounds that contain an oxygen atom bonded to a metal like PbO has also been reported.[6]

The present research is focusing on hydrolytic routes of synthesizing MAO, and more specifically on the direct hydrolysis of TMA. The main target is to investigate the initial reaction steps and intermediates formed between TMA and water in order to gain an insight into the structural characteristics of MAO. Water was molecularly dispersed in toluene, but other solvents were also employed and tested.

2.1.2 Possible Reaction Mechanisms of the Hydrolysis of TMA

In 1964 Sakharovskaya *et al.*,[5] have proposed a generic mechanism which includes a two-step reaction for the reaction of TMA with water:

$$R_3Al + H_2O \longrightarrow R_2AlOH + RH \qquad (2.1)$$

$$R_2AlOH + R_3Al \longrightarrow R_2AlOAlR_2 + RH \qquad (2.2)$$

The main intermediate of the reaction is the dialkylaluminium hydroxide.

However the exact mechanism of the reaction, the structure of the final product and the side reactions that might occur depend on many factors: concentration, temperature, duration of the reaction, mixing of the reagents, the Al/H_2O ratio and the solvent used. For example, polar solvents might decrease the reactivity of the organoaluminium compound. More specifically, Boleslawski and Serwatowski[17] chose diethyl ether as a solvent to study the hydrolysis reaction of trialkylaluminium compounds (Me_3Al, Et_3Al and *i*-Bu_3Al). Diethyl ether complexes *via* hydrogen bonding with the starting materials, intermediates and final products and decreases the reaction rate. In this way, it makes it feasible to observe the intermediates by ^1H NMR spectroscopy.

They mainly studied the hydrolysis reaction using two different Al/H_2O ratios: 1/1 and 2/1. In both cases, the first step of the reaction was the formation of a $Me_3Al–H_2O$ complex (at −70 °C) (Scheme 1):

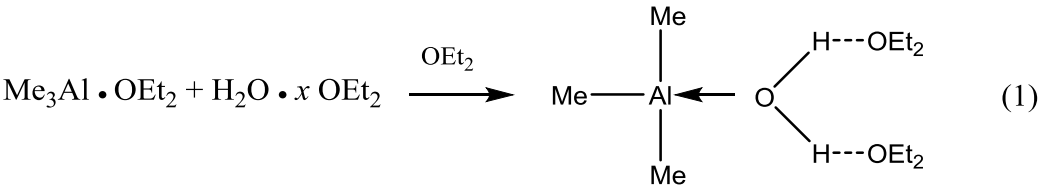

(1)

(I)

Scheme 2.1: First reaction step of the hydrolysis reaction of TMA in Et_2O, according to Boleslawski and Serwatowski.[17]

The amount of the $Me_3Al–H_2O$ complex increases as the temperature increases. At –45 °C new signals appear on the ^1H NMR spectrum, which are attributed to the formation of dimethylaluminium hydroxide and evolution of methane. This suggests that the next reaction step is the intramolecular rearrangement of the $Me_3Al–H_2O$ complex to give Me_2AlOH, as described in Scheme 2.2.

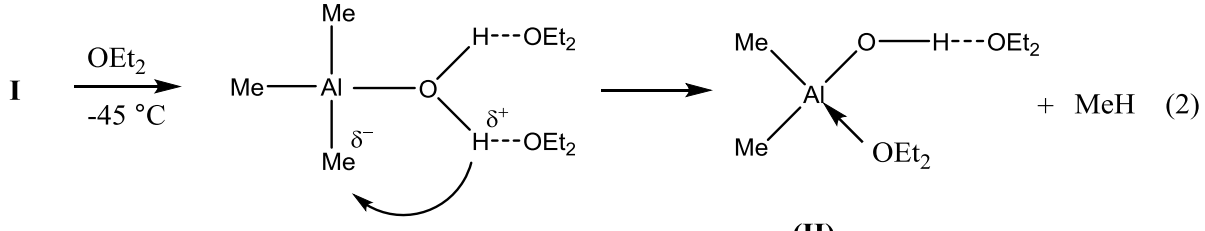

+ MeH (2)

(II)

Scheme 2.2: Second reaction step of the hydrolysis reaction of TMA in Et_2O, according to Boleslawski and Serwatowski.[17]

It is suggested that the Me_2AlOH intermediate (II) stabilizes to the dimeric form by autoassociation (see Scheme 2.3).

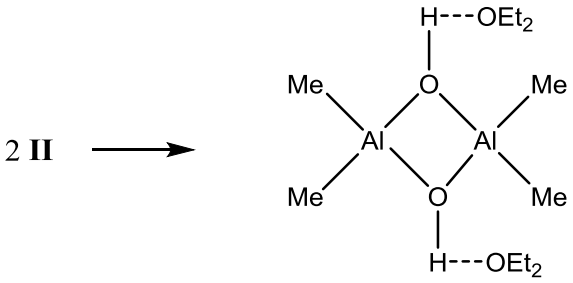

(III)

Scheme 2.3: Stabilization of Me_2AlOH by autoassociation, according to Boleslawski and Serwatowski.[17]

The hydrolysis reaction of Et_3Al and *i*-Bu_3Al proceeds by following a similar mechanism as the one described for the Me_3Al system.

When excess Me_3Al was used ($Al/H_2O = 2/1$), the conversion of (I) to (II) took place at higher temperatures (–30 °C to –20 °C), meaning that a higher activation energy was needed. The Me_2AlOH did not react further with the excess TMA to form the $Me_2AlOAlMe_2$ species, as would have been expected according to 2.2. This was attributed to the high activation energy of this reaction and high stabilization if the Me_2AlOH associates (parallel reactions of Me_2AlOH itself), causing low selectivity. High selectivity is expected for the systems where higher alkyls were used.

Pasynkiewicz *et al.*[18] have also studied the reaction of TMA with H_2O, but they performed the hydrolysis in dimethoxymethane (DMM). They employed a 2/1 ratio of TMA/ H_2O, and by using ^1H NMR spectroscopy and performing some IR measurements they observed a two step reaction. The mechanism is described below (Reactions 2.3 and 2.4).

$$2\ Me_3Al \bullet DMM + H_2O \xrightarrow[DMM]{-35\ ^\circ C} Me_2AlOH \bullet DMM + Me_3Al \bullet DMM + MeH \quad (2.3)$$

$$Me_2AlOH \bullet DMM + Me_3Al \bullet DMM \xrightarrow[DMM]{-15\ ^\circ C} Me_4Al_2O \bullet DMM + MeH \quad (2.4)$$

It is interesting to notice that two resonances are observed in the ^1H NMR spectrum attributed to the OH protons of the dimethylaluminium hydroxide. This could be explained by the presence of two different forms (see Figure 2.1), depending on the kind of hydrogen bonding with DMM.

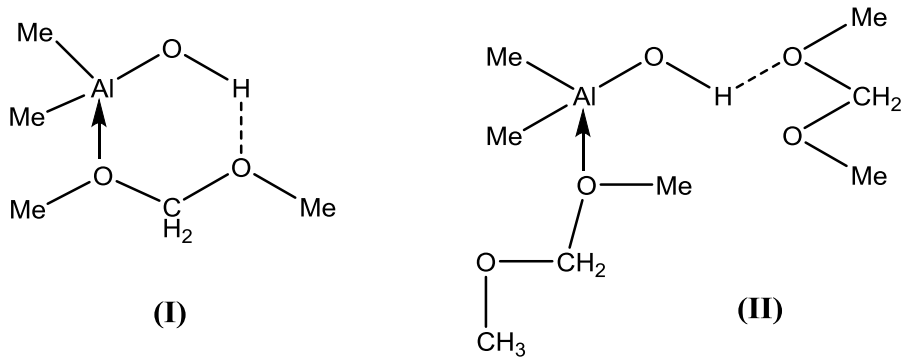

Figure 2.1: Different forms of the dimethylaluminium hydroxide (with different type of hydrogen bonding with DMM).

When Pasynkiewicz *et al.* repeated the reaction in diethyl ether, only one signal was observed for the OH protons of the dimethylaluminium hydroxide, supporting the theory that different types of hydrogen bonding occur when DMM is used as a solvent.

Storr *et al.*[7] investigated the partial hydrolysis of ethylalane compounds, $Et_{3-x}AlX_x$ (where x = 0, 1 and X = Cl, OEt), and proposed one possible reaction scheme with a hydroxyl compound as an intermediate (see Reactions 2.5 and 2.6):

$$Et_{3-x}AlX_x + H_2O \xrightarrow{\text{benzene}} Et_{2-x}Al(X)_xOH + EtH \quad (2.5)$$

$$Et_{2-x}Al(X)_xOH + Et_{3-x}AlX_x \xrightarrow{\text{benzene}} Et_{2-x}Al(X)_xEt_{2-x} + EtH \quad (2.6)$$

When Et_3Al was reacted with H_2O in a 2/1 ratio, the final product of the reaction was $(Et_2Al)_2O$ (soluble oily, trimeric product) accompanied by evolution of ethane, as described in Reaction 2.7.

$$2\ Et_3Al + H_2O \xrightarrow{\text{benzene}} (Et_2Al)_2O + 2\ EtH \qquad (2.7)$$

However, when Et_3Al was reacted with H_2O in a 1/1 ratio, formation of an insoluble amorphous material was observed; probably a cross-linked high polymer of the type EtAlO.

The reaction of Et_3Al with H_2O was investigated even earlier by Amdurski *et al.*[19] who published an article in 1961 proposing the general reaction seen in Reaction 2.8, based on the stoichiometry of the reaction and kinetic results from measuring the rate of evolution of ethane.

$$Et_3Al + H_2O \longrightarrow 0.4\ EtAlO + 0.6\ Et_2AlOH + 1.4\ EtH \qquad (2.8)$$

Barron *et al.*[20] investigated the hydrolysis of tri-*tert*-butylaluminium, $^tBu_3Al$ and provided the first structural characterization of an alkylalumoxane. Direct hydrolysis of $^tBu_3Al$ ($Al/H_2O \sim 1/1$) at low temperature (–78 °C) in pentane resulted in the formation of a trimeric hydroxide $[^tBu_2Al(\mu\text{-}OH)]_3$, accompanied by evolution of isobutene, which was verified by NMR (^1H, ^{17}O, ^{27}Al) and X-ray crystallography.

On the other hand, when $^tBu_3Al$ was hydrolyzed by the method of hydrated salts using $Al_2(SO_4)_3{\cdot}18H_2O$ ($Al/H_2O \sim 1/1$) in toluene, thermolysis of the product resulted in the formation of tetrameric $[^tBu_2Al(\mu\text{-}OAl^tBu_2)]_2$ and octameric $[^tBuAl(\mu_3\text{-}O)]_8$.[20] However, Barron *et al.*[21] found out that when the amount of H_2O added to the system was carefully controlled (thermogravimetric analysis of $Al_2(SO_4)_3{\cdot}18H_2O$ showed that the salt included only 14 H_2O molecules, so a less than stoichiometric amount of H_2O was probably used in the previous studies[20]), it resulted to the formation of the dimeric $[^tBu_2Al(\mu\text{-}OH)]_2$ (main product), and some $[Al_4(^tBu)_7(\mu_3\text{-}O)_2(\mu\text{-}OH)]$.

2.2 Results and Discussion

2.2.1 Quantitative ^{1}H NMR[22-23]

The basic principle for quantitative NMR is that the intensity of a resonance line (integrated signal area A_x) is directly proportional to the number of nuclei $N_x$which generate the corresponding signal response (see Eqn 2.1).

$$A_x = K_s N_x \qquad (2.1)$$

where K_s is a spectrometer constant.

To obtain quantitative results it is necessary to determine the relative area ratios A_x/A_y of two compounds X and Y, where X is the unknown compound that has to be determined and Y is a compound of a known weight which is used as the internal standard (see Eqn 2.2).

$$\frac{A_x}{A_y} = \frac{N_x}{N_y} \qquad (2.2)$$

The molar ratio of the compounds X and Y can be easily calculated (Eqn 2.3):

$$\frac{n_x}{n_y} = \frac{A_x}{A_y}\frac{N_y}{N_x}\frac{P_y}{P_x} \qquad (2.3)$$

where P_x and P_y are the purities of the compounds X and Y, respectively. The above equation was used to determine any quantitative NMR data presented here.

In order to ensure reliable results in quantitative NMR measurements, selection of a suitable internal standard is of great importance. A compound should be used as internal standard only if it provides unique and sharp stable signals and if it is soluble in the NMR solvent which is used. It should be non-volatile and non-reactive and it should be easy-to-use (weighing).

2.2.2 Determination of the Solubility of Water in Toluene by Quantitative NMR

The amount of water that is molecularly dispersed in toluene is very small, so is the water peak. In order to minimize the integration error when comparing two peaks of two different compounds, it is important to ensure that the peaks will be of the same level. For this reason it was necessary to initially perform a series of tests in order to estimate the

quantity of the dissolved water in toluene and optimize the concentration of 1,3,5-tri-*tert*-butylbenzene used, and subsequently minimize the error of the method. The signal of 1,3,5-tri-*tert*-butylbenzene in toluene, using a minimal amount of C_6D_6 for locking, at δ 1.47 (27 H) is far from any other signals (see Figure 2.2).

Quantitative NMR analysis, after applying the equation 2.3 with A_x = integrated area of the peak that corresponds to the water protons at δ 0.53 and A_y = integrated area that corresponds to the *t*-Bu protons of 1,3,5-tri-*tert*-butylbenzene at δ 1.47 (see Figure 2.2), it was found that the water solubility in toluene is 0.0215 mmol/mL (0.4 mL toluene were saturated with 8.6 µmol H_2O).

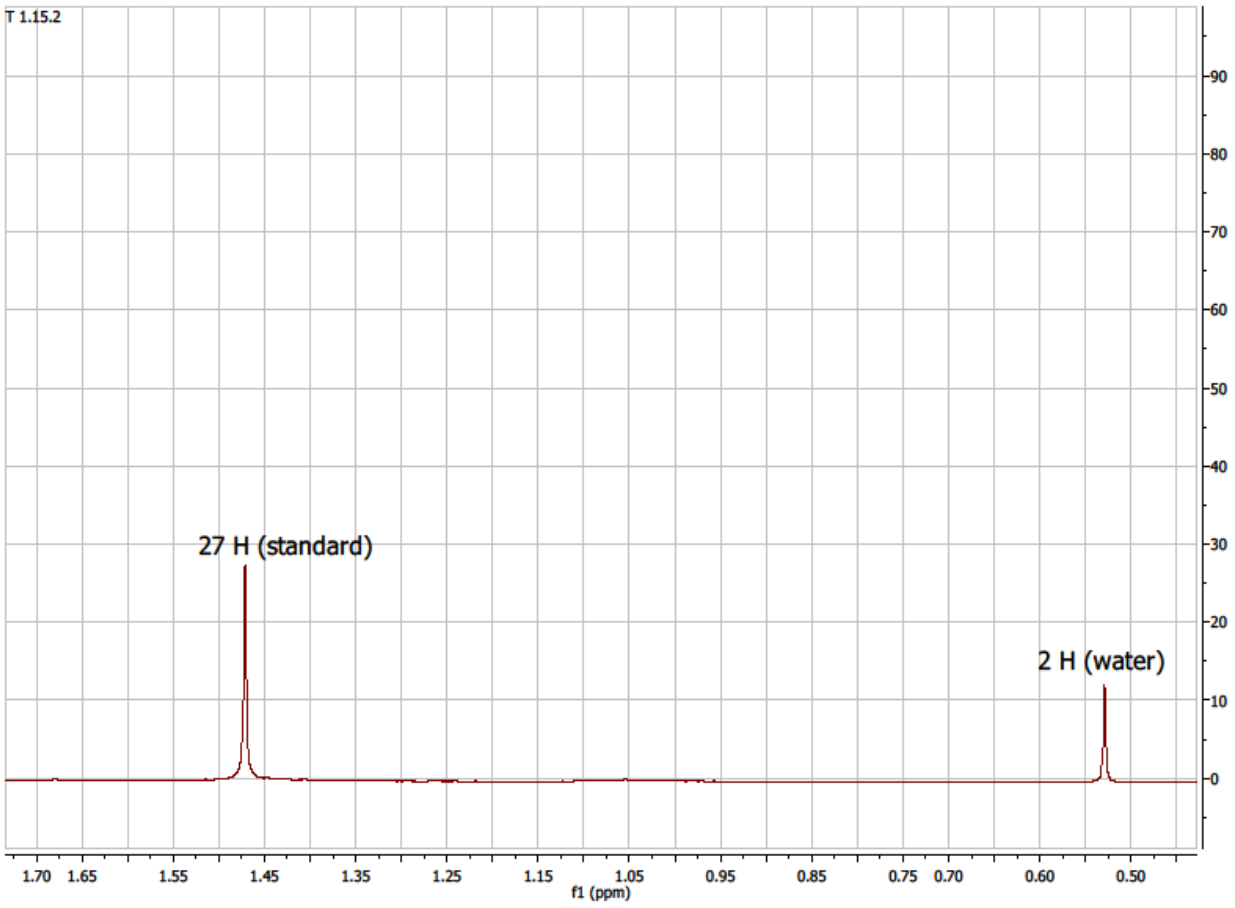

Figure 2.2: ^1H NMR spectrum of water in toluene, using 1,3,5-tri-tert-butylbenzene as internal standard and C_6D_6 as NMR reference at room temperature.

2.2.3 Non-Molecularly Dispersed Water

It was noted that when the ^{1}H NMR spectrum was recorded a short period after mixing water with toluene, a broadness of the peak that corresponds to water protons was observed, along with the presence of a shoulder peak. When the sample was left to rest for one day, the ^{1}H NMR spectrum showed a single sharp peak at the same chemical shift (δ 0.53) that appeared in previous experiments (see Figure 2.3). This indicated that H-bonded water was formed first (bottom spectrum, Figure 2.3), which was slowly converted to molecularly dispersed (top spectrum, Figure 2.3).

The chemical shift of molecular H_2O in toluene is due to the magnetic anisotropy of the arene ring of toluene; any H that points into that region is up-field shifted. Additionally bulk water will probably form aggregates; hydrogen bonding between these water aggregates will be present, leading to a downfield shift of the water protons caused by the deshielding effect of the hydrogen bonding.

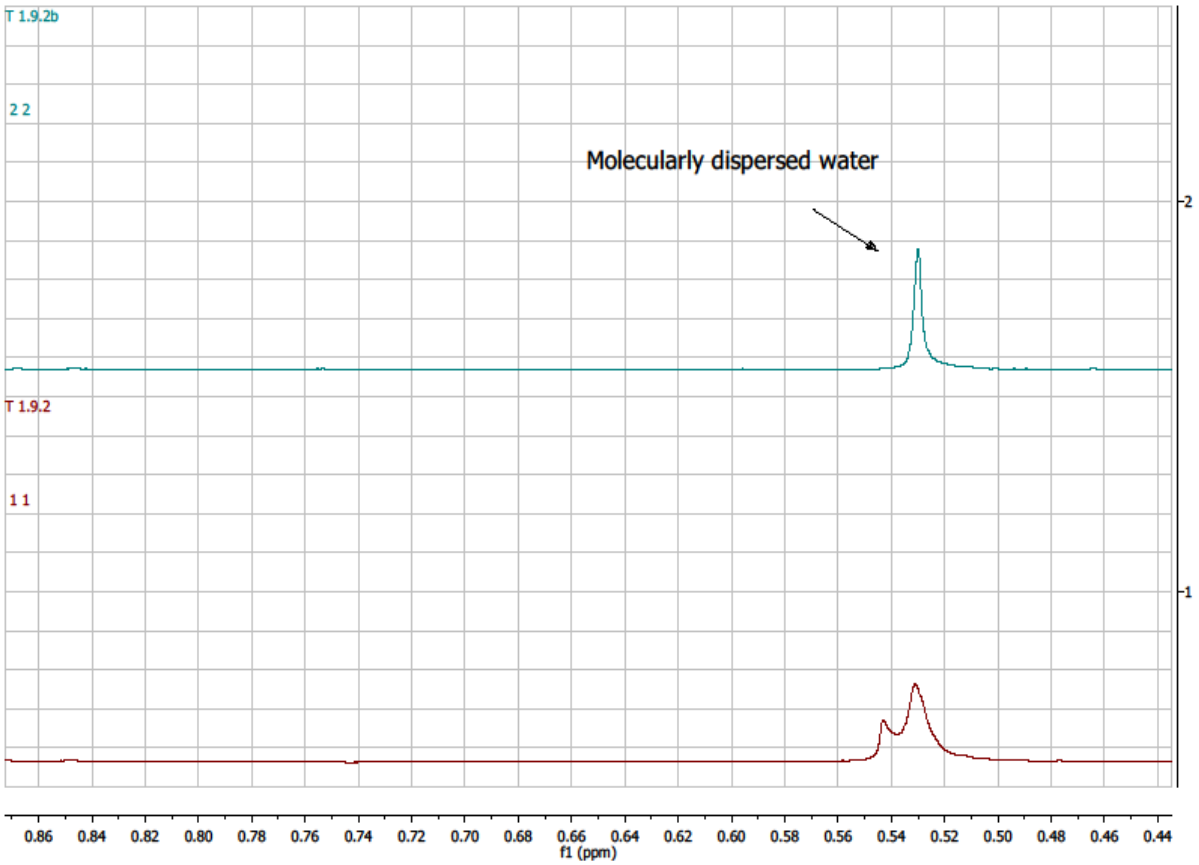

Figure 2.3: ^{1}H NMR, water chemical shift (bottom spectrum: recorded after a short period of time after mixing water and toluene; top spectrum: molecularly dispersed water in toluene)

Addition of a water droplet in the NMR tube which contained 0.6 mL distilled toluene-d8 exhibited two resonances that correspond to the water protons: molecularly dispersed water at δ 0.4 ppm and a broad resonance at δ 5 ppm that it is believed to correspond to non-molecularly dispersed water (see Figure 2.4). The broadness of the peak could be due to hydrogen bonded water (probably water droplets).

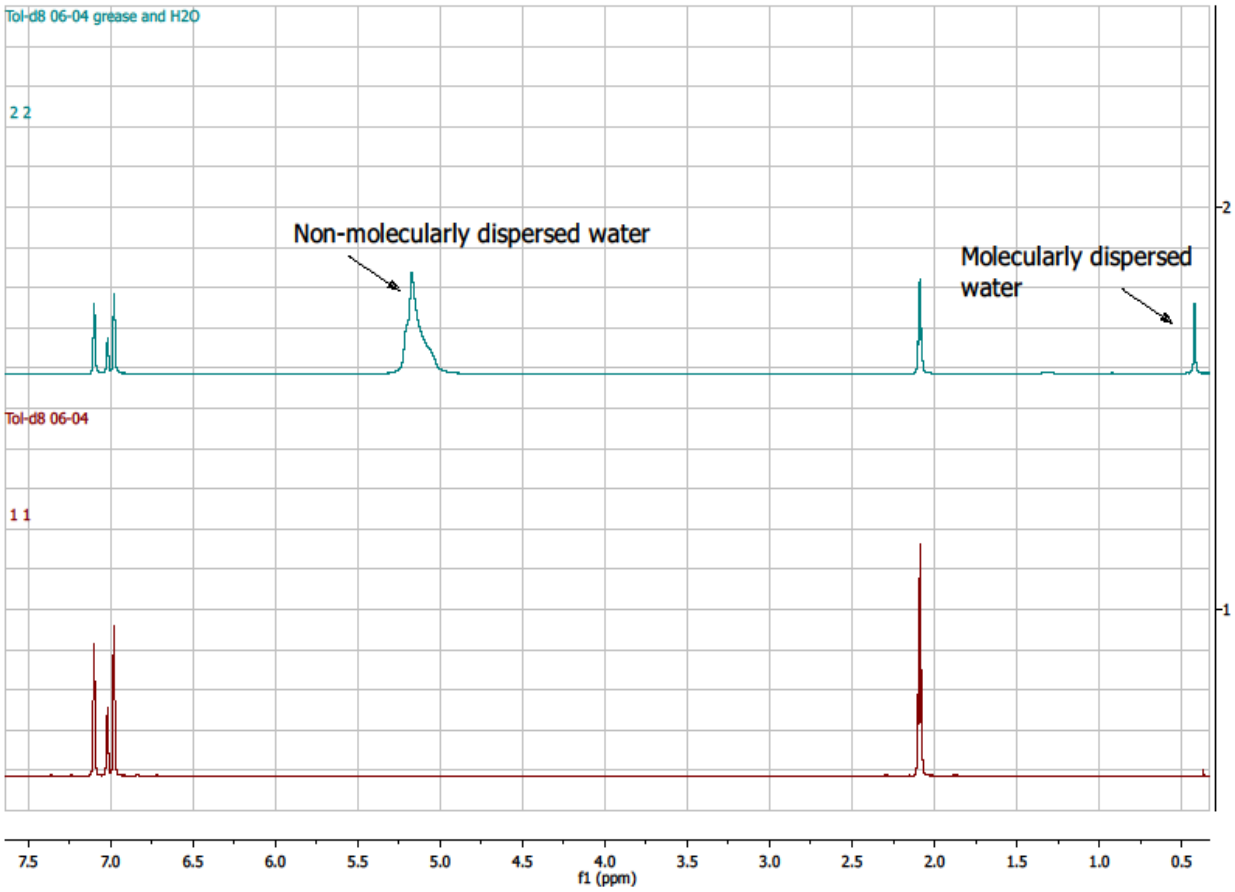

Figure 2.4: ^{1}H NMR of toluene-d^{8} (bottom spectrum) and ^{1}H NMR of toluene-d^{8} containing a droplet of water (top spectrum)

2.2.4 VT NMR Studies on the Hydrolysis Reaction of Trimethylaluminium

2.2.4.1 Toluene as a Solvent

As it has been reported in literature,[24-27] TMA exists in toluene solution as a dimer Al_2Me_6. The methyl groups of the TMA dimer display only one resonance at δ –0.36 due to their fast exchange on the ^{1}H NMR timescale (Figure 2.5, bottom spectrum). This exchange becomes slower as we reduce the temperature. The ^{1}H NMR signal of the methyl groups becomes broader (–20 °C), and eventually splits into two signals at temperatures below –40 °C. The two signals are attributed to the terminal Me groups of Al_2Me_6 (δ –0.54) and to the bridging Me groups of Al_2Me_6 (δ 0.11) at –70 °C (see Figure 2.5). These observations are in agreement with the existing literature.

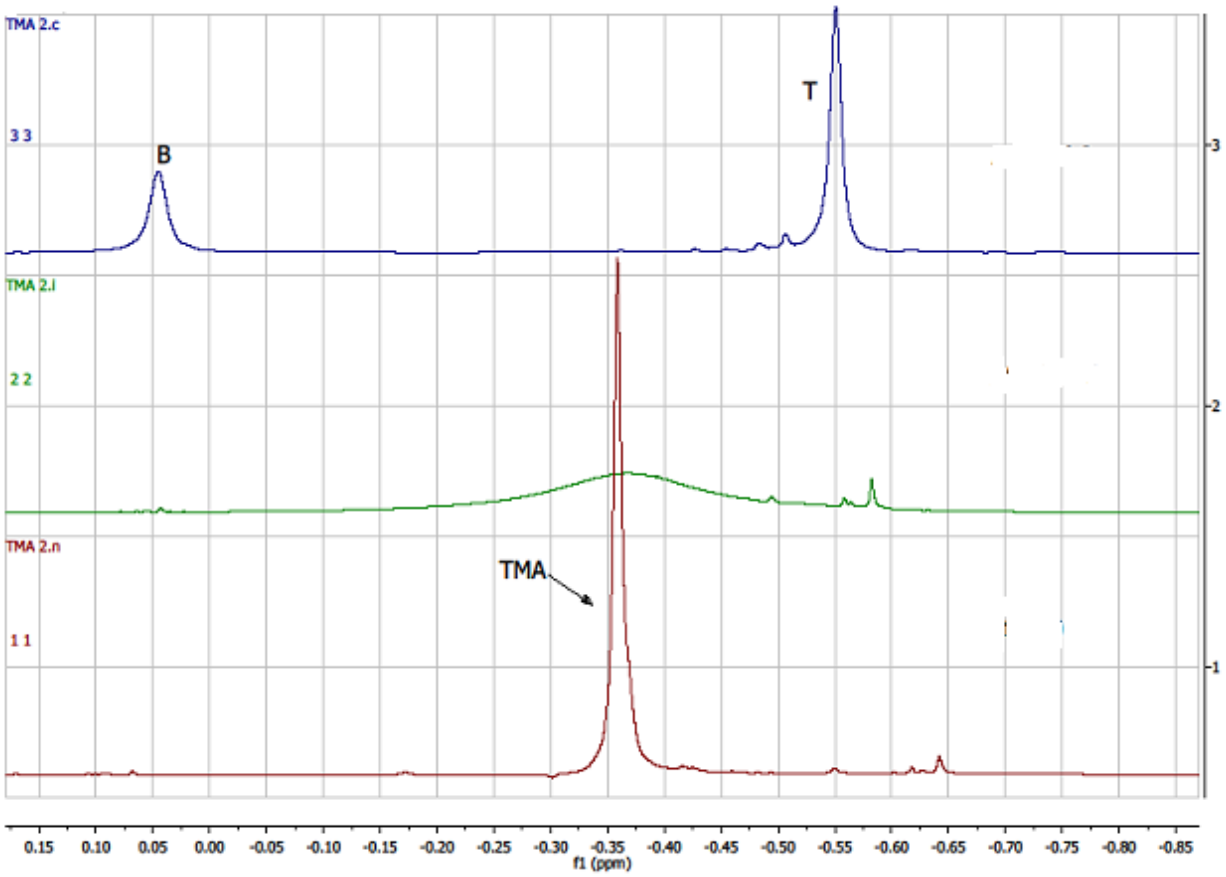

Figure 2.5: ^{1}H NMR spectra of TMA in toluene at 25 °C (bottom spectrum), –20 °C (middle spectrum) and –70 °C (top spectrum)

2.2.4.2 VT ^{1}H NMR Experiments in Toluene: Approach A

The hydrolysis of TMA was investigated by low temperature ^{1}H NMR using different TMA/H_2O ratios (Al/H_2O = 2.3/1, 3.5/1, 1.2/1 in reactions 7.1, 7.2 and 7.3 respectively).

'Reaction 7.1': Al/H_2O = 2.3/1

In reaction 7.1, a toluene solution (40 µL) of TMA (15.7 µmol) was added to an NMR tube containing 6.9 µmol of H_2O, molecularly dispersed in toluene (0.6 mL).

The ^{1}H NMR spectra of the hydrolysis reaction of TMA at increasing temperatures are presented in Figure 2.6. At low temperature (–63.7 °C) two main peaks can be detected (at δ –0.60 and –0.64). As the temperature increases (at –43.9 °C) the peak at δ –0.60, denoted as *, becomes more distinct and moves upfield (at δ –0.64), while the second smaller

peak starts to disappear. At −33.1 °C, the peak * is sharper and exhibits the highest integration area (A). As the temperature increases even more, the peak shifts further upfield and starts reducing until it disappears completely at 24.6 °C.

One assumption is that this peak could be attributed to the formation of dimethylaluminium hydroxide, Me_2AlOH, while the smaller peak at −63.7 °C could be due to the formation of a TMA and water adduct, $AlMe_3 \cdot H_2O$. This assumption could be supported by the findings during the VT NMR experiments of the hydrolysis reaction of TMA in THF (see Section 2.2.4.4). However, the intermediates detected in the experiments in THF will be more stable due to the association with THF, and we are not aware how stable they are in toluene at the same temperatures.

Several other smaller peaks are present at −43.9 °C between −0.52 to −0.59 ppm. While most of them disappear at higher temperatures, one peak remains. At room temperature there is no signal for any residual TMA, and only the peak at δ −0.57 (denoted as **) is present which is attributed to the dimethylaluminium methoxide, Me_2AlOMe, implying that some oxidation processes took place. The appearance of a small peak at δ 3.14 could be attributed to the methoxy group protons of Me_2AlOMe. The absence of any other signals apart from the one that is related to oxidation processes, leads to the conclusion that TMA was fully hydrolysed (converted to $Al(OH)_3$ or Al_2O_3) or precipitated. Actually, a careful observation of the contents of the NMR tube showed the existence of a gel on the walls of the NMR tube. This could for example mean that an insoluble amorphous material, probably a cross-linked high polymer of the type MeAlO, was formed (as Storr *et al.*[7] also mentioned formation of EtAlO products when they studied the hydrolysis of Et_3Al).

The attribution of the peak at δ −0.57 to Me_2AlOMe was proved by adding MeOH to a solution of TMA in toluene and recording the ^1H NMR spectrum. The signal attributed to the TMA (at δ −0.31) was still present but significantly reduced, and two new signals appeared at δ 3.13 and −0.57 which are attributed to the formation of Me_2AlOMe (MeO− protons and Me_2Al− protons respectively with a 1/2 integration value). Evolution of CH_4 was also observed.

Korneev *et al.*[28] identified Me_2AlOMe as a typical oxidation product of TMA when no-deoxygenated solvents were used. The assignment of the peaks comes in agreement with the results presented above.

The experiments of the *in-situ* hydrolysis reaction of TMA presented by Zhang *et al.*[29] were repeated with low [Al] = 0.095 M and high [Al] = 0.475 M TMA concentrations in toluene instead of benzene, in order to prove that the peak at −0.57 ppm is characteristic of the Me_2AlOMe and not MAO with low molecular weight. The peak at −0.57 ppm was not obvious when a higher [Al] concentration is used. When pure O_2 gas was bubbled through the reaction flask, the ^1H NMR results show clearly the formation of the oxidation product Me_2AlOMe. The appearance of the peaks at δ 3.13 and −0.57 when low concentrated TMA samples were employed shows how reactive TMA is towards oxidation.

The spectra of the hydrolysis reaction of TMA show CH_4 evolution. The signal at δ 0.25 at −63.7 °C which moves slightly upfield (δ 0.23 at 24.6 °C) as the temperature increases is attributed to the CH_4 protons. The assignment of the peak was verified by the addition of CF_3COOH in a TMA in toluene solution which results in CH_4 production. The reaction took place in an NMR tube and it was studied by VT ^1H NMR. The H^+ subtracts a methyl group from the TMA molecule to form CH_4 while the CF_3COO^- coordinates to the Al centre.

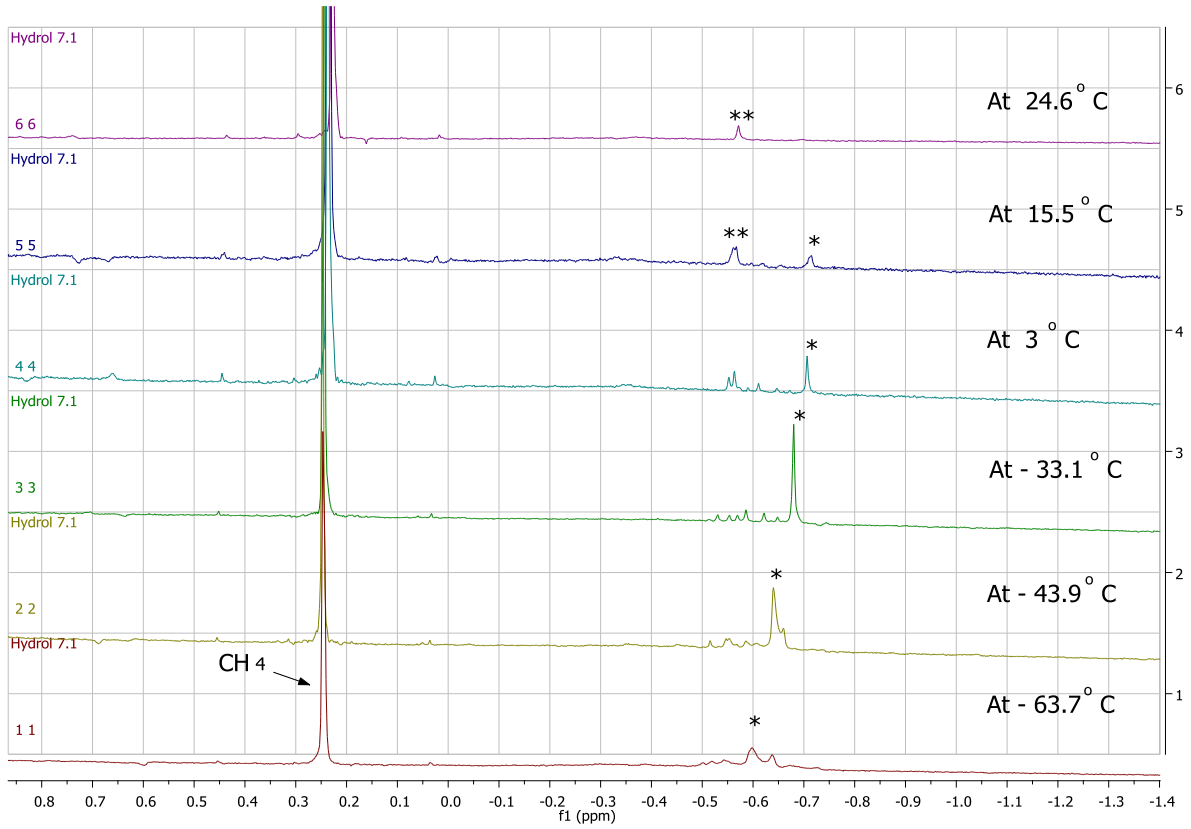

Figure 2.6: ^{1}H NMR spectra of the hydrolysis reaction 7.1 (Al/H_2O = 2.3/1): –63.7 °C (bottom spectrum), –43.9 °C, –33.1 °C, 3 °C, 15.5 °C and 24.6 °C

Quantitative ^{1}H NMR analysis showed that most of the CH_4 production took place at very low temperatures (11.09 µmol at –74.5 °C) which indicates that certain reaction processes have already happened. A small increase in CH_4 production is observed as the temperature increases, with the maximum amount of CH_4 measured at 3 °C (13.86 µmol). However, in terms of CH_4 production, the reaction is practically complete at –74.7 °C (see Figure 2.7 and Table 2.1 for methane evolution data). After 3 °C, a reduction in CH_4 is observed probably due to CH_4 loss in the gas phase. Additionally, it should be noted that a large amount of CH_4 is probably released in the gas phase while mixing, because in a few experiments the subaseal of the NMR tube flew off due to high pressure. This makes it even harder to quantify the amount of CH_4 that is produced.

Integration of the two main peaks that can be detected at the Al–Me area at –63.7 °C leads to the calculation of 0.73 µmol of Me_2AlOH and 0.17 µmol of $AlMe_3$*H_2O, if the

original assumption about the identification of these species is correct. In any case the integrated areas would result in a much smaller quantity of alkylaluminium species than the expected one, given the initial amount of TMA (15.65 μmol) inserted into the NMR. This observation would imply that mixing of the two reagents in toluene inside the NMR tube, while maintaining a very low temperature was unsuccessful, leading to full hydrolysis, or that working with such low concentrations of TMA makes oxygen insertion a detrimental problem leading to the formation of insoluble by-products. However, as mentioned earlier the insoluble products might be attributed to the formation of amorphous aluminoxane gel. Integration of the peak at δ –0.57 at 24.6 °C that is attributed to the Me_2AlOMe species shows formation of 0.25 μmol. On the other hand, in order to achieve full hydrolysis of the initial TMA there should have been an excess of H_2O (3 × 15.40). Perhaps H_2O condensation on the cold syringe needle led to introducing higher amounts of H_2O while transferring the TMA into the NMR tube.

Integration of the main Al–Me peak at –33.1 °C shows formation of 1.55 μmol of Me_2AlOH which still is a very small amount compared to the initial amount of TMA. Subtraction of the amount measured at –63.7 °C shows a rise of 0.82 μmol. The CH_4 rise from –63.7 °C to –33.1 °C corresponds to 0.97 μmol, resulting in an Al/CH_4 ratio of 0.85, relatively close to a 1/1 ratio that would have been expected if the reaction path shown in Reaction 2.9 was followed

$$Al_2Me_6 + 2\ H_2O \longrightarrow 2\ Me_2AlOH + 2\ CH_4 \qquad (2.9)$$

Determination of the Al/H_2O ratio and correlation of this ratio to a reaction path leading to the formation of an intermediate product is not possible in this case, since only a very small amount of alkylaluminium species was detected by NMR, and it is not possible to know exactly how much water was consumed for the formation of these species (because a high amount of water was probably consumed during the full hydrolysis of TMA).

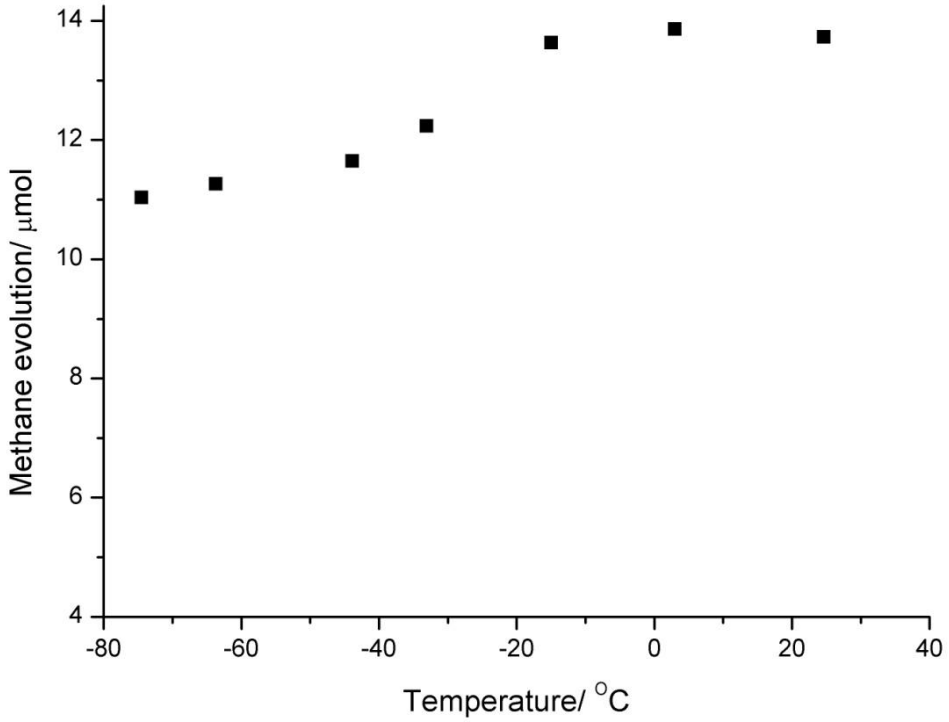

Figure 2.7: Methane evolution during the reaction 7.1

Table 2.1: Methane evolution during the reaction 7.1

T (°C)	CH_4 (μmol)
–74.7	11.1
–63.7	11.3
–43.9	11.7
–33.1	12.2
–15	13.6
3	13.9
24.6	13.7

In order to gather further quantitative data on the hydrolysis reaction of TMA another two TMA/H_2O ratios were investigated: a higher excess of TMA (3.5/1), and an almost stoichiometric ratio (1.2/1). The main quantitative data from the three different ratios employed, are summarized in Table 2.2.

'Reaction 7.2': Al/H_2O = 3.5/1

In reaction 7.2, a toluene solution (90 μL) of TMA (31.3 μmol) was added to an NMR tube containing 8.9 μmol of H_2O, molecularly dispersed in toluene (0.6 mL).

When a higher excess of TMA was employed, the signals of the terminal (δ –0.57) and bridging (δ 0.01) methyl groups of the remaining unreacted dimeric TMA are present at low temperatures (– 64.2 °C) (see Figure 2.8). As the temperature increases the bridging and terminal methyl groups of the unreacted TMA show only one broad resonance (δ –0.39 at –27.2 °C), which becomes a sharper signal at higher temperatures (e.g. δ –0.31 at 22.9 °C). At low temperature (–64.2 °C), one smaller peak at δ –0.64 appears, but it disappears with increasing temperature. If this peak corresponds to Me_2AlOH, integrating the area with respect to the internal standard would lead to 0.9 μmol. Two smaller peaks (δ –0.56, –0.54 ppm) are obvious at –27.2 °C, and only one of them (the one at δ –0.56) remains as the temperature increases. This peak is attributed to the oxidation product [$Me_2Al(OMe)$] of TMA, as it was discussed earlier (δ –0.58 at 22.9 °C, denoted as **) and corresponds to 0.8 μmol.

Integration of the unreacted TMA shows that 22.6 μmol remained into the solution. Subtracting this amount from the initial amount of TMA (31.3 μmol) would lead to 8.7 μmol of TMA that have reacted. If 0.8 μmol were oxidized, there are 7.9 μmol of TMA that has probably been fully hydrolyzed. The maximum amount of CH_4 produced was recorded at –27.2 °C (13.8 μmol), but integration of the peaks at the Al–Me area is not possible because they coincide with the broad TMA signal.

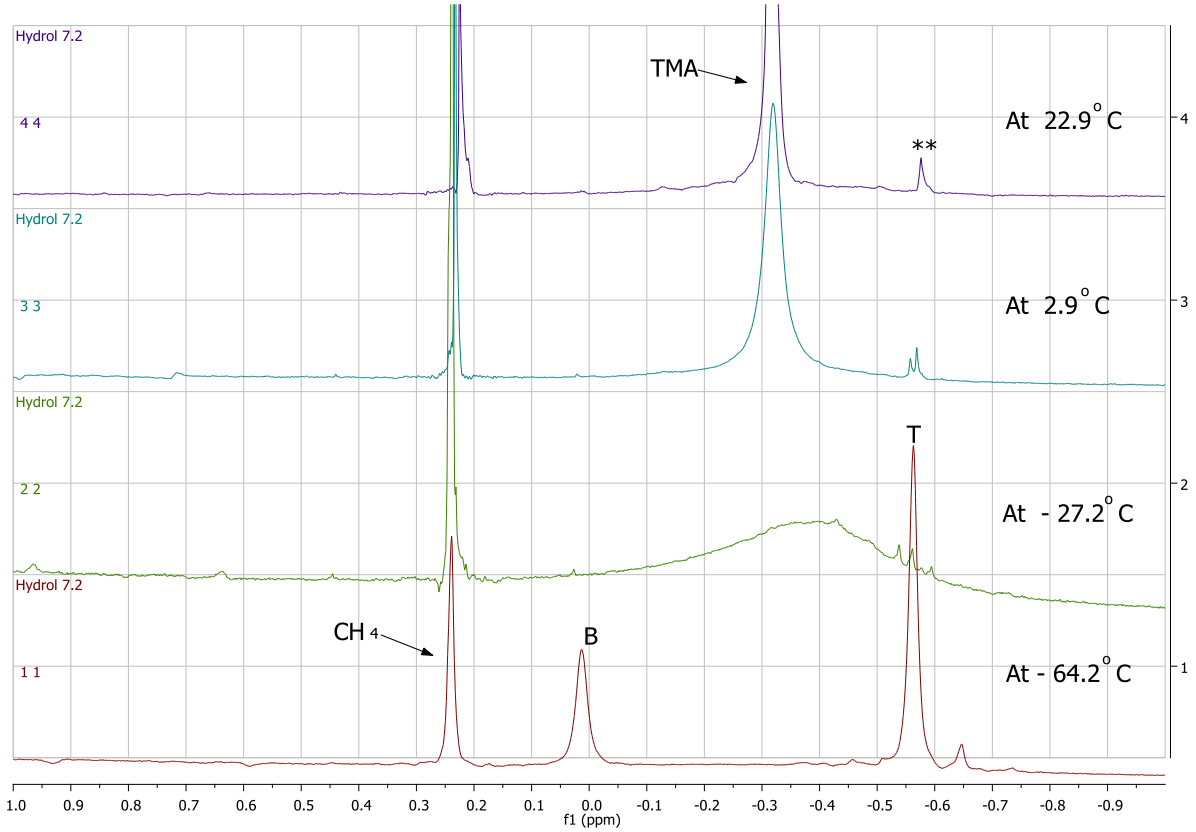

Figure 2.8: ^{1}H NMR spectra of the hydrolysis reaction 7.2 (Al/H_2O = 3.5/1): –64.2 °C (bottom spectrum), –27.2 °C, 2.9 °C and 22.9 °C.

'Reaction 7.3': Al/H_2O = 1.2/1

In reaction 7.3, a toluene solution (25 µL) of TMA (8.7 µmol) was added to an NMR tube containing 7.0 µmol of H_2O, molecularly dispersed in toluene (0.6 mL).

When a stoichiometric ratio of TMA/H_2O was employed, TMA was completely hydrolysed at higher temperatures (see Figure 2.9). At –64.2 °C one main peak (at δ –0.57) is distinct. The signal becomes sharper at –45.2 °C but starts reducing and disappears completely with increasing temperature. If this peak corresponds to Me_2AlOH, integrating the area would result to 1 µmol of Al. When the temperature reached –15.2 °C, all signals at the Al–Me area have already disappeared. The amount of CH_4 present at the lowest temperature that a measurement was taken (–75.2 °C) was 3.7 µmol, and reached a maximum (7.6 µmol) at 14.4 °C.

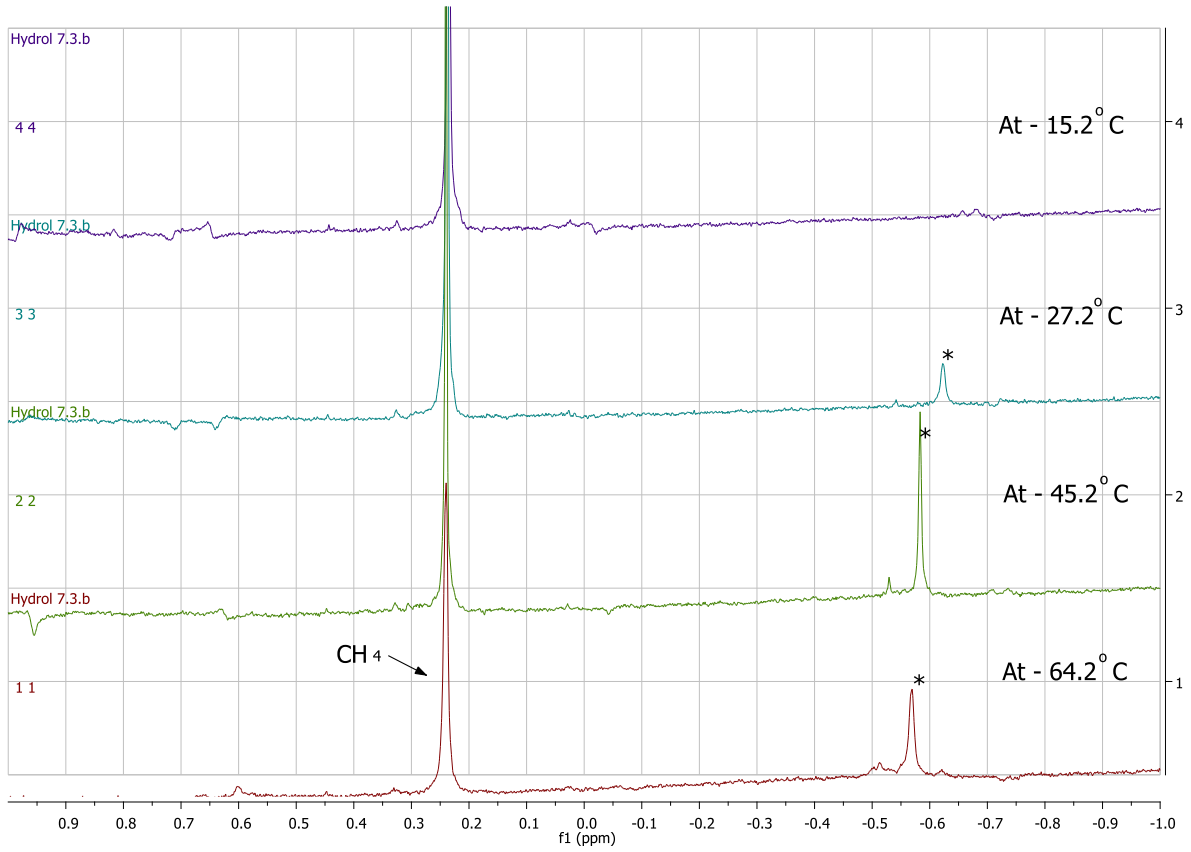

Figure 2.9: ^{1}H NMR spectra of the hydrolysis reaction 7.3 (Al/H_2O = 1.2/1): –64.2 °C (bottom spectrum), –45.2 °C, –27.2 °C and –15.2 °C.

Table 2.2: Initial conditions and quantitative data for reactions 7.1, 7.2 and 7.3

Reaction	H_2O (µmol)	TMA_{init} (µmol)	$CH_{4\ (max)}$ (µmol)	$TMA_{unreact}$ (µmol)	$Me_2Al(OMe)$ (µmol)
7.1	6.9	15.7	13.9	-	0.3
7.2	8.9	31.3	13.8	22.6	0.8
7.3	7	8.7	7.6	-	-

2.2.4.3 VT ^{1}H NMR Experiments in Toluene: Approach B

In an attempt to look at the quantitative results of the hydrolysis reaction of TMA in toluene from another aspect, the hydrolysis reaction of TMA was studied by adding first the TMA solution in toluene into the NMR tube in order to quantify the amount of methane that was initially present (before any water addition), followed by addition of a molecularly dispersed water solution in toluene. The initial TMA content was measured by integrating the peak that corresponds to the CH_3 protons of the TMA, using a longer pulse delay (d1=20 sec) in order to permit full relaxation of the methyl protons according to literature.[25] In this set of experiments excess of TMA was used in each case, due to volume limitations (addition of a relatively small volume of water/toluene mixture in order to maintain a low temperature inside the NMR tube and do not exceed the maximum permitted volume for the NMR measurements).

'Reaction 8.5': TMA/H_2O = 2.3/1

In the reaction 8.5, TMA was reacted with H_2O at an Al/H_2O ratio = 2.3 (15.4 μmol TMA, 6.7 μmol H_2O)

The background (TMA in toluene solution, before the addition of the water) was recorded at 16.2 °C, –7.4 °C, –25.4 °C, –54.2 °C and –84.9 °C, and the amount of methane present was evaluated by integration (Figure 2.10):

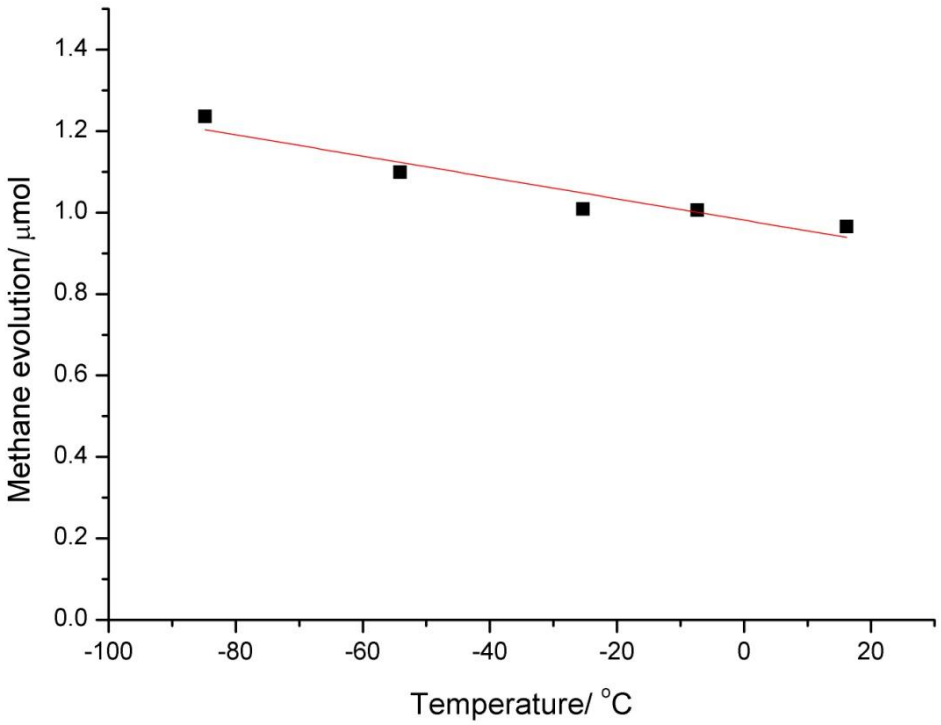

Figure 2.10: Methane background (16.2 °C, –7.4 °C, –25.4 °C, –54.2 °C, –84.9 °C)

After addition of the water/toluene mixture, the total CH_4 present at every temperature step rise was calculated by integration. The initial amount of CH_4 present at every temperature rise was calculated by applying a linear equation based on the measurements obtained for the background CH_4 (Figure 2.10). The actual amount of CH_4 produced during the reaction can be calculated by subtraction of the background CH_4 from the total amount (see Table 2.3 and Figure 2.11).

Table 2.3: Methane evolution at every temperature step of the hydrolysis reaction

T (°C)	CH_4 (total) µmol	CH_4 (background) µmol	CH_4 produced µmol
–74	2.5	1.2	1.4
–65	2.6	1.2	1.4
–54	2.9	1.1	1.8
–43.4	3.1	1.1	2.0
–34.4	3.6	1.1	2.5
–26.2	3.5	1.1	2.5
–16.4	3.8	1.0	2.8
–7.4	3.8	1.0	2.8
3.5	4.0	1.0	3.0
14.4	3.8	1.0	2.8
23.4	3.8	0.9	2.9

*produced CH_4 = CH_4 obtained by integration (total) – initial CH_4

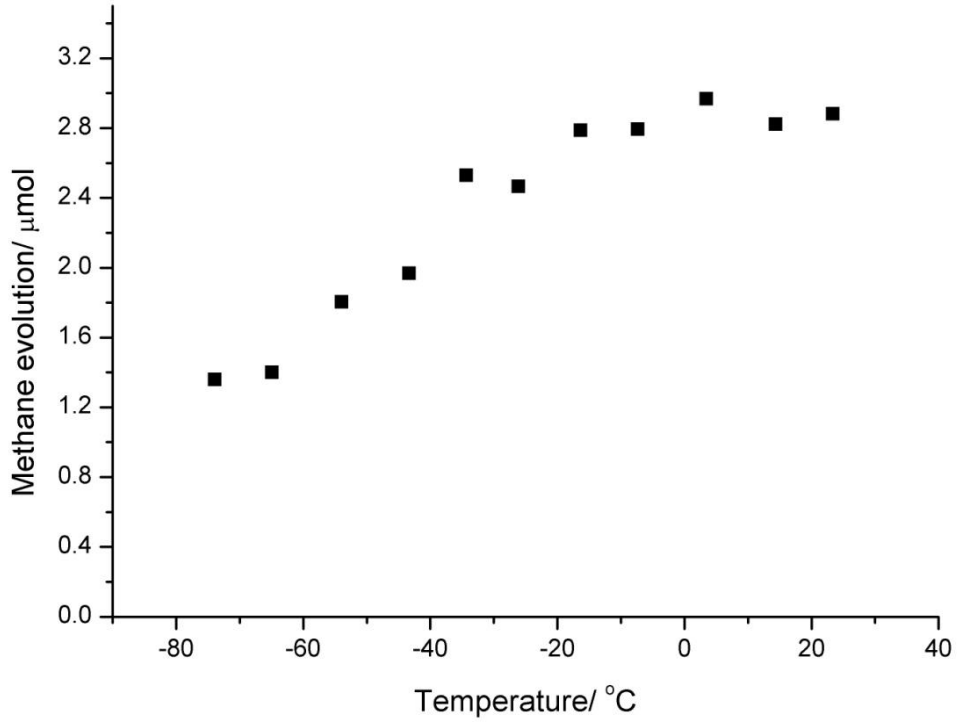

Figure 2.11: Methane evolution during the hydrolysis reaction

The maximum amount of CH_4 was produced at 3.5 °C (3.0 μmol), a value which is smaller than the expected; if the initial amount of H_2O (6.7 μmol) had reacted at 1/1 ratio with TMA, then 6.7 μmol of CH_4 would have been produced. Of course, a significant amount of CH_4 might have escaped to the gas phase. At 23.4 °C, 7.0 μmol of TMA remain unreacted, and 0.4 μmol of Me_2AlOMe are present (see Table 2.3).

Table 2.4 summarizes the main quantitative data and initial conditions of the reaction 8.5. It also includes the main quantitative data and initial conditions of the reaction 8.4 where an Al/H_2O ratio of 9.7/1 was employed (14.6 μmol of TMA were mixed with 1.5 μmol H_2O). A maximum amount of CH_4 was produced at −43.4 °C (1.9 μmol). Some CH_4 was lost as the temperature increased, but the amount of CH_4 started increasing again at 3.5 °C, reaching its maximum at 12.5 °C (2.0 μmol). At 23.4 °C, 7.2 μmol of TMA and 1.6 μmol of Me_2AlOMe

are present. The VT ^{1}H NMR spectra of these reactions were quite similar to the ones obtained for reaction 7.2 (see Figure 2.8), where an excess TMA was also used.

Table 2.4: Initial conditions and quantitative data for reactions 8.5 and 8.4

Reaction	H_2O (µmol)	TMA_{init} (µmol)	$CH_{4\ (max)}$ (µmol)	$TMA_{unreact}$ (µmol)	$Me_2Al(OMe)$ (µmol)
8.4	1.5	14.6	2.0	7.2	1.6
8.5	6.7	15.4	3.0	7.0	0.4

It was hard to obtain accurate quantitative data during the experiments. Toluene is a very poor mixing agent, which makes mixing the reagents difficult. Sufficient mixing is made harder by using an NMR tube as the mixing vessel. Cooling down the solutions to just above their melting points can also affect the solubility of water in toluene (lower solubility at lower temperatures) which can cause inaccuracies in determining the amount of water that has reacted. Varying the Al/H_2O ratio can influence the continuation of the reaction and the nature of the composition of the intermediates and reaction products.

Moreover, not the whole amount of methane produced during the reaction is detectable by NMR since some of it will escape to the gas phase.

Finally, shimming problems were observed in low temperatures because the NMR tube was already cooled down to very low temperatures before insertion to the instrument, so moisture was condensing on its surface. Properly drying the NMR tube was not possible since the temperature would have been increased.

Because of all these ambiguous results and technical difficulties a different solvent was employed, in order to prove that the general idea behind this method, the handling of the compounds and performing the necessary measurements were correct.

2.2.4.4 VT ^{1}H NMR Experiments in THF

Addition of a base like THF to TMA causes the dimeric TMA to break to monomeric TMA bonded to a THF molecule, according to the equilibrium:[25]

$$(AlMe_3)_2 + 2\ THF \rightleftharpoons 2\ (THF \bullet AlMe_3) \qquad (2.10)$$

Table 2.5: Initial conditions and quantitative data for reactions 9.8 and 9.7

Reaction		Initial TMA (µmol)	Initial H_2O (µmol)	Max. Me_2AlOH produced (µmol)
9.8	**Al/H_2O=1/1**	62	61	55.1
9.7	**Al/H_2O=2/1**	58	29	17.7

'Reaction 9.8' Al/ H_2O = 1/1

The Me signal of TMA complexed with THF appears at δ –0.65 at –84.9 °C and shifts slightly downfield as the temperature increases (δ –0.62 at 23.4 °C). The H_2O signal in THF appears at δ 3.79 at –75 °C and shifts upfield as the temperature increases (δ 2.83 at 23.4 °C).

Studying the hydrolysis reaction of TMA in THF by ^{1}H VT NMR shows a two step reaction. The formation of the $AlMe_3$*H_2O adduct (I) is the first step of the reaction, and it is observed at –84.9 °C. The resonances at δ –0.72 and 9.11 (see Figure 2.12 and 2.13) are attributed to the Me protons of TMA and H_2O protons respectively with a ratio of $(CH_3)_3/OH_2$ = 11.2/2, relatively higher than the theoretical value (9/2). The resonance of the protons of complexed H_2O (δ 9.11) with $AlMe_3$ has a great difference compared to the resonance of uncomplexed H_2O (δ 3.79). The signal of the protons of the complexed H_2O shifts upfield as the temperature increases (δ 8.57 at –43.4 °C), while the signal of the Me protons of TMA shifts slightly downfield (δ –0.68 at –43.4 °C). The signals attributed to the $AlMe_3$*H_2O adduct (at δ –0.72 and 9.11) decrease as the temperature increases. The H_2O signal is not obvious anymore at –25.4 °C, while the Me signal is significantly reduced. Trace of the Me signal is present at higher temperatures, but it disappears completely at 23.4 °C. This trace though could also perhaps be due to some unreacted TMA (since at 16.2 °C the

resonance of the peak is at δ –0.62 in THF, comparable to the resonance of the TMA complexed with THF at this temperature).

At –43.4 °C three new peaks have appeared at δ 7.54, 0.54 and –0.60 (see Figures 2.12 and 2.13) which are attributed to the product of the second step of the reaction which is the Me_2AlOH (II) and evolution of CH_4 (see Scheme 2.4). The signals at –0.60 and 7.54 are attributed to the Me and –OH protons of Me_2AlOH with a ratio of $(CH_3)_2$/OH = 6.4/1 close to the expected theoretical ratio (6/1). The two signals start to increase as the temperature increases. The peak attributed to the –OH protons shifts upfield with increasing temperature (δ 7.13 at 23.4 °C), while the peak attributed to the Me protons shifts only very slightly (δ –0.59 at 23.4 °C). A trace of Me_2AlOH is already present at –84.9 °C, but it becomes more obvious at –54.2 °C.

The Me_2AlOH should stabilize in its dimeric form (III). This exchange between II and III might explain the distortion of the OH signal at –25.4 °C due to rapid proton exchange. The third peak is attributed to CH_4, which is in agreement with the formation of Me_2AlOH. The identification of the signal is supported by addition of CF_3COOH in a TMA in THF solution in an NMR tube, followed by recording the ^1H NMR spectrum at R.T.

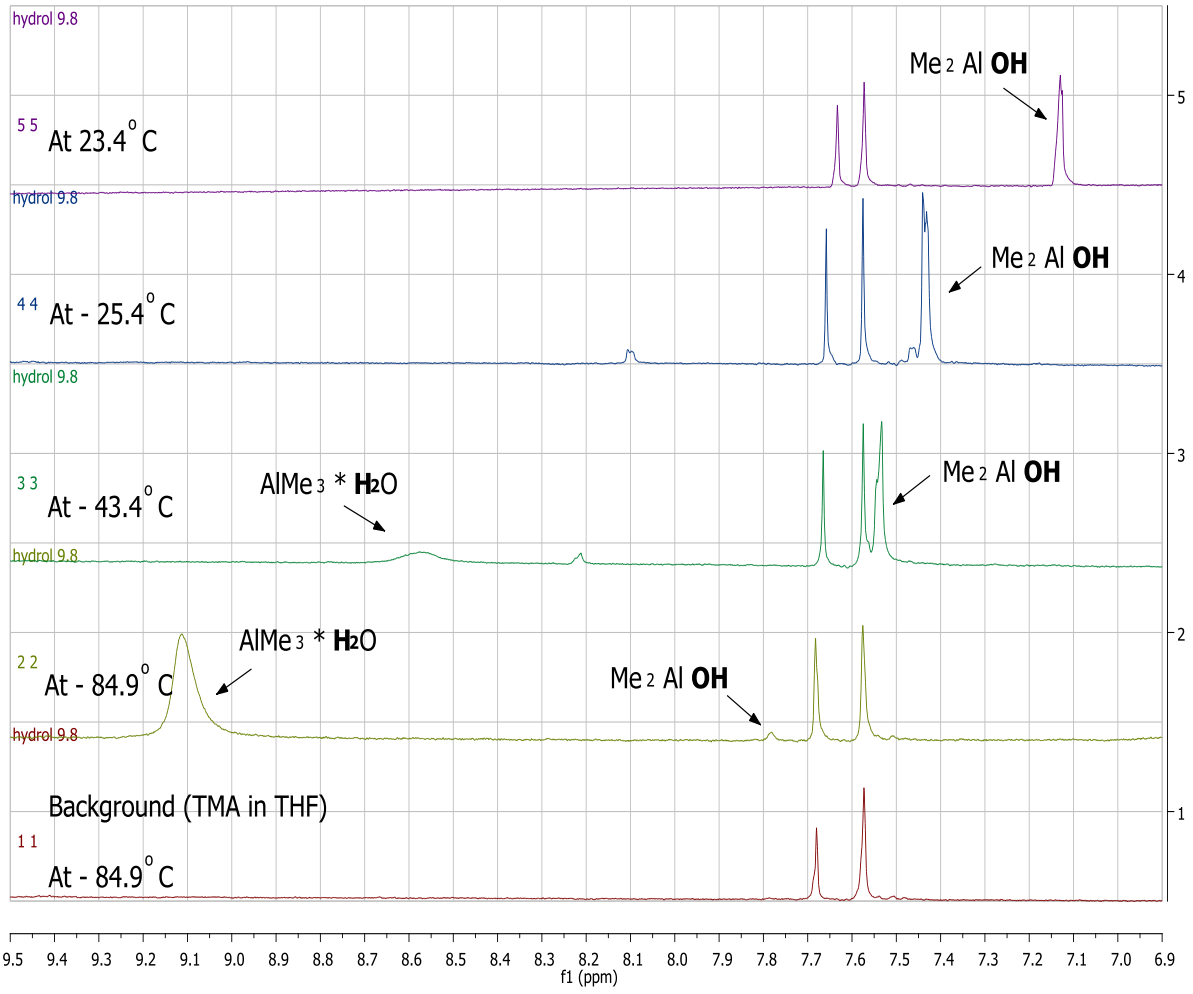

Figure 2.12: ^{1}H NMR spectra of the hydrolysis reaction 9.8 (region between 9.5 and 6.9 ppm). Background of TMA in THF at –84.9 °C (bottom spectrum), after addition of H_2O/THF at –84.9 °C, –43.4 °C, –25.4 °C and 23.4 °C.

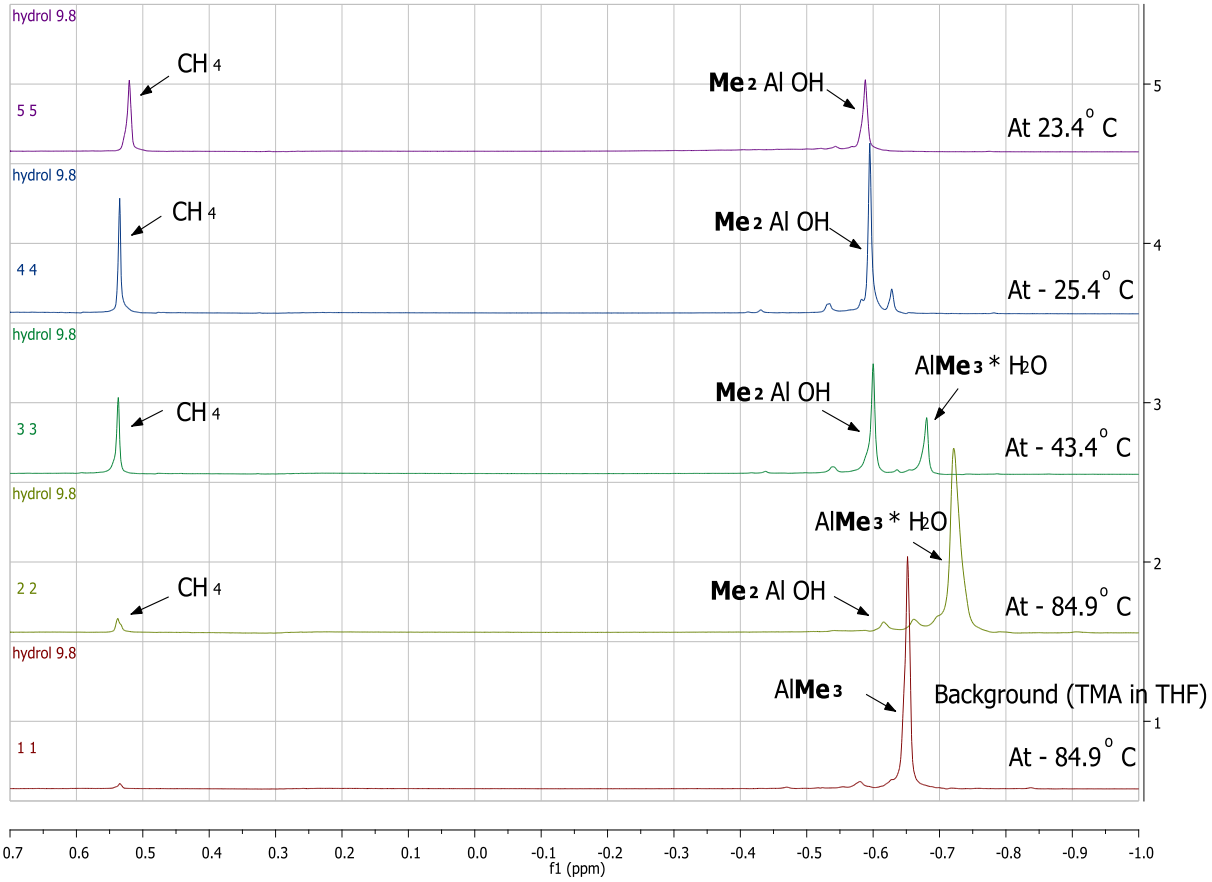

Figure 2.13: ^{1}H NMR spectra of the hydrolysis reaction 9.8 (region between 0.7 and –1.0 ppm). Background of TMA in THF at –84.9 °C (bottom spectrum), after addition of H_2O/THF at –84.9 °C, –43.4 °C, –25.4 °C and 23.4 °C.

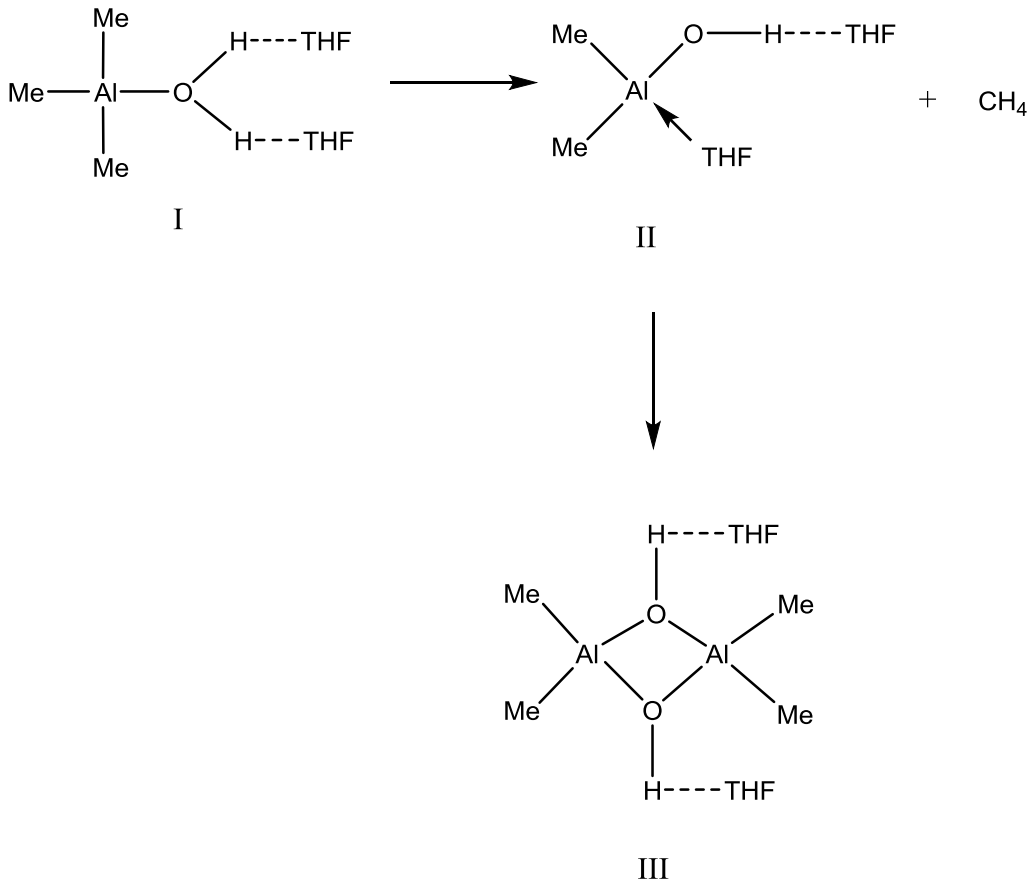

Scheme 2.4: Possible intermediates and products of the hydrolysis reaction of TMA in THF

Me_2AlOH starts reducing above –25.4 °C but the signal is still present at R.T. The noticeably stability of the product could be explained by the impact of the THF complexation. Complexation with THF would also attribute to the stability of the $AlMe_3*H_2O$ adduct. Hydrogen bonds between the –OH protons and THF and water protons and THF stabilize the intermediates.

The reduction of the signals attributed to the Me_2AlOH is not accompanied by the formation of a new product, such as $Me_2AlOAlMe_2$. This could be explained by the low selectivity of the whole reaction because of the parallel reactions of Me_2AlOH itself. As it has been reported in literature,[17] a similar study of the hydrolysis of alkylaluminium compounds in Et_2O, did not manage to observe the formation of $Me_2AlOAlMe_2$ compounds during Me_3Al hydrolysis.

As in Approach B, of the hydrolysis reaction of TMA in toluene, after addition of the water/toluene mixture, the total CH_4 present at every temperature step rise was

calculated by integration. The initial amount of CH_4 present at every temperature rise was calculated by applying a linear equation based on the measurements obtained for the background CH_4 (the background of the TMA sample used in this experiment was recorded at five different temperatures, and the amount of CH_4 already present in the sample was calculated by integration). The actual amount of CH_4 produced during the reaction was calculated by subtraction of the background CH_4 from the total amount (see Table 2.6 and Figure 2.14).

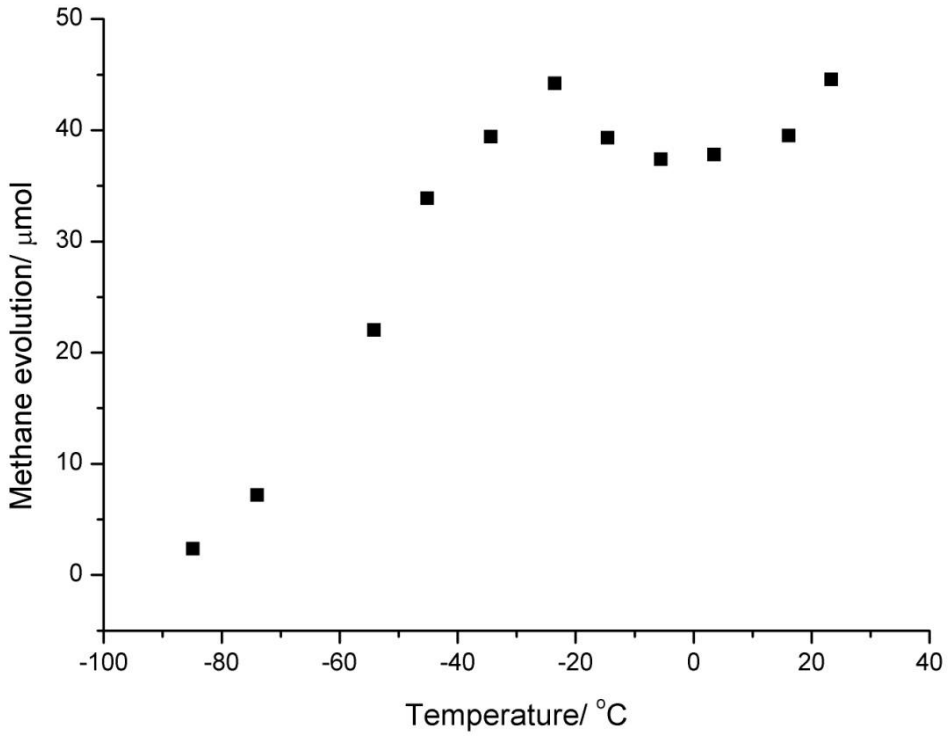

Figure 2.14: Methane evolution with increasing temperature, reaction 9.8

The initial amount of TMA (62.0 μmol) was almost all converted to the $AlMe_3*H_2O$ (57.9 μmol) adduct at −84.9 °C after addition of H_2O (based on the integration of the Me signal of TMA). Integration of the H_2O signal corresponds to a relatively lower amount (46.2 μmol). However, integration of the Me signal is a more reliable measurement since the H_2O signal is very broad. The small trace of Me_2AlOH present at this temperature according to the integration of its Me signal corresponds to production of 3.7 μmol, and it is accompanied by evolution of 2.4 μmol of CH_4. The amount of Me_2AlOH increases slowly to 6.9 μmol at

–74 °C (CH_4 evolution = 7.2 μmol, meaning an almost 1/1 ratio of Me_2AlOH/CH_4 as it would have been expected). A big increase on Me_2AlOH production is observed at –54.2 °C (21.5 μmol, which is in agreement with the 22 μmol of CH_4 present at this temperature). The maximum amount of Me_2AlOH (55.1 μmol, based on the integration of the Me signal) is produced at –14.6 °C. The amount of Me_2AlOH calculated by integration of the Me signal is quite close to the amount calculated based on the OH signal (50.2 μmol). The amount of CH_4 present at this temperature (39.3 μmol) is lower than a 1/1 ratio of Al/CH_4, but this is possibly due to loss of CH_4 in the gas phase. Loss of CH_4 in the gas phase is proved by the reduction of CH_4 from –25.4 °C (local maximum, 42.3 μmol) to –14.6 °C (39.3 μmol) (see Table 2.6).

The amount of CH_4 starts increasing again at 3.4 °C, and reaches a maximum (44.6 μmol) at 23.4 °C. Although, this increase of CH_4 is not accompanied by increase of Me_2AlOH (Me_2AlOH is actually reducing above –14.6 °C) nor accompanied by the appearance of another product. This would perhaps mean that if the dimethylyaluminium hydroxides have formed dimers or higher alkylaluminiums could eliminate one OH group accompanied by CH_4 evolution. It is hard to know the exact amount of CH_4 produced since there is a loss in the gas phase. Any unreacted or complexed with H_2O TMA could have also been converted to Me_2AlOH at higher temperatures, and cause a small increase on CH_4.

Table 2.6: Intermediates and reaction products of reaction 9.8

T (°C)	**CH_4 (μmol)**	**$(CH_3)_3$ (μmol)**	**OH_2 (μmol)**	**$(CH_3)_3/OH_2$**	**$(CH_3)_2$ (μmol)**	**OH (μmol)**	**$(CH_3)_2/OH$**
–84.9	2.4	57.9	46.2	5.6/1	3.7	*	
–74	7.2	56.3	43.6	5.8/1	6.9	*	
–54.2	22.0	35.5	*		21.5	*	
–25.4	42.3	4.2	*		53.9	50.2	6.4/1
–14.6	39.3	3.2	*		55.1	52.3	6.3/1
23.4	44.6	-	-	-	37.4	33.6	6.68/1

*These peaks were not obvious or were unreliable for integration (very small or broad signals)

'Reaction 9.7' Al/ H_2O = 2/1

In these systems the reaction proceeds in a similar way as described for the 1:1 system.

The first intermediate is the TMA-water complex at the lowest temperature (–84.9 °C). Although, as it can be seen in Figure 2.15, there is a downfield shift of the Me signal of the $AlMe_3$*H_2O adduct (δ –0.67) compared to the reaction 9.8 (δ –0.72) where the Al/H_2O ratio was 1/1. This difference could be due to an exchange between free TMA (since there is an excess) and TMA complexed with H_2O. This could be supported by the fact that integration of the Me signal results in 58.0 μmol of TMA (equal to the initial amount of TMA inserted), but integration of the H_2O signal results to just 14.6 μmol. Even though the H_2O signal might not be the most reliable peak for integration due to the nature of the signal, it clearly shows that there is a big difference when comparing the two values, meaning that the Me signal is a combination of the $AlMe_3$*H_2O adduct and the excess TMA. As in reaction 7.8, the H_2O signal is not obvious at –25.4 °C or higher temperatures (see Figures 2.16 and 2.17).

A trace of Me_2AlOH is obvious at –74 °C (Me at δ –0.61), while the OH signal is visible at –65 °C (at δ 7.61). The maximum amount of Me_2AlOH produced is observed at –5.6 °C, and is equal to 17.7 μmol according to the integration of the Me signal (which is in good agreement with the amount calculated by the integration of the OH signal = 17.8 μmol). Me_2AlOH starts reducing at higher temperatures, but it is still present at 23.4 °C (9.6 μmol).

A maximum amount of CH_4 is observed at –25.4 °C (18.8 μmol), and then it reduces slightly. It starts increasing at 3.4 °C, reaching its maximum at 23.4 °C (18.9 μmol). The production of CH_4 at –25.4 °C is in good agreement with the production of Me_2AlOH (ratio of CH_4/ Me_2AlOH = 1.1).

However, it was observed that even when excess of TMA was employed the low selectivity of the reaction does not allow it to proceed to Me_2Al-O-$AlMe_2$ formation. The excess of TMA coordinates with the THF molecules, and remained unreacted (22.9 μmol at 23.4 °C).

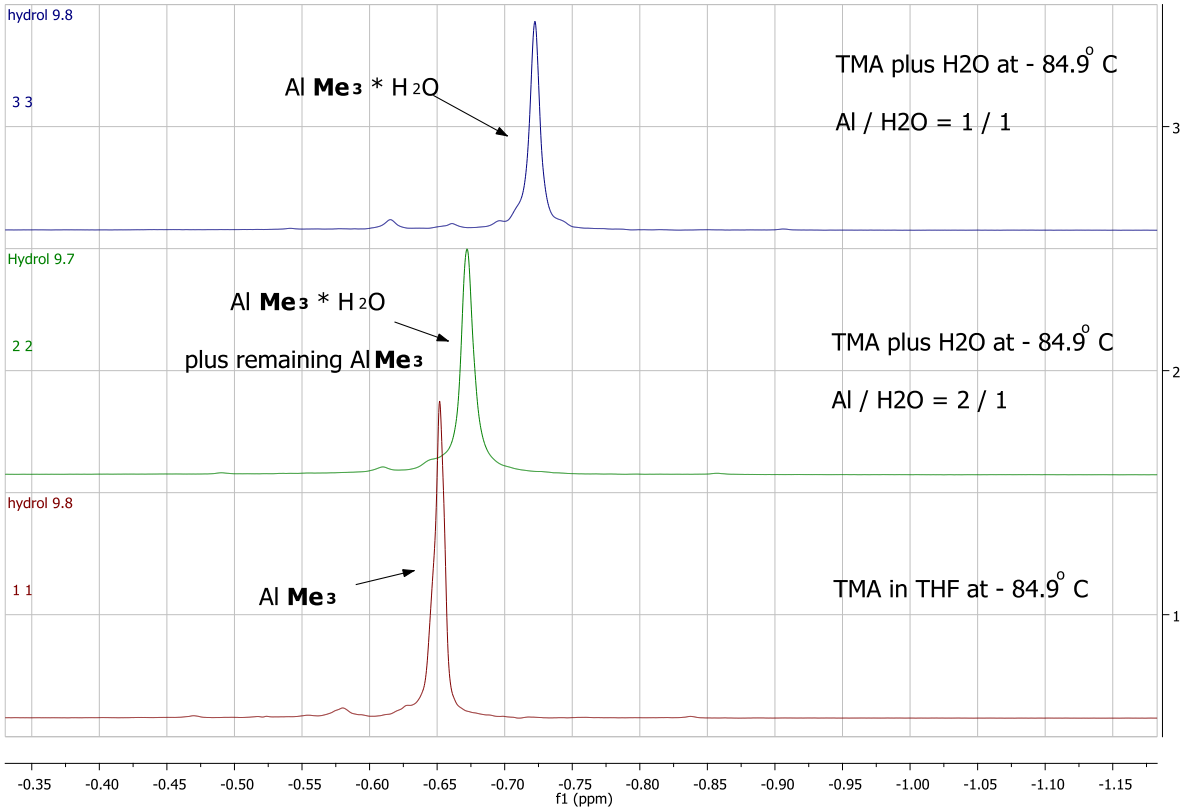

Figure 2.15: The difference of the chemical shift of the $AlMe_3*H_2O$ adduct when excess TMA is used.

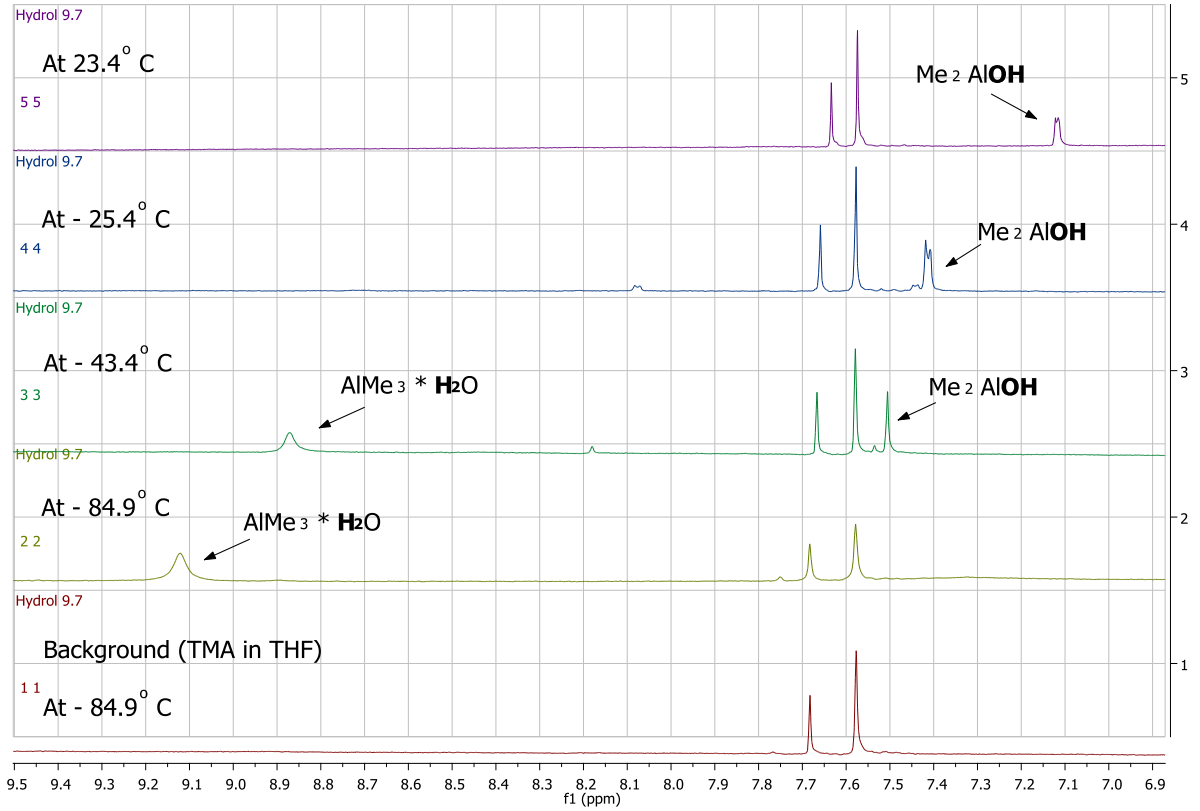

Figure 2.16: ^{1}H NMR spectra of the hydrolysis reaction 9.7 (region between 9.5 and 6.9 ppm). Background of TMA in THF at –84.9 °C (bottom spectrum), after addition of H_2O/THF at –84.9 °C, –43.4 °C, –25.4 °C and 23.4 °C.

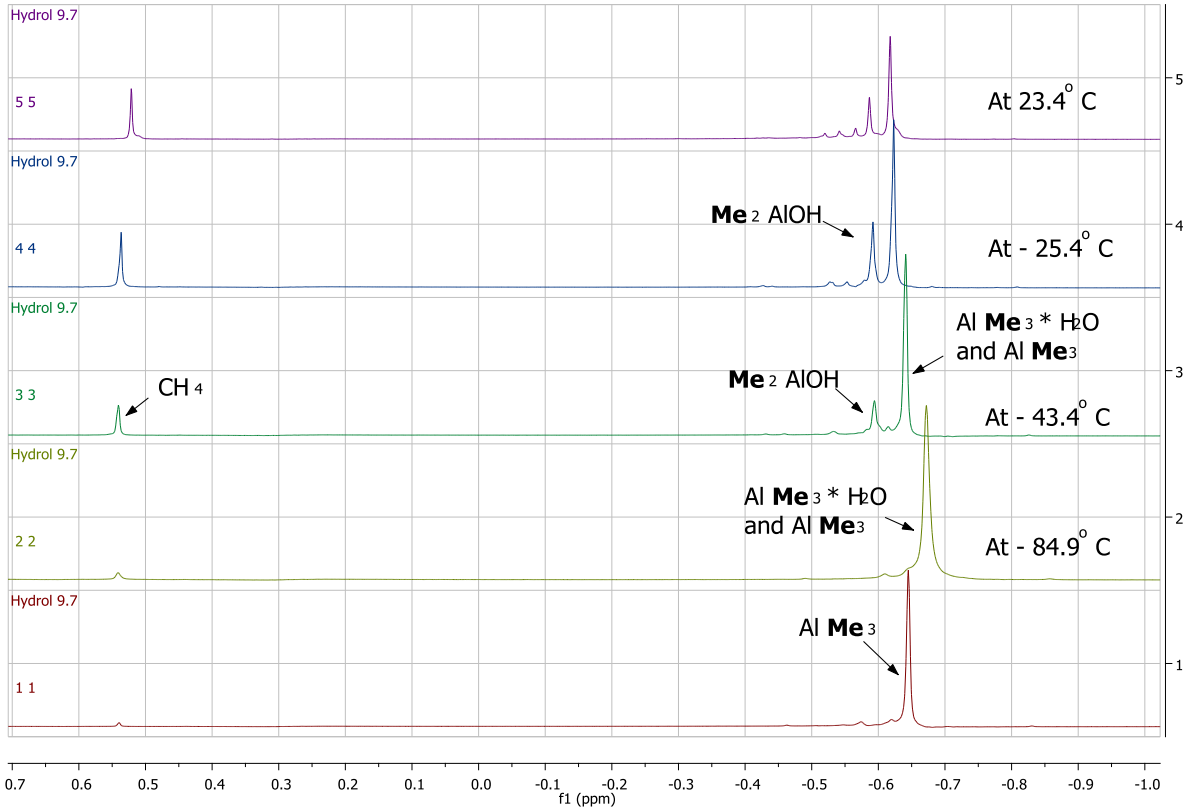

Figure 2.17: ^{1}H NMR spectra of the hydrolysis reaction 9.7 (region between 0.7 and -1.0 ppm). Background of TMA in THF at –84.9 °C (bottom spectrum), after addition of H_2O/THF at –84.9 °C, –43.4 °C, –25.4 °C and 23.4 °C.

2.3 Conclusions

The extremely low solubility of water in toluene has a crucial restrictive role in the concentration of the reagents in each experiment. Additionally, the solubility of water will undoubtedly be affected by cooling the water in toluene solution down to such low temperatures. Consequently, it could be the case that the originally molecularly dispersed water (at room temperature) will form bulk water (which could explain the full hydrolysis of TMA). Kirschenbaum and Ruekberg[30] investigated the relationship between the solubility of water in various hydrocarbons and temperature, and related it to the vapour pressure of water at those temperatures.

Working with such limited concentrations and a highly reactive compound like TMA has several disadvantages. Contamination with oxygen was impossible to avoid, and oxidation products were detected. Additionally, being unable to know the exact amount of water consumed for the formation of the alkylaluminium species that were detected in very small quantities made impossimble to determine the Al/H_2O ratio and correlate it with a reaction path. Furthermore, identification of certain peaks by NMR is very difficult since some small peaks corresponding to the water protons of the water adduct or the –OH protons of the dimethylaluminium hydroxide, both possible intermediates, are not detectable. Thus, assigning the peaks which correspond to the methyl protons of possible intermediates or impurities is very ambiguous. We could probably assume that Me_2AlOH does form, but it reacts further even at low temperatures.

When the reaction medium was changed to THF, it was proven that the method employed in this research was successful in identifying the initial products of the reaction of TMA with H_2O. Complexation with THF decreases the reaction rate and allows observation of the initial products of the reaction by ^1H VT NMR. Useful quantitative data were also collected by monitoring the hydrolysis reaction by ^1H VT NMR using an internal standard for quantification of the reactants and products at every temperature step.

The $AlMe_3*H_2O$ adduct was identified as the first intermediate of the hydrolysis reaction, and the difference between the chemical shift of the H_2O protons complexed (about 9.1 ppm) by TMA and that for uncomplexed H_2O (about 3.2 ppm) was observed.

The Me_2AlOH seems to be the main product of the partial hydrolysis of TMA in THF and it is relatively stable even at R.T. There is a reduction of Me_2AlOH as the temperature increases which is not accompanied by the appearance of other products. There were no signs indicating that the reaction proceeded further, producing $Me_2AlOAlMe_2$.

2.4 Experimental

2.4.1 General Procedures and Materials

All manipulations were conducted using standard Schlenk techniques under argon. All reagents were used as purchased without further purification unless otherwise stated. Trimethylaluminium (TMA) was provided by Chemtura Europe Ltd.

Solvents were dried over Na/benzophenone (tetrahydrofuran) or sodium (toluene) before use and purged with argon. The deuterated NMR solvents (CD_2Cl_2, C_6D_6, toluene-d8) were degassed by several freeze-thaw cycles and dried over activated 4 Å molecular sieves.

NMR spectra were recorded on a Bruker DPX-300 spectrometer operating at 300.13 MHz, 16 scans with a relaxation time (D1) of 1-20 sec. NMR chemical shifts were referenced to CD_2Cl_2 (in a capillary) which was used as the external standard. 1,3,5-Tri-*tert*-butylbenzene was used as an internal standard. Phasing was performed automatically while integration was performed manually. Shimming was necessary in every temperature in the VT NMR experiments.

2.4.2 Determination of the Solubility of Water in Toluene by Quantitative NMR

Purified toluene was mixed with distilled water in a separating funnel. The mixture was left to rest overnight. The next day the water (bottom) phase was removed and a sample was taken via a 1 mL gastight Hamilton syringe from the centre of the solvent phase. All the experiments were carried out at room temperature.

1,3,5-Tri-*tert*-butylbenzene was chosen as the most appropriate standard to use for these measurements and it was further purified by recrystalization. ^{1}H NMR spectrum were recorded in C_6D_6 for 1,3,5-tri-*tert*-butylbenzene (97%) ^{1}H NMR: δ 7.44 (s, 3H, C_6H_3), 1.34 (s, 27H, $-C(CH_3)_3$)

Several NMR tests were carried out in order to estimate the amount of 1,3,5-Tri-*tert*-butylbenzene that was needed to minimize the integration error. The optimal concentrations finally used for the determination of the solubility of water in toluene were the following: 0.2 mL of an aliquot of 1,3,5-tri-*tert*-butylbenzene in toluene (10.8 mg of 1,3,5-tri-tert-butylbenzene in 5 mL of toluene) and 0.4 mL of the toluene solution saturated with water

were added in the NMR tube and mixed. A minimal amount of C_6D_6 (0.1 mL) was also added as the NMR standard (for locking).

2.4.3 Non-Molecularly Dispersed Water

A droplet of water was added in toluene-d8 (0.5 mL), in the NMR tube, and the ^{1}H NMR spectrum was recorded. The^{1}H NMR spectrum of toluene-d8 was also recorded prior to water addition. Due to the presence of small impurities (humidity, grease) toluene-d8 was further purified by trap-to-trap distillation.

2.4.4 VT NMR Studies on the Hydrolysis Reaction of Trimethylaluminium

a. Toluene as a solvent

In order to study the reaction of TMA and water in toluene two approaches were followed.

In the 1st set of experiments (approach A), a known amount of molecularly dispersed water (6.9, 8.9 and 7 μmol for reactions 7.1, 7.2 and 7.3 respectively) in toluene (0.5 mL) was added to the NMR tube with an internal standard (1,3,5 tri-*tert*-butylbenzene, 1.3 μmol), and the ^{1}H NMR spectrum was recorded. Then, the system was cooled down slowly to −85 °C. ^{1}H NMR spectra were recorded in every 10 °C step to investigate the behaviour of water at lower temperatures. When the NMR tube was ejected from the NMR probe, it was cooled down to −116 °C using an ethanol/liquid nitrogen cooling bath. At this temperature, a known amount of TMA in toluene solution (15.6, 31.3 and 8.7 μmol of TMA in 45, 90 and 25 μL of toluene, respectively, for reactions 7.1, 7.2 and 7.3) was added via a high precision gas tight Hamilton syringe to the NMR tube with the H_2O/toluene (the TMA/toluene solution was pre-cooled to −75 °C before transferring) and the two reagents were mixed just above the melting point of toluene by shaking the NMR tube. The NMR tube was inserted into the pre-cooled

probe (–85 °C), and the NMR spectrum was recorded. Each subsequent NMR recording was preceded by a 10 °C temperature rise.

In the 2nd set of experiments (approach B), a known amount of TMA (14.6 and 15.4 μmol for reactions 8.4 and 8.5 respectively) TMA in toluene solution (0.5 mL) was added to the NMR tube with the internal standard (1,3,5 tri-*tert*-butylbenzene, 1.3 μmol) and the ^{1}H NMR spectrum was recorded between –85 °C to 25 °C. Then, the NMR tube was cooled down to –116 °C using an ethanol/liquid nitrogen cooling bath. At this temperature, a known amount of molecularly dispersed water in toluene (1.5 μmol H_2O in 50 μL and 6.7 μmol H_2O in 0.22 mL for reactions 8.4 and 8.5 respectively) was added and the two reagents were mixed just above the melting point of toluene by shaking the NMR tube. The NMR tube was inserted into the NMR probe, which was pre-cooled to –85 °C, and the NMR spectrum was recorded. Each subsequent NMR recording was preceded by a 10 °C temperature rise.

A stock solution of molecularly dispersed water in toluene was prepared by addition of H_2O (0.6 μmol) to toluene (20 mL) and stirring overnight.

b. THF as a solvent

The hydrolysis reaction of TMA was also investigated in tetrahydrofuran (THF).

The procedure detailed in approach B was followed for the THF experiments, with the exception of higher water and TMA concentrations in THF (62 and 58 μmol TMA in 0.5 mL THF in reactions 9.8 and 9.7, respectively, and 61 and 29 μmol H_2O in 0.1 mL THF in reactions 9.8 and 9.7, respectively), because water and THF are miscible. A background ^{1}H NMR spectrum was recorded between –85 °C to 25 °C (one in every 10 °C step) for a TMA in THF solution and a H_2O on THF solution.

2.4.5 Additional Experiments

i. A stock solution of TMA (1.5 mmol, 0.15 mL) in toluene (5 mL) was prepared. 0.5 mL of the solution (0.15 mmol Al) were transferred to an NMR tube and MeOH (0.15 mmol, 6 μL) were added. After shaking the NMR tube, a ^{1}H NMR spectrum was recorded.

ii. TMA (4.75 mmol, 0.46 mL) was mixed with toluene (4.5 mL). The solution was cooled down to −78 °C with a dry-ice/acetone bath. H_2O (4.75 mmol, 0.11 mL) was added to toluene (5 mL) , the mixture was stirred rapidly and after 30 min it was transferred dropwise

via cannula to the TMA/toluene solution. The mixture was allowed to reach R.T. and an NMR sample was taken for analysis after 1 hour.[29]

After the NMR sample was taken, pure O_2 gas was bubbled for 30 min through the mixture and then another NMR sample was taken.

The above experiment was repeated for a lower TMA concentration (0.95 mmol TMA, 0.95 mmol H_2O, 10 mL toluene).

iii. 0.5 mL of a stock solution of TMA (1.5 mmol, 0.15 mL) in toluene (5 mL) were transferred to an NMR tube. Two drops of CF_3COOH were added to the NMR tube. Fuming was observed. After shaking the NMR tube, a ^1H NMR spectrum was recorded. The NMR probe was gradually cooled down to –85 °C, and a ^1H NMR spectrum was recorded in every 10 °C step.

iv. The procedure described in (iii) was repeated in THF instead of toluene.

References

1. J. N. Pédeutour, K. Radhakrishnan, H. Cramail, A. Deffieux, *Macromol. Rapid Commun.*, **2001**, *22*, 1095.
2. S. Pasynkiewicz, *Polyhedron,* **1990**, *9*, 2/3, 429.
3. J. R. Severn, In *Tailor-Made Polymers. Via Immobilization of Alpha-Olefin Polymerization Catalysts*, Wiley-VCH, Weinheim, Germany, 2008, p 95
4. S. S. Reddy, S. Sivaram, *Prog. Polym. Sci.*, **1995**, *20*, 309.
5. G. B. Sakharovskaya, N. N. Koreneev, A. F. Popov, E. J. Larikov, A. F. Zhigach, *Zh. Obshch. Khim*., **1964**, *34*, 3435.
6. M. Boleslawski, S. Pasynkiewicz, *J. Organomet. Chem*., **1972**, *43*, 81.
7. A. Storr, K. Jones, A. W. Laubengayer, *J. Am. Chem. Soc.*, **1968**, *90*, 3173.
8. H. Sinn, J. Bliemeister, D. Clausnitzer, L. Tikwe, H. Winter, O. Zarncke, *Transition Metal and Organometallics as Catalysts for Olefin Polymerization* (H. Sinn and W. Kaminsky Eds.), Springer, New York,1987.
9. H. Winter, W. Schnuchel, H. Sinn, *Macromol. Symp.*, **1995**, *97*, 119.
10. E. Giannetti, G. M. Nicoletti, R. Mazzocchi, *J. Polym. Sci.: Polym. Chem. Ed*., **1985**, *23*, 2117.

11. W. Kaminsky, H. Haehnsen, US Pat. Appl. 4544762 (A), (1985, Hoechst AG)
12. G. M. Smith, S. W. Palmaka, J. S. Rogers, D. B. Malpass, US Pat. Appl. 5831109 (1998, Akzo Nobel).
13. T. Dalet, H. Cramail, A. Deffieux, *Macromol. Chem. Phys*., **2004**, *205*, 1394.
14. Y. V. Kissin, US Pat. Appl. 5258475 (1993, Mobil Oil Corp.).
15. R. L. Geerts, T. G. Hill, US Pat. Appl. 5414180 (1993, Phillips Petroleum Company).
16. W. C. Welborn, EP 0348126 A2 (1993, Exxon Chemical Patent Inc.)
17. M. Boleslawski, J. Serwatowski, *J. Organomet. Chem*., **1983**, *255*, 269.
18. S. Pasynkiewicz, A. Sadownik, A. Kunicki, *J. Organomet. Chem*., **1977**, *124*, 265.
19. S. Amdurski, C. Eden, H. Feilchenfeld, *J. Inorg. Nucl. Chem.*, **1961**, *23*, 133.
20. M. R. Mason, J. M. Smith, S. G. Bott, A. R. Barron, *J. Am. Chem. Soc*., **1993**, *115*, 4971.
21. C. J. Harlan, M. R. Mason, A. R. Barron, *Organometallics*, **1994**, *13*, 2957.
22. F. Malz, H. Jancke, *J. Pharmaceut. Biomed.*, **2005**, *38*, 813.
23. T. Rundlöf, M. Mathiasson, S. Bekiroglu, B. Hakkarainen, T. Bowden, T. Arvidsson, *J. Pharmaceut. Biomed.*, **2010**, *52*, 645.
24. L. Resconi, S. Bossi, L. Abis, *Macromolecules*, **1990**, *23*, 4489.
25. D. W. Imhoff, L. S. Simeral, S. A. Sangokoya, J. H. Peel, *Organometallics*, **1998**, *17*, 1941.
26. K. Ramey, J. O' Brien, I. Hasegawa, A. Borchert, *J. Phys. Chem*., **1965**, *69*, 10, 3418.
27. D. E. Babushkin, N. V. Semikolenova, V. N. Panchenko, A. P. Sobolev, V. A. Zakharov, E. P. Talsi, *Macromol. Chem. Phys*., **1997**, *198*, 3845.
28. N. N. Korneev, I. M. Khrapova, A. V. Polonskii, N. I. Ivanova, A. V. Kisin, V. S. Kolesov, *Russ. Chem. Bull.*, **1993**, *42*, 8, 1390.
29. Z. Zhang, X. Duan, Y. Zheng, J. Wang, G. Tu, S. Hong, *J. Appl. Polym. Sci*., **2000**, *77*, 4, 890.
30. L. J. Kirschenbaum, B. Ruekberg, *Chem. Sci.*, **2013**: 9 pages, Article ID: CSJ-101.

Chapter 3

Studies on the Initial Reaction Steps of the Hydrolysis of TMA by Matrix Isolation Infrared Technique

3.1 Introduction

3.1.1 Infrared Matrix Isolation Spectroscopy

This chapter focuses on another way to investigate the initial reaction steps and intermediates formed between water and TMA in order to gain an insight into the structural characteristics of MAO. The method used here is a combination of the matrix isolation technique with infrared spectroscopy.

Infrared (IR) spectroscopy is a useful tool for the characterization and identification of chemical compounds. IR spectroscopy on its own would not have been sufficient for the purpose of this study since the intermediates of the hydrolysis reaction of TMA are extremely reactive, so it would have been impossible to capture them to record their IR spectrum.

Additionally, the IR spectrum of most polyatomic compounds is complicated and hard to resolve, especially in the case of more than one compounds being present (which is possible when studying a reaction that might lead to the presence of the initial reactants along with the presence of more than one product). This happens because neighbouring molecules interact with each other when they are in a solid or liquid state causing perturbation of the vibrational transitions of the molecule and subsequently line broadening of the resonances of the vibrations and distortion of the fine details of the spectrum. The IR spectrum of compounds in the gas phase might not suffer from these neighbouring interactions, but usually suffers from the presence of many additional resonances due to their molecular rotations. The spectra of liquids also shows extra resonances due to rotational components.[1-5]

It was crucial to combine IR spectroscopy with another technique to overcome the above problems. The technique that fitted the profile best was the matrix isolation technique, since it has been proved to be a very effective tool for trapping unstable molecular species like free radicals, reactive intermediates or vaporizing molecules in an inert solid matrix. Matrix isolation can also achieve isolation of monomeric species of a compound that is usually dimeric or polymeric (e.g. by the Knudsen cell technique). As a consequence, the inert and rigid environment that surrounds the solute molecules reduces intermolecular

interactions and inhibits molecular rotations (with the exception of a few small molecules such as hydrogen halides, ammonia, water and methane), resulting in much sharper and narrower absorption bands which are easily identified.[1-2]

The main principle is that the molecules of the species of interest, which are often named as 'guest species' or 'trapped solute', are isolated in a large excess of a chemically inert material, 'matrix' or 'cage' material, by rapid condensation onto a spectroscopically transparent window (e.g. CsI) which is cooled to cryogenic temperatures. The inert material is usually an inert gas. Other materials have also been used but in general an appropriate matrix material should: have high levels of purity, not mask the absorption bands of the solute, not react with the solute, and it should provide a rigid matrix. The rigidity of the matrix prevents diffusion of the molecules at the chosen deposition temperature ensuring stabilization of the reactive species. Argon has been one of the most commonly used matrix materials, and it was also used in the present study.[1-2]

Argon's stable solid phase has a cubic close-packed structure, meaning that each sphere has 12 nearest neighbours and the unit cell is a face-centred cube (f.c.c.). A guest molecule in an argon lattice could replace a host molecule (substitutional site) or occupy an interstitial site. The vibrational levels of the solute are usually perturbed by the matrix resulting in a shift of their vibrational frequencies from their gas phase values. In some cases multiple bands appear due to rotation or libration of the solute in its trapping site, alternative trapping sites in the matrix or aggregation of the solute.[1-2]

The basic idea of this study was to co-deposit water and TMA, preferentially in its monomeric state, in an argon matrix and study the reaction intermediates. In order to do this, one method seemed appropriate: slow thermal annealing of the matrix up to a certain temperature that would soften the matrix and allow diffusion of the molecules and reaction with each other. It was anticipated that cooling the matrix to the lowest possible temperature would stabilize the intermediates formed and allow sufficient time to record the IR spectrum. Identification of the new species could have been possible through isotopic substitution experiments and vibrational analysis and correlation of the spectra.

3.1.2 Matrix Isolation Studies and Trimethylaluminium

The infrared spectrum of matrix-isolated trimethylaluminium has been investigated by Kvisle and Rytter; they reported the spectrum of a mixture of dimeric and monomeric TMA,[6] but they also managed to isolate purely monomeric TMA[6-7] by dissociation of the dimer at 300 °C using a Knudsen cell (deposition in argon at 12 K). Thermal annealing of the matrix led to dimerization of the monomeric TMA, and observation of intermediate species. The ratios of the monomeric, dimeric and intermediate species depended on the temperature and time of annealing. It was reported that the final matrix after annealing probably contained aggregates and crystallized dimers instead of matrix isolated dimers, and that methane slowly escaped the matrix during annealing.

Various research groups have worked on assigning the vibrational modes of TMA at ambient conditions using IR and Raman spectroscopy. These assignments correspond to the dimeric form of TMA with methyl bridges.[8-13] However, assigning the vibrational modes was quite complicated due to confusion between the skeletal stretching and the methyl rocking modes and the difficulty of distinguishing between the bridging and terminal methyl vibrations of d-TMA.[11] The calculations by Almenningen *et al.*[14] of the skeletal modes of the dimer are based on a D_{2h} symmetry, assuming that the bridging methyl groups have a C_{3v} symmetry and rotate freely and the terminal methyl groups are staggered with respect to the Al–C bonds radiating from the aluminium atoms.

The IR spectrum of the monomeric TMA was reported for the first time by Kvisle and Rytter.[6-7] O'Brien and Ozin[15] have reported a Raman gas phase spectrum; although their interpretation of data was only partly correct. In both cases, a D_{3h} symmetry was assumed as predicted by the gas phase electron diffraction study performed by Almenningen *et al.*[14] Almenningen *et al.* based their calculations on a model with freely rotating methyl groups; Kvisle and Rytter use the term 'torsional tunnelling' instead, as there is a very low rotational barrier (Almenningen estimated it to be less than 2 kcal/mol). However, Ogawa[11] presented a more complete vibrational analysis of the d-TMA molecule, assuming C_{2h} symmetry. C_{2h} or C_{2v} symmetries are possible if the methyl bridging groups are in fixed positions.

The assignment of the skeletal modes in Kvisle and Rytter's work was based on harmonic normal coordinate calculations using Wilson's GF matrix method[16] for both monomeric and dimeric TMA, assuming a trigonal D_{3h} planar configuration of the MC_3

skeleton for the monomer and the methyl group as the point of mass[14,17] and C_{2h} symmetry, following Ogawa's model theory, for the dimer using the same methyl point of masses.

More recently, Ault and Laboy[18] investigated the reaction of TMA with CH_3OH and H_2O by infrared matrix isolation. The reactants were diluted in argon and co-deposited onto the cryogenic surface. Two different matrix isolation systems were employed. In the first one called the 'twin jet system' the two reactants were diluted separately in argon and sprayed at the same time on the cold IR window from different nozzles. This technique allows only for brief mixing and reaction time before deposition. In the second system, called 'merged jet system', the two gas samples were again diluted in argon separately but their deposition lines were joined in a merged region allowing time for reaction before deposition. The system used in the present study resembles more the twin jet system.

Ault and Laboy[18] found that no reaction occurred between TMA and CH_3OH or H_2O in the twin jet system. However, when the merged jet system was used in the reaction of TMA with CH_3OH, the parent bands started to disappear and new bands appeared. Methane was also formed. Two species were distinguished: the main species was identified as $(CH_3)_2AlOCH_3$, and the two possible candidates for the second species were the dimer of $(CH_3)_2AlOCH_3$ and the dimethoxy derivative $CH_3Al(OCH_3)_2$. The C–O stretch near 1000 cm^{-1} was characteristic of the Al–O–C linkage in $(CH_3)_2AlOCH_3$. This was the first time that monomeric $(CH_3)_2AlOCH_3$ was isolated and observed. Reaction with H_2O did not show any new bands associated with new product formation, but a reduction of the parent bands was observed along with methane formation. Ault and Laboy explained this observation by the fact that the new species did not survive the transit to the matrix.

A similar study by Ault[19] investigated the reaction of TMA with O_2 in an argon matrix, resulting in the same reaction products described above when a merged jet system was used. Co-deposition using the twin jet system did not show any new species formed. Ault[20] had also investigated the reaction of TMA with H_2S and ethyl and methyl mercaptans in an argon matrix at 14 K, which led to the formation of molecular Al_2S_3, $(CH_3)_2AlSCH_3$ and $(CH_3)_2AlSC_2H_5$ respectively. Earlier, Sanchez *et al.*[21] investigated the reaction of TMA with CO in argon matrix and their data showed the formation of a weakly bound complex $(CH_3)_3Al–CO$.

3.2 Results and Discussion

3.2.1 General

The matrix isolation technique has been used in conjunction with infrared spectroscopy (see Section 3.5.1 for further details about the technique and a schematic diagram of the system) in order to investigate the initial reaction products and intermediates of the hydrolysis reaction of TMA. To achieve this it was decided to co-deposit TMA and water in an argon matrix (water was premixed with argon in the tank) at low temperatures (~ 20 K). It was initially assumed that there would have been little or no interaction between the two reagents at such low temperatures.

The plan was to anneal the matrix up to a certain temperature to allow the molecules to diffuse and react, and then cool the matrix down and record an IR spectrum to observe changes in the spectrum (appearance of new signals and disappearance of existing ones) that would make the identification of new species feasible (intermediate products of the hydrolysis reaction). If that step proved to be successful, the next step would include annealing up to a higher temperature to allow the continuation of the reaction and gradual identification of the next species formed. The intermediates of the hydrolysis reaction of TMA are very reactive, and this is the reason why they have not been identified before. A technique like matrix isolation seemed a promising choice for isolating and studying these reactive intermediates.

Prior to any co-deposition experiments (of water and TMA), it was necessary to deposit TMA on its own in an argon matrix to gather data that could be used for comparison with the spectra of the hydrolysis reaction, and to perform control experiments in order to find the ideal conditions (argon deposition rate, cooling temperature of the TMA flask, deposition time, deposition temperature, behaviour of the matrix during annealing) to be used in the co-deposition experiments.

It should be noted that under the current experimental conditions and with the given equipment it was not possible to eliminate completely the rotational features of small molecules like atmospheric CO_2 and water. The areas that were affected were the OH stretching region of water between 3900-3500 cm^{-1}, the CO_2 asymmetric stretching region between 2400-2300 cm^{-1} with two peaks at ~2344 and ~2339 cm^{-1}, the bending region of water between 1850-1350 cm^{-1} and the deformation/bending region of CO_2 between 680-650

cm^{-1} with a characteristic peak at 667 cm^{-1} (for characteristic peaks in the water regions see section 3.2.3). Interference fringes were also observed, depending on the thickness of the matrix material deposited in each experiment. Finally, in some cases imperfect background subtraction was observed due to very small band shifts caused by the instability of the spectrometer through temperature changes inside and out, leading to high levels of noise and appearance of a number of artefacts that could have been mistaken for actual signals. For this reason, the background single spectra were studied thoroughly and compared with the actual spectrum of each deposition experiment (the background spectra for all experiments are presented in section 3.5-Additional Information). The background noise was more persistent in areas affected by the rotational structures of remaining water or CO_2.

When thermal annealing of the argon matrix containing both reagents did not show any spectral changes, meaning that no reaction had occurred, a different route was followed. It was decided to test a new idea; not to use an inert gas as the matrix material, but to co-deposit TMA and water directly on the cold surface of the window (~20 K).

The results of all the experiments performed are presented below. It should be noted that repeated break-downs of the turbopump delayed this series of experiments significantly, as well as failure of other parts (e.g. temperature controller, repair of the IR spectrometer). Although the results of the new experiments seemed promising, due to a final failure of a part of the equipment it was decided to terminate this work and continue with the research presented in the next three chapters. The nature of the matrix isolation system ('homebuilt', consisted of many different parts, operating at extreme pressures and temperatures) had a crucial impact on the progress of this work. Additionally, the long preparation time of the matrix isolation system prior to each experiment (at least 2-3 days of pumping, especially when water was introduced into the system), the long duration of each experiment (~ 10 h), and the careful disassembly and thorough cleaning of the system after the end of each experiment (e.g. polishing of the CsI window after TMA deposition required several hours every time) were a significant time constraint.

3.2.2 Deposition of TMA in Argon Matrix

TMA was in a liquid state in the flask, which meant that before exposing it to the high pressure of the system to deposit it onto the cold surface of the window, it needed to be

significantly cooled down (otherwise a huge amount of TMA would have been pumped onto the window once opening the valve). For this reason, several trials using different cooling temperatures were made.

It was found that cooling the flask down to –100 °C or –60 °C would not allow any TMA to vaporize (mp 15 °C) and deposited onto the window upon exposure to the very low pressure of the system (no bands were detected after recording the spectrum of the argon matrix).

When a higher cooling temperature was used (–35±2 °C) in Exp. 1.1 new bands were observed when the IR spectrum of the matrix was recorded. For the assignment of the bands, the infrared matrix isolation studies of Kvisle and Rytter[6-7] on TMA, and the Raman studies on TMA vapour by O'Brien and Ozin[15] were used for comparison of the IR vibrations. It was found that the spectrum consisted of a mixture of monomeric and dimeric TMA (m-TMA and d-TMA, respectively). The spectrum of TMA is presented in Figures 3.1 and 3.2; the two main areas of the TMA spectrum are presented in two different graphs for clarity. The monomer seems to be dominant, due to the very low pressure of the system causing the equilibrium to shift to the side of the monomeric species.

The target of experiment 1.2 was to isolate only m-TMA, as m-TMA would ideally be the first candidate to study its reaction with water (simpler spectrum to interpret and easier to identify intermediate products). As is already known, TMA in gas and liquid state exists both as a monomer and dimer, according to the equilibrium:[6-7,22]

$$2\ Al(CH_3)_3 \rightleftharpoons Al_2(CH_3)_6 \qquad (3.1)$$

Isolation of m-TMA or a mixture of m- and d-TMA is possible depending on the conditions used during deposition. It was found that the temperature of the cooling bath of the TMA flask and the argon deposition rate played a crucial role on the form of TMA isolated in the argon matrix. Exp. 1.2 was a successful attempt to isolate only the m-TMA species in the argon matrix by using a lower cooling temperature (–47±2 °C) and a higher argon deposition rate. A large argon/TMA ratio would lead to low concentration of TMA, causing the equilibrium presented in (3.1) to shift to the left to form m-TMA.[6,23] The argon deposition rate of Exp. 1.1 was 3 mbar/min and the argon deposition rate of Exp. 1.2 was more than tripled, 10.7 mbar/min (calculations are based on the argon deposition and deposition time

reported in Table 3.12). Similarly, lowering the cooling temperature would lead to a lower [TMA]. The spectrum of m-TMA is also presented in Figures 3.1 and 3.2.

The transmittance values (Y-axis) of the spectrum are multiplied by a scaling factor of 2, in order for the spectrum to be comparable with the one of the mixture of m- and d-TMA; the vibration of CH_3 rock which is a characteristic monomer band at 741 cm^{-1} (strong and distinct signal in both spectra) was chosen for comparison and adjustment of the m-TMA spectrum. The monomer/dimer absorbance ratio, A_m/A_d for this experiment was 5.4, based on the intensity ratio (see Table 3.3 for integration values of the corresponding peaks) of the CH_3 rock band (741 cm^{-1}) for the m-TMA and the band at 771 cm^{-1} which is also a characteristic band that corresponds to the d-TMA (for comparison with literature data on the A_m/A_d ratio and relation with experimental conditions see ref 7)

The observed frequencies of the spectrum for the m-TMA and d-TMA are listed on Tables 3.1 and 3.2 respectively, along with the frequencies reported in existing literature.[6,15]

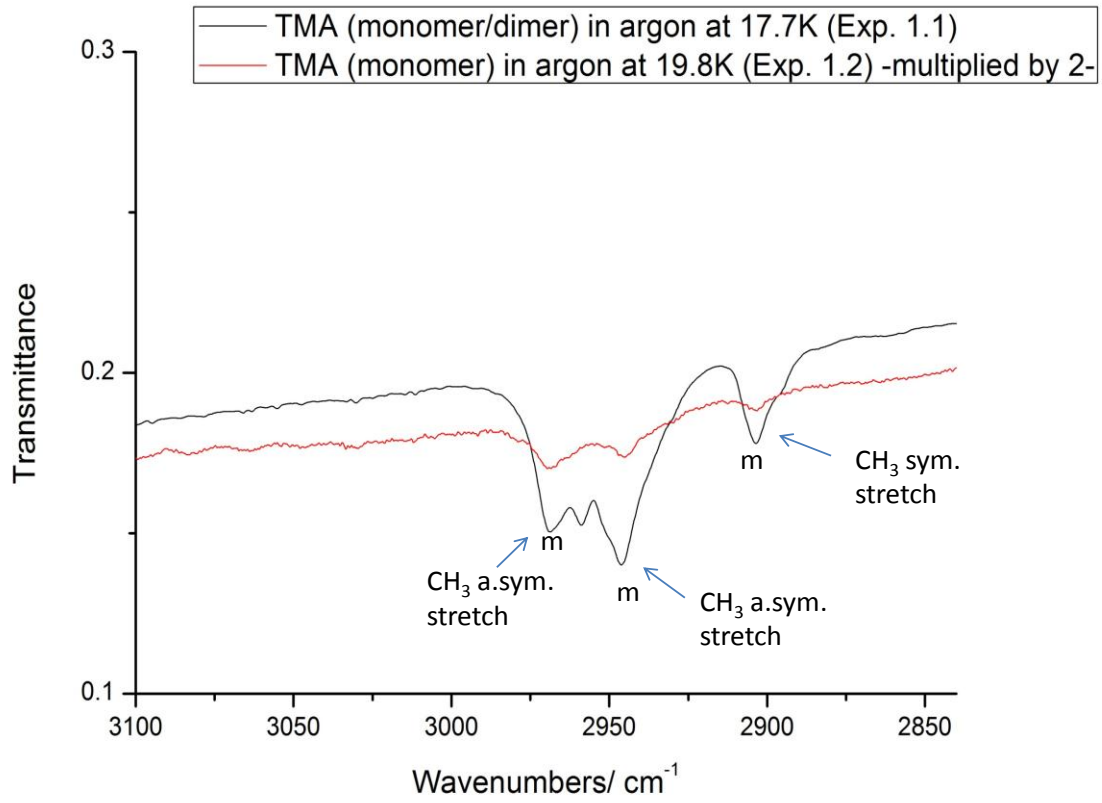

Figure 3.1: Infrared spectrum of m-TMA in argon (Exp. 1.2) compared with m-/d-TMA in argon (Exp. 1.1). The region presented here is between 3100 – 2840 cm^{-1}.

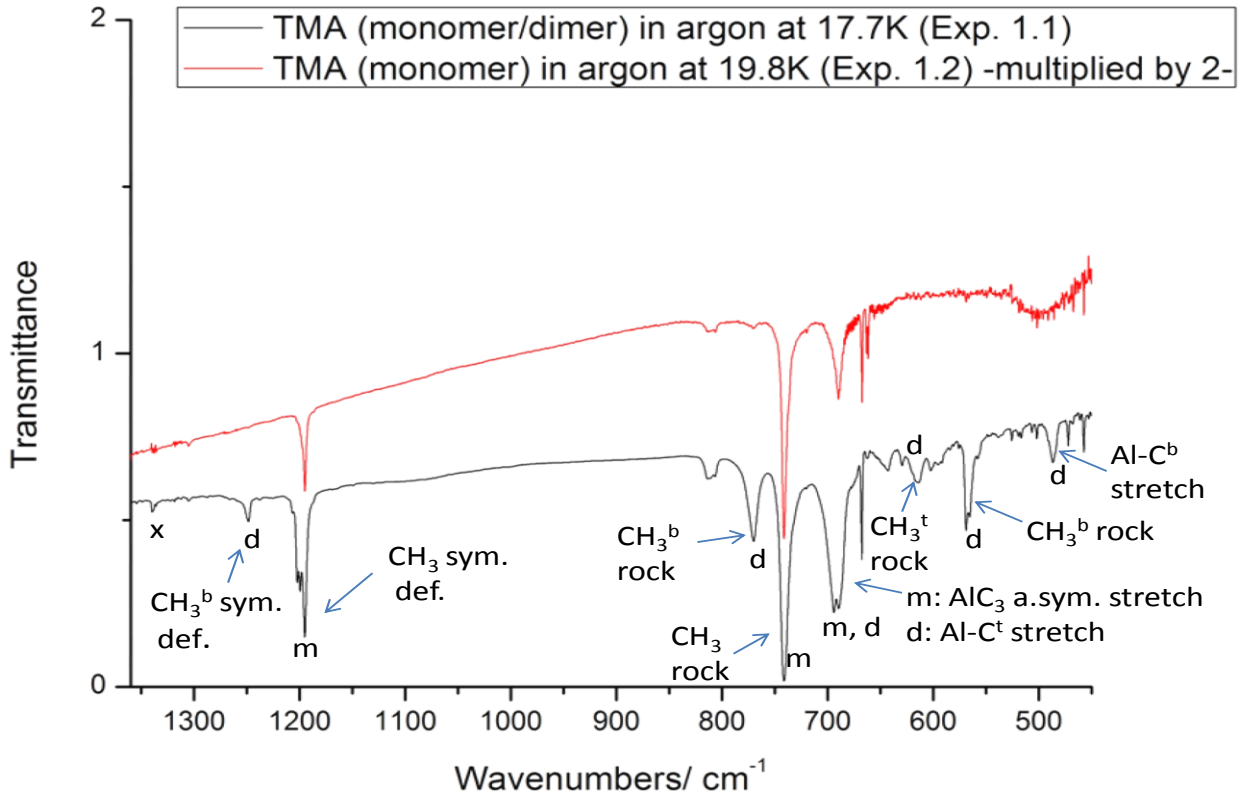

Figure 3.2: Infrared spectrum of m-TMA (Exp. 1.2) in argon compared with m-/d-TMA in argon (Exp. 1.1). The region presented here is between 1360 – 450 cm^{-1}. The CH_4 band is annotated with 'x'.

Table 3.1: Observed frequencies and assignments for monomeric trimethylaluminium (m-TMA) with effective point group D_{3h}

Vibrational modes	**Raman vapour** **O' Brian et al.**	**IR Ar matrix 12 K** **Kvisle and Rytter**	**IR Ar matrix** **19.8 K (Exp. 1.2)**
A_1' ν_1 CH_3 sym. stretch	2900		
ν_2 CH_3 sym. def.	1200 m	1226 vw	
ν_3 MC_3 sym. stretch	530 vs, p		

A_2'' ν_7 CH_3 a. sym. stretch ν_8 CH_3 a. sym. def. ν_9 CH_3 rock		2948 s - 643 w	2947 w
E' ν_{11} CH_3 a. sym. stretch ν_{12} CH_3 sym. stretch ν_{13} CH_3 a. sym. def. ν_{14} CH_3 sym def. ν_{15} CH_3 rock ν_{16} MC_3 a. sym. stretch ν_{17} MC_3 in-plane def.	2996 2920 1440 vw 1035 vw 893 w 760 vw 170 s	2971 s 2905 m ~1430 vw 1196 s 742 s 689 s -	2968 w 2903 w 1195 s 741 vs 690 s
E'' ν_{18} CH_3 a. sym. stretch ν_{19} CH_3 a. sym. def. 2 ν_{13} (A_1'+E')	2951 1440 vw	 2830 w	
Additional overtones and Combination bands		1267 vw 1167 vw 717 vw	 (720 vw)*
CH_4 ν_3		3035 vs 3014 sh	
CH_4 ν_4		1310 sh 1306 s	 1305 vw

*Abbreviations: vw, very weak; w, weak; m, medium; s, strong; sh, shoulder; br, broad; p, polarized.

Careful comparison of the experimental vibrational frequencies shows good agreement with the literature data for the m-TMA (Exp. 1.2). Only a few weak or very weak bands presented in Kvisle and Rytter's study[6] were not detected (at 2830, 1430, 1267, 1226, 1167 and 643 cm^{-1}), probably because of the low concentration of TMA in the matrix. There are some differences on the band shifts but this can be due to many factors: different concentration of TMA on the matrix material, differences on the deposition temperature, and possible matrix perturbation caused by the crystal packing effects.

One difference in our experimental data is that the bands corresponding to vibrations ν_7, ν_{11} and ν_{12} were relatively weak compared to their intensity characterization in Rytter's work. The bands observed in Exp. 1.2 for the m-TMA were of course observed in Exp. 1.1 which also contains m-TMA. However it seems that the vibrations presented in Figure 3.1 are weaker in Exp. 1.2, which contains only m-TMA, than in Exp. 1.1 which contains the m/d-TMA mixture. The full range (3900 – 450 cm^{-1}) of the spectra of Exp. 1.1 and 1.2 are presented in Figure 3.13 in the additional information section for a better understanding and comparison of the intensity of the bands.

A small peak appears at 810 cm^{-1} that is not assigned and a trace of d-TMA at 771 cm^{-1}. Some weaker bands are also observed at 667, 663 and 661 cm^{-1}. The band at 667 cm^{-1} is due to CO_2 and the bands at 663 and 661 cm^{-1} are probably artefacts.

The data gathered for d-TMA from Exp. 1.1 are also in good agreement with the existing literature data, as can be seen in Table 3.2. There is a band reported by Kvisle and Rytter[6] for d-TMA in argon matrix at 2935 cm^{-1}. An observation of a band at this wavelength under the current experimental conditions (Exp. 1.1) was not possible, but an observation of an additional band at 2958 cm^{-1} apart from those that correspond to m-TMA was made. (All the bands attributed to m-TMA reported in Table 3.1 were observed in the spectrum of Exp. 1.1, as expected.) The weak bands at 1435 and 2830 cm^{-1} were not observed. Kvisle and Rytter[6] also report a strong band at 378 cm^{-1} and a shoulder at 368 cm^{-1}. The spectra presented in Figure 3.2 contain interference fringes below 680 cm^{-1} making it difficult to identify weak vibrations, and it was not possible to identify any bands below 450 cm^{-1}.

The band at 810 cm^{-1} observed in the spectrum of Exp. 1.2 is also observed in Exp. 1.1. The band at 1195 cm^{-1}, attributed to m-TMA is present in the spectrum of Exp. 1.2 as expected, but two more signals are distinguishable next to this band at 1199 and 1202 cm^{-1}. These signals can be seen more clearly in Figure 3.10. Kvisle and Rytter[6] reported the frequencies of the vibrations of a single-bridged intermediate form of TMA (i-TMA) observed when they annealed the matrix of m-TMA (m-TMA dimerises after thermal annealing of the matrix). A shoulder at 1200 cm^{-1} was attributed to the i-TMA, which could be the explanation for one the bands observed here. Observation of additional bands is not impossible since multiple bands may appear due to rotation or libration of the solute molecule in its trapping site, alternative trapping sites in the matrix or aggregation of the solute.

Some additional weak or very weak bands are observed on the spectrum of Exp. 1.1 at 1148, 1174, 1130, 629, 602, 525 and 516 cm^{-1}. The bands at 1174, 525 and 516 cm^{-1} also exist in the background spectrum (see Figures 3.14 - 3.18), so they are not related to the material deposited, and the bands at 629 and 602 cm^{-1} could possibly be due to improper background subtraction (the noise level at this area is relatively high). The band at 1130 cm^{-1} might be due to the existence of some i-TMA in the matrix (Kvisle and Rytter[6] reported a band at 1132 cm^{-1} that was attributed to i-TMA). Some additional weak bands were also observed by Kvisle and Rytter[6] when TMA was deposited onto the argon matrix; these were not assigned to any vibrations.

A trace of methane was observed in this spectrum (band at 1305 cm^{-1}). The vibrational modes of methane have been studied thoroughly in infrared matrix isolation experiments and assigned.[24-27]

Thermal annealing of the matrix produced in Exp. 1.1 up to 54 K (the matrix was kept at 54 K for 20 min and then cooled down to the original deposition temperature to record the IR spectrum) did not cause any spectral changes. Originally it was expected that thermal annealing to a higher temperature would allow the molecules of m-TMA to diffuse and form dimers, so a lower A_m/A_d ratio would have been observed. However the A_m/A_d ratio remained the same, meaning that interaction between neighboring monomeric molecules of TMA did not occur.

Thermal annealing of the matrix in Exp. 1.2, containing only (or mainly) m-TMA also did not cause any spectral changes, whilst annealing of the matrix of m-TMA produced by Kvisle and Rytter[6] up to 40 K over short periods of time (max. time = 60 min), caused the

appearance of new bands assigned to intermediate or dimeric species. Annealing of the matrix in the present experiment even up to temperatures of 74 K and accumulated time reaching 1 h was not successful in allowing the m-TMA molecules to react with each other. One possible explanation is that [TMA] in the matrix was very low and the TMA molecules were too far from each other to react.

Table 3.2: Observed frequencies and assignments for dimeric trimethylaluminium (d-TMA) assuming C_{2h} symmetry

Vibrational modes		**Vapour 298 K** **Kvisle and Rytter**	**Solid 12 K** **Kvisle and Rytter**	**Ar matrix 12 K** **Kvisle and Rytter**	**Ar matrix 17.7 K**
A_u	CH_3 a. sym. stretch	2944 s	2936 s	2935 s	2958 m
	CH_3 sym. stretch	2904 m	2894 m	2892 m	2895 sh
	CH_3 a. sym. def.	-	~1435 w	~1435 w	
	CH_3^t sym. def.	-	-	1235 sh	1237 vw
	CH_3^b rock	774 s	768 s	766 vs	771 s
	CH_3^t rock	-	725 s	720 sh	(720 vw)
	CH_3^t rock	-	683 m		
	ν_{16} Al-C^t stretch	567 s	563 vs	563 vs	569 s
	ν_{17} Al-C^b stretch	368 s	370 s	378 s	
B_u	CH_3 a. sym. stretch	2944 s	2936 s	2935 s	2958 m
	CH_3 sym. stretch	2904 m	2894 m	2892 m	2895 sh
	CH_3 a. sym. def.	-	~1435 w	~1435 w	
	CH_3^b sym. def.	1255 m	1252 m	1249 s	1249 s

CH_3^t sym. def.	1208 s	1196 s	1193 vs	1199 vs 1202 vs
ν_8 Al-C^t stretch	700 vs	701 vs	697 vs	695 vs
CH_3^t rock	~650 vw	645 m	645 m	643 m
CH_3^t rock	609 m	611 s	612 s	614 s
CH_3^b rock	-	597 sh	597 sh	602 vw and 595 sh
ν_{13} Al-C^b stretch	480 m	488 s	491 s	487 m
2 x CH_3 a. sym. def.	2845 w	2832 w	~2830 w	2826 vw
Additional unassigned bands		674 sh 519 w	521 vw 368 sh	520 vw
CH_4 ν_3	3008 vw	3007 w		
CH_4 ν_4		1301 m		1305 vw

*Abbreviations: , terminal; b, bridge; see also Table 3.1

**The skeletal modes are numbered according to D_{2h} symmetry, see Ref. [28]

Table 3.3: Integration values of the absorbance of the main peaks observed in the spectra of Exp. 1.1 and 1.2.

Exp. 1.1: m+d- TMA		**Exp. 1.2: m-TMA**	
Peak Position (cm^{-1})	**Intensity (Abs. Units)**	**Peak Position (cm^{-1})**	**Intensity (Abs. Units)**
2968, 2958, 2947	4.756	2968, 2947	1.223
2903	0.593	2903	0.069
1305	0.025	1305	0.016
1249	0.230		
1202, 1199, 1195	3.632	1195	0.668
771	**1.592**	771	0.073
741	**8.591**	**741**	**2.479**
695, 690	6.288	690	0.974
643	0.278		
614	0.441		
569	1.378		

*When more than one peak is reported, the whole region including these peaks was integrated.

3.2.3 Co-deposition of TMA and Water in Argon Matrix

In Exp. 2.1 in order to study the hydrolysis reaction of TMA, a 1% gas mixture of H_2O in argon was co-deposited with the TMA. The same experimental conditions as in Exp. 1.2 were used in order to deposit only m-TMA. The aim was to allow the molecules of water and TMA to diffuse and react with each other after thermal annealing, and trap the initial intermediates of the reaction. Exp. 2.2 is the same as Exp. 2.1, but using a lower water concentration in argon (0.15% gas mixture of H_2O in argon).

The two regions of the spectra (for Exp. 2.1 and 2.2) where the alkylaluminium vibrations appear are presented in Figures 3.5 and 3.6, along with the spectrum of m-TMA (Exp. 1.2) for comparison. Figure 3.7 zooms in on the area between 1330 – 1280 cm^{-1} to observe the very weak band of methane more closely. Figure 3.8 zooms in on the area between 800 – 600 cm^{-1} to observe the small shift of the bands between Exp. 2.1 and 2.2 and Exp. 1.2. The observed frequencies from the spectra presented in the graphs (Exp. 2.1, Exp. 2.2 and Exp. 1.2) are listed in Table 3.4.

The transmittance values (Y-axis) of the spectrum of Exp. 2.1 presented in Figure 3.6 are multiplied by a scaling factor of 10, in order for the spectrum to be comparable with that

of Exp. 2.2. The transmittance values of Exp. 1.2 are multiplied by a scaling factor of 1.5; the characteristic monomer band at 741 cm^{-1} (strong and distinct signal in both spectra) was chosen for comparison and adjustment of the m-TMA spectrum. The same scaling factors were used in Figures 3.7 and 3.8, however it was not possible to keep the same multiplication factors for the spectra presented in Figure 3.5. In Figure 3.5 the transmittance values of Exp. 2.1 and Exp 1.2 were multiplied by a scaling factor of 5 and 4 respectively in order to result to comparable peak heights.

Figures 3.3 and 3.4 present the OH stretching (3900-3300 cm^{-1}) and bending (1850-1350 cm^{-1}) regions of water respectively, for Exp. 2.1 and 2.2 in comparison with those from Exp. 1.2. The main bands observed in these regions are reported on Table 3.5. The transmittance values of the spectra presented in these figures have not been normalized by a factor.

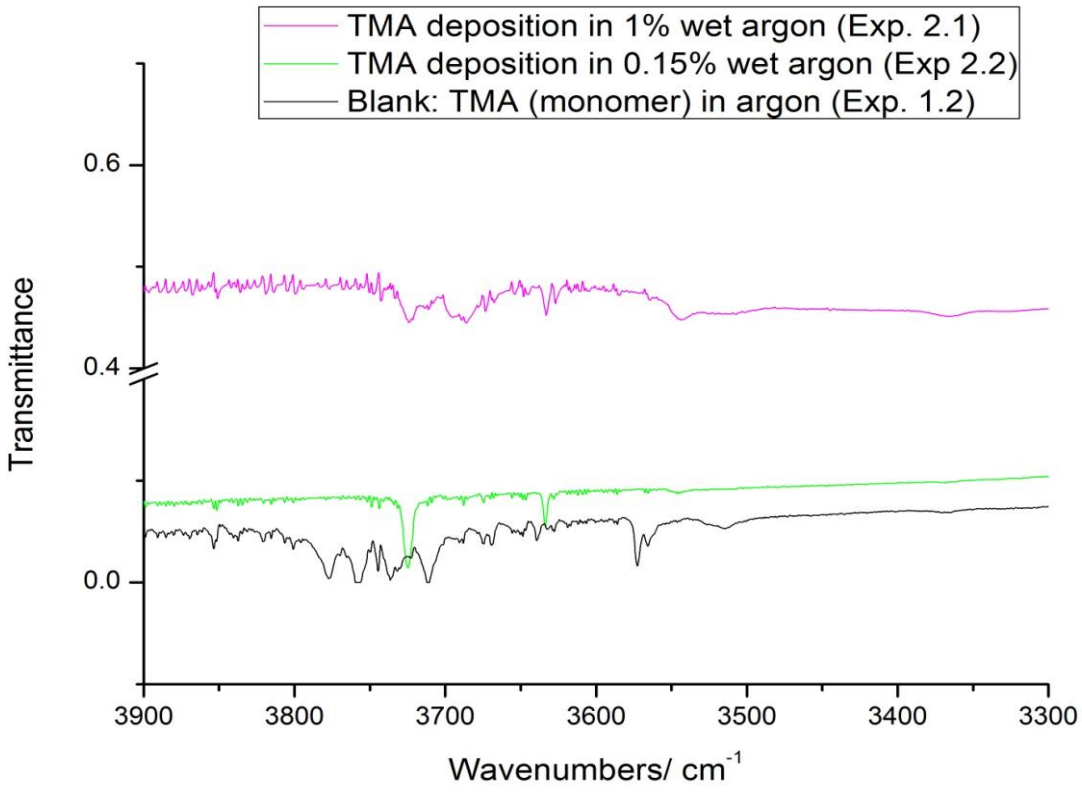

Figure 3.3: Infrared spectrum of m-TMA in 1% gas mixture of water in argon (Exp. 2.1) and m-TMA in 0.15% gas mixture of water in argon, compared with m-TMA in argon (Exp. 1.2). The region presented here is between 3900 – 3300 cm^{-1}.

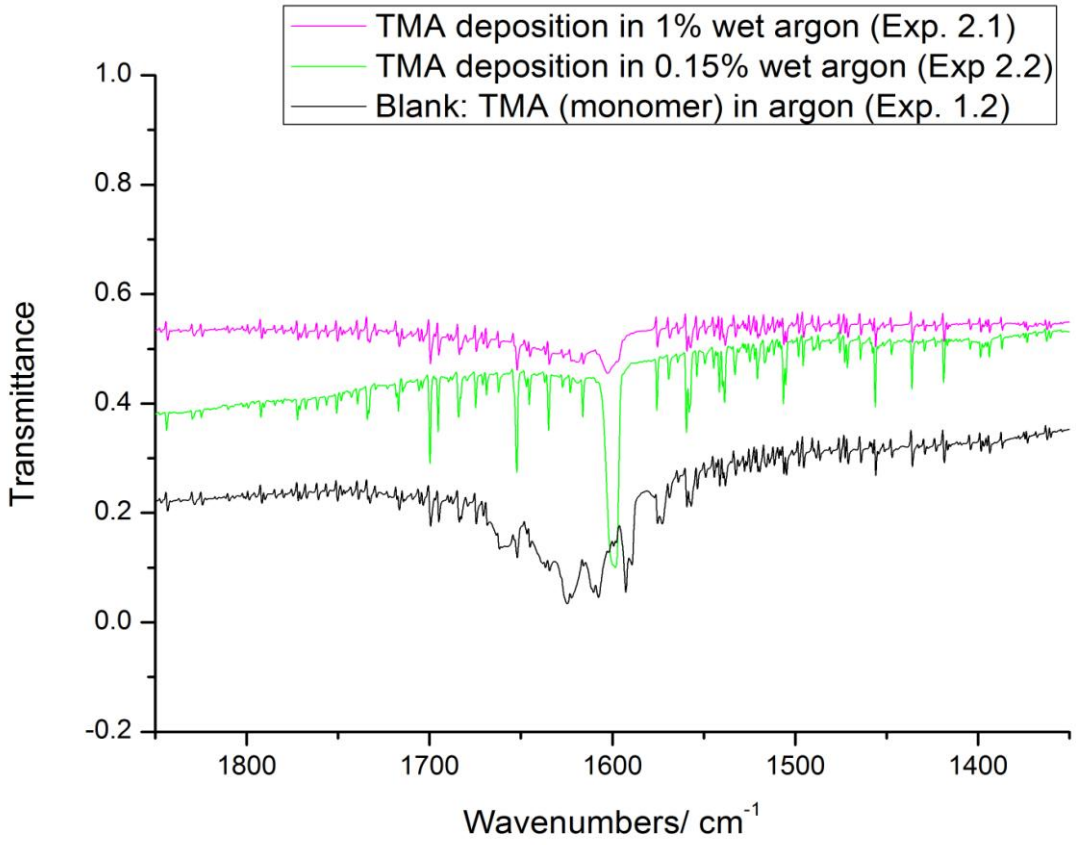

Figure 3.4: Infrared spectrum of m-TMA in 1% gas mixture of water in argon (Exp. 2.1) and m-TMA in 0.15% gas mixture of water in argon, compared with m-TMA in argon (Exp. 1.2). The region presented here is between 1850 – 1350 cm^{-1}.

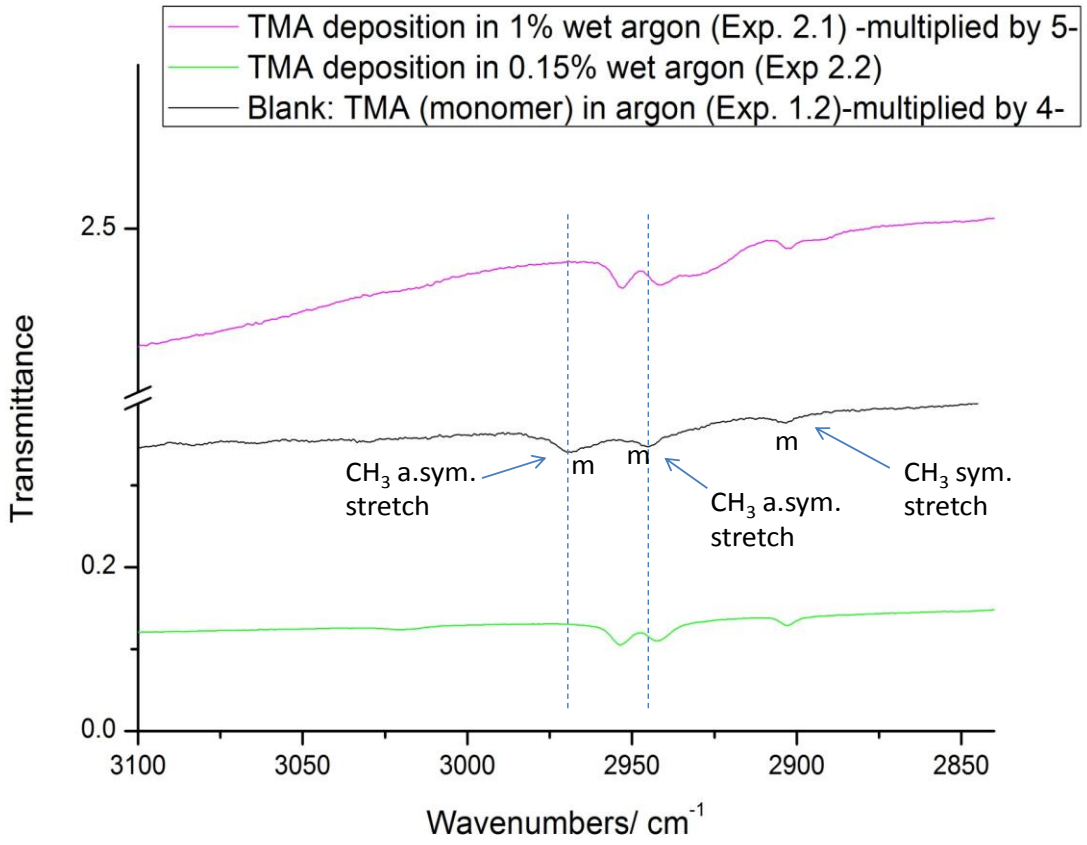

Figure 3.5: Infrared spectrum of m-TMA in 1% gas mixture of water in argon (Exp. 2.1) and m-TMA in 0.15% gas mixture of water in argon, compared with m-TMA in argon (Exp. 1.2). The region presented here is between 3100 – 2840 cm^{-1}.

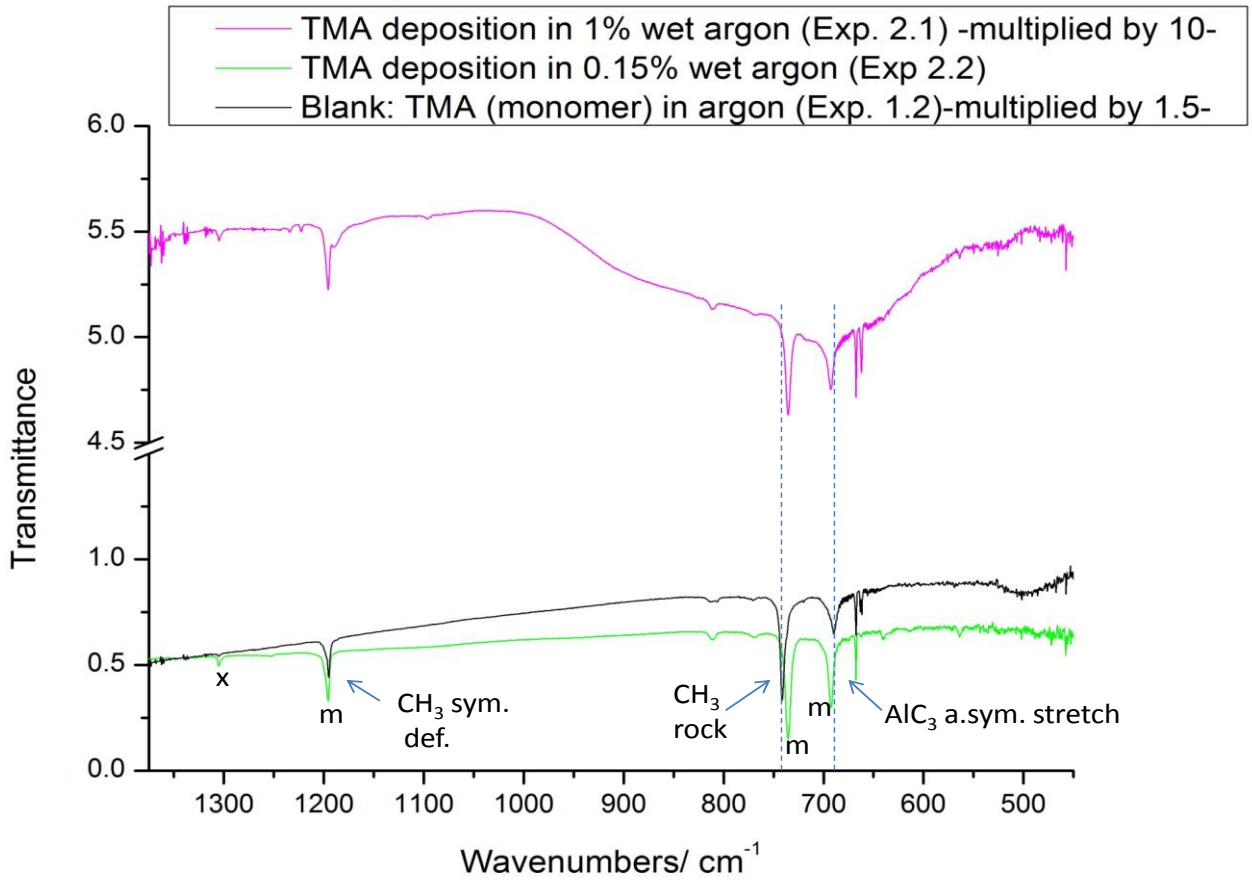

Figure 3.6: Infrared spectrum of m-TMA in 1% gas mixture of water in argon (Exp. 2.1) and m-TMA in 0.15% gas mixture of water in argon, compared with m-TMA in argon (Exp. 1.2). The region presented here is between 1360 – 450 cm^{-1}. The band attributed to methane is annotated with 'x'.

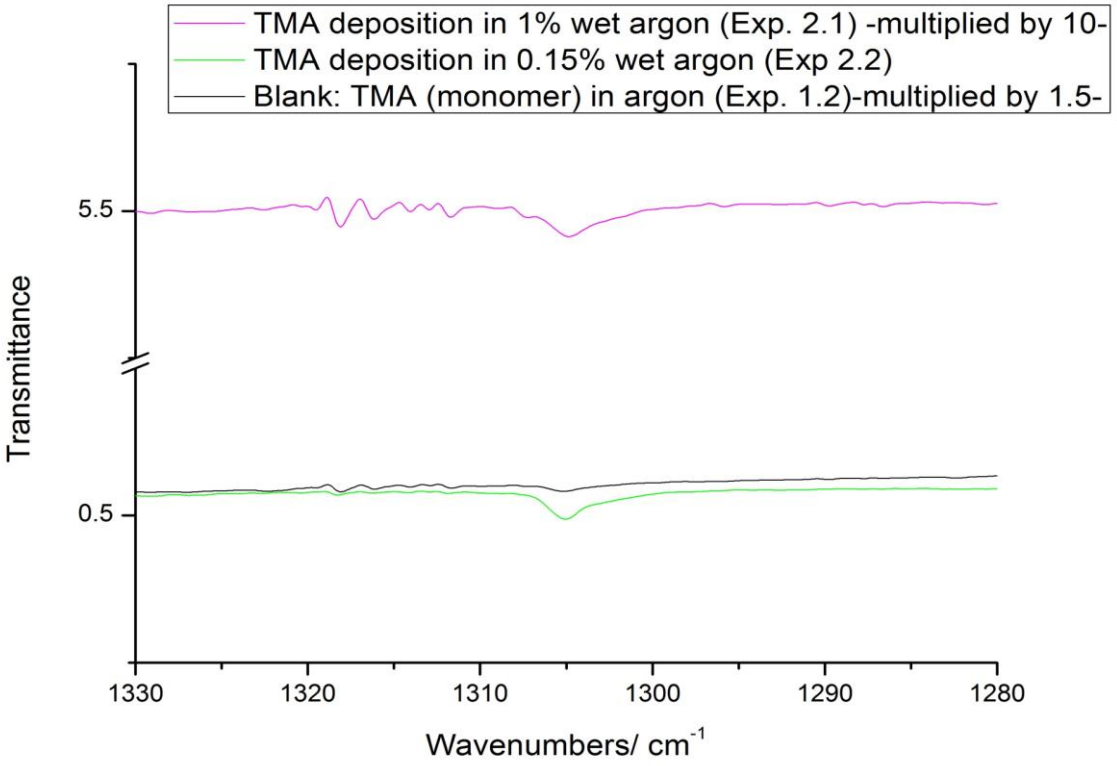

Figure 3.7: A magnification of the region where the ν_4 methane band appears in the infrared spectrum of m-TMA in 1% gas mixture of water in argon (Exp. 2.1) and m-TMA in 0.15% gas mixture of water in argon (Exp. 2.2), compared with m-TMA in argon (Exp. 1.2).

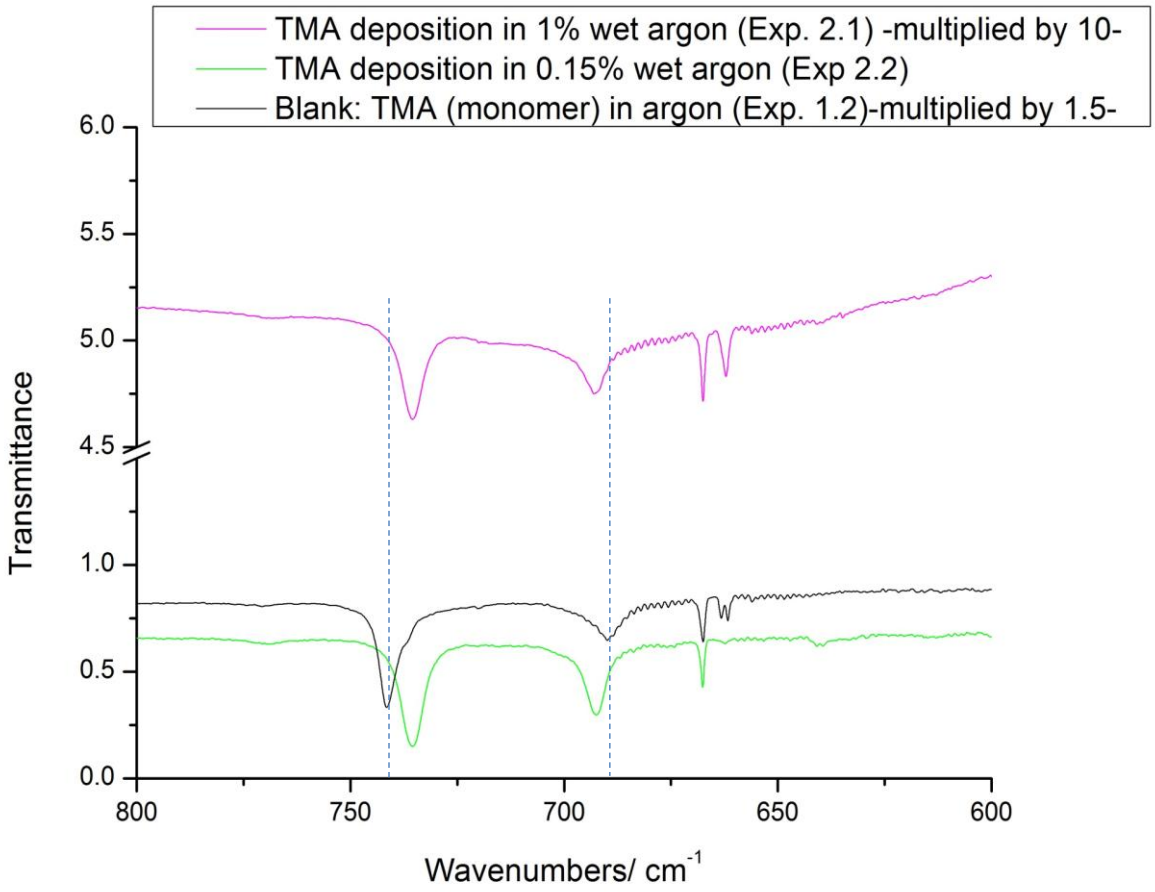

Figure 3.8: A magnification of the region between 800 – 600 cm^{-1} for a closer observation of the shift of the bands in the infrared spectra of m-TMA in 1% gas mixture of water in argon (Exp. 2.1) and m-TMA in 0.15% gas mixture of water in argon (Exp. 2.2), compared with m-TMA in argon (Exp. 1.2).

Observation of the spectra between isolated m-TMA in argon matrix and m-TMA in a H_2O/argon matrix reveals some distinct differences. These differences could be described as appearance of new bands and disappearance of other characteristic bands of the m-TMA or by a shift of existing bands (e.g. 2947 → 2942, 2968 → 2953, 741 → 735, 690 → 693) and appearance of some new signals. Some very weak additional bands that are not listed in Table 3.4 were observed in Exp. 2.1 and 2.2 at 770, 565 and 640 cm^{-1}. These bands might be associated with traces of d-TMA (d-TMA from Exp. 1.1: 771, 564 and 643 cm^{-1}). The spectrum of Exp. 2.1 also shows some very weak bands at 1234, 1223 and 1097 cm^{-1}. A very

careful observation of Figure 3.6 might reveal these very tiny signals. It should also be noted that Exp. 2.1 shows the additional shoulder peaks at 2932, 2893 and 1190 cm^{-1} (reported in Table 3.4) that are not present in Exp. 2.2. This might be due to the higher water concentration leading to matrix perturbation caused by the crystal packing effects or to the formation of new reaction products (higher concentration of water→ higher chance of collision of a water and a TMA molecule when they meet in the gas phase, before they solidify on the cold surface).

Obvious differences are also observed in the areas of the spectrum where the OH vibrations appear (see Figures 3.3 and 3.4 and Table 3.5). These differences might simply be related to the different water concentrations (e.g. water might form dimers, trimers or larger aggregates in an argon matrix depending on the concentration) or to the formation of new species (e.g. formation of $AlMe_3$*H_2O adduct or $AlMe_2OH$). Some of the peaks in Exp. 1.2 where the [H_2O] must be very low (only traces of atmospheric water) might be attributed to the water monomer or dimer e.g. the band at 3735 cm^{-1} might be due to ν_3 of the monomer, the bands at 3711 cm^{-1} and 3753 cm^{-1} due to the ν_2 and ν_1 of the dimer respectively, the bands at 1611, 1593 cm^{-1} due to the dimer and the band at 1590 cm^{-1} due to non-rotational monomer. However, some of the bands (3515, 1625, 1622) are close to the frequencies reported for polymeric H_2O. Exp. 2.1 and 2.2 which contain higher [H_2O] show bands at 3694 or 1602 cm^{-1} that were attributed to polymeric H_2O (trimer or tetramer). The band at 3633 cm^{-1} is close to the one reported for the dimer. A list of the observed frequencies and assignments of the H_2O spectrum in argon matrix that have been reported in literature[29-31] is also listed on Table 3.5.

Unfortunately, due to time constraints and systematic failure of the equipment we were unable to study the spectrum of isolated water molecules in an argon matrix. Careful infrared matrix isolation studies, varying the [H_2O] would have added a valuable insight to the information presented here.

The shift of the main bands reported earlier (2947 → 2942, 2968 → 2953, 741 → 735, 690 → 693) was originally explained by the hypothesis that an intermediate between a H_2O molecule and a TMA monomer was formed possibly at the moment the two gas streams hit the cold cell. However, the presence of such species should have shown a strong band around 500 cm^{-1} due to the rocking mode of the water molecule as was predicted by computational studies by our collaboration partners, the Linnolahti group at the University of

Eastern Finland (UEF); but such a vibration did not appear in the spectra of the present experiments (the Linnolahti group also reported two distinct bands between 3900-3800 cm^{-1}, one at 1624 cm^{-1} and a band around 300 cm^{-1} due to Al–O vibrations).

Another possible explanation for the shift of the bands referred to earlier, could be lattice disorders in the argon matrix due to the addition of water molecules in the close packed system of argon molecules (1 water molecule between 11 argon molecules). However, a careful observation of the shift of the bands at 735 (ν_{15} CH_3 rock) and 693 cm^{-1} (ν_{16} MC_3 a. sym. stretch) shows that these bands move in opposite directions, meaning that this phenomenon is less likely to be simply due to a change in the matrix packing. Of course, it should be taken into consideration that the shift of the bands is so small in energy terms that it is difficult to interpret them.

This observation might actually be an indication of the initial interaction of TMA with water, associated with the effect of hydrogen bonding, as when a H_2O molecule approaches, the symmetry of the TMA molecule changes from planar to tetrahedral.

In the case of the formation of a TMA-water adduct as the only reaction product no methane should have been evolved; however, an amount of methane was traceable (bands at 1305 cm^{-1} for Exp. 2.1 and 2.2 and 3019 cm^{-1} for Exp 2.2, see Tables 3.4 and 3.6, and Figure 3.7).

In fact, careful comparison of the $A_{m\text{-}TMA}/A_{CH_4}$ of Exp. 2.1 (= 31.2) and Exp 2.2 (= 26.3) with that of Exp. 1.2 (= 154.9), where only m-TMA was deposited without the presence of water, shows that a lot more CH_4 was detected in the co-deposition experiments of TMA and water in argon than in experiments of just TMA deposition in argon. The calculation of the ratios was based on the integration values of the absorbance of the peaks at 735 cm^{-1} for Exp. 2.1 and 2.2 and at 741 cm^{-1} for Exp. 1.2 for the $A_{m\text{-}TMA}$, and the peak at 1305 cm^{-1} for the A_{CH_4} for all experiments. The integration values of the main absorbance peaks observed in the spectra of Exp. 2.1 and 2.2 are presented on Table 3.6.

The existence of methane in the matrix could mean that the reaction between H_2O and TMA proceeded further, forming additional products. The CH_3 vibrations of the new products would show only small differences, so identification of the new species would not have been easy without identification of characteristic bands. Computational studies by the Linnolahti group about the IR vibrations of $AlMe_2OH$ which could have been a possible

intermediate of the reaction revealed a band around 3900 cm^{-1} and a new one at 856 cm^{-1}. They also reported bands at lower wavenumbers, 500-300 cm^{-1}, related to the Al-O vibrations. No new band was observed around 856 cm^{-1} in our experiments, and identifications of peaks below 450 cm^{-1} was not possible.

Thermal annealing of the matrix of Exp. 2.1 up to 80 K and annealing of the matrix of Exp 2.2 up to 82 K did not cause any spectral changes. Although the highest possible annealing temperature was used for the argon matrix (getting close to the m.p. of argon = 83.3 K[1]), it seemed like the temperature was not high enough to overcome the energy barrier and allow molecules to react. As observed earlier, perhaps the low concentration of m-TMA in the matrix makes it more difficult; the molecules have to travel a larger distance until they meet another molecule.

Table 3.4: Observed frequencies and assignments for monomeric trimethylaluminium (m-TMA) with effective point group D_{3h} (Exp. 1.2) and main observed frequencies in Exp. 2.1 and 2.2.

Vibrational modes	**Exp. 1.2: IR Ar matrix 19.8 K**	**Exp. 2.1**	**Exp. 2.2**
A_2'' ν_7 CH_3 a. sym. stretch	2947 w	2942 w and 2932 sh	2942 w
E' ν_{11} CH_3 a. sym. stretch	2968 w	2953 w	2953 w
ν_{12} CH_3 sym. stretch	2903 w	2903 w 2893 sh	2903 w
ν_{14} CH_3 sym def.	1195 s	1196 s and 1190 sh	1196 s
ν_{15} CH_3 rock	741 vs	735 vs	735 vs
ν_{16} MC_3 a. sym. stretch	690 s	693 s	693 s
CH_4 ν_3			3019 vw
CH_4 ν_4	1305 vw	1305 w	1305 w

*Abbreviations: vw, very weak; w, weak; m, medium; s, strong; sh, shoulder; br, broad; p, polarized.

Table 3.5: Observed frequencies in the OH stretching region (3900-3300 cm^{-1}) and the bending region of water (1850-1350 cm^{-1}) for Exp. 2.1 and 2.2 in comparison with Exp. 1.2.

H_2O frequencies reported in literature[29-31]		**Exp. 1.2: TMA in Ar matrix 19.8 K**	**Exp. 2.1 Ar/H_2O = 100/1**	**Exp. 2.2 Ar/H_2O= 1000/1.5**
		3777		
		3758		
3736	non-rot. monomer	3735		
3722	non-rot. monomer		3724	3724
3709.5	dimer	3711		
3702.5	polymer			
3693.8	polymer		3694 sh, 3687	
3634.1	dimer		3633	3634
3574.5	dimer	3573		
3568	?	3567		
			3544, 3514 sh	(3546)
3517	polymer	3515		
3372	polymer	(3367)	(3366)	
1623	polymer	1625, 1622		
1611.2	dimer	1611, 1607		
1602.3	polymer		1602	1602
1593.6	dimer	1593		

1591.4 **1590.1**	non-rot. monomer non-rot. monomer	1590		

Table 3.6: Integration values of the absorbance of the main peaks observed on the spectra of Exp. 2.1 and 2.2.

Exp. 2.1		**Exp. 2.2**	
Peak Position (cm^{-1})	Intensity (Abs. Units)	Peak Position (cm^{-1})	Intensity (Abs. Units)
		3019	0.177
2953, 2942, 2932	1.728	2953, 2942	1.823
2903, 2893	0.153	2903	0.201
1305	0.069	1305	0.132
		1253	0.073
1234	0.023		
1223	0.032		
1196, 1190	1.110	1196	1.177
(771)	0.005	(771)	0.098
735	**2.151**	**735**	**3.469**
693	1.492	693	2.067
564	0.064	564	0.127

3.2.4 Co-deposition of TMA and Water (without inert gas)

Since thermal annealing of the argon matrix containing water and TMA (Exp. 2.1 and 2.2) did not produce the desired results and we were unable to follow a reaction between the two reagents and identify possible intermediates, a different technique was employed in this series of experiments.

The temperature limitations due to the low melting point of argon made it necessary to look for another matrix material. An interesting idea was to attempt to use water as the matrix material and reagent simultaneously. In this case, the TMA molecules will be trapped in a water matrix and react either the moment the two streams hit the cold surface, before they solidify, or during the thermal annealing which can now reach higher temperatures.

Although the attempt to trap TMA in a water matrix was successful, most areas of the spectrum are saturated because of the higher refractive index of the matrix and due to scattering. The areas that were mainly studied were between 3050 – 2750 cm^{-1} and 1375 –

1050 cm^{-1}. Initially, the two reagents were co-deposited on the surface of the cold window at very low temperatures (Exp. 3.1, T_{dep} = 17.6 K). However when thermal annealing of the matrix of water and TMA neglected to show any spectral changes, a new series of experiments was designed. The idea was to co-deposit water and TMA at gradually higher temperatures allowing more time for the molecules to interact with each other before they solidify. Different deposition temperatures could vary the liquid transition state life time and thus capture different intermediates.

Figures 3.9 and 3.10 present the spectra obtained for Exp. 3.1 and Exp. 3.2, including the spectrum of the m- and d-TMA of Exp. 1.1 for comparison, and Figures 3.11 and 3.12 present the spectra obtained for Exp. 3.3 and 3.5, including the spectrum of the m-TMA (Exp. 1.2) for comparison. Table 3.7 contains the observed frequencies for all experiments, and a comparison with the frequencies observed in the same regions for m-TMA and d-TMA, while Tables 3.8 and 3.9 contain the intensity values of the bands seen on absorbance units (based on integration of the area of the absorbance peaks).

In Figures 3.9 and 3.10 the transmittance values (Y-axis) of the spectrum of Exp. 3.1 are multiplied by a scaling factor of 4 and the one of Exp. 3.2 by a factor of 12, in order the spectra to be comparable with each other and the one of the mixture of m- and d-TMA; the vibration of the d-TMA (CH_3^b sym. def.) at 1249 cm^{-1} was chosen for comparison and adjustment of the other spectra. In Figure 3.12 the transmittance values (Y-axis) of the spectrum of Exp. 3.3 are multiplied by a scaling factor of 2.5 and the spectrum of Exp. 3.5 by 15, in order for the spectra to be comparable with each other and the one of the m-TMA; the vibration of the m-TMA (ν_{14} CH_3 sym. def.) at 1195 cm^{-1} was chosen for comparison and adjustment of the other spectra. However, the spectrum of m-TMA (Exp. 1.2) in Figure 3.11 needed a further multiplication by 4, in order for the bands to be visible.

Experiment 3.1 reveals the presence of a high amount of CH_4 compared to the amount of TMA (see the intensity of the bands on Table 3.8). The A_m/A_{CH4} is very low (= 0.9) compared to the A_m/A_{CH4} (=41.8) of Exp. 1.2 (see Table 3.11 for details), due to the high amount of CH_4 produced. The band at 3009 cm^{-1} is attributable to the ν_3 vibration of CH_4, and the band at 1301 cm^{-1} is assigned to the ν_4 vibration

The three TMA bands that are close together in the 3050 – 2750 cm^{-1} region [2969 (m), 2958 (d), 2946 (m) cm^{-1}], are not distinguishable in the spectrum of Exp. 3.1: a broad band appears at 2926 cm^{-1} instead. The broadness of the signal might be due to the nature of the new matrix. Also the signal of m-TMA at 2903 cm^{-1} seems to have been shifted to 2887 cm^{-1}. A new, weak signal also appears at 2815 cm^{-1}.

Examining the second region of the spectrum at 1375 – 1050 cm^{-1} also reveals differences when it is compared to the spectrum m/d-TMA. The band of the d-TMA at 1249 cm^{-1} seems to have shifted to 1246 cm^{-1}. A very weak band at 1237 cm^{-1} was also observed for the d-TMA in argon matrix. For Exp. 3.1, a shoulder band is present at 1237 cm^{-1} which is much stronger than the one in Exp. 1.1 (in comparison with their neighboring bands at 1246 and 1249 cm^{-1} respectively), indicating a change in the nature of the species trapped in the matrix. Another broad signal is also obvious at 1186 cm^{-1}, which is comparable with the one of m-TMA at 1195 cm^{-1}. The broadness of the signal would shadow the separation of smaller signals related to the d-TMA as the ones observed in the spectrum of Exp. 1.1 (at 1199 and 1202 cm^{-1}). Some weaker additional bands were also observed (1094, 1083 and 1031 cm^{-1}).

All these spectral differences, along with the obvious production of methane could lead to the conclusion that an intermediate of the reaction could have been formed. In this case, a logical explanation would be that the two streams (TMA and water) interact with each other in the liquid state the moment they hit the cold surface of the window. It should be recalled at this point that the matrix isolation system used in this study could be characterized as a 'twin-jet system', allowing only a brief mixing and reaction time before deposition. For this reason, co-deposition of TMA and water was attempted at higher temperatures (100 K and 200 K) in order to prolong the time the molecules remain in the liquid state.

The matrix was annealed up to 270 K for 1 h but no changes were observed. The matrix can start subliming at these temperatures, so the reagents were sublimed before they started reacting. Failing to observe spectral changes after annealing to temperatures lower than 270 K can only be explained by the fact that the reagents don't react when they are both in the solid state or that the activation energy needed is higher.

In experiment 3.2 the T_{dep} was raised to 100 K. Unfortunately, apart from the methane band at 3009 cm^{-1} no other bands were obvious in the 3050 – 2750 cm^{-1} region. The most dominant band at the 1375 – 1050 cm^{-1} region is also the methane band at 1299 cm^{-1}. Another two bands are however distinct, at 1245 and 1186 cm^{-1}, which are in alignment with the

bands observed in Exp. 3.1. Here, the shoulder at 1237 cm^{-1} was not observed which could attribute to the belief that perhaps that band on Exp. 3.1 was due to an early intermediate of the reaction. In this experiment more CH_4 was produced as was expected due to the higher deposition temperature. The A_m/A_{CH_4} was even lower (= 0.6) than in Exp. 3.1 and the A_d/A_{CH_4} (= 0.4) was also lower than the A_m/A_{CH_4} (= 0.5) in Exp. 3.1. Thermal annealing of the matrix did not cause any spectral changes, as observed in Exp. 3.1.

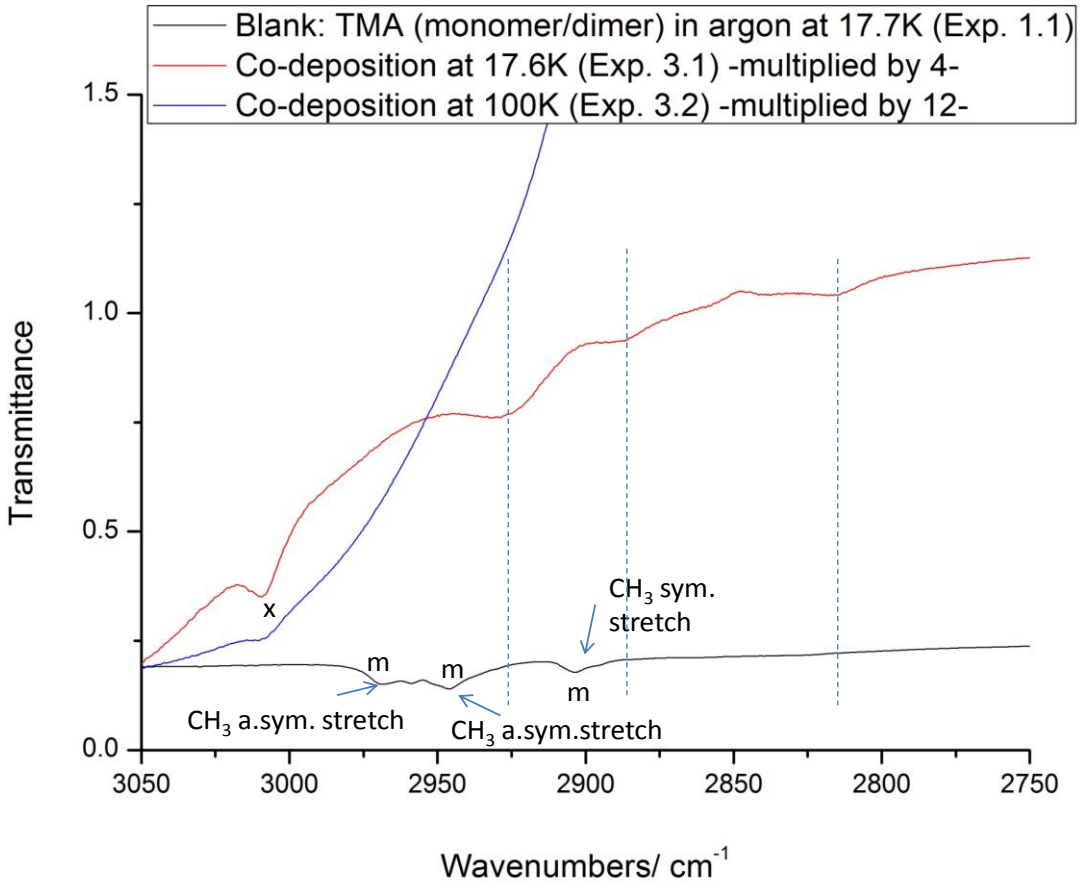

Figure 3.9: Infrared spectrum of co-deposited TMA and water at 17.6 K (Exp. 3.1) and at 100K (Exp. 3.2), compared with the spectrum of the mixture of m/d-TMA in argon at 17.7 K (Exp. 1.1). The region presented here is between 3050 – 2750 cm^{-1}. The band attributed to methane is annotated with 'x'.

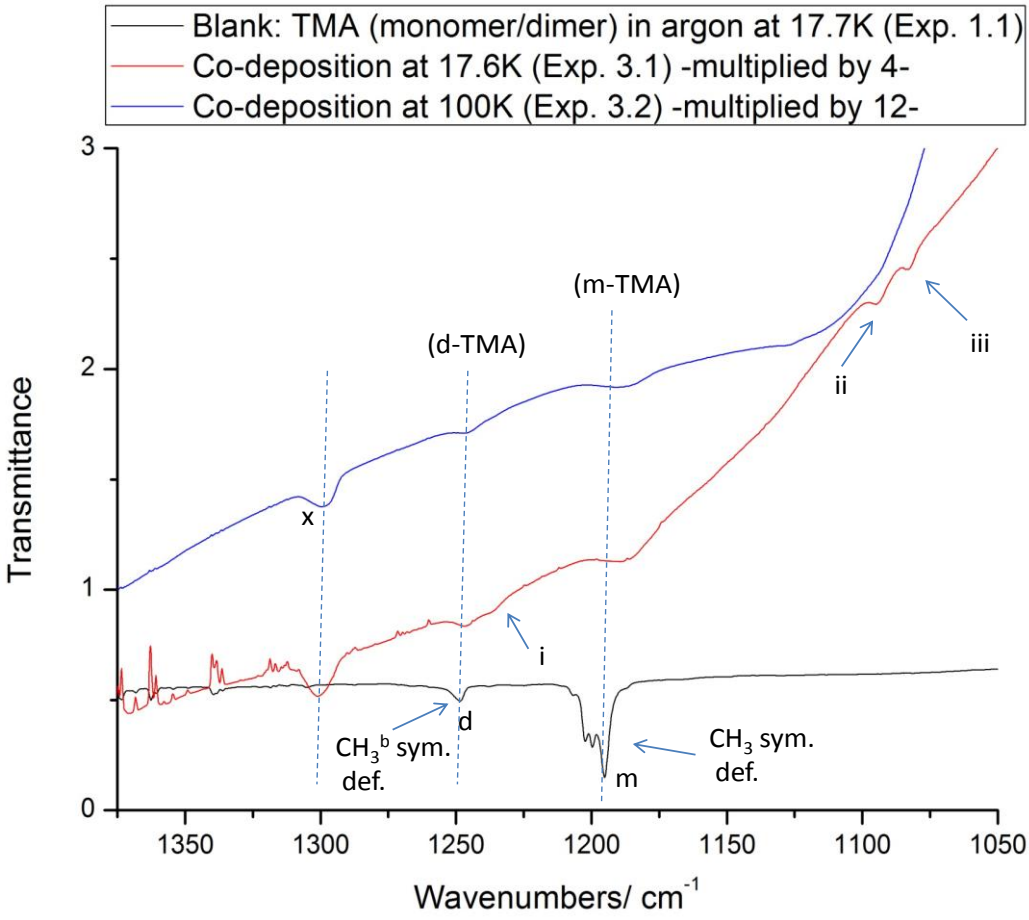

Figure 3.10: Infrared spectrum of co-deposited TMA and water at 17.6 K (Exp. 3.1) and at 100K (Exp. 3.2), compared with the spectrum of the mixture of m/d-TMA in argon at 17.7 K (Exp. 1.1). The region presented here is between 1375 – 1050 cm^{-1}. The band attributed to methane is annotated with 'x'.

While in Exp. 3.1 and 3.2 the bands at 1246-5 and 1237 cm^{-1} are related to d-TMA or a product of d-TMA after reaction with water, Exp. 3.3 and 3.5 do not show any bands in this region, leading to the conclusion that only m-TMA was isolated on the matrix. This series of experiments was performed after a few months due to equipment failure, and the system was re-assembled. The position of the radiation shield was in a slightly different position allowing a lower amount of TMA to be deposited on the cold surface of the window. Additionally, the amount of water was slightly higher in these experiments, as can be seen in Table 3.13. To

conclude, a lower concentration of TMA in the water matrix might have shifted the equilibrium to the side of the monomer.

The T_{dep} in Exp. 3.3 was 21.5 K. It was relatively hard to see the bands in the 3050 – 2750 cm^{-1} region, but three bands seem to exist at 2922, 2887 and 2814 cm^{-1}. No band for methane was observed in this region. The second region of the spectrum contains just one band at 1186 cm^{-1} (same frequency as in Exp. 3.1 and 3.2). No methane band is observed here either, meaning that TMA did not react with water during this deposition (a water-TMA adduct formation is not excluded).

In Exp. 3.5 the T_{dep} was raised to 200 K. The same bands were observed here as in Exp. 3.3 (the band centred at 2922 cm^{-1}, is now centred at 2925 cm^{-1}), with the only difference being that methane evolution is observed. The methane signals at 3009 cm^{-1} and 1300 cm^{-1} are easily identified. The A_m/A_{CH_4} is also very low (= 0.8) here (see Table 3.11). This observation leads to the conclusion that increasing the lifetime of the liquid transition state of the two streams by increasing the T_{dep} could allow the reaction to proceed and trap different intermediates.

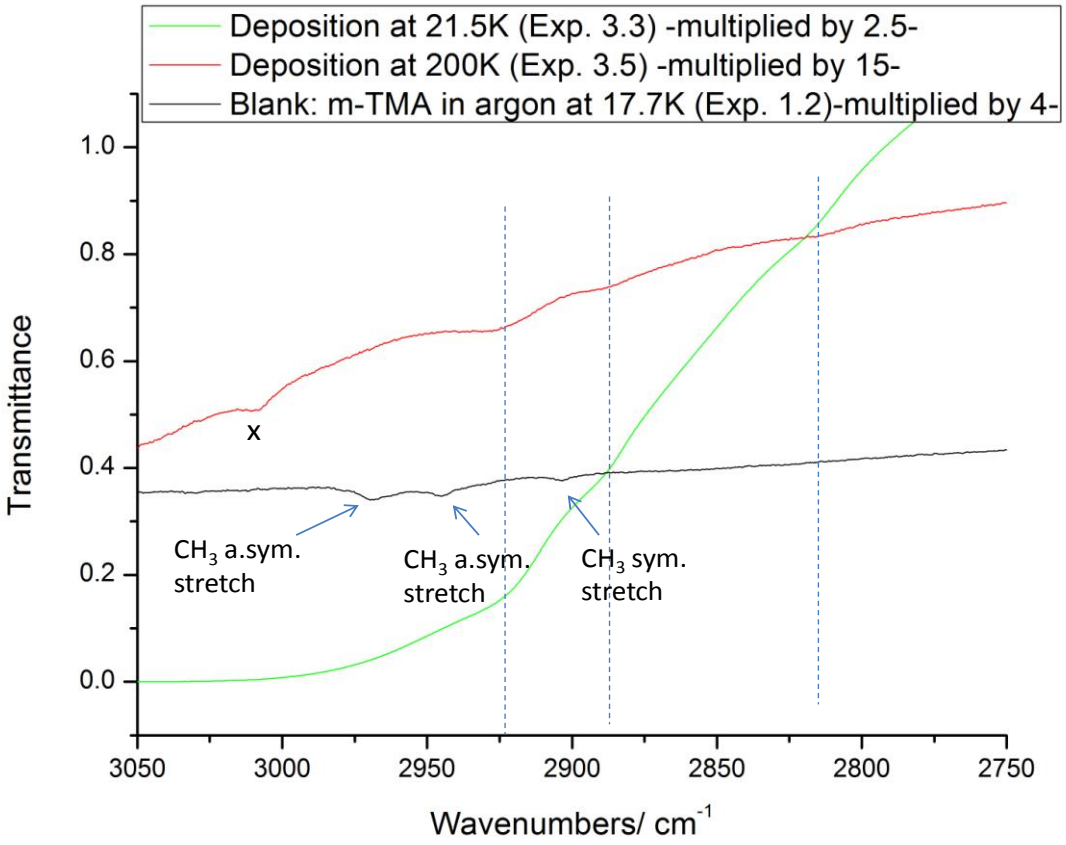

Figure 3.11: Infrared spectrum of co-deposited TMA and water at 21.5 K (Exp. 3.3) and at 200K (Exp. 3.5), compared with the spectrum of m-TMA in argon at 17.7 K (Exp. 1.2). The region presented here is between 3050 – 2750 cm^{-1}. The band attributed to methane is annotated with 'x'.

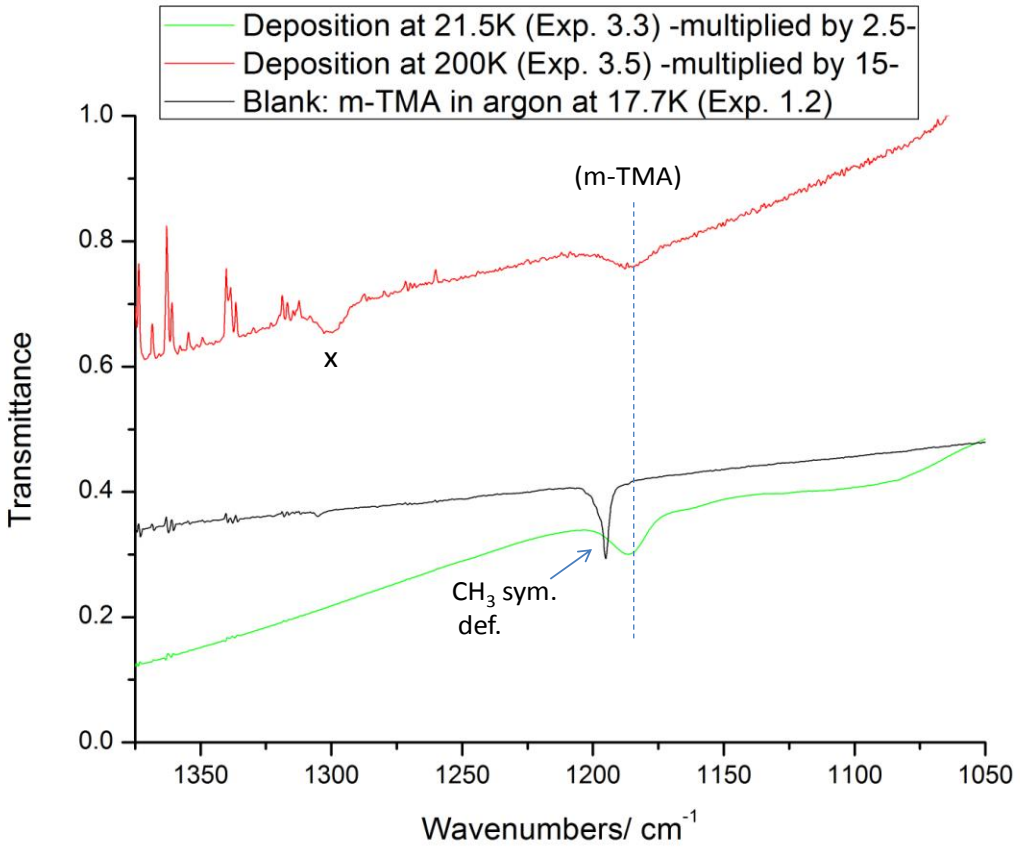

Figure 3.12: Infrared spectrum of co-deposited TMA and water at 21.5 K (Exp. 3.3) and at 200K (Exp. 3.5), compared with the spectrum of m-TMA in argon at 17.7 K (Exp. 1.2). The region presented here is between 1375 – 1050 cm^{-1}. The band attributed to methane is annotated with 'x'.

Table 3.7: Observed frequencies and assignments for m/d-TMA (Exp. 1.1 and 1.2) and main observed frequencies of Exp. 3.1, 3.2, 3.3 and 3.5 for the regions 3050 – 2750 cm^{-1} and 1375 – 1050 cm^{-1}.

Vibrational modes	**m-TMA**	**d-TMA**	**Exp. 3.1**	**Exp. 3.2**	**Exp. 3.3**	**Exp. 3.5**
ν_{11} CH_3 a. sym. str.	2968		2926	-	2922*	2925

CH_3 a. sym. stretch		(2958)				
ν_7 CH_3 a. sym. Str.	2947		2887		(2887)	2887
ν_{12} CH_3 sym. Stretch	2903		2815		(2814)*	2814
CH_3^b sym. def.		1249	1246	1245		
CH_3^t sym. def.		1237 vw	1237sh			
ν_{14} CH_3 sym. def.	1195		1186	1186	1186	1186
CH_3^t sym. def.		1199 1202				
Additional unassigned bands			1094 1083 1031			
CH_4 ν_3		-	3009	3009	-	3009
CH_4 ν_4	1305	1305	1301	1299	-	1300

Table 3.8: Integration values of the absorbance of the main peaks observed on the spectra of Exp. 3.1 and 3.2.

Exp. 3.1		**Exp. 3.2**	
Peak Position (cm^{-1})	Intensity (Abs. Units)	Peak Position (cm^{-1})	Intensity (Abs. Units)
3009	1.026	3009	0.378
2926	1.011		
2887	0.076		
1301	1.065	1299	0.315
1246, 1237	**0.559**	**1245**	**0.123**
1186	**0.919**	**1186**	**0.192**
1094	0.057		
1083	0.034		

Table 3.9: Integration values of the absorbance of the main peaks observed on the spectra of Exp. 3.3 and 3.5.

Exp. 3.3		**Exp. 3.5**	
Peak Position (cm^{-1})	Intensity (Abs. Units)	Peak Position (cm^{-1})	Intensity (Abs. Units)
		3009	0.228
2922	0.842	2925	0.398
		2887	0.050
1186	**1.050**	**1186**	**0.387**
		1300	0.510

Table 3.10: The A_m/A_d ratios of Exp. 1.1, 2.2, 3.1 and 3.2 based on the absorbance of the peak ~1195 cm^{-1} for m-TMA and the peak ~1249 cm^{-1} for d-TMA

Experiment	**A_m/A_d**	**m-band (cm^{-1})**	**d-band (cm^{-1})**
1.1	15.8	1195 (+d: 1202, 1199)	1249
2.2	47.1	1196	1253
3.1	1.6	1186	1246, 1237
3.2	1.6	1186	1245

*In Exp. 1.1 the whole area including the peaks at 1195, 1199 and 1202 cm^{-1} was integrated.

Table 3.11: The A_m/A_{CH_4} and A_d/A_{CH_4} ratios of all experiments presented in this study based on the absorbance of the peak ~1195 cm^{-1} for m-TMA, the peak ~1249 cm^{-1} for d-TMA and the absorbance of the peak ~ 1305 cm^{-1} for CH_4.

Experiment	A_m/A_{CH_4}	m-band(cm^{-1})	A_d/A_{CH_4}	d-band (cm^{-1})
1.1	145.3	1195 (+d: 1202, 1199)	9.2	1249
1.2	41.8	1195	-	-
2.1	16.1	1196 (1190 sh)	-	-
2.2	8.9	1196	0.2	1253
3.1	0.9	1186	0.5	1246, 1237
3.2	0.6	1186	0.4	1245
3.3	-	1186	-	-
3.5	0.8	1186	-	-

*Integration of absorbance peak of CH_4 at 1305 cm^{-1} for Exp. 1.1, 1.2, 2.1 and 2.2 and ~1300 cm^{-1} for Exp. 3.1, 3.2, 3.3 and 3.5.

**In Exp. 1.1 the whole area including the peaks at 1195, 1199 and 1202 cm^{-1} was integrated.

3.3 Conclusions

Although thermal annealing of the matrix of TMA and water co-deposited in argon (Exp. 2.1 and 2.2) did not produce the desired results (that is, no changes were observed, meaning that no further reaction took place), some spectral changes were observed when water was introduced to the system, compared to the TMA deposition in argon (Exp. 1.2). These differences were attributed either to an early, weak interaction of a water molecule with a TMA molecule or to the perturbation of the packing in the matrix because of the presence of a significant percentage of water.

However it should be noted that it was the first time that CH_4 was observed in matrix isolation experiments containing water and TMA in argon using a twin-jet system that allows only a brief mixing and reaction time before deposition.

When TMA and water were co-deposited without using argon, the evolution of CH_4 was predominant (Exp. 3.1 and 3.3). Increasing the deposition temperature from ~20 K to 100 K (Exp. 3.2) or 200 K (Exp. 3.5) shows an even higher evolution of CH_4. This observation led to the conclusion that increasing the lifetime of the liquid transition state of the two streams by increasing the T_{dep} could allow the reaction to proceed and trap different intermediates.

Unfortunately characterization of the trapped species was not possible, because we were unable to see most regions of the spectrum due to saturation and scattering effects in regions where it was most likely to observe and identify characteristic bands of new species. Surprisingly in this series of experiments, TMA and water did not react after thermal annealing; leading to the hypothesis that perhaps when the two reagents are both in the solid state they do not react with one another.

Table 3.11 presents a comparison of the A_m/A_{CH_4} and A_d/A_{CH_4} in all experiments (using the same bands), showing a gradual increase in the evolution of CH_4 as we move from a system were no water was added (only traces of atmospheric water vapour), to a system containing a small percentage of water in argon, and finally to a system containing a high percentage of water (without argon as a matrix material).

Unfortunately, under the current experimental conditions and with the current equipment, it was not possible to achieve total elimination of the rotational features of small molecules like atmospheric CO_2 and water. Removal of these traces is very difficult, but it could perhaps be achieved by replacing certain parts of the vacuum system and sealing all the joints perfectly. Working at high resolution (0.5 cm^{-1}) increases the noise of the spectrum. To reduce the noise, a high number of scans was required. It is the long running time of each individual experiment that limits the optimization of these parameters.

Additionally, other improvements might be possible, such as using an automated system to regulate the deposition flow rate and consequently control the concentration of the reagents in the matrix. The pressure control was performed manually in the present experiments, so the concentration of the reagents was unknown (TMA) or estimated roughly (water).

Finally, it has to be stated that each experiment is unique and it was impossible to reproduce exactly the same experiment under identical conditions. The factors that add to the limitations of the method were: being able to reproduce an experiment with the exact same concentration of reactants and the exact same material deposited on the window each time (e.g. the position of the radiation shield was manually adjusted before each experiment and a few cm could make a huge difference on the material deposited), the exact same temperature of the interior window (deposition at the lowest temperature could vary from temperatures between 17 to 23K, as the lowest achievable temperature was dependent on the system since the system had to be taken down and reassembled each time), keeping the same the pressure

in the system as this could depend on many factors (e.g. the whole system had to be disassembled and cleaned after each experiment and then reassembled; screwing all the different parts together was done manually), evacuation of the entire system or even the atmospheric conditions (e.g. humidity). For all these reasons, it is hard to comment on the reproducibility of each experiment separately, but performing a series of experiments varying deliberately specific parameters each time led to the observations of specific patterns that can definitely be used to extract useful information and conclusions.

3.4 Additional Information

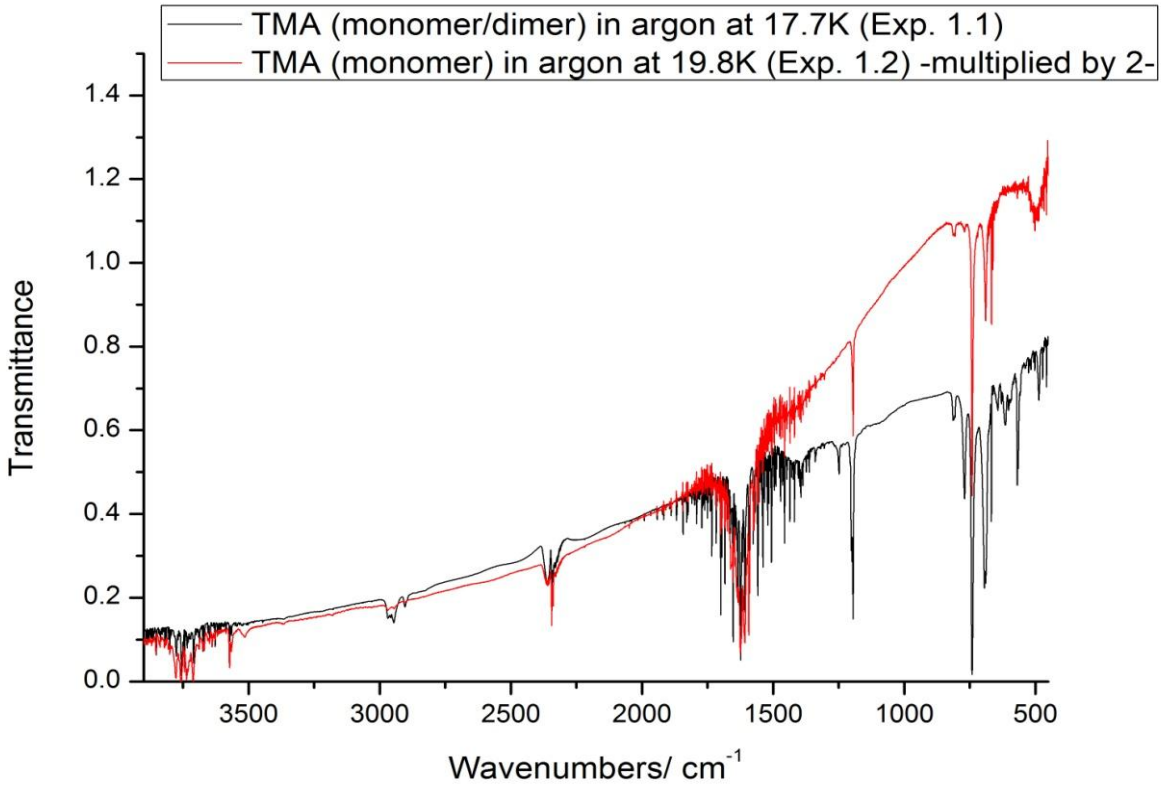

Figure 3.13: Infrared spectra of m-TMA (Exp. 1.2) in argon compared with m-/d-TMA in argon (Exp. 1.1).

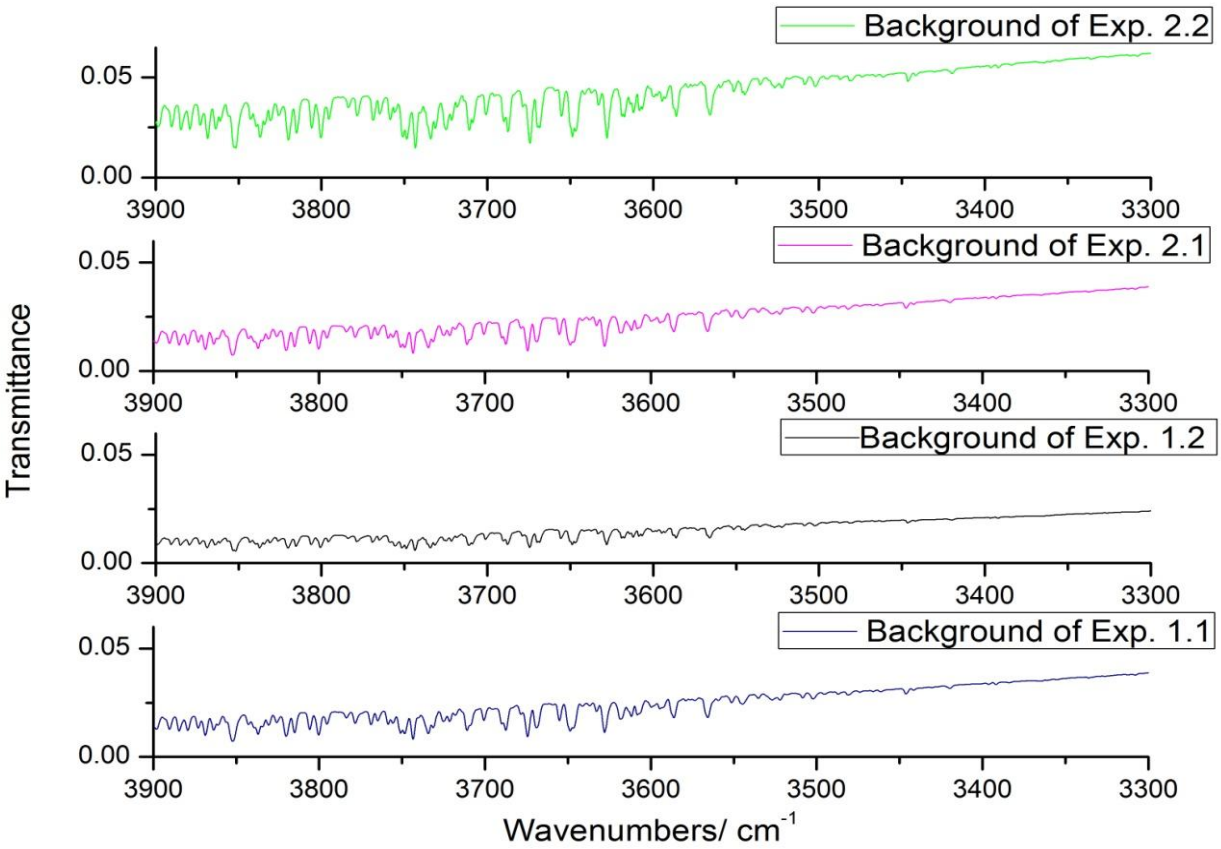

Figure 3.14: Infrared spectra of the background of Exp. 1.1 (20 mbar of argon), Exp. 1.2 (20 mbar of argon), Exp. 2.1 (20 mbar of 1% water mixture in argon) and Exp. 2.2 (20 mbar of a 0.15% water mixture in argon). The region presented here is 3900-3300 cm^{-1}.

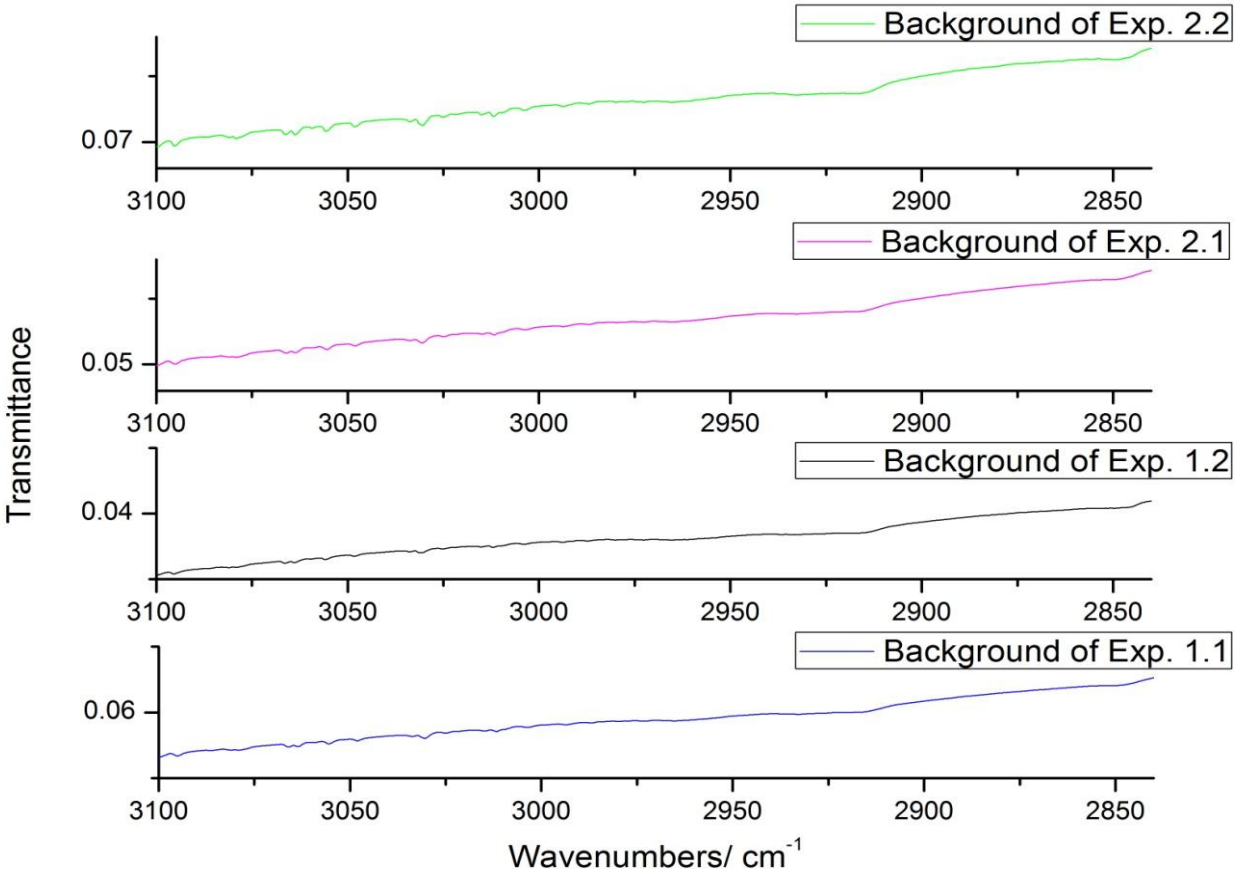

Figure 3.15: Infrared spectra of the background of Exp. 1.1 (20 mbar of argon), Exp. 1.2 (20 mbar of argon), Exp. 2.1 (20 mbar of 1% water mixture in argon) and Exp. 2.2 (20 mbar of a 0.15% water mixture in argon). The region presented here is 3100-2840 cm^{-1}.

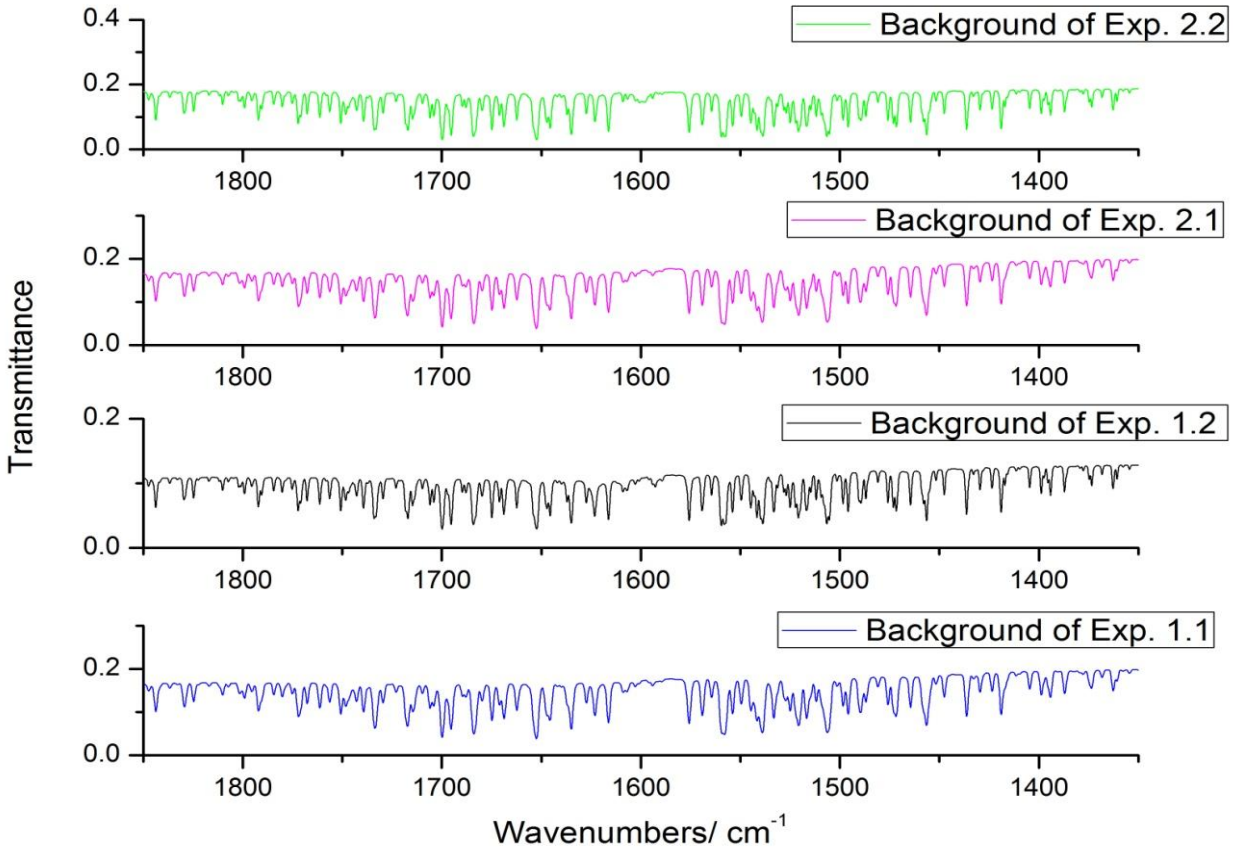

Figure 3.16: Infrared spectra of the background of Exp. 1.1 (20 mbar of argon), Exp. 1.2 (20 mbar of argon), Exp. 2.1 (20 mbar of 1% water mixture in argon) and Exp. 2.2 (20 mbar of a 0.15% water mixture in argon). The region presented here is 1850-1350 cm^{-1}.

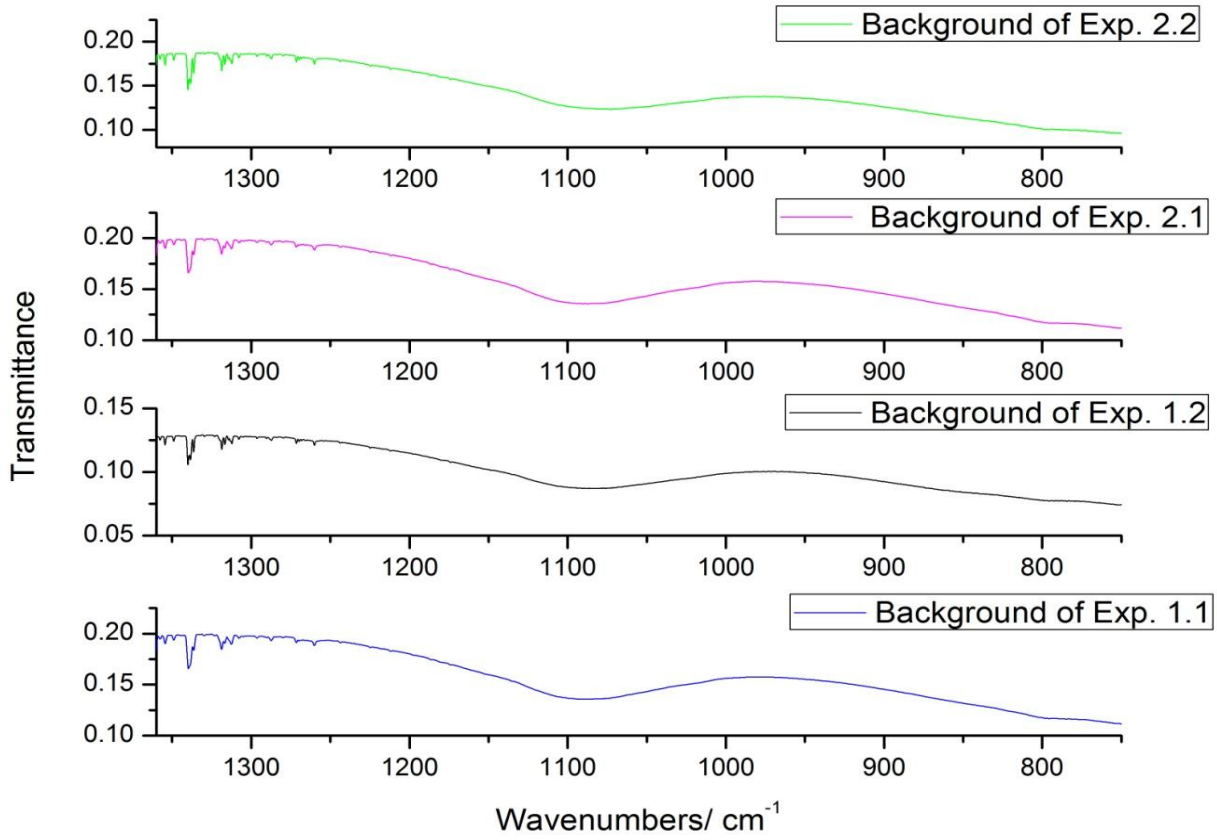

Figure 3.17: Infrared spectra of the background of Exp. 1.1 (20 mbar of argon), Exp. 1.2 (20 mbar of argon), Exp. 2.1 (20 mbar of 1% water mixture in argon) and Exp. 2.2 (20 mbar of a 0.15% water mixture in argon). The region presented here is 1360-750 cm^{-1}.

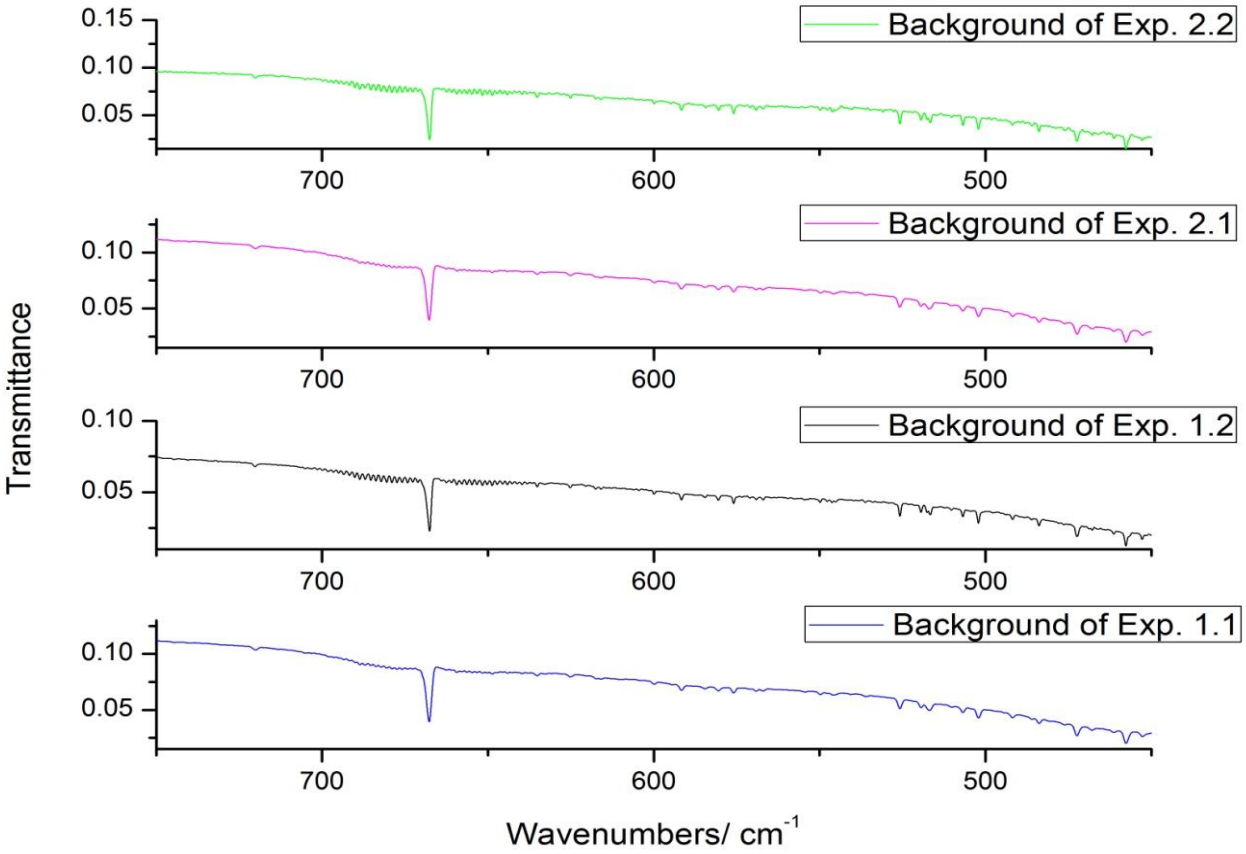

Figure 3.18: Infrared spectra of the background of Exp. 1.1 (20 mbar of argon), Exp. 1.2 (20 mbar of argon), Exp. 2.1 (20 mbar of 1% water mixture in argon) and Exp. 2.2 (20 mbar of a 0.15% water mixture in argon). The region presented here is 750-450 cm^{-1}.

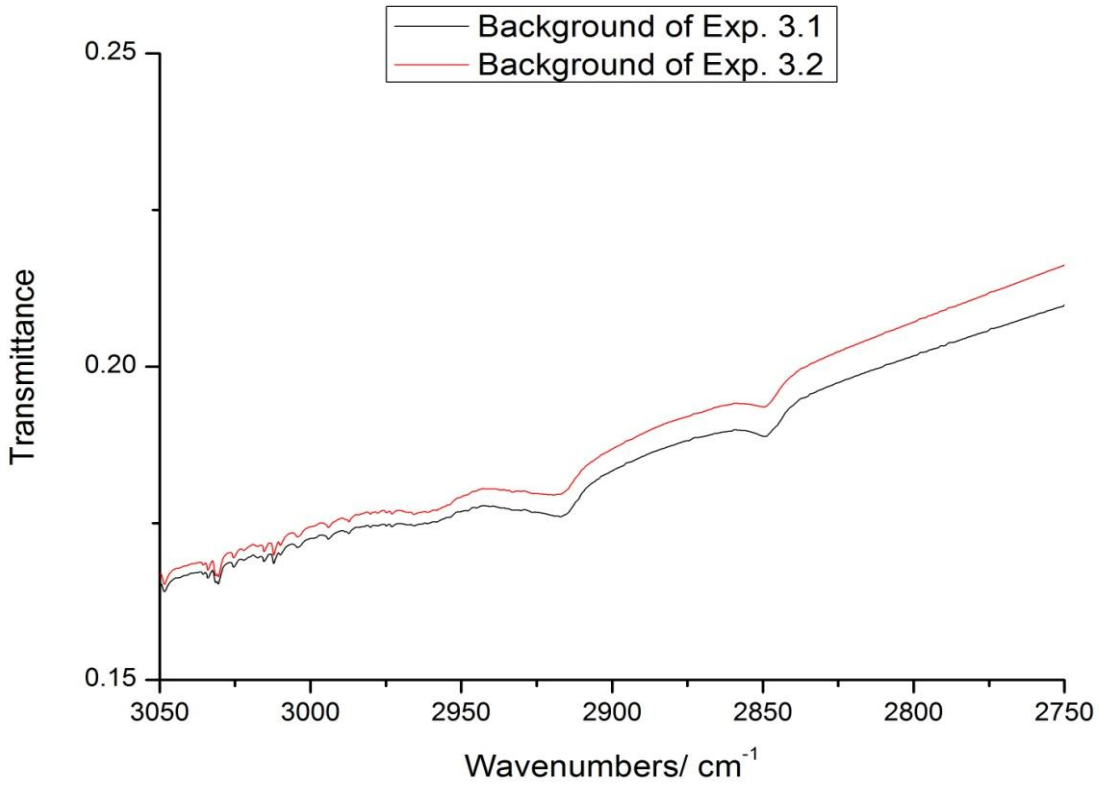

Figure 3.19: Infrared spectra of the background of Exp. 3.1 (IR window at 17.6 K) and the background spectrum of Exp. 3.2 (IR window at 100 K). The background of Exp. 3.2 is exactly the same as the one of Exp. 3.3 and 3.5. The region presented here is 3050-2750 cm^{-1}.

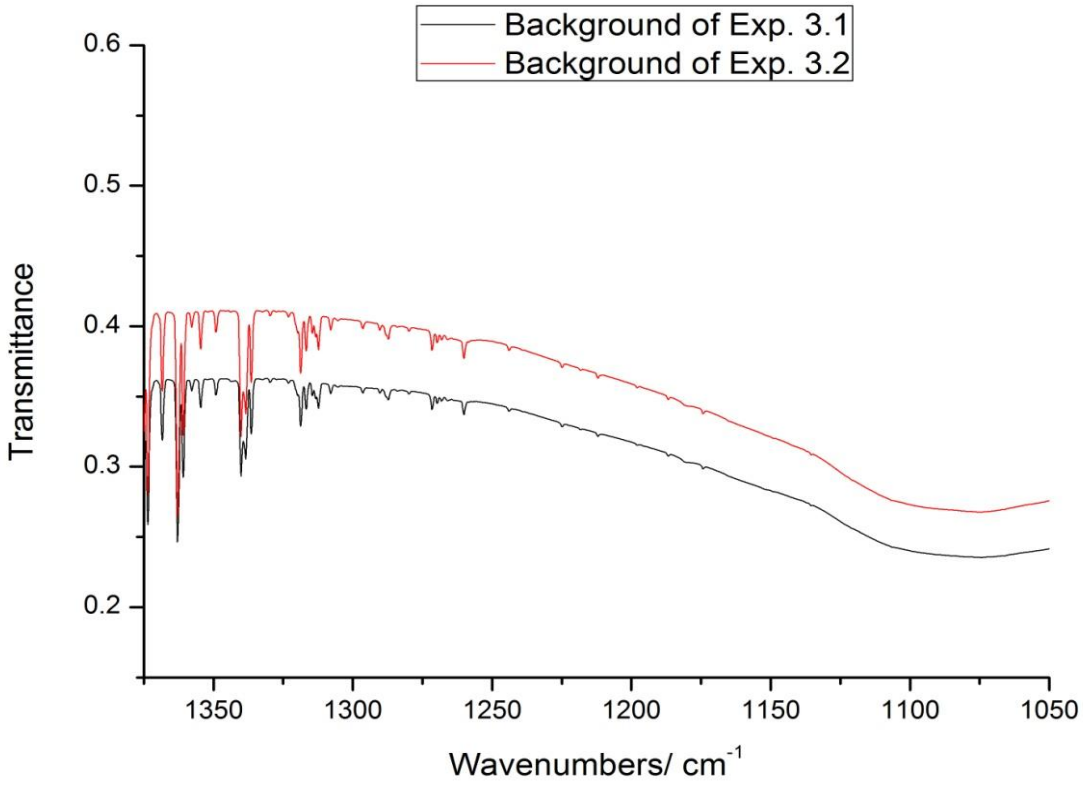

Figure 3.20: Infrared spectra of the background of Exp. 3.1 (IR window at 17.6 K) and the background of Exp. 3.2 (IR window at 100 K). The background of Exp. 3.2 is exactly the same as the one of Exp. 3.3 and 3.5. The region presented here is 1375-1050 cm^{-1}.

3.5 Experimental

3.5.1 General Method

All experiments were carried out in a stainless vacuum system, equipped with a Divac pump and a turbopump (Leybold BMH70) (Part A, Figure 3.21), reaching pressures of 10^{-6} mbar at the gauge (near the pump system). The Divac pump was running constantly, and the turbopump was turned on one day before the beginning of a new experiment to achieve evacuation of the entire system to the minimum possible pressure (and both pumps kept on during the experiments). The pressure was recorded at the beginning of each experiment. The gas handling system was constructed using Swagelok fittings and stainless steel pipes. A helium pump (closed cycle cryostat) was used, operating at temperatures down to 17-22 K.

Matrix samples were deposited onto the cold interior window (CsI) of the IR cell. The two external windows of the cell were KBr windows (see Figure 3.22). The temperature at the cold CsI window was measured by a thermocouple and controlled by a 1 W heating system, when higher temperatures than 17-22 K were required, during thermal annealing or deposition of the reagents at higher temperatures. The temperature was measured with an accuracy of ± 3 K (Part E). The cold cell assembly fits into the chamber (called 'sample chamber') of a Bruker IR spectrometer (IFS-66 operated by the OPUS v6.0 software) in order to record IR spectra during the experiments.

Figure 3.21 presents a simple schematic diagram of the most important parts of the matrix isolation system. During deposition the upright section of the cryostat was placed perpendicular to the deposition line coming from the TMA sample can; in this way the interior CsI window had the position presented in the left image of Figure 3.22. When it was time to record an IR spectrum of the matrix deposited on the window, the cryostat was rotated in order the interior CsI window to face the IR beam path (right image on Figure 3.22).

Argon was kept in a stainless steel tank (part J in Figure 3.21) equipped with a pressure gauge (part I) to determine the total amount and a needle valve (part H) to control the deposition rate of argon during every experiment (argon passed through a column of P_2O_5 before transferring to the tank to remove any traces of water). In experiments where an argon matrix (or a mixture of water/argon) was used, a small amount, associated with a pressure drop of 20 mbar in the tank, was deposited onto the cold window. Although, argon was coming from a needle valve of a small diameter (2 mm), it coated the whole window (which

had a diameter of 20 mm), along with the metal bracket that was holding the window. Quantification of the volume of the deposited gas (or other reagents) was not possible with the current equipment. After deposition of this small amount of argon, an IR spectrum was recorded as a background spectrum, which was also useful as a ‘check point’ to ensure that the gas spray was targeted correctly and that the system did not show excess levels of moisture or atmospheric contamination.

The interior of the spectrometer was constantly purged with dry nitrogen (constant pressure of ~750 mbar), and it was sealed as best as possible in order to provide a stable inert atmosphere.

Neat TMA was kept in a flask (part O) with a Young tap and connected to the vacuum system through a glass window attached onto the IR cell. The sample was pumped for three freeze-thaw cycles before each experiment to remove any volatiles and decomposition products like methane. A cooling bath was used to control the vapor pressure of TMA, before opening the tap and expose it to the vacuum. The tap of the TMA is much larger than the diameter of the argon needle, but a low deposition rate was maintained by controlling the temperature of the cooling bath.

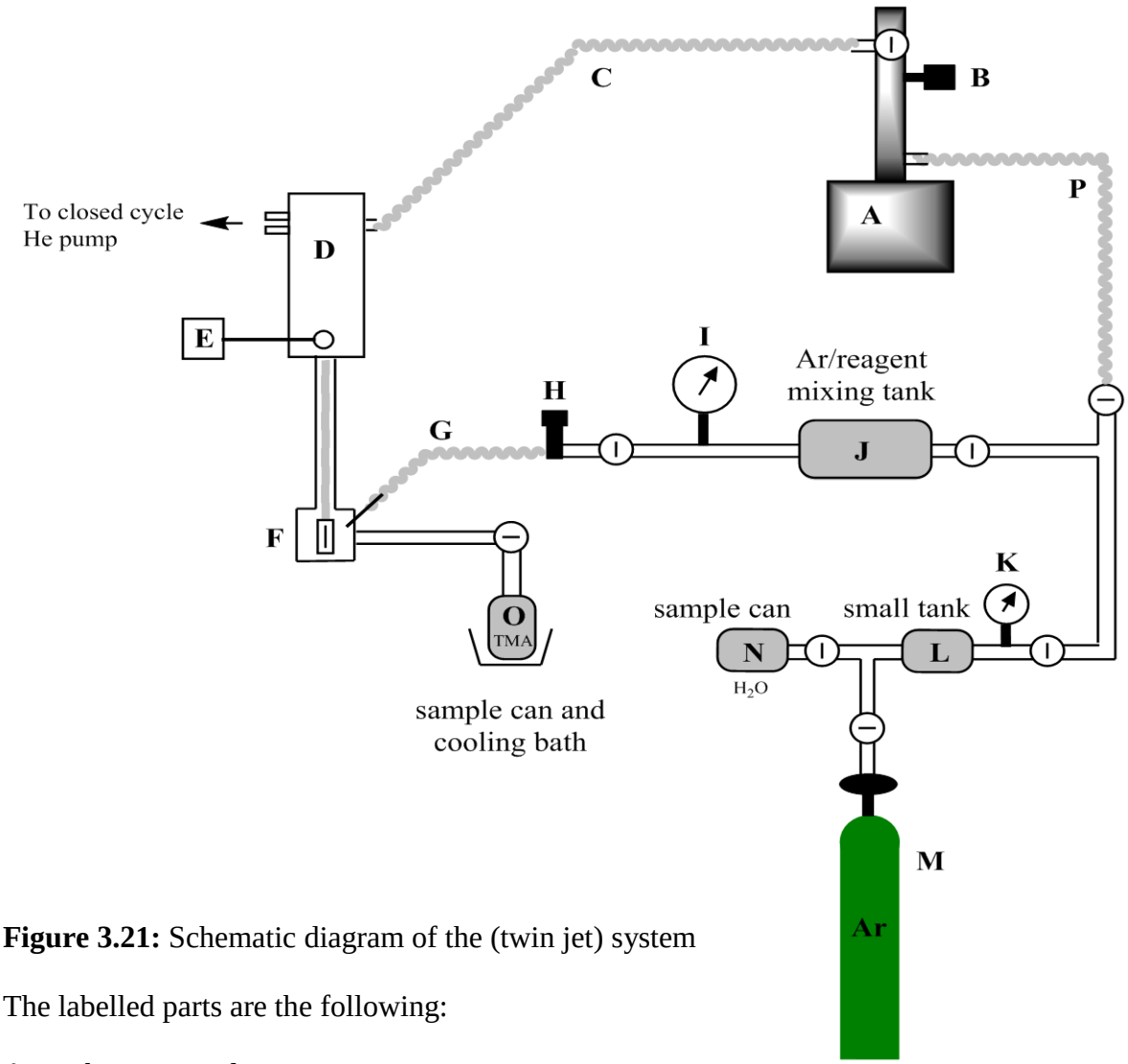

Figure 3.21: Schematic diagram of the (twin jet) system

The labelled parts are the following:

A: Turbopump and Divac pump

B: Digital pressure sensor (HV emission detector)

C: 0.5 cm internal diameter flexible pipe

D: Double stage He expander cryostat (arm extends down to sample chamber F)

E: Combination of digital thermometer and heater

F: Sample chamber (see Figure 3.22 for detailed structure)

G: 0.5 cm internal diameter flexible pipe

H: Needle valve to control sample spray pressure

I: Analog pressure gauge, 0-1000 mbar

J: 2250 cm^3 volume primary tank

K: Analog pressure gauge, 0-100 mbar

L: 40 cm^3 volume small tank

M: Argon gas supply (after the argon gas cylinder, a drying tube containing powdered P_2O_5 is attached, that is not drawn in this diagram)

N: sample can (for water)

O: sample can and cooling bath (for TMA)

and where ◯ is a tap.

In the experiments where the reaction of TMA and water in an argon matrix was studied, distilled water was used and kept in a flask (part N) with a Young tap and connected to the vacuum system for several freeze-thaw cycles. Water vapour was firstly introduced in a smaller tank (part L), ideal for fine measurements of gas pressures (ideal gas behavior was assumed for the calculation of gas mixtures by pressure) and the pressure was determined by a pressure gauge (part K), before mixing with argon in the main tank (part J). The water sample was also exposed to three freeze-thaw cycles before each experiment to remove any traces of O_2. Taps were used where noted to close off sections of the system during the mixing procedure.

For the experiments performed without inert gas, the water flask was exposed to the system's vacuum for 30 min in order to allow maximum diffusion into the tank. The two gas samples, TMA and argon or argon/water were co-deposited from the two different nozzles onto the window allowing only for brief mixing and short reaction time before deposition.

During deposition of any of the reagents (even during deposition of 20 mbar of argon) small increases in pressure were observed. It should be noted that pressure was measured only in the sections indicated in Figure 3.21.

After each deposition or thermal annealing the system was allowed to 'rest' for five minutes before recording the IR spectrum. High quality scans (1024-512 scans) were performed in the range of 4000 – 400 cm^{-1} with a resolution of 1 – 0.5 cm^{-1} for Exp. 1.1, 1.2, 2.1, 2.2 and a resolution of 0.5 cm^{-1} for Exp. 3.1, 3.2, 3.3 and 3.5. In each case the background was collected at the same resolution as the sample. The infrared spectra were collected using a deuterated triglycine sulphate (DTGS) detector, and a zero-filling factor of four (meaning that spectra of 0.5 cm^{-1} resolution contain 59156 data points).

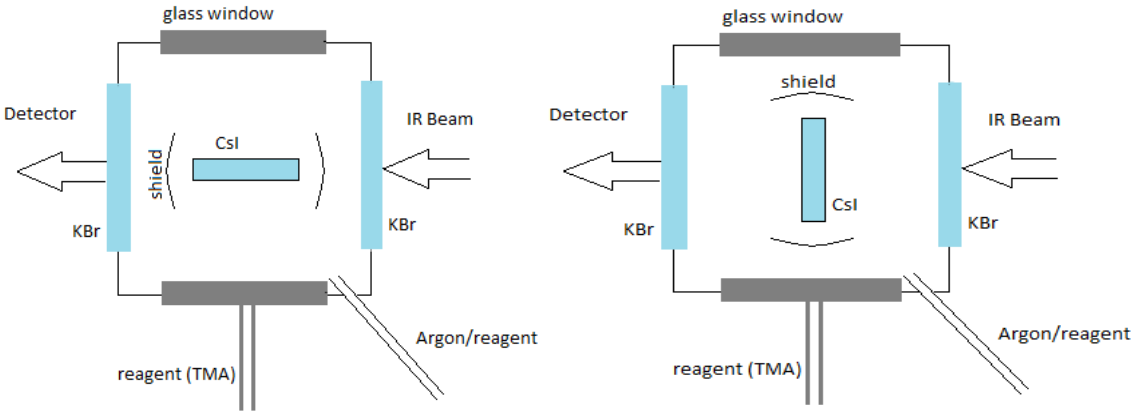

Figure 3.22: Left: Window position during deposition of the two streams. Right: Recording the IR spectrum

At the end of each experiment the sample chamber had to be disassembled and thoroughly cleaned. The CsI and the two KBr windows had to be polished. Deposition of the reagents without argon required several hours of polishing the windows. After cleaning, the system was reassembled and the Divac pump was kept on for several days, until reaching a satisfactory low pressure. Then, the turbopump could be turned on for 1 day before performing another experiment (the sensitivity of the turbopump would not allow usage when the system was under high pressure).

3.5.2 Deposition of TMA in Argon Matrix

Experiment 1.1

The system reached a pressure of 1.23×10^{-6} mbar and a temperature of 17.7 K before deposition of 20 mbar of argon. After argon deposition a background spectrum was recorded. Then, the TMA can was cooled down to −100±2 °C and exposed to the system vacuum. However, no traces of TMA were detected after the IR spectrum was recorded, meaning that no TMA was deposited at this temperature.

The same procedure was repeated for cooling temperatures at −60±2 °C and −35±2 °C. No TMA was deposited at −60 °C, but IR signals showed TMA deposition at −35°C. The deposition time (duration), exact temperature of the CsI window and pressure of the system for this deposition are summarised in Table 3.12.

It should be noted that during TMA deposition, argon was co-deposited on the CsI window (the argon tap was turned on and off before and after turning on and off the TMA tap). The amount of argon deposited during the successful attempt to deposit TMA onto the window is also present in Table 3.12.

Thermal annealing of the argon matrix containing TMA (monomeric and dimeric) was performed. The matrix was heated up to 32 K for 20 min, then cooled back down to 17.7 K before recording the IR spectrum. The same procedure was repeated for annealing up to 44 K and 54 K.

Experiment 1.2

The system reached a pressure of 1.55×10^{-6} mbar and a temperature of 20.4 K before deposition of 20 mbar of argon. After argon deposition a background spectrum was recorded. Then, the TMA can was cooled down to –47±2 °C and exposed to the system vacuum. The same procedure as in Exp. 1.1 was followed and the experimental conditions are summarised in Table 3.12.

Thermal annealing of the argon matrix containing TMA (monomeric) was performed. The matrix was heated up to 44 K for 30 min, and then cooled back down to 19.8 K before recording the IR spectrum. The same procedure was repeated for annealing up to 64 K and 74 K (the matrix was kept at 74 K for 1 h).

Table 3.12: Experimental conditions in experiments of deposition of TMA and TMA and water in argon matrix

Experiment	**1.1**	**1.2**	**2.1**	**2.2**
Deposition temperature/ K	17.7	19.8	17.9	17.1
Deposition time/ min	20	28	20	30
Argon/ mbar	60	300	200	200
Temperature of cooling bath/ °C (TMA flask)	–35±2	–47±2	–47±2	–47±2
Water/ mbar	-	-	2	0.3
Pressure/ mbar	1.30×10^{-6}	1.25×10^{-6}	9.9×10^{-7}	7.7×10^{-7}

3.5.3 Co-deposition of TMA and Water in Argon Matrix

Experiment 2.1

A 1% gas mixture of water in argon was prepared (e.g. 4 mbar of water were firstly introduced and measured in tank D, then approximately 200 mbar of argon were transferred to tank B; the 4 mbar of water in tank D were transferred to tank B, and tank B was topped up with argon up to 400 mbar).

The system reached a pressure of 8.9×10^{-7} mbar at 17.6 K, before deposition of 20 mbar of the 1% gas mixture of water in argon. After deposition of the mixture a background spectrum was recorded. Then, the TMA can was cooled down to −47±2 °C and exposed to the system vacuum. The deposition time (duration), exact temperature of the CsI window and pressure of the system for this deposition are summarised in Table 3.13.

During TMA deposition, the 1% gas mixture of water in argon was co-deposited on the CsI. The amount deposited is also present in Table 3.13.

Thermal annealing was performed: the matrix was heated up to 44 K, 54 K, 64 K and 80 K and kept for 40 min in each one of these temperatures. After every annealing the matrix was cooled down to 17.9 K and an IR spectrum was recorded. The matrix was kept at 17.9 K overnight, and an IR spectrum was recorded the next day, followed by thermal annealing at 80 K for 4 h and recording of the IR spectrum after cooling back down to 17.9 K.

Experiment 2.2

The same procedure was followed for this experiment, as in Exp. 2.1 with the only difference that a 0.15% gas mixture of water in argon was prepared. The system reached a pressure of 8.9×10^{-7} mbar at 17.7 K, before deposition of 20 mbar of the 0.15% gas mixture of water in argon.

The matrix was annealed to 82 K for 1 h, and the IR spectrum was recorded after cooling it down to 17.1 K.

3.5.4 Co-deposition of TMA and Water (without inert gas)

Experiment 3.1

The system reached a pressure of 1.05×10^{-6} mbar at 19.6 K, before recording the background spectrum of the empty cell (without any material deposited).

20 mbar of water vapour were transferred to tank D, and the TMA can was cooled down to −47±2 °C. Then, the TMA and water vapour were co-deposited on the cold interior window, by exposing them to the system vacuum. The exact experimental conditions during the deposition are reported in Table 3.13.

The matrix was anneal to 200 K for 20 min, and to 274 K for 25 min and the IR spectrum was recorded after cooling it down to 17.6 K.

Experiment 3.2

The system reached a pressure of 2.9×10^{-6} mbar at 21 K. Then the cold window was warmed up to 100 K by using the 1 W heating system. When the temperature reached 100 K, the pressure was 2.48×10^{-6} mbar. The IR spectrum of the empty cell was recorded at this temperature, and used as a background spectrum.

Then, the same experimental procedure was followed as in Exp. 3.1; the conditions are summarized in Table 3.13.

The matrix was annealed to 150 K, 200 K and 250 K and kept for 20 min in each one of these temperatures. After every annealing the matrix was cooled down to 100 K and an IR spectrum was recorded.

Experiment 3.3

The system reached a pressure of 2.67×10^{-6} mbar at 21.8 K before recording the background spectrum of the empty cell.

Then, the same experimental procedure was followed as in Exp. 3.1; the conditions are summarized in Table 3.13.

Experiment 3.5

The system reached a pressure of 3.0×10^{-6} mbar at 22.4 K. Then the cold window was warmed up to 200 K by using the 1 W heating system. When the temperature reached 200 K, the pressure was 3.1×10^{-6} mbar. The IR spectrum of the empty cell was recorded at this temperature, and used as a background spectrum.

Then, the same experimental procedure was followed as in Exp. 3.1; the conditions are summarized in Table 3.13.

Table 3.13: Experimental conditions in experiments with co-deposition of TMA and water

Experiment	**3.1**	**3.2**	**3.3**	**3.5**
Deposition temperature/ K	17.6	100	21.5	200
Deposition time/ min	15	15	15	15
Temperature of cooling bath/ °C (TMA flask)	–47±2	–47±2	–47±2	–47±2
Water/ mbar	8	8.5	10	9
Pressure/ mbar	1.01×10^{-6}	2.53×10^{-6}	2.68×10^{-6}	3.10×10^{-6}

References

1. A. J. Barnes, W. J. Orville-Thomas, A. Müller, R. Gaufres, *Matrix Isolation Spectroscopy*, D. Reidel Publishing Company, Dodrecht, Holland, 1981.
2. H. E. Hallam, *Vibrational Spectroscopy of Trapped Species*, Wiley. Bristol, England, 1973.
3. C. N. Banwell, E. McCash, *Fundamentals of Molecular Spectroscopy, Fourth Edition*, McGraw-Hill Publishing, Avon, Great Britain, 1994.
4. L. Iverson, PhD Thesis A Study of Inter- and Intramolecular Interactions through Neutron Compton Scattering and Low Temperature Matrix Isolation Infrared Spectroscopy, University of East Anglia, 2014.

5. L. Iverson, M. Sc. By research Thesis, Natural Isotope abundance using Infrared Spectroscopy, University of East Anglia, 2009.
6. S. Kvisle, E. Rytter, *Spectrochim. Acta*, **1984**, *40A*, 939.
7. S. Kvisle, E. Rytter, *J. Mol. Struct.*, **1984**, *117*, 51.
8. A. P. Gray, A. B. Callear, F. H. C. Edgecombe, *Can. J. Chem*., **1963**, *41*, 1502.
9. A. P. Gray, *Can. J. Chem*., **1963**, *41*, 1511.
10. T. Ogawa, K. Hirota, T. Miyazawa, *Bull. Chem. Soc. Japan*, **1965**, *38*, 1105.
11. T. Ogawa, *Spectrochim. Acta*, **1968**, *24A*, 15.
12. E. G. Hoffmann, *Z. Elektrochem*., **1960**, *64*, 616.
13. T. Onishi, T. Shimanouchi, *Spectrochim. Acta*, **1964**, *20*, 325.
14. A. Almenningen, S. Halvorsen, A. Haaland, *Acta Chem. Scand.*, **1971**, *25*, 1937.
15. R. J. O' Brien, G. A. Ozin, *J. Chem. Soc. A*, **1971**, *9*, 1136.
16. E. B. Wilson, J. C. Decius, P. C. Cross, *Molecular Vibrations*, McGraw-Hill, New York, 1955.
17. J. R. Durig, K. K. Chatterjee, *J. Raman Spectrosc*., **1981**, *11*, 168.
18. B. S. Ault, J. L. Laboy, *J. Mol. Struct*., **1999**, *475*, 193.
19. B. S. Ault, *J. Organomet. Chem*., **1999**, *572*, 169.
20. B. S. Ault, *J. Phys. Chem*., **1994**, *98*, 77.
21. R. Sanchez, C. Arrington, C. A. Arrington, *J. Am. Chem. Soc*., **1989**, *111*, 9110.
22. S. Balasubramanian, C. J. Mundy, M. L. Klein, *J. Phys. Chem. B*, **1998**, *102*, 10136.
23. H. Phan, Master Thesis, Infrared Matrix Isolation Studies of Trimethylaluminium with Ozone, HoChiMinh City University of Pedagogy, 2004.
24. A. Chamberland, R. Belzile, A. Cabana, *Can. J. Chem*., **1970**, *48*, 1129.
25. F. H. Frayer, G. E. Ewing, *J. Chem. Phys*., **1968**, *48*, 781.
26. L. H. Jones, S. A. Ekberg, B. I. Swanson, *J. Chem. Phys*., **1986**, *85*, 3203.
27. M. G. Govender, T. A. Ford, *J. Mol. Struct*., **2000**, *550-551*, 445.
28. R. P. Bell, H. C. Longuet-Higgins, *Proc. R. Soc*., **1945**, *183A*, 357.
29. G. P. Ayers, A. D. E. Pullin, *Spectrochim. Acta*, **1976**, *32A*, 1629.
30. G. P. Ayers, A. D. E. Pullin, *Spectrochim. Acta*, **1976**, *32A*, 1695.
31. R. M. Bentwood, A. J. Barnes, W. J. Orville-Thomas, *J. Mol. Spectrosc*., **1980**, *84*, 391.

Chapter 4

Quantification of Lewis Acidic Sites of Methylaluminoxane (MAO) by NMR Spectroscopic Techniques

4.1 Introduction

4.1.1 Determination of TMA in MAO

NMR spectroscopy (^{1}H, ^{13}C or ^{27}Al) reveals the existence of residual TMA in commercial MAO solutions in toluene[1-2]. However, there are several different theories in the existing literature on the interaction of TMA with MAO, distinguishing between two forms: 'free' TMA and 'bound' or 'associated' TMA. 'Free' TMA can be removed when the MAO solution is dried under vacuum, but 'bound' TMA can be removed only by a chemical reaction.[3-7] The possibility of occlusion of a TMA molecule inside an MAO cage has also been suggested, which could explain why TMA is not quantitatively removed under vacuum.[3,8] In general the following equilibrium has been proposed:[9-11]

$$(AlOMe)_n + (m/2)\ (AlMe_3)_2 \rightleftharpoons (AlOMe)_n \bullet (AlMe_3)_m \qquad (4.1)$$

'Free' TMA exists as a dimer in toluene solutions, as it would have been expected (see Chapter 2 and 3 for detailed information on TMA). This is proved by low temperature NMR studies (^{1}H and ^{13}C); the signal attributed to TMA splits into two different signals upon cooling the MAO solution (–70°C), one attributed to the terminal methyl (Me) groups and one attributed to the bridging Me groups, with the latter moving downfield. Talsi and co-workers stated that these signals correspond to the 'free' TMA, and it is likely that 'bound' TMA signals are 'hidden' in the area of the broad MAO resonance.[2]

Tritto and co-workers claim that TMA is mainly bound on MAO; their investigations were focused on low temperature NMR experiments, and suggested that the line broadening of the 'sharp' Al-Me signal consists of contributions from both free and bound or exchanging TMA with MAO.[12] On the other hand, Ystenes *et al.* reported that there is no reaction between TMA and TMA-depleted MAO. This conclusion was based on IR spectroscopic

studies that showed that the spectrum of TMA-depleted MAO and the spectrum of TMA are superimposable when the IR spectrum of a TMA-depleted MAO solution after addition of TMA is recorded. Had there been some reaction between MAO and TMA, additional changes in the IR spectrum would have been anticipated.[13-14]

^{1}H NMR spectroscopic studies by Fabio Ghiotto in our research group revealed that upon addition of the donors $OPPh_3$, PMe_3 and PCy_3 polymeric MAO precipitates which contains about 1/4 of the total TMA content. This amount is attributed to the 'bound' TMA, while the rest 3/4 of the total TMA, the 'free' TMA, remain in the supernatant phase. This conclusion was also confirmed by pulsed field gradient spin echo NMR measurements by Nicole Lühmann at the Research Centre Jülich.[15]

Determination of the TMA content in MAO solutions, either in its 'free' or 'bound' state, is a very important step for the characterization of MAO that would lead to a better understanding of the catalytic properties of MAO. The influence of TMA content on catalyst activity is described in detail in the next chapter. Although various research groups have developed different methods to measure the TMA content, a systematic comparison between them has not been made. For this reason, the present research study was focused on developing a reliable and reproducible method of determining the TMA content of commercial MAO solutions in toluene, and comparing the various methods that have been reported so far.

Two main direct methods have been reported in literature: titration of an MAO solution with pyridine using phenazine as an indicator[16] and ^{1}H NMR spectroscopy. Pyridine complexes TMA and provides an easy and fast method for measuring the TMA content. However, pyridine also reacts with MAO sites that possess some Lewis acidity, leading to apparently higher TMA values.[17]

This research was focused on the second method, ^{1}H NMR spectroscopy. The overlapping of MAO and TMA signals does not allow direct quantification of the TMA content in MAO solutions in toluene by NMR. However, as it has been already reported[17], addition of excess THF to the MAO solution complexes TMA; dimeric TMA will break to monomeric TMA bonded to a THF molecule, according to the equilibrium:

$$(AlMe_3)_2 + 2\ THF \rightleftharpoons 2\ (THF \bullet AlMe_3) \qquad (4.2)$$

Computational studies by Tossell[18] have also shown that the bond between THF and TMA and polyhedral methylaluminoxanes is so strong that will complex all the TMA liberated, by decomposing any aluminoxane–TMA complexes. The peak attributed to TMA after complexation with THF becomes sharper and moves to higher field, allowing integration and quantification by NMR. Imhoff *et al*[17]. integrated the TMA peak after addition of THF to an MAO solution by curve fitting on both sides of the peak to remove the broad MAO resonance. The ratio of total Al to THF was 1/4, although the influence of the quantity of the THF added has not been explored.

The present research focuses on the determination of the TMA content of commercial MAO solutions after addition of THF or other Lewis bases like pyridine and investigates the influence of the ratio of these bases to the total Al.

4.1.2 Other Lewis Acidic Sites on MAO

Apart from the TMA content of MAO samples, further information about the structural characteristics of MAO is needed. Since MAO is an important activator in olefin polymerization, determining the nature of the species (within the MAO framework) involved in catalyst activation is crucial.

Many researchers have tried to identify the Lewis acidic sites that MAO contains, which are responsible for catalyst activation. Talsi and his co-workers[19] performed EPR measurements after addition of 2,2,6,6-tetramethylpiperidine-N-oxyl (TEMPO) to MAO. TEMPO coordinated to two types of acidic sites which were identified as $-OAlMe_2$ and $-O_2AlMe$, where Al is unsaturated. Quantitative EPR showed that one Lewis acidic site corresponds to every 100 ± 30 Al atoms, meaning that not every oligomeric MAO molecule contains an acidic site.

The formation of cationic species, $[AlMe_2]^+$, during the interaction of MAO with metallocene catalyst precursors, has been discussed in a recent patent proposing that these cations are responsible for/ or improve the activation efficiency of MAO.[20] This follows a previous study by Klosin and co-workers, who synthesized $[AlMe_2(OEt_2)_2]^+$ salts and used them as catalyst activators.[21-22] However, as proven, non-solvated $[AlMe_2]^+$ cations are extremely unstable and reactive.[23]

4.2 Results and Discussion

4.2.1 VT NMR Studies of an MAO Solution in Toluene

The ^{1}H NMR spectrum of an MAO solution in toluene consists of a broad signal at δ 0 to –0.6, and a sharper peak at δ –0.30, which is attributed to the TMA present in the solution, either as 'free' or 'bound'. When the temperature was decreased the TMA signal becomes broader (–20 °C), and eventually splits into two signals at temperatures below – 40 °C. The two signals are attributed to the terminal Me groups of Al_2Me_6 (δ –0.54, labeled T) and to the bridging Me groups of Al_2Me_6 (δ 0.11, labeled B) at –70 °C (see Figure 4.1). These observations come in agreement with the existing literature.[1-2,24]

Although it is possible to see the ^{1}H NMR signal attributed to the TMA in an MAO sample, quantification of the TMA content by integration of the peak is impossible because it overlaps with the MAO signal.

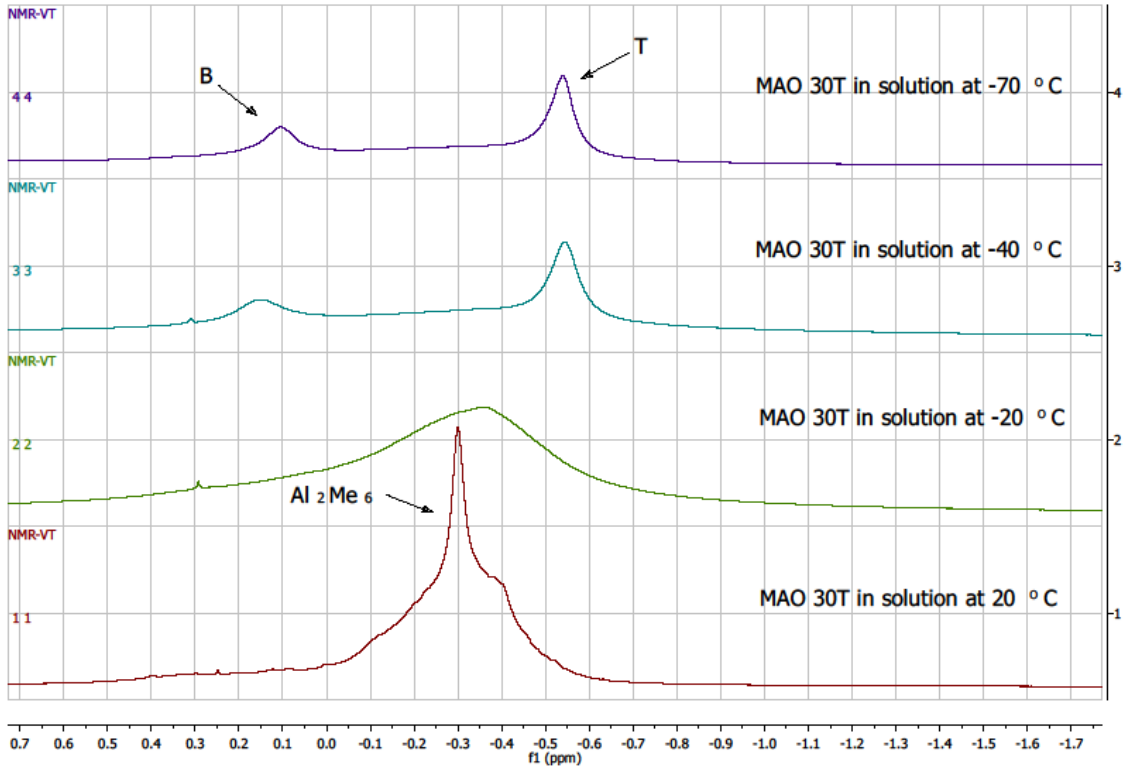

Figure 4.1: ^{1}H NMR spectra of an MAO solution in toluene from 20 °C (bottom spectrum) to –70 °C (top spectrum), showing the temperature-dependent splitting of the TMA signal into terminal (T) and bridging (B) components.

4.2.2 Interaction of MAO with O and N donors

When THF was added to the MAO solution the peak attributed to the TMA in a ^{1}H NMR spectrum of an MAO sample became sharper and was shifted to higher field, δ –0.60 (see Figure 4.2). This allows integration of the peak and consequently quantification of the TMA content.

Addition of THF to MAO cleaves the dimeric Al_2Me_6 to give monomeric $AlMe_3$ coordinated with a THF molecule: $AlMe_3$·THF. This was validated by low temperature NMR experiments: when THF is added to an MAO solution, the signal attributed to the TMA remained intact as the temperature decreased (no splitting into two signals was observed in temperatures below –40 °C since there are no bridging Me groups).

The influence of adding increasing amounts of THF ($pK_b = 5$)[25] was also investigated. For Al/THF ratios between 1/1 and 1/10, the calculated TMA content of the samples of MAO is consistent and reproducible at 3.3 ± 0.1 wt% (see Table 4.2). When a higher amount of THF was added (Al/THF = 1/15 and 1/26), the wt% of TMA seemed to decrease (3.1 and 2.7 wt% respectively). The lower wt% of TMA when a low amount of THF was added (Al/THF = 6/1) might be explained by the fact that the amount of THF was not sufficient to extract TMA quantitatively. The ratio of Al/THF suggested by Imhoff *et al.*[17] (1/4) for the determination of the TMA content lies within the optimal range of Al/THF ratios found in this study.

Furthermore, observation of the spectra presented in Figure 4.2 show the appearance of a new smaller peak upon THF addition. This peak appears at δ –0.65, high field of TMA, for Al/THF = 6/1 and moves to lower field at higher THF concentrations (δ –0.3 for Al/THF = 1/26).

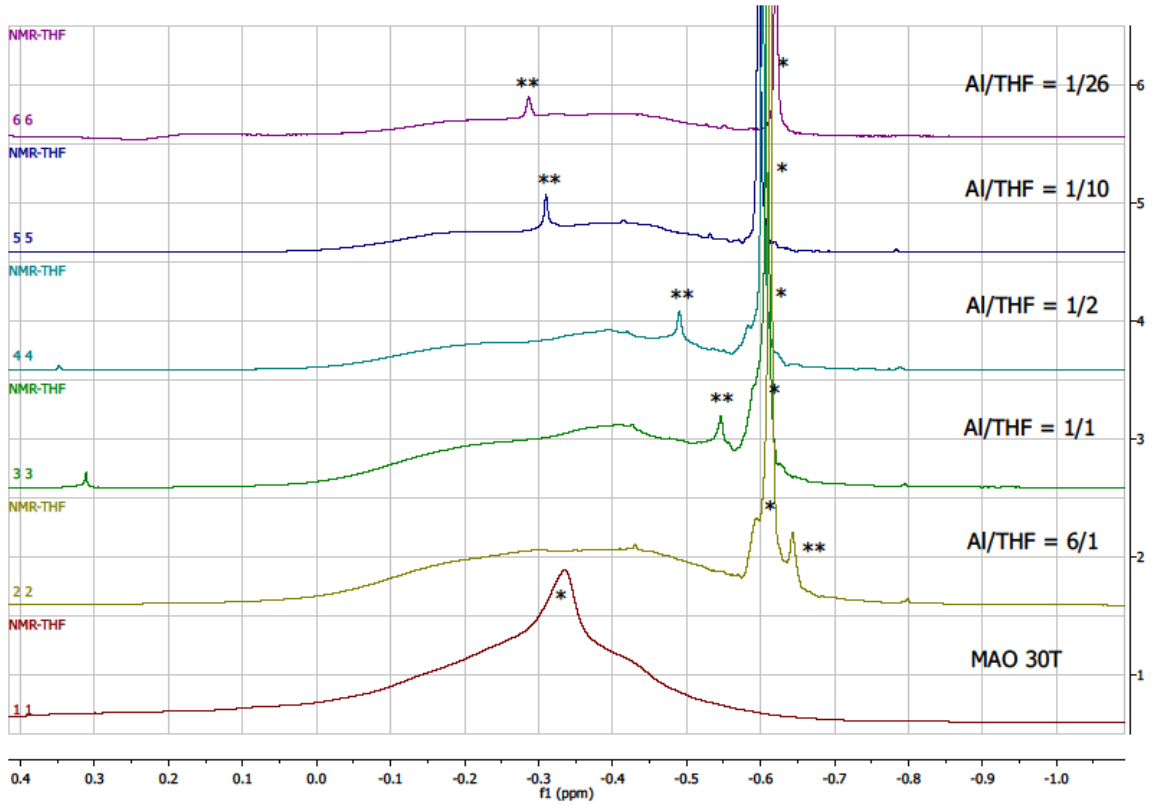

Figure 4.2: ^{1}H NMR spectra of MAO with increasing quantities of THF. The Al:THF ratio is reported as total Al present in the sample. * denotes the Al*Me*$_3$·THF signal, ** the [*Me*$_2$Al(THF)$_2$]$^+$ peak.

In order to explore the nature of the species that gave rise to the aforementioned peak, $[AlMe_2(THF)_2]^+[MeB(C_6F_5)_3]^-$ was synthesised and added to a solution of MAO in toluene/THF. The ^{1}H NMR spectrum of the MAO solution after addition of THF (Al/THF = 1/4) was recorded (bottom spectrum, Figure 4.3). A small amount of the $[AlMe_2(THF)_2]^+[MeB(C_6F_5)_3]^-$ was added to the NMR tube; after mixing the spectrum was recorded (middle spectrum, Figure 4.3). Finally a higher amount of the $[AlMe_2(THF)_2]^+$ was added and the spectrum was recorded again (top spectrum, Figure 4.3). As it can be seen in Figure 4.3, addition of $[AlMe_2(THF)_2]^+$ does not lead to the formation of a new peak at the Al–Me area. Instead, an increase of the small signal that appeared after addition of THF to the MAO solution at δ -0.38 is observed, after addition of increasing amounts of $[AlMe_2(THF)_2]^+$. By integrating the peak of the TMA (the TMA content of the sample does

not change after addition of $[AlMe_2(THF)_2]^+$) with respect to the the 'new peak' shows the relative increase of this peak (A_{cat}/A_{TMA} = 1/3.36 to A_{cat}/A_{TMA} = 1/0.79).

The above observation allows the assignment of the new peak to the cationic complex of $[AlMe_2(THF)_2]^+$ and comes in agreement with a similar observation by Sangokoya[20] and co-workers who synthesised the cationic $[AlMe_2(THF)_2]^+$ from the reaction of $[(C_6F_5)_4B]^-[PhNMe_2H]^+$ with $AlMe_3$ in THF, and then added a small amount of the product of the reaction to an MAO in THF solution.

Quantification of $[AlMe_2(THF)_2]^+$ with increasing THF concentrations follows a similar trend as the one observed for the TMA content. For Al/THF ratios between 1/1 and 1/10, the calculated $[AlMe_2(THF)_2]^+$ content of the MAO samples is consistent and reproducible at at 0.12 mol/L (see Table 4.2). When a higher or lower amount of THF was added (Al/THF = 1/15 and 1/26 or Al/THF = 6/1), the amount of $[AlMe_2(THF)_2]^+$ seemed to decrease (0.09, 0.06 and 0.08 mol/L respectively).

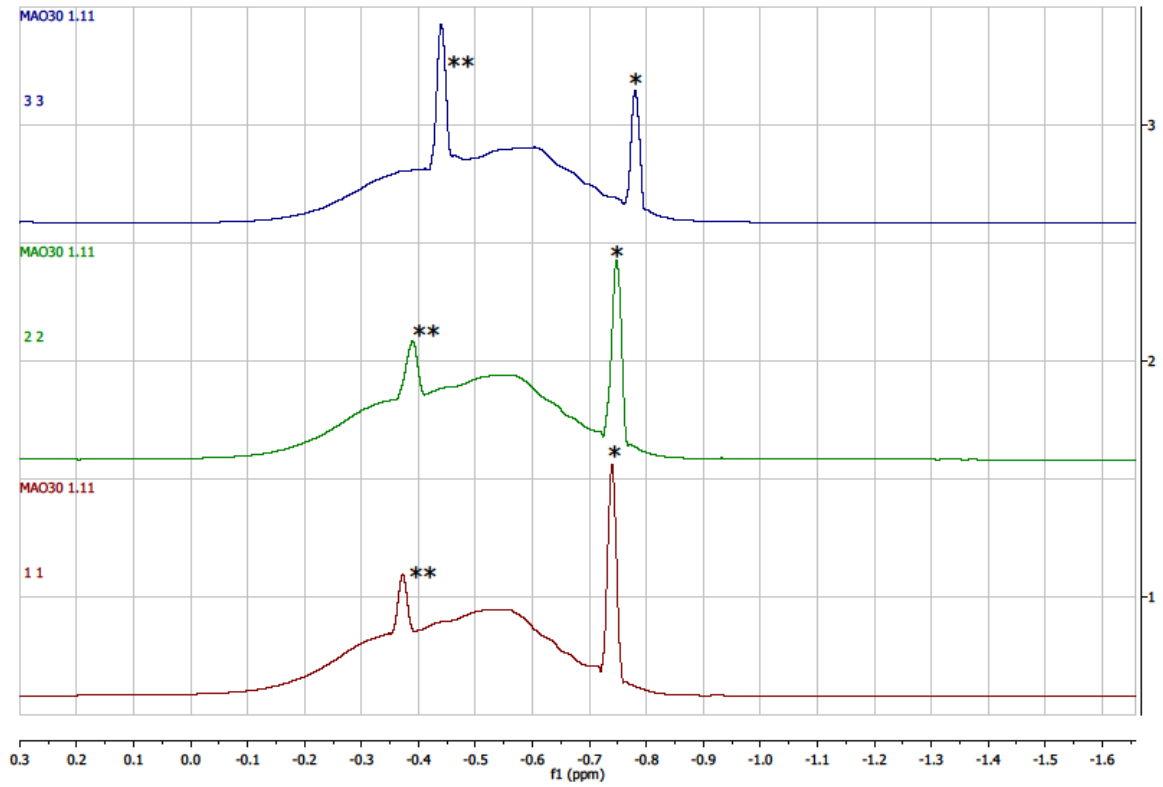

Figure 4.3: Addition of increasing amounts of $[AlMe_2(THF)_2]^+$ to a toluene/THF solution of MAO. (Bottom spectrum: MAO in THF/toluene without addition of $[AlMe_2(THF)_2]^+$)

Addition of pyridine (Py, $pK_b = 8.8$)[26] to an MAO 30T solution led to similar results to the ones observed with addition of THF. For Al/py ratios between 1/1 and 1/10, the calculated TMA content of the MAO samples was consistent and reproducible at 3.5 ± 0.2 wt%, very close to the values obtained with THF addition (see Table 4.1). For Al/py = 6/1, a lower TMA value was obtained (2.2 wt%), perhaps because the amount of pyridine added is not sufficient to extract all TMA. When larger amounts of pyridine were employed (for ratios Al/py = 1/15 or 1/26), the value obtained for the TMA content was also lower (2.3 and 2.1 wt% respectively). At these ratios, the ^{1}H NMR spectrum also showed the appearance of new signals at δ 0.15, –0.30 and –0.55, indicating the formation of side products. This might explain the decreased values of the TMA concentration, and perhaps the higher values obtained for TMA by the pyridine titration method, as pyridine does not simply form a 1/1 complex with TMA (see Figure 4.4).

Again, as with THF addition, the formation of a new smaller peak is observed. This peak is assigned to the cationic species $[AlMe_2(py)_2]^+$. It appears at δ –0.32 for Al/py = 6/1 and moves to lower field as the pyridine concentration increases (at δ 0.02 for Al/Py = 1/26). Quantification of the amount of $[AlMe_2(py)_2]^+$ shows an increase with higher pyridine concentrations (up to Al/py = 1/10), possibly because a higher amount of pyridine binds to more Lewis acidic MAO sites (see Table 4.1). Although, when a large excess of pyridine was used (Al/py = 1/15 and 1/26) a decrease of the $[AlMe_2(py)_2]^+$ content was observed.

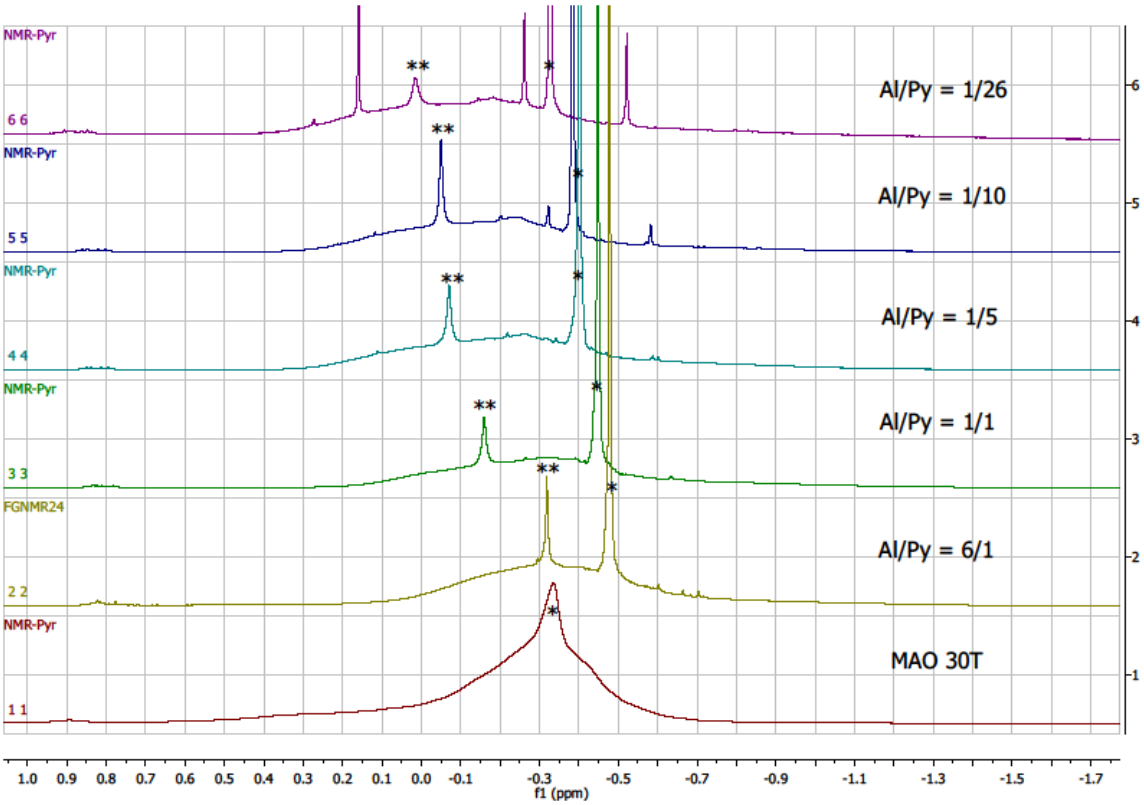

Figure 4.4: ^{1}H NMR spectra of MAO 30T with increasing Al/Py ratios. The Al/Py ratio is reported as total Al present in the sample. * denotes the AlMe_3·Py signal, ** the $[Me_2Al(Py)_2]^+$ peak.

Table 4.1: The TMA and $[Me_2Al(L)_2]^+$ content of the MAO 30T sample as a function of L and the TMA/L ratio (L = THF, Py).

Ratio Al : L	L = THF			L = Py		
	TMA weight-%	TMA (M)	$[Me_2Al(L)_2]^+$ (M)	TMA weight-%	TMA (M)	$[Me_2Al(L)_2]^+$ (M)
6 : 1	2.8	0.35	0.08	2.2	0.28	0.11
1 : 1	3.3	0.41	0.12	3.3	0.41	0.11
1 : 2	3.4	0.42	0.12	3.6	0.45	0.12
1 : 5	3.2	0.40	0.12	3.4	0.42	0.14
1 : 10	3.4	0.42	0.12	3.6	0.45	0.16
1 : 15	3.1	0.39	0.09	2.3	0.29	0.09
1 : 26	2.7	0.34	0.06	2.1	0.26	0.06

4.2.3 Reaction of MAO with 1,2-Difluorobenzene (FF)

Indications for the presence of specific Lewis acidic sites in MAO capable of preferential binding of donor ligands are not only found with typical O and N ligands. The addition of 1,2-difluorobenzene (FF) to MAO solutions leads to the formation of a well-defined triplet at δ –0.45 (J_{HF} = 2.4 Hz) (Figure 4.5). The chemical shift of this peak does not change upon addition of increasing amounts of FF. The J_{HF} value is in agreement with the existence of Al-F single bonds (e.g. in $[^nBu_4N][Me_2AlF_2]$: δ –1.25, t, J_{HF} = 2.4 Hz, in THF).[27] The ^{19}F NMR of the MAO solution upon addition of FF shows a peak at δ –131.5 and a smaller peak at δ –132.8 (besides FF). These disappear after addition of a small quantity of THF. Attempts to generate a defined dissociated cationic dimethylaluminium complex in solution, $[AlMe_2(1,2\text{-difluorobenzene})]^+$, from $AlMe_3$ and $B(C_6F_5)_3$ in FF/toluene did not succeed: no reaction was observed at RT, and only decomposition products at 40 °C.

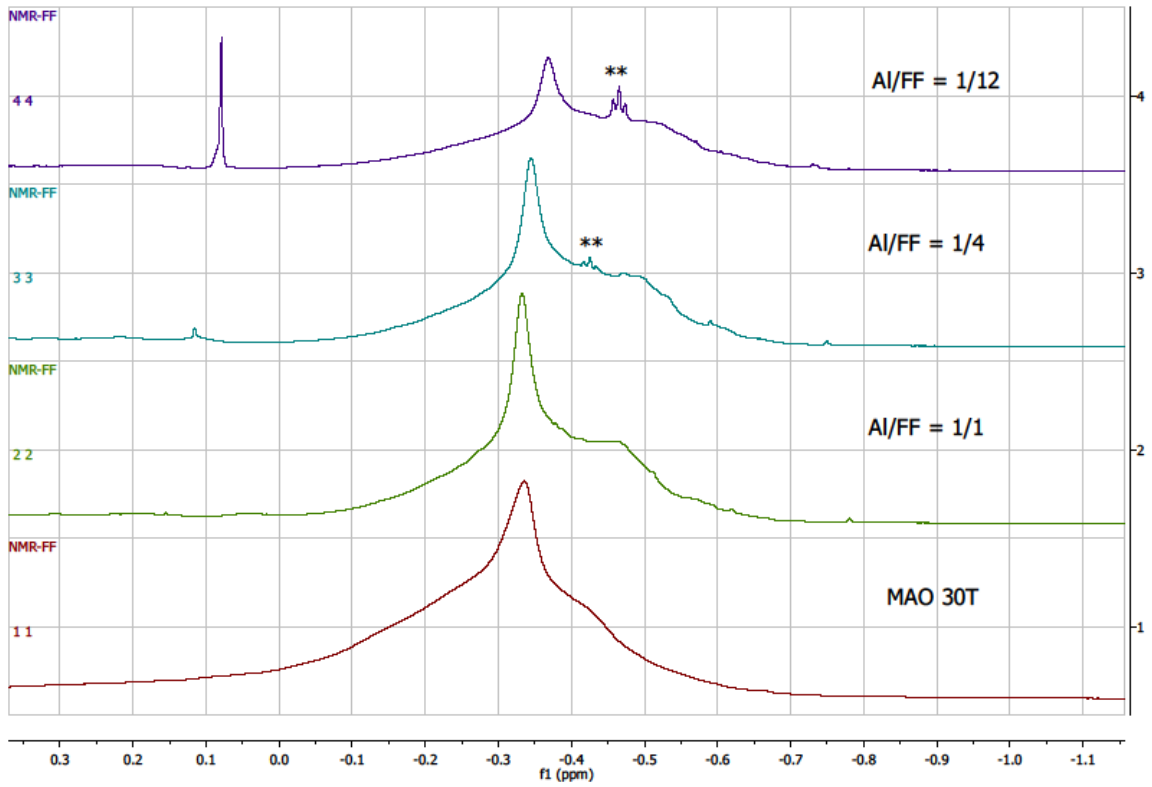

Figure 4.5: ^{1}H NMR spectra of MAO 30T with increasing quantities of 1,2-difluorobenzene

4.3 Conclusions

The present research provides a fast and reliable method for quantification of the TMA content of commercial MAO solutions by ^{1}H NMR spectroscopy with addition of donors like THF and pyridine. It also adds an insight to the comparison between existing techniques: ^{1}H NMR spectroscopy upon THF addition and pyridine titration, and explains why pryridine titration leads to higher values. Another method that was employed by the post-doctoral researcher Fabio Ghiotto[15] was addition of PPh_3 and use of ^{31}P NMR. The TMA content was determined by establishing a correlation relationship between Al/P. This method has been used before by other researchers, although, more than one calibration curve has been reported.[12,28] The results obtained by F. Ghiotto using this method are in good agreement with those obtained by addition of THF and pyridine.

The results of this research also show that MAO contains a small amount of certain structures, which upon addition of suitable bases like THF or pyridine can lead to the formation of cationic species $[AlMe_2L_2]^+$, where L= base, and may even bind 1,2-difluorobenzene. These Lewis acidic sites might have an important role in the activation process of metallocene catalysts by MAO in olefin polymerization. Addition of PPh_3 to MAO did not lead to the formation of similar cationic species. The match of the results from this method with the results from THF and pyridine addition show that the $[AlMe_2L_2]^+$ species do not arise from TMA. Their discovery and quantification, apart from the determination of the TMA content, is another important step to a better understanding of the performance of MAO as a catalyst activator. Computational modelling by M. Linnolahti and co-workers[15] showed that it is likely that these structures are associated with $Al_2(\mu\text{-Me})(\mu\text{-O})$ and $Al_2(\mu\text{-O})_2$ 4-rings, and that similar processes are highly likely involved in catalyst activation.

4.4 Experimental Part

4.4.1 General Procedures and Materials

All manipulations were conducted using standard Schlenk techniques under argon. All reagents were used as purchased without further purification unless otherwise stated. Samples of trimethylaluminium (TMA), and "MAO 30T" (10 and 30 weight-% MAO+TMA in toluene, respectively) were provided by Chemtura Europe Ltd. Their specifications are summarised in Table 4.2 MAO 30T was stored at –28 °C and it was 10 months old at the time of the analysis.

Table 4.2: Specifications of the MAO samples, as provided by Chemtura

Specifications	MAO 30T
Al content (%w/w)	13.58
Me/Al (mol/mol)	1.68
TMA (% w/w)	7 – 9
MAO (% w/w)	21 – 23
Toluene (% w/w)	70
Density (g/mL)	0.90

Solvents were dried over Na/benzophenone (tetrahydrofuran and light petroleum) or sodium (toluene) before use and purged with argon. 1,2-Difluorobenzene (FF, Apollo Scientific) and extra-dry pyridine (Py, Acros) were degassed with a stream of argon and stored over activated molecular sieves (4 Å). The deuterated NMR solvent (CD_2Cl_2) was degassed by several freeze-thaw cycles and dried over activated 4 Å molecular sieves.

NMR spectra were recorded on a Bruker Avance DPX-300 spectrometer operating at 300.13 MHz, 16 scans with a pulse delay (D1) of 25 s. ^{1}H NMR chemical shifts were referenced to the residual solvent peaks of CD_2Cl_2 (in a capillary) which was used as the external standard. 1,3,5-Tri-*tert*-butylbenzene was used as an internal standard. Phasing was performed automatically while integration was performed manually. In order to compensate for sloping baselines and peak overlaps, the ^{1}H NMR signals were integrated by printing the spectra on large sheets of paper (80 g/m^2), cutting the peaks and weighing on an analytical balance.

4.4.2 VT NMR Studies of an MAO Solution in Toluene

Low temperature ^{1}H NMR experiments were carried out for an MAO solution in toluene. 0.5 mL of an MAO 30T solution in toluene was transferred to an NMR tube, equipped with a CD_2Cl_2 capillary, and the ^{1}H NMR spectrum was recorded at R.T. (20 $^\circ$C). Then, the probe of the instrument was gradually (by 10 $^\circ$C each time) cooled down, and ^{1}H NMR spectra were recorded at every 10 $^\circ$C step. The lowest temperature that a spectrum was

recorded was −80 °C. Shimming was necessary in every temperature step that a spectrum was recorded.

4.4.3 Characterization of MAO: Quantification of $AlMe_3$ and $[AlMe_2]^+$ content by THF and Py

MAO 30T (2 mL, 9.06 mmol Al) and THF (1.5 – 245 mmol) were stirred for 30 min at RT. An aliquot (0.5 mL) of the resulting solution was transferred to an NMR tube containing a CD_2Cl_2 capillary and 1,3,5-tri-*tert*-butylbenzene (10 – 40 μL, 0.5 *M* in toluene) and ^1H NMR spectra were recorded. The same procedure was followed for MAO 30T (2 mL, 9.06 mmol Al) and pyridine (1.5 – 245 mmol) solutions.

4.4.4 Reaction of MAO with 1,2-Difluorobenzene (FF)

MAO 30T (2 mL, 9.06 mmol Al) and FF (9.06 – 109 mmol) were stirred for 30 min at RT. An aliquot (0.5 mL) of the resulting solution was transferred to an NMR tube containing a CD_2Cl_2 capillary and ^1H NMR spectra were recorded.

4.4.5 Synthesis of $[AlMe_2(THF)_2]^+[MeB(C_6F_5)_3]^-$ [21-22,29]

A solution of $AlMe_3$ (0.14 mL, 1.46 mmol) in a mixture of petroleum ether (4 mL) and THF (4 mL) was added dropwise to a solution of $B(C_6F_5)_3$ (0.75 g, 1.46 mmol) in THF (25 mL). The resulting mixture was stirred for 1 h at RT and dried under vacuum to yield a viscous colourless oil. ^1H NMR (toluene-d_8): δ –0.45 (s, 6H, $(CH_3)_2Al$–), 0.32 (s, br., 3H, CH_3-B–), 1.31 (m, THF), 3.48 (m, THF).

References

1. L. Resconi, S. Bossi, L. Abis, *Macromolecules*, **1990**, *23*, 4489.
2. D. E. Babushkin, N. V. Semikolenova, V. N. Panchenko, A. P. Sobolev, V. A. Zakharov, E. P. Talsi, *Macromol. Chem. Phys*., **1997**, *198*, 3845.
3. H. Sinn, *Macromol. Symp*., **1995**, *97*, 27.
4. W. Kaminsky, *Macromol. Symp*., **1995**, *97*, 79.

5. H. Sinn, W. Kaminsky, H. J. Vollmer, R. Woldt, *Angew. Chem., Int. Ed. Engl*., **1980**, *19*, 390.
6. H. Sinn, W. Kaminsky, *Adv. Organomet. Chem*., **1980**, *18*, 99.
7. J. R. Severn, In *Tailor-Made Polymers. Via Immobilization of Alpha-Olefin Polymerization Catalysts;* Wiley-VCH: Weinheim, Germany, 2008, p 95.
8. J. Bliemeister, W. Hagendorf, A. Harder, B. Heitmann, I. Schimmel, E. Schmedt, W. Schnuchel, H. Sinn, L. Tikwe, N. Vonthienen, K. Urlass, H. Winter, O. Zarncke, In *Ziegler Catalysts: Recent Scientific Innovations and Technological Improvements*; Springer: Heidelberg, Germany, 1995; pp 57-82.
9. E. Zurek, T. Ziegler, *Prog. Polym. Sci.* **2004**, *29*, 107.
10. E. Zurek, T. Ziegler, *Inorg. Chem.* **2001**, *40*, 3279.
11. I. I. Zakharov, V. A. Zakharov, A. G. Potapov, G. M. Zhidomirov, *Macromol. Theory Simul.* **1999**, *8*, 272.
12. I. Tritto, C. Mealares, M. C. Sacchi, P. Locatelli, *Macromol. Chem. Phys*., **1997**, *198*, 3963.
13. J. L. Eilertsen, E. Rytter, M. Ystenes, *Vib. Spectrosc*., **2000**, *24*, 257.
14. M. Ystenes, J. L. Eilertsen, J. K. Liu, M. Ott, E. Rytter, J. A. Stonveng, *J. Polym. Sci., Part A: Polym. Chem.*, **2000**, *38*, 3106.
15. F. Ghiotto, C. Pateraki, J. Tanskanen, J. R. Severn, N. Luehmann, A. Kusmin, J. Stellbrink, M. Linnolahti, M. Bochmann, *Organometallics*, **2013**, *32*, 3354.
16. D. E. Jordon, *Anal. Chem*., **1968**, *40*, 2150.
17. D. W. Imhoff, L. S. Simeral, S. A. Sangokoya, J. H. Peel, *Organometallics*, **1998**, *17*, 1941.
18. J. A. Tossell, *Organometallics*, **2002**, *21*, 4523.
19. E. P. Talsi, N. V. Semikolenova, V. N. Panchenko, A. P. Sobolev, D. E. Babushkin, A. A. Shubin, V. A. Zakharov, *J. Mol. Catal. A: Chem.* **1999**, *139*, 131.
20. L. Luo, S. A. Sangokoya, X. Wu, S. P. Diefenbach, B. Kneale, U.S. Pat. Appl. 2009/0062492 A1 (2009, Albemarle Corp.).
21. J. Klosin, G. R. Roof, E. Y.-X. Chen, *Organometallics* **2000**, *19*, 4684.
22. J. Klosin, PCT Int. Appl. WO2000/11006 (2000, Dow Chemical Co.)
23. M. Bochmann, M. J. Sarsfield, *Organometallics*, **1998**, *17*, 5908.
24. K. C. Ramey, J. F. O'Brien, I. Hasegawa, A. E. Borchert, *J. Phys. Chem*., **1965**, *69*, 3418.

25. Y. Yamashita, H. Kasahara, K. Suyama, M. Okada, *Makromol. Chem*., **1968**, *117*, 242.
26. Quin, L. D.; Tyrell, J. *Fundamentals of Heterocyclic Chemistry*; Wiley, Hoboken, New Jersey, 2010.
27. Roesky, A. Stasch, H. Hatop, C. Rennekamp, D. H. Hamilton, M. Noltemeyer, H. G. Schmidt, *Angew. Chem. Int. Ed.*, **2000**, *39*, 171.
28. A. R. Barron, *Organometallics*, **1995**, *14*, 3581.
29. E. Y.-X. Chen, W. J. Kruper, PCT Int. Appl. WO 2001/5642 (2001, Dow Chemical Co.).

Chapter 5

Investigating the Performance of Modified MAO Catalyst Systems in Aliphatic Hydrocarbons by Studying the Kinetics of 1-Hexene Polymerization

5.1 Introduction

5.1.1 Modification of MAO by Silanols and Higher Trialkylaluminium Compounds

As it has been described in Chapter 1, methylaluminoxane (MAO) is a very important cocatalyst in solution-phase olefin polymerization with group 4 metallocenes. One major drawback derived from its use when solution-based technologies are employed, is that it is insoluble in aliphatic hydrocarbons, which are the preferred solvents in industrial polymerization processes.[1-2]

Previous studies have shown that incorporation of longer alkyl chains into the MAO structure by the use of branched or straight chain alkylaluminium compounds, with at least two carbon atoms, substantially improves the solubility[3] of MAO in saturated hydrocarbons.[4-9] These modified MAOs (MMAOs) can be synthesized by three different routes:

(i) mixing of trimethylaluminium (TMA) with a higher alkylaluminium compound in a hydrocarbon solvent, followed by hydrolysis (by direct addition of water or addition of hydrated salts)[5],

(ii) mixing a methylaluminoxane solution with a higher alkylaluminium compound in an aliphatic solvent or in toluene (mixing in toluene was followed by removal of the solvent, leaving an oily product behind which was re-dissolved in an aliphatic solvent)[6] and

(iii) addition of higher alkylaluminium compounds to a methylaluminoxane solution prepared via non-hydrolytic routes[10-14], usually by reacting TMA with a compound that contains a C–O bond or by mixing the higher alkylaluminium compound with TMA first, followed by reaction with the oxygenating agent[15].

The most commonly used compounds that achieve high solubility are: triethylaluminium (TEA), tri*iso*butylaluminium (TIBA) and trioctylaluminium (TOA). This increased solubility is probably due to partial exchange of their alkyl groups with the methyl groups of the aluminoxane. TOA is the preferred additive since it is a very effective solubilizing agent and it does not cause any noticeable changes in the catalytic properties of MAO. The molar ratios of methylaluminoxane or trimethylaluminium versus the trialkylaluminium compound that is used as an additive varies, but are often between 1: 1 and 10: 1, depending on the trialkylaluminium compound used each time.[4,6,9] The patent applications[6,9] claim that the MMAOs produced following their synthetic procedures, exhibited high activities in olefin polymerizations which were comparable to or even higher than conventional MAO.

However, taking a closer look at the existing literature on MMAOs shows different catalytic behaviors in olefin polymerization. For example, Kurokawa and Sugano[16] reported that the ethylene polymerization activity of the MMAO produced by direct hydrolysis of a mixture of TMA and TIBA, when using $Me_2Si(H_4Ind)_2ZrCl_2$ as catalyst, exhibited lower activities with increasing amounts of TIBA, while a maximum activity was obtained for propylene polymerization when a 1: 1 molar ratio of TMA : TIBA was employed. Charpentier *et al.*[17] reported that the molecular weight of the polymer and the molecular weight distribution do not seem to be influenced by the different MAOs (Cp_2ZrCl_2 catalyst, ethylene polymerization).

Our studies[18] have proven that heptane-soluble MAO is produced by removal of all volatiles from MAO solutions in toluene, followed by suspending the TMA-depleted residue in heptane and adding a sufficient amount of TIBA or TOA. The MMAOs produced were evaluated according to their performance in 1-hexene polymerizations in heptane. Some of the results of this study are presented later in this chapter.

TIBA has been used as an additive in silica supported catalysts SiO_2/MAO/SBIZrCl_2, and it has been found that it solubilizes parts of the MAO and zirconocene into the heptane solution, leading to the production of polyethylene with bimodal molecular mass distribution. The polymer produced by the catalyst system in solution is believed to be of lower molecular mass.[4]

Silica supported catalysts

Silica supports are used widely in heterogeneous α-olefin polymerizations with single-site catalysts. The most commonly used forms of silica are amorphous silica and surface-hydroxylated amorphous silica. The unmodified silica surfaces which are saturated with silanol groups and contain residual water have to be thermally or chemically processed in order to remove the residual water and hydroxyl groups which could deactivate the catalyst. At high temperatures (above 180 °C) the adjacent hydroxyl groups start condensing to siloxanes, and the final density of silanol groups ranges between 1-5 OH/nm^2.[1-2] As the surface silanol groups are the most reactive groups present on silica, it is necessary to control the amount that exists on a silica support and subsequently the properties of that surface.[19] One major advantage coming from supporting MAO on silica gel surfaces is that the required amount of MAO versus the amount of catalyst can be reduced significantly from 10^3-10^4 equivalents to about 100-500 equivalents.[8]

The interactions of MAO and other alkylaluminiums with silica surfaces have been investigated by many research groups. Zakharov *et al.*[20-21] suggested that TMA reacts rapidly with surface silanols via protolysis releasing methane, while MAO reacts slowly with the silica surface via chemisorption. The idea of the chemisorption of MAO on the silica surface was introduced by Bartram *et al.*,[22] who based their observations on the Si–Me and Al–Me ratio, while Soga and Kaminaka[23] suggested a quantitative reaction between TMA and MAO with the surface silanols. Santos *et al.*[24] supported that MAO shields the surface silanol groups preventing them from further reactions due its steric effect.

Later on Scott *et al.*[25] studied the reaction of TMA with silica surface by deposition of TMA onto Aerosil 380, and suggested the formation of an intermediate product due to the strong interaction between a siloxide, which acts as a bridge between the two Al centers of the dimeric TMA: $[Me_2Al]_2(\mu\text{-}Me)(\mu\text{-}OSi\equiv)$. They proposed that the bridging Me group of the intermediate is transformed to a methylene group by C–H activation due to the electron-withdrawing silica ligand forming $\equiv SiOAl_2Me_3(CH_2)$ and releasing methane. The second Al centre is likely to coordinate with a nearby siloxide oxygen in order to maintain a tetracoordinated form. Deactivation reactions[26-27] that lead to the formation of M–CH_2–Al and M–CH_2–M species in homogenous MAO/ metallocene systems seem to be suppressed when the catalyst system is supported on silica which inhibits α-hydrogen transfer.[26] Li *et al.*[28] added TMA to a suspension of a silica gel surface in toluene or cyclohexane and claimed

the formation of mainly five-coordinate Al species. Three main types of aluminium species containing Me groups were distinguished: $Al(CH_3)_n$ with Si–O–Al linkages, Si–O–CH_3 and $(Si–O)_{4-n}Si(CH_3)_n$. The $Al(CH_3)_n$ and Si–O–CH_3 species were converted to four- and six-coordinate Al after addition of water in diethyl ether. An example is illustrated on Scheme 5.1.

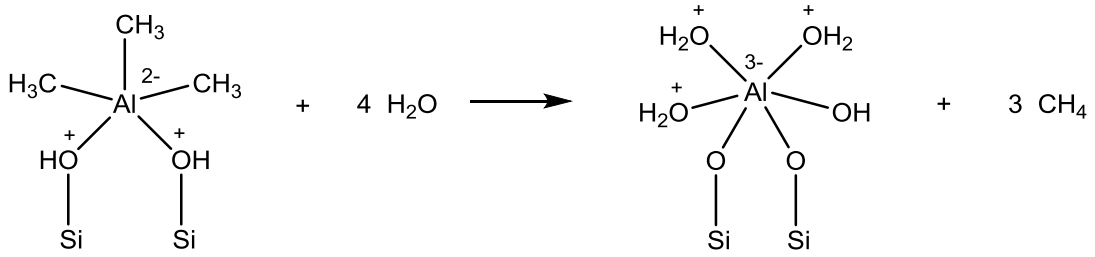

Scheme 5.1: Example of a conversion of a five-coordinate Al structure on silica gel to a six-coordinate structure, after addition of water [28]

Additionally, there are several studies investigating the possible reactions of alkylaluminiums with silica based compounds which resemble the interactions between alkylaluminiums and silica gel surfaces. Seeking a better understanding of the reaction between alkyl aluminiums and the surface Si-OH groups, Skowronska-Ptasinska *et al.*[29] studied the reaction of TMA with methyl aluminosilsesquioxanes : treatment of $(c\text{-}C_5H_9)_7Si_8O_{12}(OH)$ with TMA yielded polymeric $\{[c\text{-}C_5H_9)_7Si_8O_{13}]AlMe_2\}_n$, while $(c\text{-}C_5H_9)_7Si_7O_9(OH)_2OSiMePh_2$ reacted with TMA to give $\{[(c\text{-}C_5H_9)_7Si_7O_{11}\text{-}(OSiMePh_2)]AlMe_\}2$ as the main product as well as $\{[(c\text{-}C_5H_9)_7Si_7O_{11}\text{-}(OSiMePh_2)](AlMe_2)_2\}_2$ and a Bronsted acidic product, $\{[(c\text{-}C_5H_9)_7Si_7O_{11}\text{-}(OSiMePh_2)]_2Al^-\}\{H^+\}$.

Other research groups have studied the reaction of silanols with TMA. The stoichiometric reaction of Ph_3SiOH with TMA produces $[Me_2Al(\mu\text{-}OSiPh_3)]_2$ [10,30-31], while the reaction of $(^tBuO)_3SiOH$, $(Me_3SiO)_3SiOH$ or $^tBuMe_2SiOH$ with one equivalent of TMA has been found to produce the dimeric siloxyaluminium compounds $[(^tBuO)_3SiOAlMe_2]_2$ (1a), $[(Me_3SiO)_3SiOAlMe_2]_2$ (1b) and $[^tBuMe_2SiOAlMe_2]_2$ (1c) respectively. Their reactivity towards catalytic activators has been studied in order to provide models for comparison for TMA-treated silica surfaces. The compounds (1b) and (1c) were treated with the proton donor $[Me_2NHPh]^+[B(C_6F_5)_4]^-$ in a 1:1 molar ratio, to produce $Me_2Al(\mu\text{-}OSiR_3)_2AlMe(NMe_2(C_6H_5)^+$ (2b, 2c) and CH_4 (see Scheme 5.2). The cationic aluminium

complexes were then used to activate zirconocene dimethyl species. Reaction with L_2ZrMe_2 proceeds *via* Me abstraction from 2b or 2c and leads to the formation of neutral $[R_3SiOAlMe_2]_2$ species. The siloxalanes exhibit lower reactivity than the TMA-treated silica gel surfaces which is probably due to the two bridging O–SiR_3 ligands between the metal centers.[32]

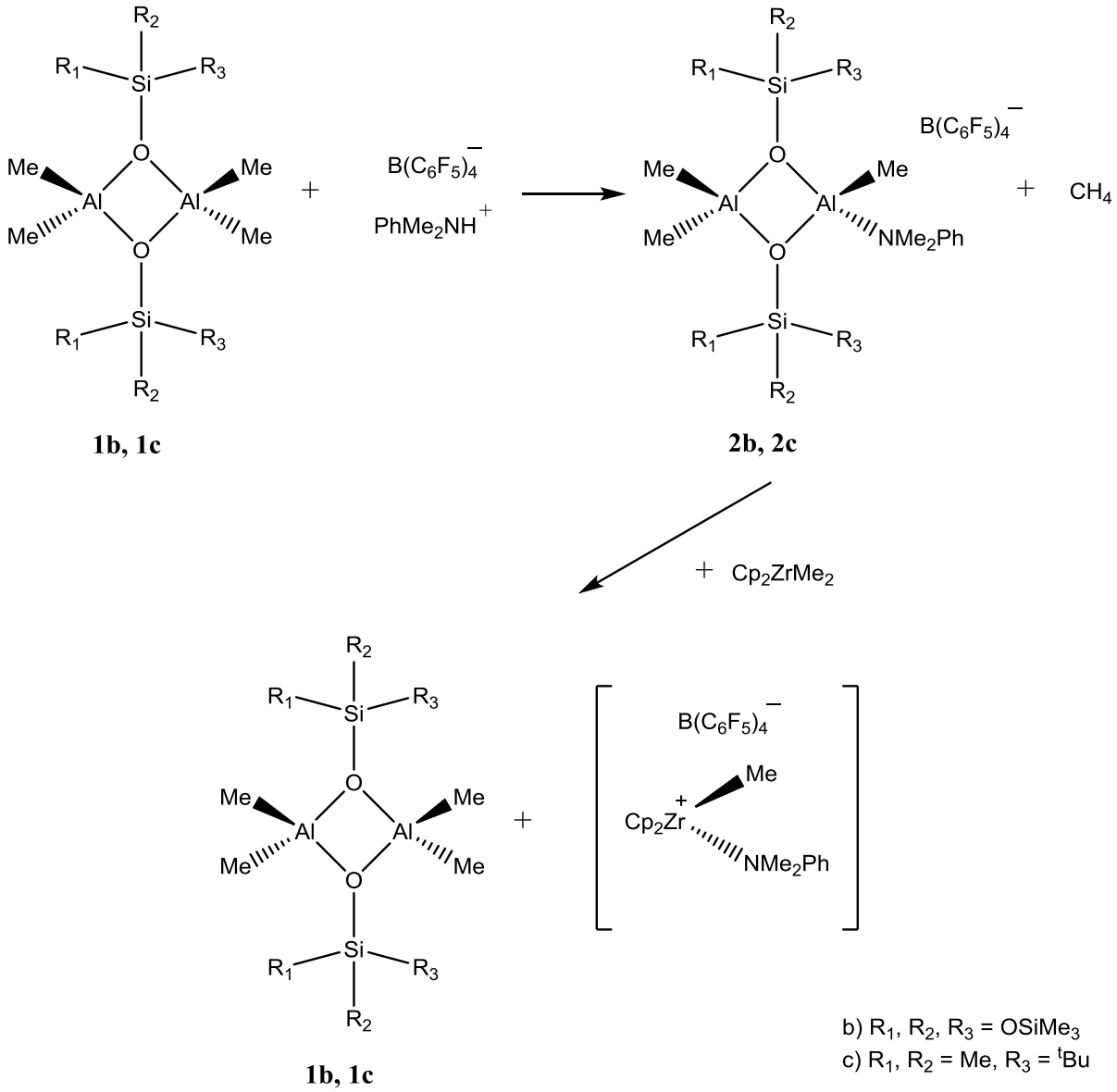

Scheme 5.2: Reaction scheme of compounds (1b) and (1c) after treatment with the proton donor $[Me_2NHPh]^+[B(C_6F_5)_4]^-$ and reaction of the product $Me_2Al(\mu\text{-}OSiR_3)_2AlMe(NMe_2(C_6H_5)^+$ (2b, 2c) with zirconocene dimethyl species.

The system that results after treatment of a toluene solution of TMA with Me_3SiOH, followed by reaction with Cp_2ZrCl_2 is active in ethylene polymerization (best yield for a molar ratio of Si/Al = 1:10), but has a lower activity than a system where the reaction of Cp_2ZrCl_2 with Me_3SiOH takes place before addition of TMA[33]. Brintzinger *et al.*[34] studied the reaction of very bulky silanols like $(2,4,6\text{-}Me_3C_6H_2)_3SiOH$ with TMA. These systems did not produce dimeric siloxyaluminium alkyl compounds but gave a binuclear siloxalane with one siloxy and one methyl bridge, $Me_2Al(\mu\text{-}OSi(2,4,6\text{-}Me_3C_6H_2)_3)(\mu\text{-}Me)AlMe_2$ (Scheme 5.3). This species, unlike siloxalanes with two siloxy bridges, react with L_2ZrCl_2 (L= (C_5H_5), $Me_2Si(C_5H_4)_2$, *n*-BuC_5H_4 *via* Me/Cl exchange, and it is believed that they represent a closer model for the activation reaction of metallocenes on TMA-treated silica gel surfaces (Scheme 5.4).

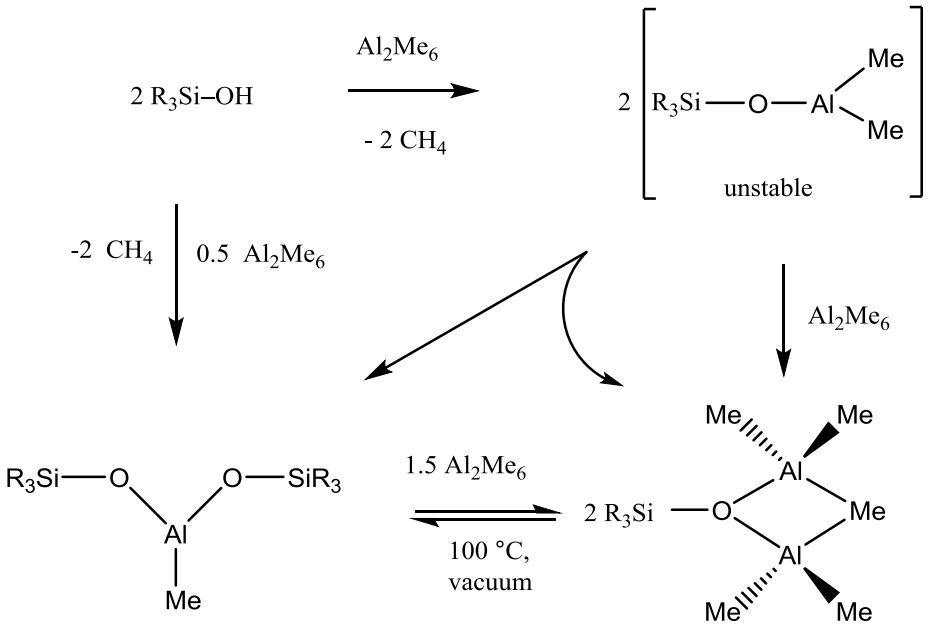

Scheme 5.3: Reaction scheme of some very bulky silanols like the $(2,4,6\text{-}Me_3C_6H_2)_3SiOH$ with TMA, as suggested by Brintzinger *et al.*[34]

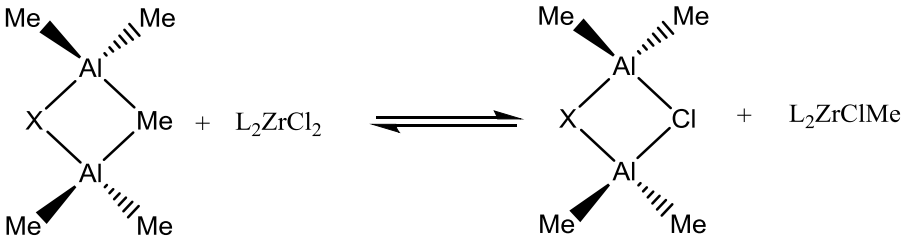

X = Me, (2,4,6-$Me_3C_6H_2)_3SiO$, surface Si-OH
L_2 = $(C_5H_5)_2$, $Me_2Si(C_5H_4)_2$, $(^nBuC_5H_4)_2$

Scheme 5.4: Reaction of binuclear siloxalane with one siloxy and one methyl bridge with L_2ZrCl_2 *via* Me/Cl exchange, as suggested by Brintzinger *et al.*[34]

The reaction of TMA with poly-organosiloxanes or cyclic siloxane oligomers has been investigated as well. TMA cleaves the Si-O-Si bond by alkylation of the silicon and formation of an Al-O bond. Reaction of TMA with silicon grease, poly(dimethylsiloxane) oil or poly(dimethylsiloxane) rubber in refluxing toluene[35], or reaction of TMA with octamethyltetrasiloxane[36] (180 °C, 24 hours) results in the formation of $[Me_2Al(OSiMe_3)]_2$. $[Et_2Al(OSiMe_2Et)]_2$ is a widely used and the least expensive siloxalane[36] and is synthesized by reaction of TEA with octamethyltetrasiloxane. $[Me_2Al(OSiMe_3)]_2$ has been used in the preparation of a modified aluminoxane and tested in ethylene polymerization, achieving activities comparable to conventional MAO with specific TMA/$[Me_2Al(OSiMe_3)]_2$ ratios.[37]

MAO has been treated with additives such as hydrocarbylsiloxanes essentially free of Si-OH groups[38], with hydroxysiloxanes and especially with siloxane diols[39] and then tested in olefin polymerization. These studies claim higher polymerization activities and higher stability of the siloxy-aluminoxane compositions compared to the unmodified methylaluminoxanes. The TMA content of the original MAO solution is reduced after addition of the organosiloxane compound, so the higher activity that is reported might be simply a consequence of the reduced TMA concentration.[18]

Finally, aluminoxane salt compositions soluble in aromatic and aliphatic solvents, have been prepared[40-42] by mixing octamethyltrisiloxane (OMTS) with MAO. These aluminoxane salts have then been treated with TIBA or more importantly TOA, and the resulting compositions tested in ethylene polymerizations with the *rac*-$C_2H_4(Ind)_2ZrMe_2$ catalyst, where they exhibited higher activities than unmodified MAO systems.[40]

Taking into consideration the existing literature data, this study aims to produce a modified methylaluminoxane composition that will be soluble in aliphatic hydrocarbons with enhanced polymerization performance after treatment of MAO with branched or long chain silanols or di-silanols.

5.1.2 Kinetic studies of 1-Hexene Polymerizations

The difficulty to extract detailed mechanistic information from MAO-based catalytic systems due to the complex nature of the structural characteristics of MAO, and the complications that arise from the fact that different MAO grades and formulations exhibit different catalytic performance, highlighted the necessity to study the kinetic profile of each different polymerization system concerned in detail, in order to be able to quantify and compare the parameters that govern the catalyst initiation, propagation and termination. Modification of MAO with various additives causes changes to the structural characteristics of MAO and can be expected to lead to different catalytic results. The easiest and quickest way to access the effectiveness of each modified-MAO catalytic system is to study the reaction kinetics of the system.[8,43-44]

For this reason, this study was focused on the evaluation of the modified MAO systems produced based on kinetic studies. 1-Hexene polymerization was chosen as the standard polymerization test reaction and *rac*-Me_2Si(2-Me-Benz[e]Ind)$_2ZrCl_2$ (1; Ind = 1-indenyl)[45] as the standard catalyst. The polymerization of 1-hexene was selected because the reaction remains homogeneous throughout and produces a polymer soluble in hydrocarbon solvents at room temperature; it is also slower than ethylene or propylene polymerization which allows collection of data during all stages (initiation, propagation) without the need to use time consuming quenched-flow techniques.

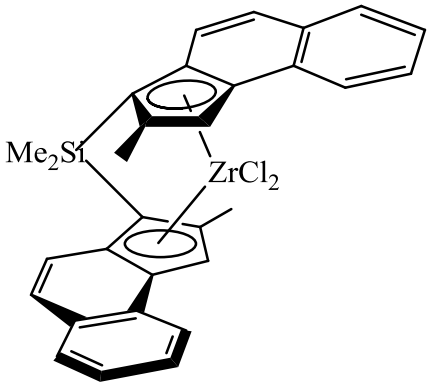

The tailored metallocene used in this study (its structure is shown above), was carefully selected in order to have the desired catalytic activity (e.g. zirconocene catalysts are more active than titanocene or hafnocene), and produce poly-hexene with a molecular weight within the rage that we could easily and accurately study with the given equipment. Most importantly, this catalyst was specifically chosen because it is an ansa-metallocene; its Me_2Si bridge produces a rigid, C_2-symmetric framework that leads to the production on an isoatactic polymer (the monomer coordinates enantioface regardless of the side it coordinates to). By using this catalyst system, β-hydride elimination as a termination pathway is prevented; chain transfer to aluminium is the main termination mechanism. This makes comparison of the different catalyst systems in this study easier and more focused on specific factors (e.g. amount of Al as TMA present).

The methods used in this study: quantitative NMR and gel permeation chromatography (GPC), allowed the quantification of the catalyst performance in 1-hexene polymerizations by establishing the kinetics under non-steady-state conditions through the simultaneous determination of rate constants and active species count.[18]

The kinetics of alkene polymerization with metallocene catalysts follows the empirical rate law shown in eqn. 5.1.[46]

$$\text{Rate} = -\frac{\mathrm{d[M]}}{\mathrm{dt}} = \mathrm{k\,[C]_T[M]} \qquad (5.1)$$

where [M] = monomer concentration, $[C]_T$ = catalyst concentration (usually taken to be equal to the total concentration of the precatalyst added), t = reaction time and k is the chain propagation rate constant. The rate constant k is the apparent propagation rate constant, which will be referred to as k_p^{app}, to distinguish from the actual rate of growth of the polymer chains, k_p. Calculation of k_p^{app} was possible by measuring the 1-hexene consumption by ^{1}H

NMR spectroscopy using an internal standard and taking samples at regular time intervals (quenching the samples in THF-MeOH-HCl was necessary).

A second measure of propagation rate is obtained by determining the average growth rate of the polymer chains by monitoring the degree of polymerization $< n >$ as a function of time. This is possible either by observing very short reaction times or by slowing the polymerization reaction down to allow sufficiently fast sampling to take place during the initial phase of the polymerization. For fast polymerizations, such as ethylene and propylene polymerizations, measurement of the time dependence of $< n >$ requires, as mentioned above, quenched-flow techniques to sample the time range before steady-state conditions are attained, which may be as short as a few seconds[47].

In quenched-flow polymerisations there are two reservoirs: one contains the catalyst and the other the co-catalyst in a solvent (e.g. toluene); they are usually saturated with the monomer. To start the polymerisation pressure is applied to the two reservoirs (e.g. by the monomer if it is a gas, otherwise an inert gas is used) and the two streams are mixed in a short, thin tube. The polymerisation conditions can be changed by varying the length or width of the reactor tube (subsequently varying the reaction time). However, such quenched-flow techniques are slow, laborious and can suffer from polymer deposition in the reactor tubes (the reactor tubes must be cleaned after each polymerization reaction); quenched-flow techniques do not lend themselves to automation or fast monitoring.

The analysis of $< n >$ (eqn. 5.2) provides essential information, because unlike eqn. (5.1), it makes no assumption about the catalyst concentration and is a function only of the initial monomer concentration $[M]_0$ and the rate constants of propagation (k_p), termination (k_t) and initiation (k_i) (eqn. 5.2).

$$< n > = f\left([M], k_p, k_t, k_i\right) \qquad (5.2)$$

With fast activating catalysts, where monomer consumption grows linearly with time, the k_i term may be neglected,[47] but under non-steady state conditions k_i needs to be taken into account.

The data needed to calculate the parameters k_p, k_t and k_i were extracted from the GPC measurements. Calculation of the k_p^{app} / k_p ratio is very important since it gives the mol fraction $[C^*]$ of the catalyst that is involved in polymer chain growth at any time (eqn. 5.3).

$$[C^*] \propto k_p^{app}/k_p \qquad (5.3)$$

For metallocene catalysts, this fraction is typically around 0.1-0.3 and in any case much less than 100% of the catalyst added.[47-49] This type of measurement of the active species concentration differs from the determination by isotopic labeling[50-52] which measures the concentration of the total Zr–C bonds formed during the polymerization experiment.

The polymerization of 1-hexene with the given metallocene catalyst is sufficiently slow at 30 °C to allow sampling for about an hour before steady-state conditions are reached. This, coupled with fast size exclusion chromatography, allows the time dependence of both conversion and the number-average molecular weight $\overline{M_n}$ to be established within a few hours, whereas previous measurements of this kind on propene polymerizations may have taken days or weeks.[47] For the above reasons, the method used in this study is suitable for evaluating the influence of a variety of different MMAOs and experimental conditions within an acceptable time frame.

5.2 Results and Discussion

5.2.1 Reaction of TMA with ^{t}Bu$_2$Si(OH)$_2$

The reaction of TMA with ^{t}Bu$_2$Si(OH)$_2$ in toluene is surprisingly complex and gives a number of different products, which were difficult to identify. NMR spectroscopy shows many different signals (see Figure 5.2, top spectrum). When the reaction was performed at higher temperatures broadening of the signals was observed. Several attempts to crystallize any reaction products failed. The reaction in THF (see Figure 5.2, bottom spectrum) shows two distinct resonances in the Al-Me region (δ –0.61, –0.63) and a smaller peak at –0.57 ppm. Integration of the peaks was not possible because the signals overlap. Evolution of methane (δ 0.22 and 0.52, in toluene and THF respectively) was observed in both cases as expected.

The reaction of TMA with ^{t}Bu$_2$Si(OH)$_2$ in an Al/Si ratio of 2/1 would be expected to give [^{t}Bu$_2$SiOAlMe$_2$]$_2$ as the main product, due to the steric effect of the bulky ^{t}Bu groups (Figure 5.1, structure ii). Other possible reaction products are depicted in Figure 5.1. When

reaction is performed in toluene, it is likely that polymeric products such as structure iv (Figure 5.1) are formed.

The main focus was to study the interactions of $^{t}Bu_2Si(OH)_2$ with alkylaluminium compounds in toluene, because toluene is the primary solvent used in 1-hexene polymerizations with modified MAO by addition of $^{t}Bu_2Si(OH)_2$. It was for this reason that the reaction of TMA with $^{t}Bu_2Si(OH)_2$ in THF was not studied further.

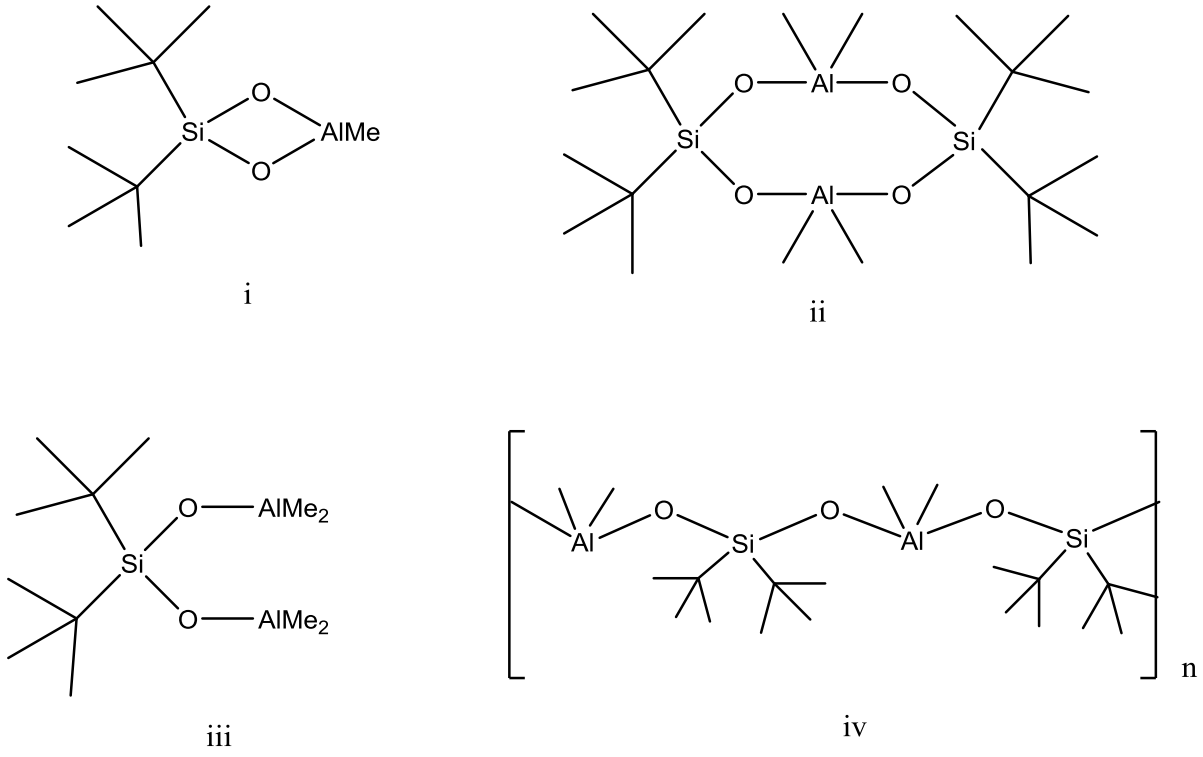

Figure 5.1: Possible reaction products from the reaction between TMA and $^{t}Bu_2Si(OH)_2$ in an Al/Si ratio of 2/1 or 1/1

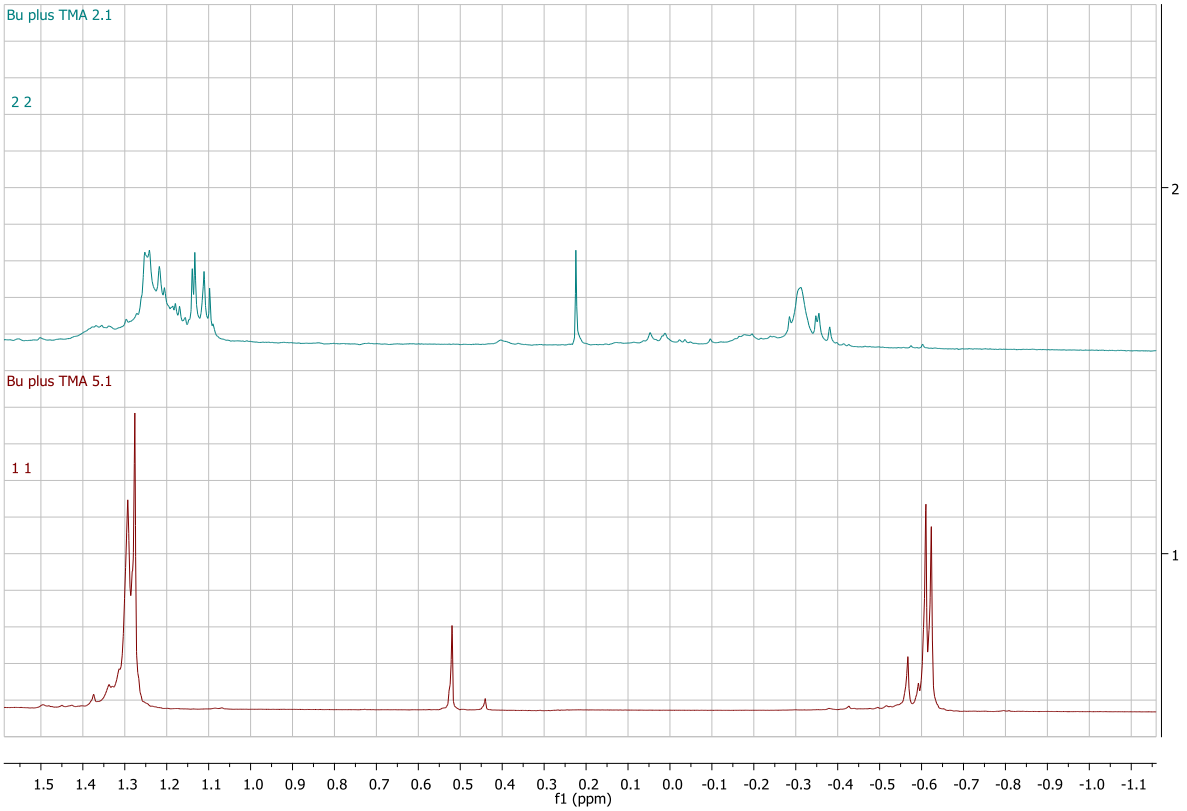

Figure 5.2: ^{1}H NMR spectra of the reaction products for the reaction between TMA and $^{t}Bu_2Si(OH)_2$ with an Al/Si ratio of 2/1 and addition of $^{t}Bu_2Si(OH)_2$ at –78 °C. (Top spectrum: reaction in toluene. Bottom spectrum: reaction in THF)

5.2.2 Reaction of TMA with Ph_3SiOH, $(C_8H_{17})_3SiOH$ and $^{i}Pr_3SiOH$

TMA + Ph_3SiOH

As it has been suggested[10, 30-31], the product of the stoichiometric reaction between TMA and Ph_3SiOH is the dimer $[Me_2Al(\mu\text{-}OSiPh_3)]_2$ (^{1}H NMR: δ –0.68 Me; top spectrum, Figure 5.3) formed by methane elimination (Reaction 5.1), which was crystallized from toluene. Some residual $AlMe_3$ (δ –0.46) is observed. The crystal structure is presented in Figure 5.4 and it has not been previously reported.

$$AlMe_3 + Ph_3SiOH \longrightarrow 1/2\ [Me_2Al(\mu\text{-}OSiPh_3)]_2 + CH_4 \qquad (5.1)$$

No evidence of Ph_3MeSi (^{1}H NMR: δ 0.81 ppm for the Me signal) was observed when addition of Ph_3SiOH took place at –78 °C. Barron *et al.*[10] reported that when the

reaction of $AlMe_3$ with Ph_3SiOH took place at low temperatures (−78 °C) hydroxide/methyl exchange was observed along with the main alkane elimination reaction. This was explained by the fact that at low temperatures Lewis acid-base complexes of $AlMe_3$ are formed, and their formation inhibits alkane elimination. Additionally, when $AlMe_3$ coordinates to Ph_3SiOH, the acidity of the hydoxy proton increases, leading to an increase of the electrophilicity of the Si atom which favours its alkylation by $AlMe_3$. The proposed reaction of $AlMe_3$ with Ph_3SiOH at low temperature via hydroxide/methyl exchange is described in Scheme 5.5.

It was reported by Barron that when the reaction mixture was held for 1 h at −78 °C, only 5% of the relative fraction of the hydroxide exchange reaction was observed. This means that in the present study where the reaction mixture was kept for less than 20 min at −78 °C before starting to increase the temperature of the mixture gradually, the relative fraction of the hydroxide exchange reaction would have probably been negligible. It should however be noted that some broadening of the spectrum (δ −0.40 to −0.75) was observed (bottom spectrum, Figure 5.3), which is in agreement with Barron's observations.

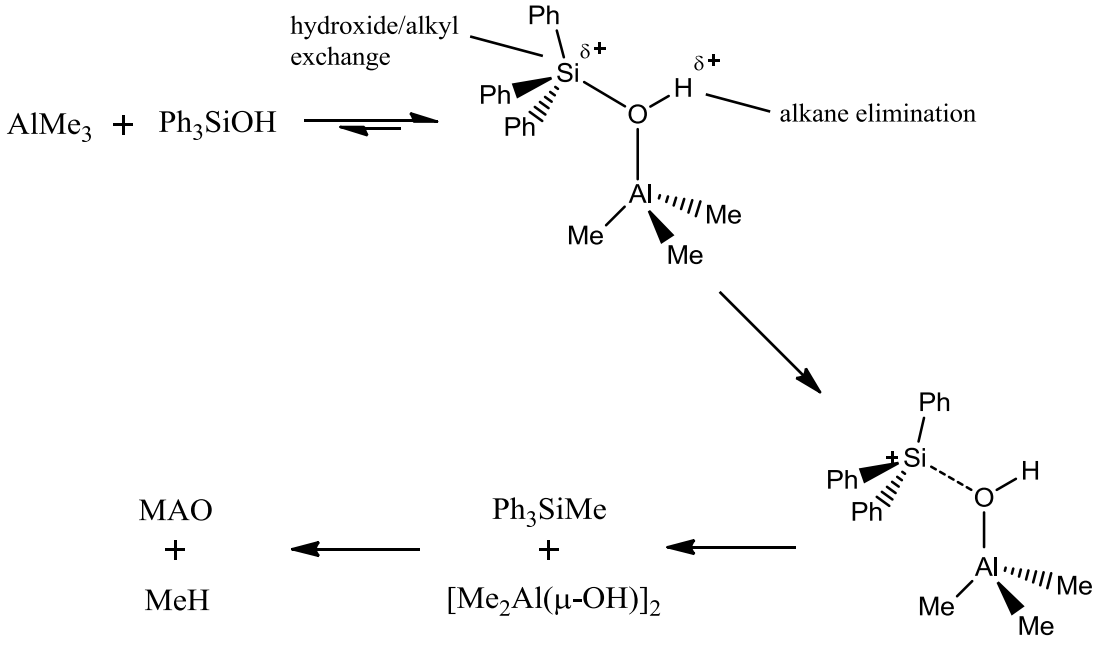

Scheme 5.5: The proposed reaction by Barron *et al.*[10] of $AlMe_3$ with Ph_3SiOH at low temperature via hydroxide/methyl exchange

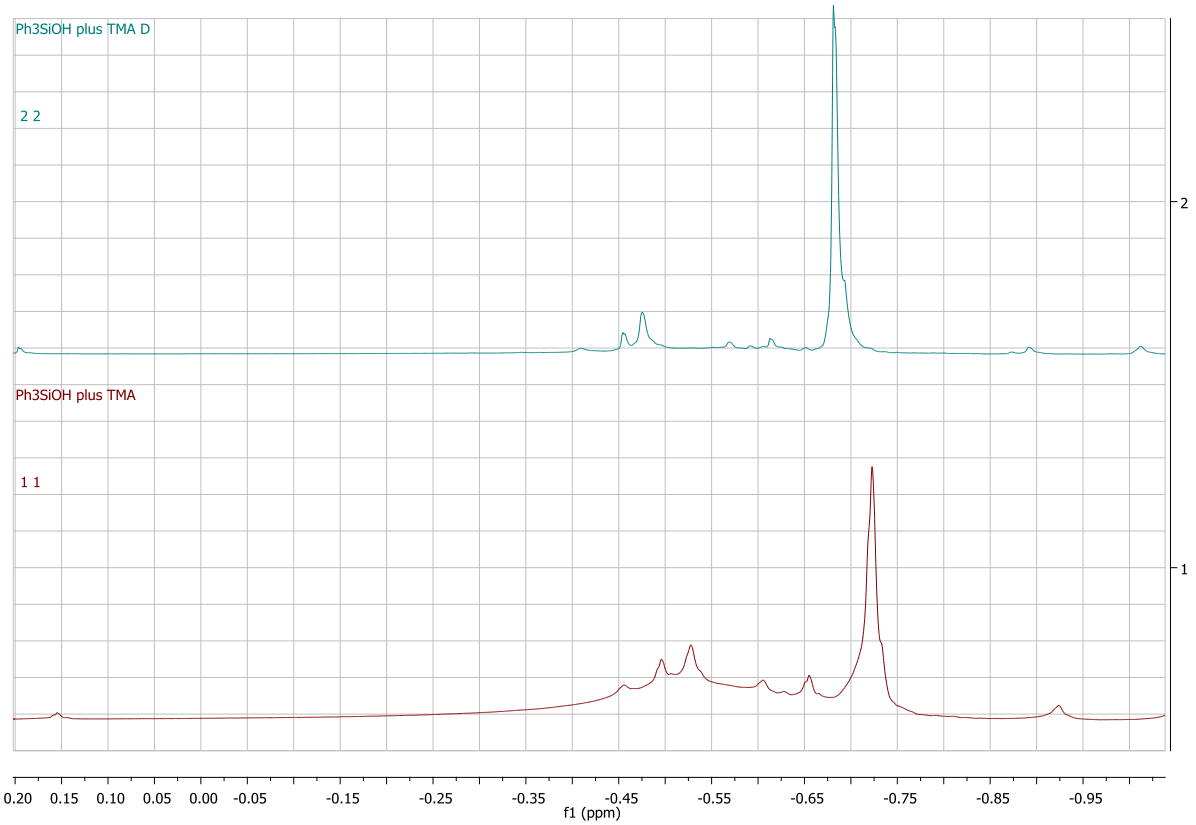

Figure 5.3: ^{1}H NMR spectra of TMA+ Ph_3SiOH in toluene. The spectrum at the top is from addition of Ph_3SiOH at –15 °C, and the spectrum at the bottom from addition at –78 °C.

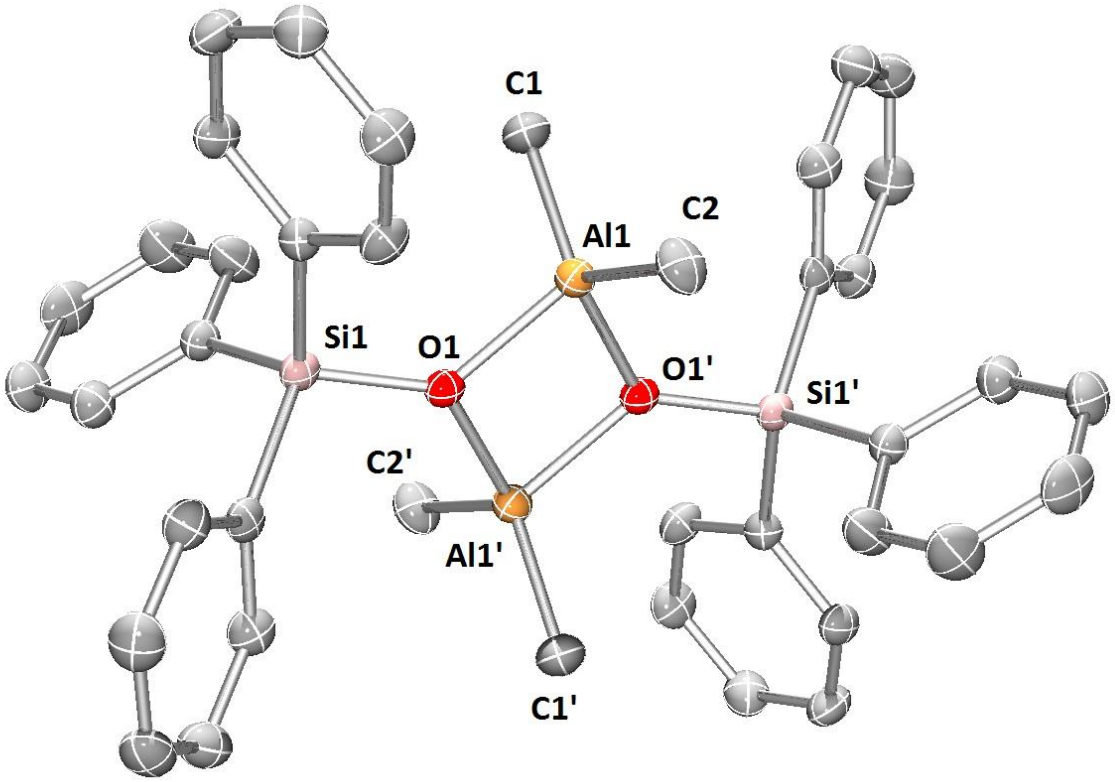

Figure 5.4: Crystal structure of the $[Me_2Al(\mu\text{-}OSiPh_3)]_2$ dimer.

TMA + $(C_8H_{17})_3SiOH$

The ^{1}H NMR spectrum of the products from the reaction of TMA with $(C_8H_{17})_3SiOH$ shows that there are 3 different Al-Me environments; there are three main peaks at the Al-Me area at –0.24, –0.31 and –0.37 ppm (Figure 5.5) with a ratio of 1.4/1.0/3 respectively. If the only product of the reaction was the dimer $[Me_2Al(\mu\text{-}OSiOct_3)]_2$, then only one signal should appear at the Al–Me area. So, perhaps apart from the dimer, the trimer or higher oligomers were also formed.

When the reaction product was dried under vacuum overnight the middle peak (δ –0.31 ppm) was reduced.

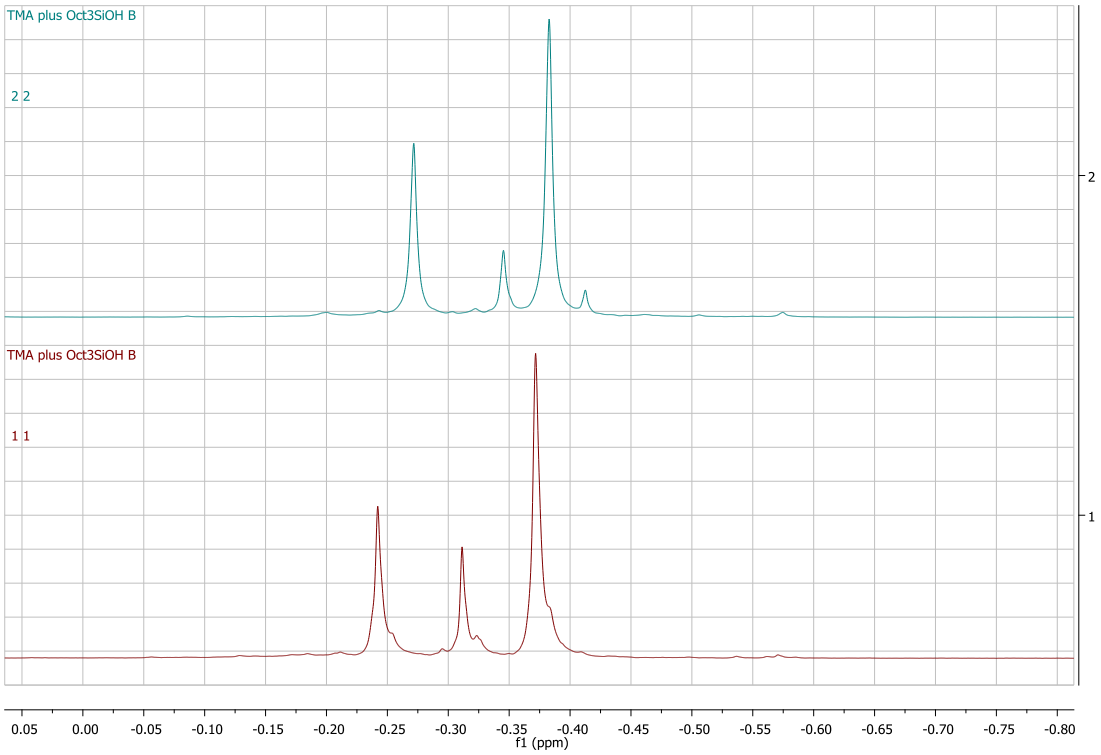

Figure 5.5: ^{1}H NMR spectra of the product of the TMA + Oct_3SiOH reaction in toluene. The upper spectrum corresponds to the reaction mixture that was dried overnight and re-dissolved in toluene. (Different concentrations might explain the differences we observe in the chemical shifts.)

TMA + $^{i}Pr_3SiOH$

When $^{i}Pr_3SiOH$ was added to TMA at −78 °C, two main peaks appeared in the Al–Me region at δ −0.25 (Peak A) and −0.38 ppm (Peak B) with a ratio of 1/2.8. The most favourable product of the reaction should be the dimer $[Me_2Al(\mu\text{-}OSi(i\text{-}Pr_3))]_2$, but the ^{1}H NMR spectrum of the compound shows that two different products are competing (Figure 5.7, bottom spectrum).

When addition of $^{i}Pr_3SiOH$ takes place at higher temperature (−15 °C), the intensity of the peak at δ −0.25 increases (ratio of Peak A/Peak B = 1/0.9), while two smaller peaks appear (δ −0.21, −0.22) (Figure 5.6, top spectrum). Reaction at lower temperatures results in less reaction products. In both cases, methane is formed as expected (verified by a peak at δ 0.26).

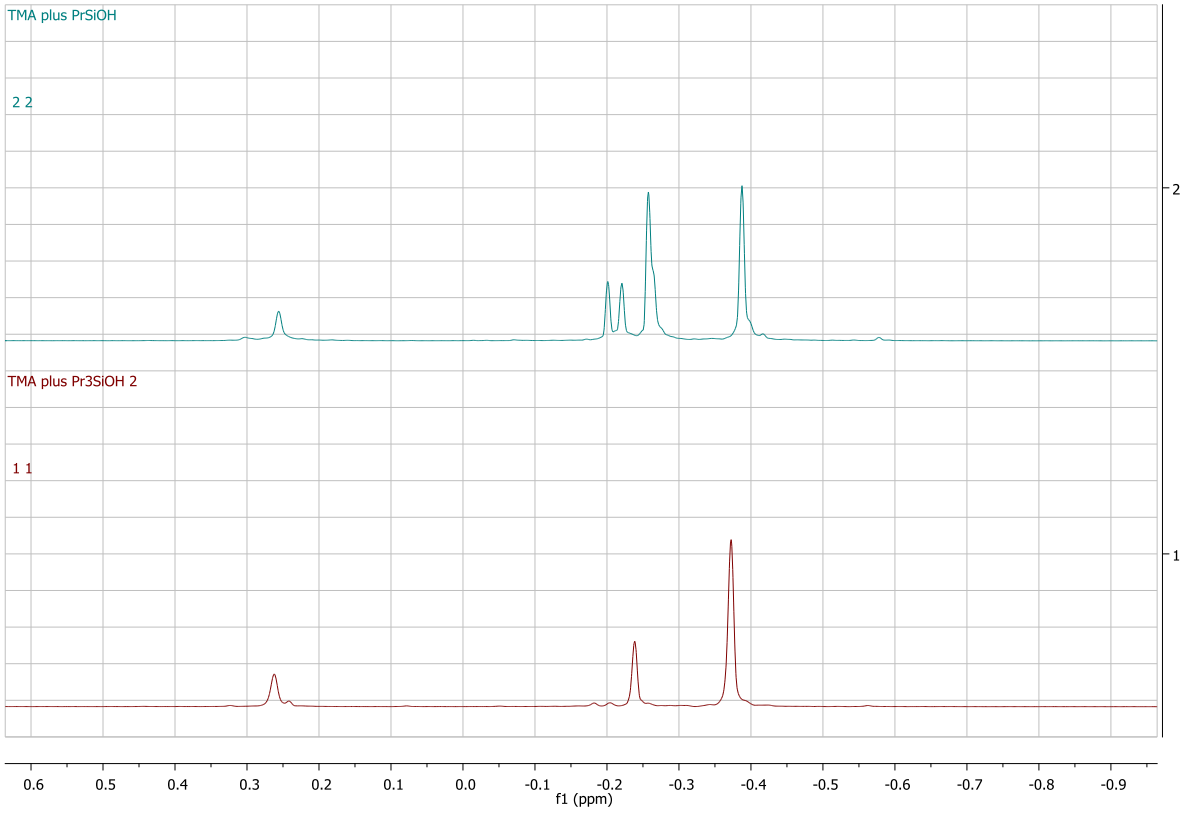

Figure 5.6: ^{1}H NMR spectra of TMA+$^{i}Pr_3SiOH$ in toluene (bottom spectrum: addition of $^{i}Pr_3SiOH$ at −78 °C, top spectrum: addition of $^{i}Pr_3SiOH$ at −15 °C)

The main product of the reaction of TMA with $(C_8H_{17})_3SiOH$ and $^{i}Pr_3SiOH$ is most possibly a dimeric Al siloxide $\{[Me_2Al(\mu\text{-}OSiOct_3)]_2$ and $[Me_2Al(\mu\text{-}OSi(i\text{-}Pr_3))]_2$,

respectively}, as it was similarly observed in the reaction of TMA and Ph_3SiOH. However, the low selectivity of the reaction is probably responsible for the formation of a mixture of higher oligomers that give rise to the additional peaks on the ^1H NMR spectra.

5.2.3 Polymerizations in Toluene

5.2.3.1 General Information

Four different commercial MAO solutions, supplied by Chemtura, were used in this study; the labels "MAO" and "MAOb" refer to toluene solutions of MAOs prepared by two different proprietary processes. All samples were supplied as toluene solutions containing 10 or 30 weight % of Al compounds ("MAO-10" and "MAO-30"): the weight % being a percentage of the combined weight of MAO + TMA. The TMA content of these MAO grades was determined by NMR spectroscopy following the addition of THF as discussed previously[53-55:] their specifications are summarized in the Experimental Section (Table 5.1).

The performance of catalysts generated with modified MAOs using additives such as silanols with long alkyl chains ($C_{12}H_{25}Ph_2SiOH$, Oct_3SiOH), branched disilanols [$^tBu_2Si(OH)_2$] or higher alkylaluminium compounds [Al(*i*-Bu)$_3$, Al(Oct)$_3$] was tested in heptane. The aim of adding such additives was to produce a heptane-soluble aluminoxane and achieve better performance. However, in order to better understand the behaviour of a modified MAO with silanols, some polymerization studies were performed firstly in toluene (with $^tBu_2Si(OH)_2$, $C_{12}H_{25}Ph_2SiOH$ and Ph_3SiOH). These studies highlighted the importance of the TMA content of the MAO solution used in the polymerization, which affects the activity of the catalyst and the final $\overline{M_n}$of the polymer. This initiated a new series of investigations on the performance of the catalyst system with varying amounts of TMA: increasing the amount by adding TMA or reducing it by adding DBP (a TMA scavenger).[18]

For the A1 and A2 series the general protocol was:

(i) the required amount of the MAO solution was allowed to react with the additive (the silanol $^tBu_2Si(OH)_2$ or $C_{12}H_{25}Ph_2SiOH$ or TMA and DBP) for 1-2 h at 30 °C (other reaction conditions were investigated: varying temperature up to reflux temperature, varying the reaction time up to ~12 hours, but no enhancement of the polymerization performance was observed so the study was focused on the procedure described in detail in the experimental part.)

(ii) the catalyst precursor *rac*-Me_2Si(2-Me-Benz[e]Ind)$_2ZrCl_2$ was added and allowed to react with the modified MAO in toluene for 1 h at 30 °C before addition of 1-hexene. For the A3 series the first step was to remove all volatiles from the required amount of MAO by drying it under vacuum overnight. It was then suspended in heptane and allowed to react with Ph_3SiOH for 2 hrs at 45 °C before addition of the catalyst precursor.

When the polymerization started, samples were taken at regular intervals over a period of 3 h at 30 °C and quenched in THF-MeOH-HCl (100 : 1 : 1 v/v). The 1-hexene conversion was followed by NMR spectroscopy using pentamethylbenzene as the internal standard (e.g. Figure 5.7); the number-average molecular weight $\overline{M_n}$ was determined by gel permeation chromatography (GPC) techniques (e.g. Figure 5.8). The samples for NMR analysis were filtered and spectra recorded as soon as possible (within a few hours); samples for GPC investigation were left to dry overnight and analysed as THF solutions.

As required by eqn. 5.1 the initial monomer consumption proceeds linearly with time. Deviation from linearity in the latter stages of the reaction reflects monomer depletion. As reported previously by Song *et al.*[47], the time dependence of $\overline{M_n}$ under non-steady-state conditions (before the final equilibrium molecular weight is reached), given by eqn. 5.4.

$$\langle n\rangle = \frac{\frac{(k_p[M]_0 + k_t)t}{k_t} + \frac{k_p[M]_0 + k_t - k_i[M]_0}{k_i[M]_0(k_t - k_i[M]_0)}\left(e^{-k_i[M]_0 t} - 1\right) - \frac{(k_p[M]_0\, k_i[M]_0}{{k_t}^2\,(k_t - k_i[M]_0)}\left(e^{-k_t t} - 1\right)}{t + \frac{1}{k_i[M]_0}\, e^{-k_i[M]_0 t} - \frac{1}{k_i[M]_0}} \qquad (5.4)$$

where $\langle n\rangle = \overline{M_n}/m_M$ is the degree of polymerization (m_M is the relative molar mass of the monomer), $[M]_0$ is the monomer concentration at t = 0, k_i is the initiation rate constant, k_t the termination rate constant, k_p the propagation rate constant, and t the reaction time.

Curve fitting gives acceptable estimates of k_p and k_t. Varying k_i over a wide range of values has only a small effect on the curve fitting (e.g. varying k_i over 30 orders of magnitude results in variations in k_p and k_t of less than 50%). The best estimate of k_i was obtained for MAO-30 solutions and then used as a constant for the other MAO grades.

The NMR data gathered by all polymerization runs were fitted according to eqn. 5.5, as previously reported:[56]

$$\text{Slope} = m_M \cdot [M]_0 \cdot C^0 \cdot k_p^{app} \qquad (5.5)$$

where C^0 = concentration of total catalyst precursor and k_p^{app} = apparent propagation rate.

As explained in the Introduction section, k_p as determined by eqn. 5.4 describes the rate of growth of the polymer chain, irrespective of the number of metal centres involved, while k_p^{app} (eqn. 5.5) takes into account the total catalyst concentration, whether active or dormant. Eqn. 5.3 is a very useful tool because the k_p^{app} / k_p ratio gives an estimate of the active species concentration involved in chain growth at any one time.

5.2.3.2 Polymerizations in Toluene with Addition of ^{t}Bu$_2$Si(OH)$_2$ and C$_{12}$H$_{25}$Ph$_2$SiOH (A1 series of experiments)

As shown in Table 5.1, modification of MAO with 0.53 mmol of ^{t}Bu$_2$Si(OH)$_2$ (i) enhanced the polymer yield (3.4 g) relative to the test polymerization, which used unmodified MAO and produced 2.6 g of poly(1-hexene). The highest polymer yield (3.5 g) arose from the reaction containing MAO modified with 1.06 mmol of ^{t}Bu$_2$Si(OH)$_2$ (ii), however when a higher amount (2.12 mmol) of ^{t}Bu$_2$Si(OH)$_2$ (iii) was employed the polymer yield reduced to 2.4 g. Modification of MAO with C$_{12}$H$_{25}$Ph$_2$SiOH also enhanced the polymer yield (3.2 g) compared to the test polymerization. As expected the MMAO with 1.06 mmol and 0.53 mmol of ^{t}Bu$_2$Si(OH)$_2$ showed the highest k_p^{app} (0.25 L mol^{-1}s^{-1}), followed by the MMAO with 0.53 mmol of C$_{12}$H$_{25}$Ph$_2$SiOH (see Table 5.2). The k_p^{app} of the test polymerization was lower (0.19 L mol^{-1}s^{-1}) and the MMAO with the highest amount of ^{t}Bu$_2$Si(OH)$_2$ showed the lowest k_p^{app} (0.17 L mol^{-1}s^{-1}).

MMAOs with ^{t}Bu$_2$Si(OH)$_2$ or C$_{12}$H$_{25}$Ph$_2$SiOH generate polymers with a lower final $\overline{M_n}$ (ranging from 46000 to 38500) compared to the final $\overline{M_n}$ (66200) of the poly(1-hexene) produced by the unmodified MAO. As expected, the unmodified MAO showed the lowest k_p and k_t values, with the k_t value ($2.35 * 10^{-3}$s^{-1}) being significantly lower than the those associated with the MMAOs (ranging from 4.88 to $3.53 * 10^{-3}$s^{-1}) , which comes into agreement with the lower $\overline{M_n}$ values observed. The active species count was higher for MMAOs with 1.06 mmol and 0.53 mmol of ^{t}Bu$_2$Si(OH)$_2$ (0.20 and 0.19 respectively) as a consequence of their higher k_p^{app}; the active species count for the unmodified MAO was not

significantly different (0.17). The polydispersities, $\overline{M_w}/\overline{M_n}$, of the polymers produced with MMAOs were ≈ 1.9 - 2.1, with the same value being obtained by unmodified MAO (2.0).

Polymerizations with MMAO with $^{t}Bu_2Si(OH)_2$ (i and ii) show a higher catalytic activity, but this can simply be the result of the silanol acting as a TMA scavenger. Since the MAO solution has not been dried before addition of the silanol, it contains its initial amount of TMA. Therefore it is a possibility that the silanol reacts preferentially with the free TMA, since TMA is the most reactive component.

When MAO was treated with additives essentially free of Si-OH groups, such as hydrocarbylsiloxanes,[38] enhanced activity in ethylene polymerization was observed for certain siloxy-aluminium compositions. However, a substantial reduction of free TMA is reported which could imply that the hydrocarbylsiloxanes act, like in the present study, as TMA scavengers, with the enhancement of polymerization being attributed to this fact. The study where hydroxysiloxanes and especially where siloxane diols[39] were used as additives does not state if MAO had been previously dried to remove any free TMA or not.

Table 5.1: Polymerization conditions, productivity and equilibrium $\overline{M_n}$ of 1-hexene polymerizations in toluene.

Polym. Run A1	**[TMA][a] (mmol L^{-1})**	**[Al as MAO][b] (mol L^{-1})**	**Si (mmol L^{-1})**	**Al_{MAO} /Si/ Al_{TMA}**	**Polymer (g)**	**Final $\overline{M_n}$**
MAO-30 (I)	22	0.18	-	-	2.6	66200
MAO-30 (I) + $^{t}Bu_2Si(OH)_2$ (i)	22[b]	0.18	11	17.1 : 1 : 2.1	3.4	43400
MAO-30 (I) + $^{t}Bu_2Si(OH)_2$ (ii)	22	0.18	21	8.6 : 1 : 1.0	3.5	44500
MAO-30 (I) + $^{t}Bu_2Si(OH)_2$ (iii)	22	0.18	42	4.3 : 1 : 0.5	2.4	46000
MAO-30 (I) + $C_{12}H_{25}Ph_2SiOH$	22	0.18	11	17.1 : 1 : 2.1	3.2	38500

[a]Concentration of TMA in the polymerization reaction mixture

[b] This is the theoretical amount of TMA that would have been present in the reaction, without addition of the silanol. It is verified by NMR studies (see section 5.2.5) that [TMA] is reduced after addition of a silanol or silanediol.

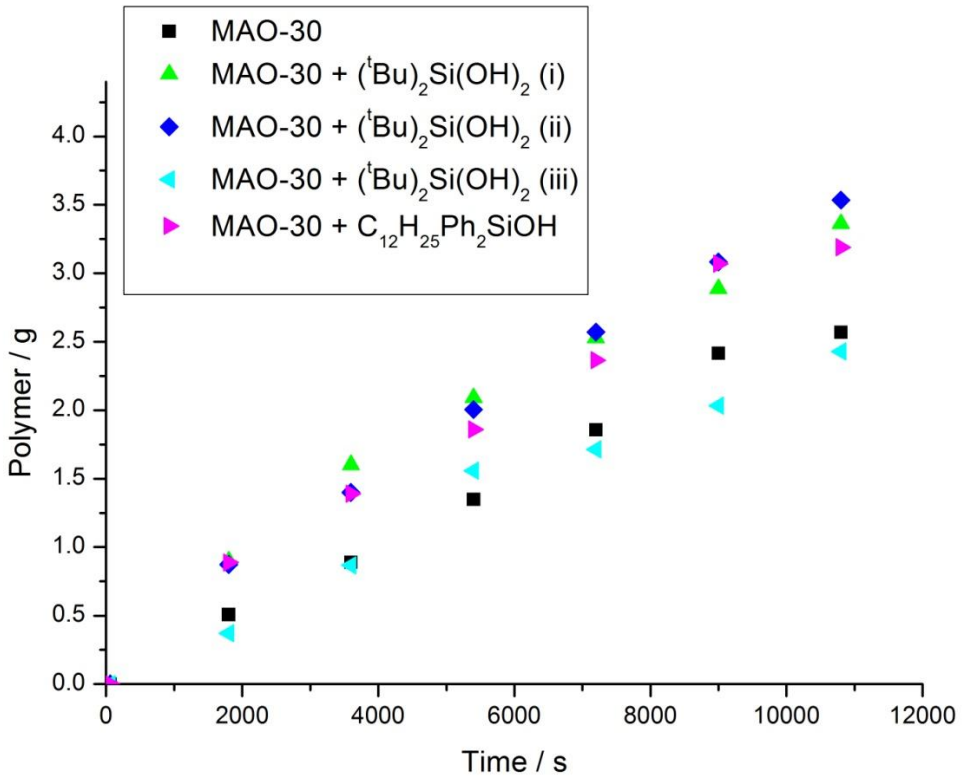

Figure 5.7: Productivity as a function of reaction time for MAOs modified with $^{t}Bu_2Si(OH)_2$ or $C_{12}H_{25}Ph_2SiOH$ in toluene. A test polymerization with unmodified MAO is displayed for comparison.

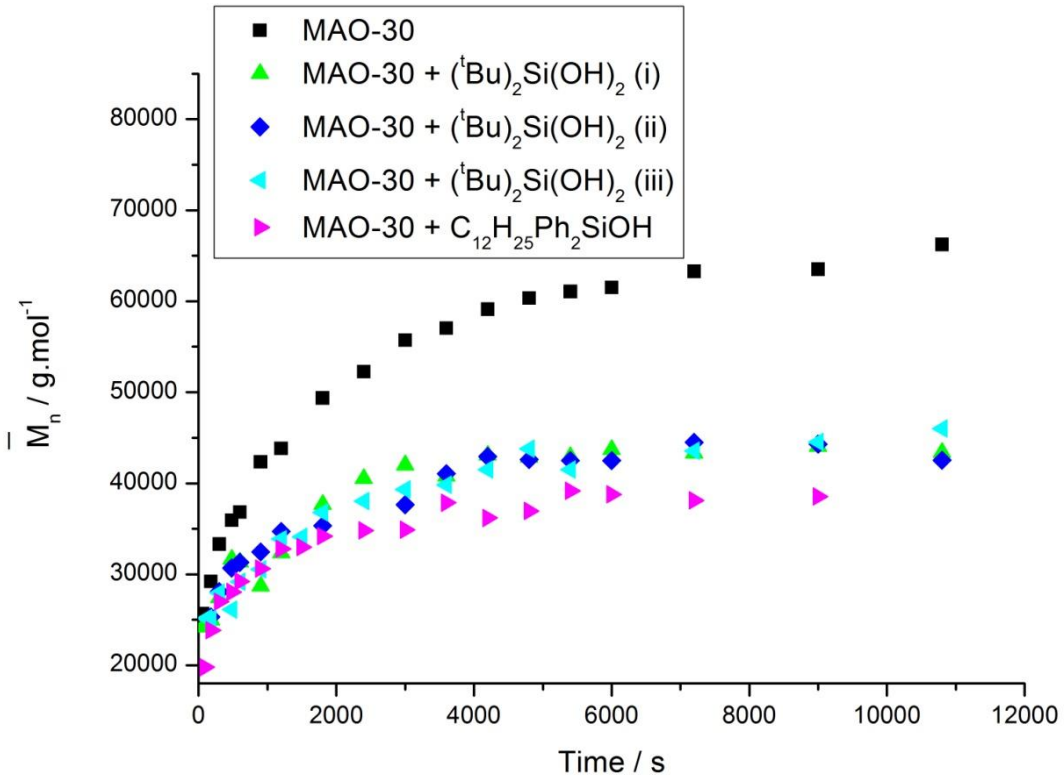

Figure 5.8: Time dependence of $\overline{M_n}$ for MAOs modified with $^{t}Bu_2Si(OH)_2$ or $C_{12}H_{25}Ph_2SiOH$ in toluene. A test polymerization with unmodified MAO is displayed for comparison.

Table 5.2: Summary of the kinetic parameters for modified MAOs with $^{t}Bu_2Si(OH)_2$ or $C_{12}H_{25}Ph_2SiOH$ in toluene. The results from a test polymerization with unmodified MAO are presented.

Aluminoxane	k_p $(L\,mol^{-1}s^{-1})$	k_t $(10^{-3}s^{-1})$	k_i $(L\,mol^{-1}s^{-1})$	k_p^{app} $(L\,mol^{-1}s^{-1})$	k_p^{app}/k_p
MAO-30	1.10 ± 0.04	2.35 ± 0.12	3.8	0.19 (± 0.004)	0.17
+ $^{t}Bu_2Si(OH)_2$ (i)	1.34 ± 0.08	4.19 ± 0.31	3.8	0.25 ± 0.01	0.19
+ $^{t}Bu_2Si(OH)_2$ (ii)	1.24 ± 0.07	3.93 ± 0.28	3.8	0.25 (± 0.007)	0.20
+ $^{t}Bu_2Si(OH)_2$ (iii)	1.12 ± 0.07	3.53 ± 0.28	3.8	0.17 (± 0.006)	0.15
+ $C_{12}H_{25}Ph_2SiOH$	1.35 ± 0.06	4.88 ± 0.26	3.8	0.24 (± 0.009)	0.18

The higher productivity of the polymerizations with MMAO with $^{t}Bu_2Si(OH)_2$ (i and ii) and $C_{12}H_{25}Ph_2SiOH$, shown in Figure 5.7, is probably a result of the reduction of [TMA] due to addition of the silanols. However, polymerizations with MMAO with $^{t}Bu_2Si(OH)_2$ (i and ii) and $C_{12}H_{25}Ph_2SiOH$ show an obvious decrease in $\overline{M_w}$, which was not anticipated (reduction of [TMA] should have inhibited chain termination due to transfer to TMA, and thus result in higher molecular weights). This phenomenon could only be associated with the formation of new species due to side reactions of MAO with the silanols which may be responsible for early chain termination.

5.2.3.3 Polymerizations in Toluene with Addition of TMA or 2,6-di-*tert*-butylphenol (DBP), (A2 series of experiments)

The results of the A1 series of polymerizations highlighted the importance of the TMA concentration in the polymerization reaction for the performance of the catalyst system in 1-hexene polymerizations in toluene. This initiated a new series of experiments with the aim to establish the exact relationship between the TMA content and the polymer yield and final $\overline{M_n}$ of the polymer produced. Two different MAO solutions were used for this study, MAO-10 and MAO-30-II (coming from a second batch of MAO-30 solutions supplied by Chemtura); both solutions were two months old at the time of the analysis. Figures 5.9 and 5.10 show the productivity and $\overline{M_n}$ of MAO solutions with different TMA concentrations as a function of reaction time, and prove that TMA has a primary role in determining catalyst productivity and molecular weight.

MAO-10 has a higher TMA content than MAO-30-II, which probably explains the lower polymer yield (2.4 g) and $\overline{M_n}$ (52300) when compared to the MAO-30-II (4.9 g and 70200). When BHT was added to the MAO-10 solution an enhancement of the polymer yield (4.4 g) and $\overline{M_n}$ (76900) was observed (see Table 5.3). DBP acts as a TMA scavenger[57-59], thus reducing the amount present in the polymerization reaction. The final TMA content in this polymerization mixture should be close to that of the MAO-30-II reaction mixture, justifying the similar performance of the two systems. Conversely, when extra TMA was added to the MAO-30-II solution, a decrease of the polymer yield (2.6 g) and final $\overline{M_n}$ (48700) was observed; this performance being almost identical to that exhibited by the MAO-10 system. This could be explained by the fact that the two systems have the same concentration of TMA. As expected the MAOs with the lower TMA concentration showed

the highest k_p^{app} (0.37 – 0.31 L $mol^{-1}s^{-1}$) compared to the k_p^{app} of the MAOs with the higher TMA concentrations (0.18 – 0.19 L $mol^{-1}s^{-1}$); and the lowest k_t values (2.20 – 2.98 $* 10^{-3}s^{-1}$) compared to the k_t values (3.29 – 4.17 $* 10^{-3}s^{-1}$) of the high TMA concentration MAOs (see Table 5.4). Their k_p values are also relatively lower and the active species count is higher, as expected (0.29 – 0.30 for low TMA concentrations and 0.12 – 0.15 for high).

The comparison of the kinetic parameters shown in Table 5.4 with catalyst productivities taken from the literature is not meaningful due to the scarcity of data available for 1-hexene polymerizations and the variety of reaction conditions used (cocatalyst, Al/Zr, temperature, [monomer]). The active site counts of $k_p^{app} / k_p = 0.12 - 0.30$ are higher than reported for *rac*-Me_2Si(1-indenyl)$_2ZrCl_2$/MAO (0.08; 40 °C, Al/Zr = 2400, propene)[47] and resembles that found for trityl borate activated metallocenes;[48-49] the values found here are however in line with data reported by Busico *et al.* for propene polymerizations with *rac*-Me_2Si(2-Me-4-Ph-Ind)$_2ZrCl_2$/MAO, for which quenched-flow kinetic studies suggested an active site count of 0.58 (at 40 °C, Al/Zr = 2200).[60] The polydispersities were 1.7 – 2.3 for all MAO grades, which are close the values reported in the literature[61] for the catalyst system used in this study.

The relationship between catalyst productivity or $\overline{M_n}$ and TMA concentration was also investigated by the post-doctoral researcher Fabio Ghiotto of the Bochmann group by studying the polymerization performance of MAOs with different preparative histories ('MAOb-30', 'MAOb-10', provided also by Chemtura, but they were synthesized using a different proprietary process, and 'MAO-30HT' which is an MAO prepared with the same process as 'MAO-30-II' but it has a higher TMA content). A summative comparison of the MAOs examined in the current study and the study of F.Ghiotto in relation to the [TMA] is presented in Ref. 18. The influence on catalyst productivity is due to the well-known[60, 62-64] competition between the monomer substrate and TMA for catalyst binding sites; depicted in Scheme 5.6. When a graph of the productivity vs [TMA] is plotted, the MAOs with different preparative history do not fall into the same line, which could be explained by the fact that they form counter-ions with subtly different structures, resulting in ion pairs [L_nZr(polymeryl)$^+$...Me-MAO$^-$] that have slightly different energies from one another.[18]

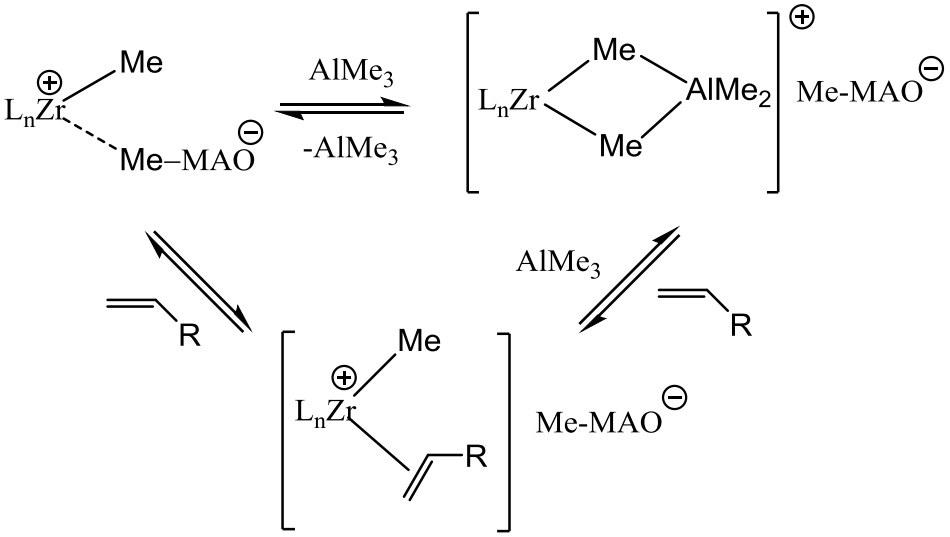

Scheme 5.6: Competition between the monomer substrate and TMA for catalyst binding sites

End-group analysis of the poly(1-hexene) produced by MAO-10 and MAO-30-II, showed absence of unsaturated vinyl and vinylidene end groups, so β-H processes (β-H transfer to metal or β-H transfer to monomer) are absent or below the detection limit. This means that the major contribution to chain termination and hence to the equilibrium molecular weight limit is chain transfer to the aluminium (i.e. to TMA). The MAO/TMA activation system differs in this respect from hexene polymerizations with borate-activated metallocene, where anion-dependent unsaturated end groups prevail[65].

The rate of the transfer of the polymeryl chain to TMA depends on the concentration of B (see Scheme 5.7), which is a function of the TMA association equilibrium K_{ass}. This could explain the different behaviour of MAOs with different preparative history when the $\overline{M_n}$ is plotted against [TMA][18].

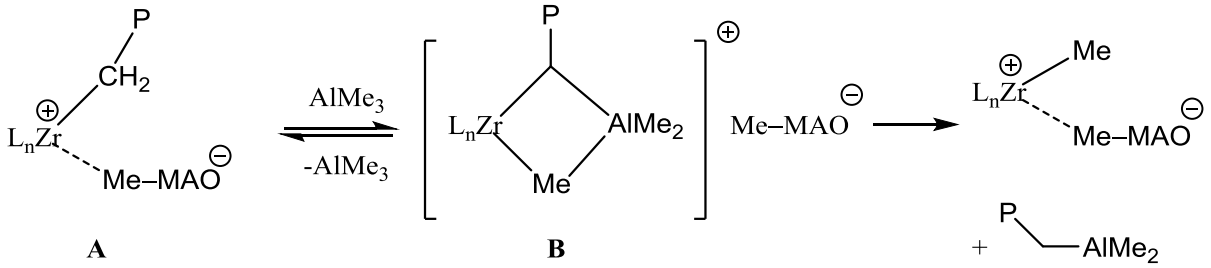

Scheme 5.7: Transfer of the polymeryl chain to TMA

Table 5.3: Polymerization conditions, catalyst productivity and equilibrium $\overline{M_n}$ of 1-hexene polymerizations in toluene.

Polym. Run A2	**[TMA][a] (mmol L^{-1})**	**[Al as MAO][b] (mol L^{-1})**	**TMA added (mmol L^{-1})**	**DBP added (mmol L^{-1})**	**Polymer (g)**	**Final $\overline{M_n}$**
MAO-10	61	0.14	-	-	2.4	52300
MAO-10 + DBP	61	0.14	-	48	4.4	76900
MAO-30 (II)	13	0.19	-	-	4.9	70200
MAO-30 (II) + TMA	13	0.19	48	-	2.6	48700

[a] Concentration of TMA in the reaction mixture, without taking into account addition of TMA or DBP

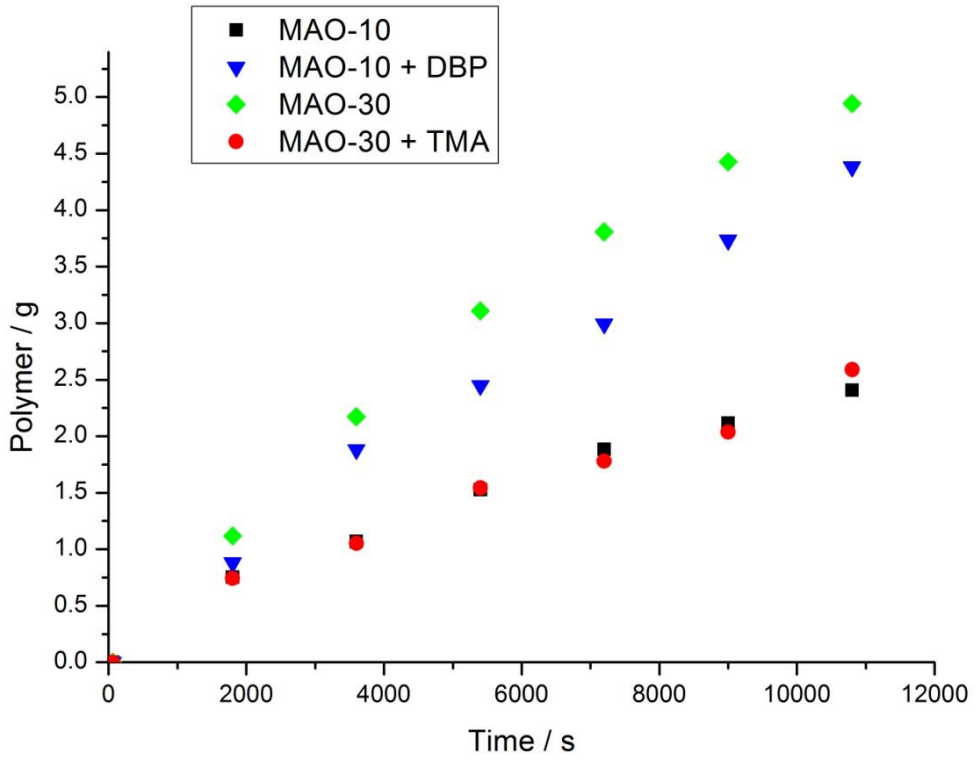

Figure 5.9: Productivity as a function of reaction time for different MAOs after adjusting the TMA content

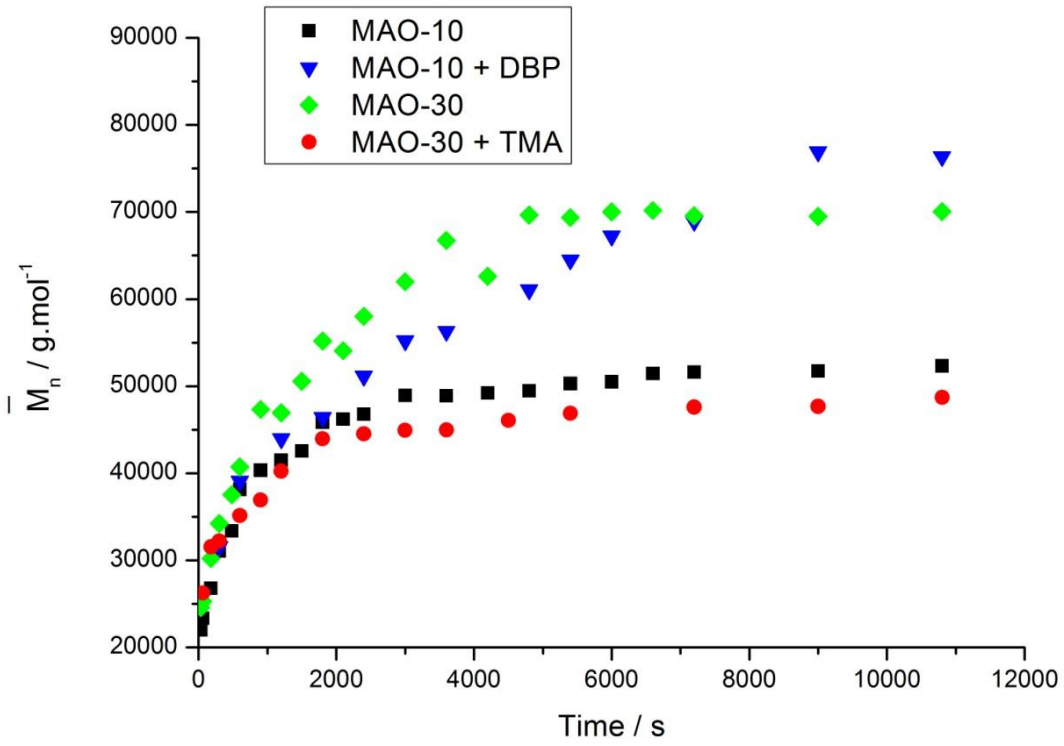

Figure 5.10: Time dependence of $\overline{M_n}$ for different MAOs after adjusting the TMA content

Table 5.4: Summary of the kinetic parameters for different MAOs and MAOs after addition of TMA or DBP in toluene.

Aluminoxane	k_p $(L\,mol^{-1}s^{-1})$	k_t $(10^{-3}s^{-1})$	k_i $(L\,mol^{-1}s^{-1})$	k_p^{app} $(L\,mol^{-1}s^{-1})$	k_p^{app}/k_p
MAO-10	1.25 ± 0.03	3.29 ± 0.10	3.8	0.19 (± 0.009)	0.15
MAO-10 + DBP	1.06 ± 0.08	2.20 ± 0.24	3.8	0.31 ± (0.008)	0.29
MAO-30 (II)	1.24 ± 0.06	2.98 ± 0.17	3.8	0.37 ± 0.01	0.30
MAO-30 (II) + TMA	1.45 ± 0.09	4.17 ± 0.29	3.8	0.18 (± 0.008)	0.12

5.2.3.4 Polymerizations in Toluene with Addition of Ph_3SiOH (A3 series of experiments)

The results of the A1 series of polymerizations showed that it was important to investigate the behaviour of a modified MAO with a silanol after the MAO solution has been pre-dried in order to remove any 'free' TMA and re-dissolved in toluene. This procedure was essential in order to be able to understand the effect on the catalyst system's polymerization

performance in the presence of silanol, when it is incorporated into the MAO structure without the TMA-silanol reaction blurring MAO's behaviour in the catalytic process. The silanol that was chosen here was Ph_3SiOH, because it is commercially available and because the products of the reaction of TMA with Ph_3SiOH have been further investigated with success in this study.

The productivity of the polymerization with unmodified 'MAO-10' and MMAO with Ph_3SiOH, and the $\overline{M_n}$ as a function of reaction time is given in Figures 5.11 and 5.12. The polymerization conditions, final productivity and final $\overline{M_n}$ are presented in Table 5.5 and the kinetic parameters are presented in Table 5.6.

The modified MAO produces a lower polymer yield (2.0 g) compared to unmodified MAO (2.5 g), and as expected, is associated with a lower k_p^{app} ($0.14 * L\,mol^{-1}s^{-1}$) compared to the k_p^{app} ($0.18 * L\,mol^{-1}s^{-1}$) of the unmodified MAO. It also has a lower $\overline{M_n}$ (44600 compared to the 64700), and as expected this would mean a higher k_t ($3.58 * 10^{-3}s^{-1}$ compared to $2.42 * 10^{-3}s^{-1}$). As it can be predicted, the MMAO is associated with a lower active species count (0.13 compared to 0.17 of the test polymerization). The polydispersities of the polymer produced with MMAO was 1.6; very close to the value obtained for unmodified MAO (1.7), with the catalyst retaining its single-site character, as expected.

Table 5.5: Polymerization conditions, productivity and equilibrium $\overline{M_n}$ of 1-hexene polymerizations for MAO and MAO+Ph_3SiOH activators in toluene

Polym. Run A3	**[TMA] added (mmol L^{-1})**	**[Al as MAO] (mol L^{-1})**	**Si (mmol L^{-1})**	**Al_{MAO} : Si : Al_{TMA}**	**Polymer (g)**	**Final $\overline{M_n}$**
MAO-10	23[a]	0.14	-	-	2.5	64700
MAO-10 + Ph_3SiOH	23	0.14	42	3.3 : 1 : 0.9	2.0	44600

[a] The MAO-10 contains an additional amount of ~15 mmol L^{-1} TMA, due to 'bound' TMA. After reaction of MAO-10 with the Ph_3SiOH any remaining TMA after drying has disappeared (see Section 5.2.5).

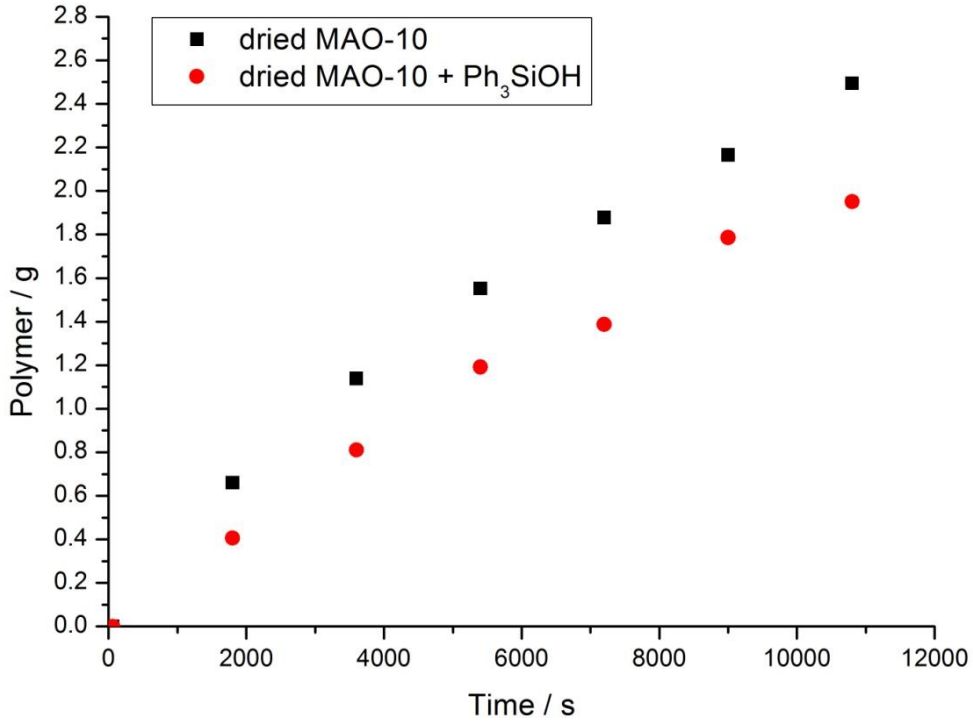

Figure 5.11: Productivity as a function of reaction time for modified MAO with Ph_3SiOH in toluene. A test polymerization with unmodified MAO is displayed for comparison.

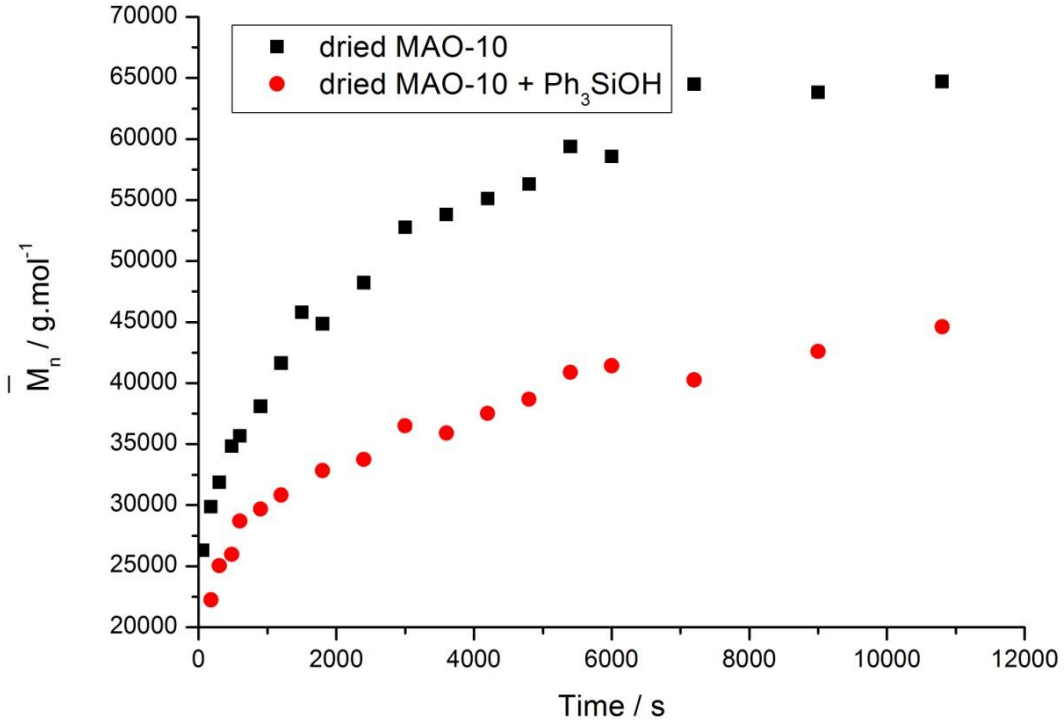

Figure 5.12: Time dependence of $\overline{M_n}$ for modified MAO with Ph_3SiOH in toluene. A test polymerization with unmodified MAO is displayed for comparison.

Table 5.6: Summary of the kinetic parameters for MAO modified with Ph_3SiOH in toluene. The MAO solution was pre-dried. The results from a test polymerization with unmodified MAO are presented.

Aluminoxane	k_p $(L\ mol^{-1}s^{-1})$	k_t $(10^{-3}s^{-1})$	k_i $(L\ mol^{-1}s^{-1})$	k_p^{app} $(L\ mol^{-1}s^{-1})$	k_p^{app}/k_p
dried MAO-10	1.08±0.06	2.42±0.19	3.8	0.18 (± 0.008)	0.17
+Ph_3SiOH	1.05±0.07	3.58±0.29	3.8	0.14 (± 0.004)	0.13

5.2.4 Polymerizations in Heptane

5.2.4.1 General Information

Industrially relevant solution-phase polymerizations are carried out not in saturated hydrocarbons rather than toluene. Since the catalyst precursor is practically insoluble in non-aromatic hydrocarbons, the success of such polymerizations depends on the method of

catalyst activation. Unmodified MAO is also poorly soluble in heptane. The solubility of MAO is improved slightly when Al(*i*-Bu)$_3$ (TIBA) is added, in agreement with the observations of Panchenko *et al*. about the solubilisation effect of TIBA on supported MAO[4.] Heptane-soluble MAO was produced by removing all volatiles from MAO solutions in toluene, suspending the TMA-depleted residue in heptane, and adding sufficient Al(Oct)$_3$ (TOA) to obtain a clear homogeneous solution. The solubilising effect of TOA on MAO is known[6]. A concentration of [TOA] = 32 mmol L^{-1} was chosen as the standard so that the AlR_3 concentration is roughly comparable to those used for polymerizations in toluene, where [TMA] = 13 – 61 mmol L^{-1}.

In the present study, the solubilizing effect of long chain silanols on MAO was investigated. Adding a sufficient amount of Oct_3SiOH or the reaction product of Oct_3SiOH + TMA results in a clear homogeneous MMAO solution in heptane. When $OctPh_2SiOH$ or $^tBu_2Si(OH)_2$ were used as additives, the same phenomenon was not observed: a clear homogeneous solution of MMAO in heptane was not produced.

Two different strategies were investigated to overcome solubility problems of the catalyst precursor in heptane:

(1) Dissolution of L_2ZrCl_2 in a minimal amount of toluene, followed by activation with modified MAO in heptane.

(2) Pre-activation of the catalyst in toluene, followed by removal of volatiles. Here, L_2ZrCl_2 was reacted with unmodified MAO in toluene for 10 minutes, followed by removal of the volatiles in vacuo (1 h). The residue was then suspended in heptane, and the specified amount of AlR_3 was added to obtain a homogeneous mixture. It proved important to avoid ageing of the catalyst, as pre-activated catalysts that had been left under vacuum overnight resulted in bimodal polymer molecular weight distributions.

Polymerizations with addition of AlR_3 with the method A follow strategy (1), while the ones with methods B and C follow strategy (2). Method B differs because the catalyst was allowed to react with the MAO for longer (1 h) and then the mixture was left to dry overnight. This resulted in a bimodal polymer molecular weight distribution, and for this reason this research focused on methods A and C and no results from method B are presented.

Polymerizations with modification of MAO by silanols or silanol products follow the 1st strategy.

The polymerization kinetics was studied following the same protocol as for reactions in toluene: using NMR spectroscopy to determine the monomer consumption and GPC techniques to obtain $\overline{M_n}$ values.

5.2.4.2 Polymerizations in Heptane with Addition of AlR_3 (B1 series of experiments)

The productivity of the polymerizations with addition of $AlMe_3$, Al(*i*-Bu)$_3$ or Al(Oct)$_3$ and the $\overline{M_n}$ as a function of reaction time are given in Figures 5.13 – 5.16.

The different dried MAO-30/AlR_3 compositions show very close k_p^{app} values ($0.10 - 0.13\ L\,mol^{-1}s^{-1}$) and productivities (1.4 – 1.8 g). On the other hand, the final $\overline{M_n}$ values are strongly influenced by the nature of the AlR_3 additive and decreases in the order R = *i*-Bu > Oct >> Me. TMA is a more efficient chain transfer reagent than the longer-chain aluminium alkyls. As expected, polymerizations with $AlMe_3$ as the additive show higher k_t ($6.31 - 7.34 * 10^{-3}s^{-1}$) compared to the ones with Al(*i*-Bu)$_3$ or Al(Oct)$_3$ ($2.51 - 3.48 * 10^{-3}s^{-1}$).

The results obtained by method A come in agreement with method C. The polydispersities of the polymers produced here were ≈ 1.8 – 2.6.

Table 5.7: Polymerization conditions, productivity and equilibrium $\overline{M_n}$ of 1-hexene polymerizations in heptanes.

Polym. Run B1 MAO-30 (II)	[AlR_3] added (mmol L^{-1})[a]	[Al as MAO][b] (mol L^{-1})	Polymer (g)	Final $\overline{M_n}$
dried MAO-30 + $AlMe_3$ (A)	32	0.19	1.6	26600
dried MAO-30 + Al(i-Bu)$_3$ (A)	32	0.19	1.8	51600
dried MAO-30 + $AlOct_3$ (A)	32	0.19	1.6	50000
dried MAO-30 + $AlMe_3$ (C)	32	0.19	1.5	24200
dried MAO-30 + Al(i-Bu)$_3$ (C)	32	0.19	1.6	62100
dried MAO-30 + $AlOct_3$ (C)	32	0.19	1.4	51000

[a] Concentration of AlR_3 added to the polymerization reaction mixture

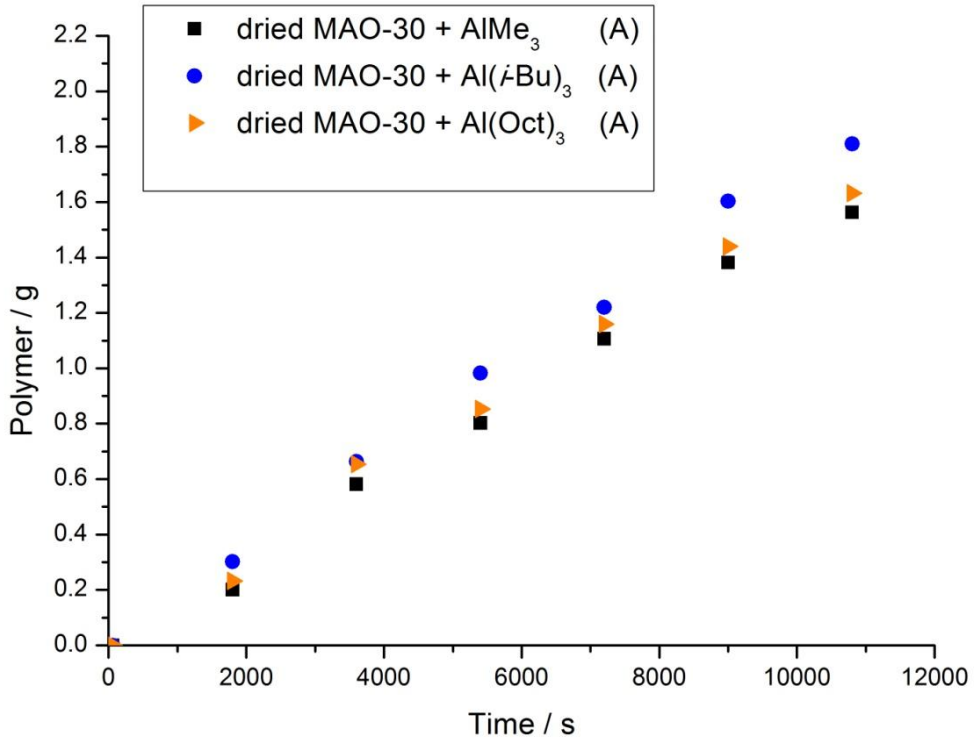

Figure 5.13: Productivity as a function of reaction time for different dried MAOs/AlR_3 compositions in heptane (Method A)

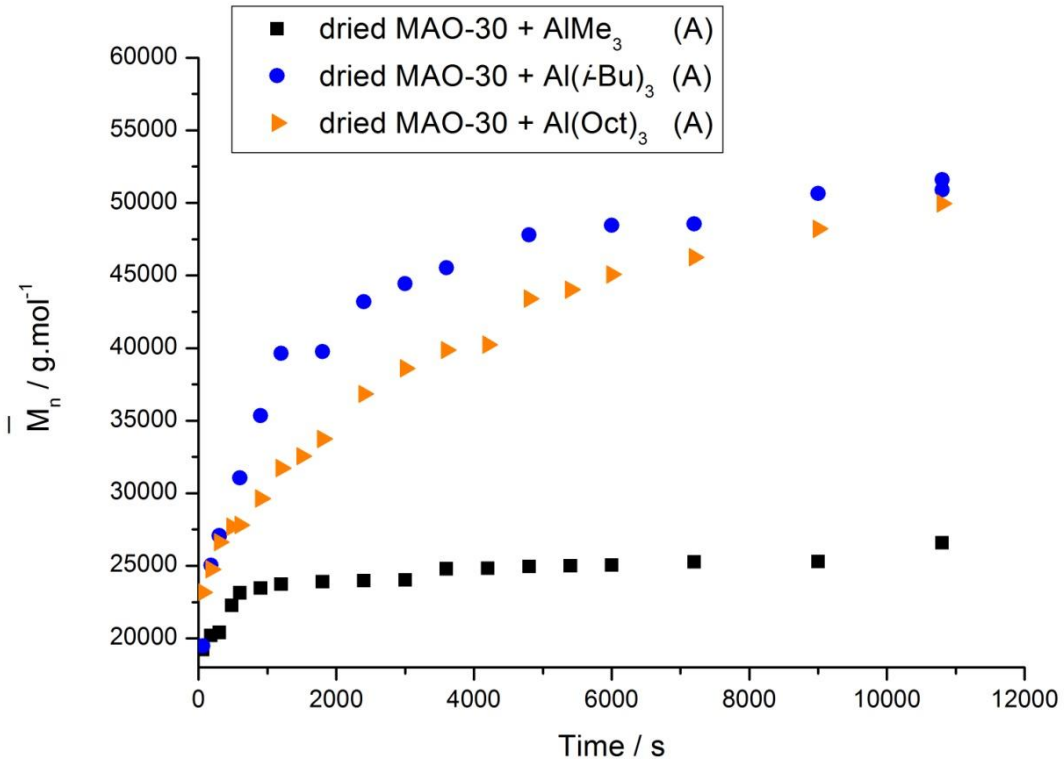

Figure 5.14: Time dependence of $\overline{M_n}$ for different dried MAOs/AlR_3 compositions in heptane (Method A)

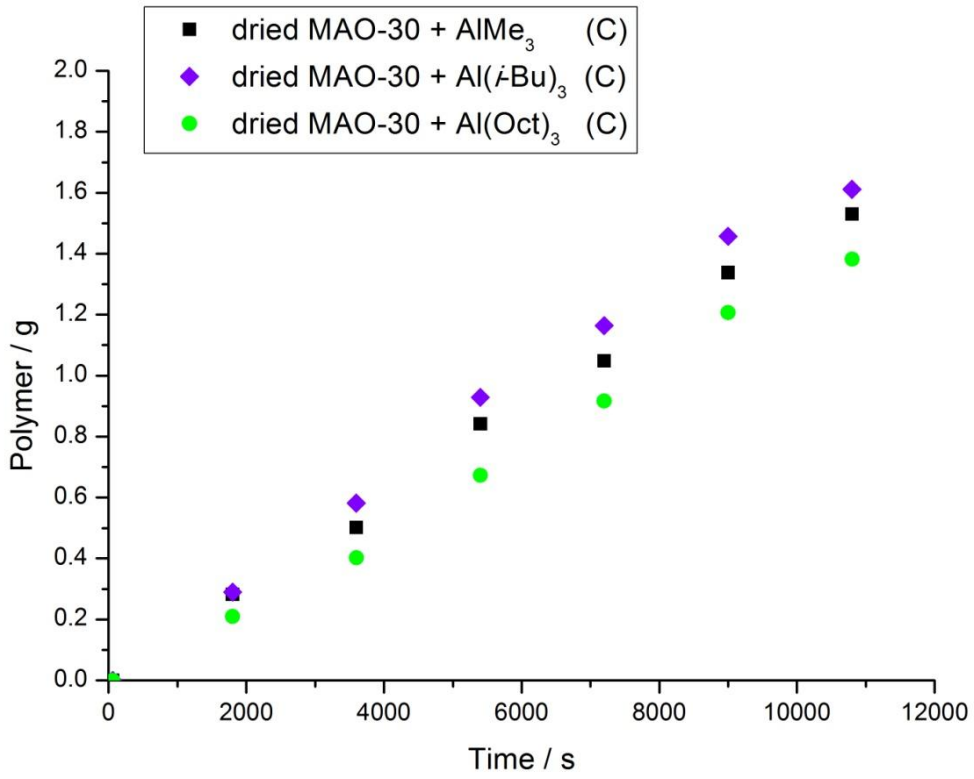

Figure 5.15: Productivity as a function of reaction time for different dried MAOs/AlR_3 compositions in heptane (Method C)

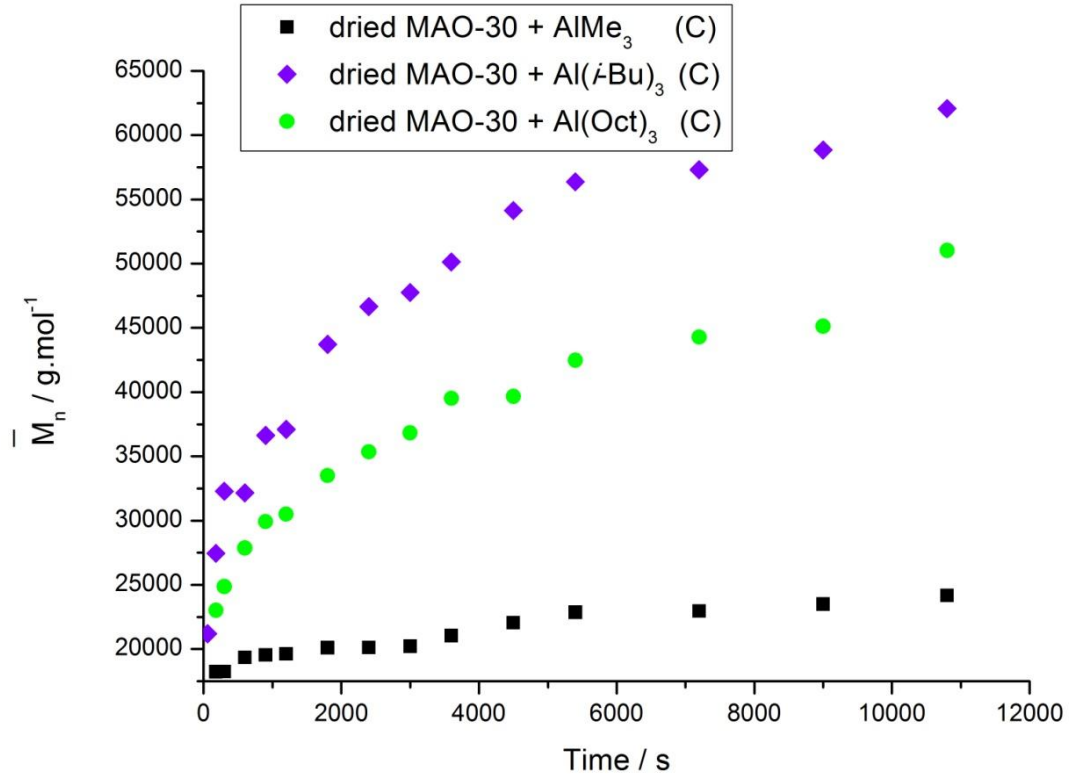

Figure 5.16: Time dependence of $\overline{M_n}$ for different dried MAOs/AlR_3 compositions in heptane (Method C)

Table 5.8: Summary of the kinetic parameters for different dried MAOs/AlR_3 compositions in heptane

Aluminoxane	k_p $(L\,mol^{-1}s^{-1})$	k_t $(10^{-3}s^{-1})$	k_i $(L\,mol^{-1}s^{-1})$	k_p^{app} $(L\,mol^{-1}s^{-1})$	k_p^{app}/k_p
dried MAO-30 + $AlMe_3$ (A)	1.37 ± 0.15	7.34 ± 0.88	3.8	0.11 (± 0.002)	0.08
dried MAO-30 + Al(*i*-Bu)$_3$ (A)	1.09 ± 0.04	3.02 ± 0.15	3.8	0.13 (± 0.002)	0.12
dried MAO-30 + Al(Oct)$_3$ (A)	1.11 ± 0.10	3.48 ± 0.39	3.8	0.12 (± 0.002)	0.11
dried MAO-30 + $AlMe_3$ (C)	1.05 ± 0.12	6.31 ± 0.83	3.8	0.11 (± 0.005)	0.10
dried MAO-30 + Al(*i*-Bu)$_3$ (C)	1.05 ± 0.07	2.51 ± 0.22	3.8	0.12 (± 0.006)	0.11
dried MAO-30 + Al(Oct)$_3$ (C)	0.97 ± 0.08	3.12 ± 0.31	3.8	0.10 (± 0.002)	0.10

5.2.4.3 Polymerization with Addition of $^{t}Bu_2Si(OH)_2$

Polymerization of MAO in heptane after addition of $^{t}Bu_2Si(OH)_2$ (11–21 mmol L^{-1}) gave very poor results. MAO was pre-dried in order to remove any free TMA and prevent preferential reaction of the silanediol with TMA.

5.2.4.4 Polymerizations with Addition of $C_{12}H_{25}Ph_2SiOH$ (B2 series of experiments)

As has already been stated, addition of $C_{12}H_{25}Ph_2SiOH$ to a pre-dried MAO suspension in heptane does not produce a clear homogeneous solution. The results presented in this study are associated with heterogeneous mixtures in heptane. Addition of a higher amount of $C_{12}H_{25}Ph_2SiOH$ (up to 64 mmol L^{-1}) has been tested, along with longer reaction times (~12 h) and higher temperatures (refluxing temperatures), although these attempts did not result to a heptane soluble MMAO.

The MAO used in this series of polymerization runs was a 'MAOb-30' solution. The productivity of the polymerizations with addition of $C_{12}H_{25}Ph_2SiOH$ (11 and 21 mmol L^{-1}) and the $\overline{M_n}$ as a function of reaction time are given in Figures 5.17 and 5.18.

Addition of $C_{12}H_{25}Ph_2SiOH$ does not seem to cause a decrease in the productivity (as was observed in the A3 series in toluene). The polymer yield (2.1 g) is similar with the unmodified MAOb-30 (2.2 g) (see Table 5.9 for polymerization conditions, productivity and equilibrium $\overline{M_n}$). In this test polymerization the unmodified MAO was dried under vacuum overnight and the same amount of TMA that was added in the polymerizations with $C_{12}H_{25}Ph_2SiOH$, was added back to the system in order to keep the other parameters that could affect the polymerization performance of the catalyst system the same. As expected, the three polymerization runs show similar k_p^{app}values (see Table 5.10 for kinetic parameters).

On the other hand, $\overline{M_n}$ values are strongly influenced by addition of $C_{12}H_{25}Ph_2SiOH$. A decrease in the final $\overline{M_n}$ of the polymer is obvious when the MMAO is used (24,600-28,000 compared to the 38,500). This decrease in $\overline{M_n}$ is of course associated with higher k_t values ($7.88 - 10.22 * 10^{-3} s^{-1}$) of the MMAO polymerizations, relative to the test polymerization with unmodified MAO ($4.89 * 10^{-3} s^{-1}$). MMAOs with $C_{12}H_{25}Ph_2SiOH$ also exhibit higher k_p values ($1.60 - 1.80\ \mathrm{L\ mol^{-1} s^{-1}}$) relative to the unmodified MAO

(1.33 L $mol^{-1}s^{-1}$), resulting in lower active species count (0.08 – 0.10 compared to 0.13). The polydispersities of the polymers produced here with MMAO or unmodified MAO were ≈ 1.9 - 2.0.

Table 5.9: Polymerization conditions, productivity and equilibrium $\overline{M_n}$ of 1-hexene polymerizations in heptane.

Polym. Run B2 MAOb-30	**[TMA] added (mmol L^{-1})**	**[Al as MAO][b] (mol L^{-1})**	**Si (mmol L^{-1})**	**Al_{MAO} : Si : Al_{TMA}**	**Polymer (g)**	**Final $\overline{M_n}$**
dried MAOb-30	41.8[a]	0.18	-	-	2.2	38500
dried MAOb-30 + $C_{12}H_{25}Ph_2SiOH$ (i)	41.8[b]	0.18	11	17.4 : 1 : 4.3	2.1	24600
dried MAOb-30 + $C_{12}H_{25}Ph_2SiOH$ (ii)	41.8[c]	0.18	21	8.7 : 1 : 2.2	2.1	28000

[a] This MAO contains an additional amount of ~4 mmol L^{-1} TMA, due to the 'bound' TMA

[b, c] The reaction mixture probably contains an additional amount of TMA < 4 mmol due to 'bound' TMA. The values can be estimated by comparison with Table 5.15.

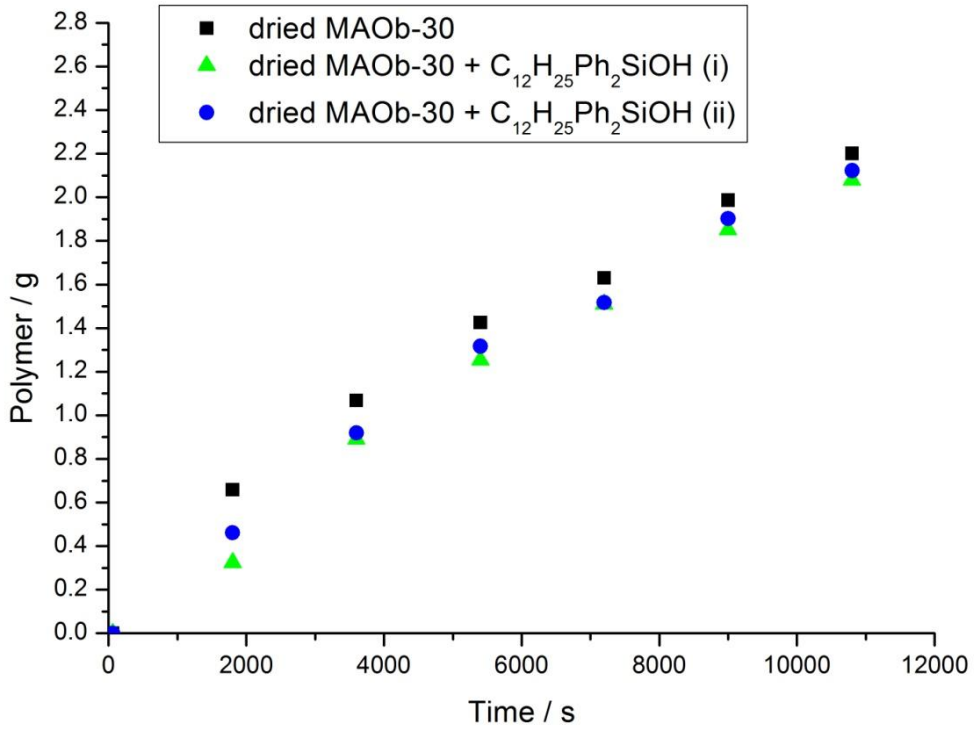

Figure 5.17: Productivity as a function of reaction time for modified MAO with $C_{12}H_{25}Ph_2SiOH$ in heptane. A test polymerization with unmodified MAO is displayed for comparison.

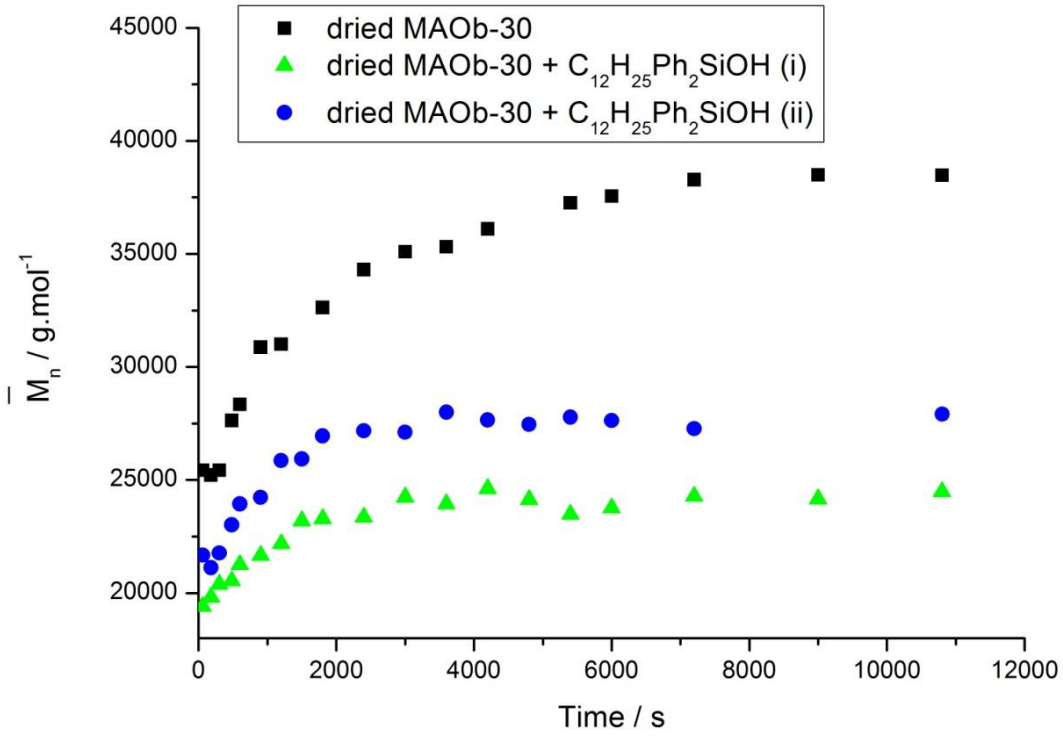

Figure 5.18: Time dependence of $\overline{M_n}$ for modified MAO with $C_{12}H_{25}Ph_2SiOH$ in heptane. A test polymerization with unmodified MAO is displayed for comparison.

Table 5.10: Summary of the kinetic parameters for modified MAO with $OctPh_2SiOH$ in heptane. The MAO solution was pre-dried. The results from a test polymerization with unmodified MAO are also presented.

Aluminoxane	k_p $(L\,mol^{-1}s^{-1})$	k_t $(10^{-3}s^{-1})$	k_i $(L\,mol^{-1}s^{-1})$	k_p^{app} $(L\,mol^{-1}s^{-1})$	k_p^{app}/k_p
dried MAO-30	1.33±0.08	4.89±0.35	3.8	0.17 (± 0.008)	0.13
+ $C_{12}H_{25}Ph_2SiOH$ (i)	1.80±0.13	10.22±0.78	3.8	0.15 (± 0.005)	0.08
+ $C_{12}H_{25}Ph_2SiOH$ (ii)	1.60±0.08	7.88±0.43	3.8	0.16 (± 0.005)	0.10

5.2.4.5 Polymerizations with Addition of Oct_3SiOH (B3 series of experiements)

Since addition of a silanol with just one long alkyl chain ($OctPh_2SiOH$) did not produce a clear homogeneous solution of MMAO in heptane, synthesis of Oct_3SiOH was the next step. When the required amount of Oct_3SiOH (2.4 mmol) was mixed with 'MAO-10' (which had been pre-dried under vacuum overnight), a clear solution was obtained. Addition of TMA before addition of the catalyst precursor causes the solution to become slightly cloudy; the cloudiness disappears after ~30 min. Addition of TMA to the mixture was necessary for the alkylation step of the polymerization when this protocol was followed: when addition of TMA did not take place, initiation of the polymerization did not occur (no colour change was observed after addition of the monomer).

Although modification of MAO with long chain silanols helped in overcoming the solubility problems and producing a homogeneous system (that should theoretically achieve higher catalyst activity), unfortunately it was proven that addition of silanols led to lower molecular weights.

For the catalyst systems of MAO and MMAO with approximately the same TMA concentrations, a similar productivity to that of the test polymerization (1.6 g) was observed for the system with Oct_3SiOH (1.7 g), and identical k_p^{app}values were observed (see Tables 5.13 – 5.14). However, the problem with the significant decrease of the $\overline{M_n}$ remained (reducing from 30400 to 22100), and is associated with higher k_t values ($10.68 * 10^{-3}s^{-1}$) compared to the test polymerization ($5.55 * 10^{-3}s^{-1}$). A lower active species count (0.07 compared to 0.10) was also observed. The polydispersities of the polymers produced here with MMAO or MAO were ≈ 1.4 – 1.6.

The results of another two polymerizations with Oct_3SiOH as a modifier for the MAO are presented, although in these polymerizations a lower (23 mmol L^{-1}) and a higher (84 mmol L^{-1}) amount of TMA were employed to see if the [TMA] would cause any significant difference in the polymerization performance. The results obtained are quite similar to the polymerization with MMAO and 57 mmol L^{-1} of TMA, apart from the fact that the polymerization with the higher [TMA] shows slightly lower productivity (1.4 g).

Table 5.11: Polymerization conditions, productivity and equilibrium $\overline{M_n}$ of 1-hexene polymerizations in heptane.

Polym. Run B3 MAO-10	**[TMA] added (mmol L^{-1})**	**[Al as MAO][b] (mol L^{-1})**	**Si (mmol L^{-1})**	**Al_{MAO} : Si : Al_{TMA}**	**Polymer (g)**	**Final $\overline{M_n}$**
dried MAO-10	42[a]	0.14	-	-	1.6	30400
dried MAO-10 + Oct_3SiOH (i)	23[b]	0.14	48	2.9 : 1 : 0.8	1.8	22500
dried MAO-10 + Oct_3SiOH (ii)	42[b]	0.14	48	2.9 : 1 : 1.2	1.7	22100
dried MAO-10 + Oct_3SiOH (iii)	84[b]	0.14	48	2.9 : 1 : 2.1	1.4	21800

[a] This MAO contains an additional amount of ~15 mmol L^{-1} TMA, due to the 'bound' TMA

[b] The MMAOs are probably depleted of any remaining 'bound' TMA after reaction with the Oct_3SiOH (see Table 5.15).

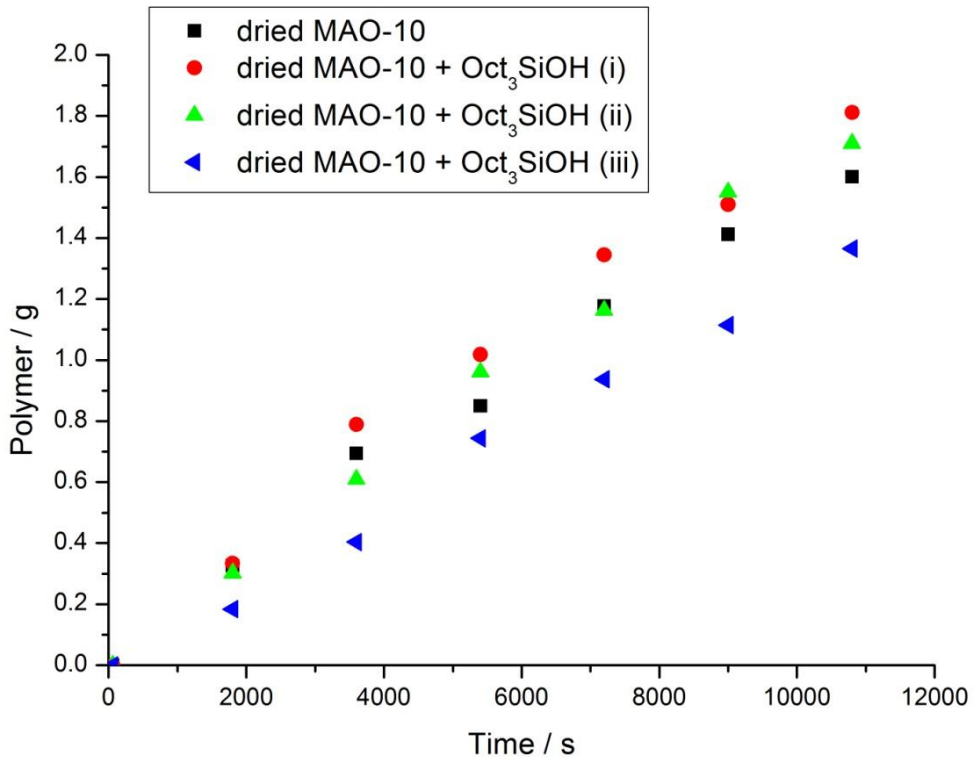

Figure 5.19: Productivity as a function of reaction time for modified MAO with Oct_3SiOH in heptane. A test polymerization with unmodified MAO is displayed for comparison.

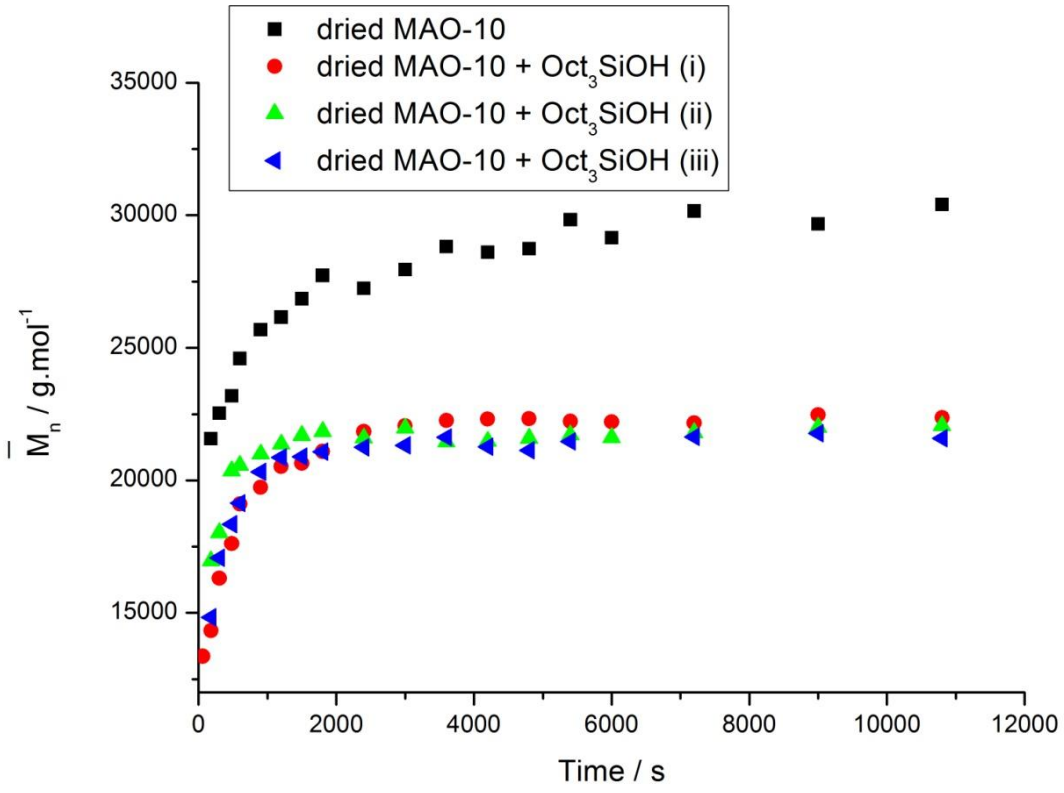

Figure 5.20: Time dependence of $\overline{M_n}$ for modified MAO with Oct_3SiOH in heptane. A test polymerization with unmodified MAO is displayed for comparison.

Table 5.12: Summary of the kinetic parameters for modified MAO with Oct_3SiOH in heptane. The MAO solution was pre-dried. The results from a test polymerization with unmodified MAO are also presented.

Aluminoxane	k_p $(L\,mol^{-1}s^{-1})$	k_t $(10^{-3}s^{-1})$	k_i $(L\,mol^{-1}s^{-1})$	k_p^{app} $(L\,mol^{-1}s^{-1})$	k_p^{app}/k_p
dried MAO-10	1.21±0.05	5.55±0.27	3.8	0.12 (± 0.003)	0.10
+Oct_3SiOH (i)	1.32±0.06	8.07±0.40	3.8	0.13 (± 0.004)	0.10
+Oct_3SiOH (ii)	1.72±0.06	10.68±0.40	3.8	0.12 (± 0.002)	0.07
+Oct_3SiOH (iii)	1.35±0.02	8.45±0.15	3.8	0.09 (± 0.002)	0.07

5.2.4.6 Polymerizations with the Product of the Reaction of Oct_3SiOH + TMA (B4 series of experiments)

When compared to the reaction of MAO with silica bound Si-OH groups, to form a silica supported MAO system, it is believed that the reaction of MAO with free silanols leads to the formation of structures that facilitate chain termination: a conclusion arising from the fact that the addition of a silanol to the MAO has a negative effect on the $\overline{M_n}$ and usually on the productivity of the polymer (see A3 series in toluene).

For this reason it was decided to test the impact that addition of Oct_3SiOH would have if it was pre-reacted with TMA, so that no Si-OH groups would have been present to cause an immediate reaction with certain MAO features. In order to produce a clear homogeneous solution of MAOb-30 in heptane, 4 mmol of the reaction product of Oct_3SiOH/TMA were needed as opposed to just 3.2 mmol when Oct_3SiOH is used alone (showing that a larger amount of the Oct_3SiOH/TMA mixture is needed to solubilise MAO than when Oct_3SiOH is used), and longer reaction times were necessary (~ 12 h).

Figures 5.21 and 5.22 present the productivity and $\overline{M_n}$ vs the reaction time of a polymerization with Oct_3SiOH/TMA as an MAO additive. The results from a test polymerization with unmodified MAO and a polymerization with Oct_3SiOH as an MAO additive are also presented for comparison.

As can be seen from the graph of $\overline{M_n}$ *vs* reaction time (Figure 5.22) and the Tables 5.15 – 5.16, addition of the product of the Oct_3SiOH/TMA mixture still causes: a significant decrease of the final $\overline{M_n}$ of the polymer (26200 compared to 38500 of the test polymerization); shows higher k_t values ($8.05 * 10^{-3}s^{-1}$) compared to the unmodified MAO catalyst systems ($4.89 * 10^{-3}s^{-1}$); has a lower polymer yield (1.8 g compared to 2.2 g for the test polymerization); slightly lower k_p^{app}values and higher k_p values, resulting in a lower active species count (0.09 compared to 0.13 for the test polymerization). The polydispersities of the polymers produced here with MMAO or MAO were ≈ 1.6 – 1.7

Table 5.13: Polymerization conditions, productivity and equilibrium $\overline{M_n}$ of 1-hexene polymerizations in toluene.

Polym. Run B4 MAOb-30	**[TMA]added (mmol L^{-1})**	**[Al as MAO][b] (mol L^{-1})**	**Si (mmol L^{-1})**	**Al_{MAO} : Si : Al_{TMA}**	**Polymer (g)**	**Final $\overline{M_n}$**
dried MAOb-30	41.8[a]	0.18	-	-	2.2	38500
dried MAOb-30 + TMA/Oct_3SiOH	41.8[b]	0.18	80	2.3 : 1 : 1.6	1.8	26200
dried MAOb-30 + Oct_3SiOH	41.8	0.18	64	2.9 : 1 : 0.7	1.9	26000

[a] This MAO contains an additional amount of ~4 mmol L^{-1} TMA, due to the 'bound' TMA

[b]The reaction mixture of TMA/Oct_3SiOH contains additional [$AlMe_3$] structures (80 mmol L^{-1}). So, the total TMA of this MMAO is probably higher.

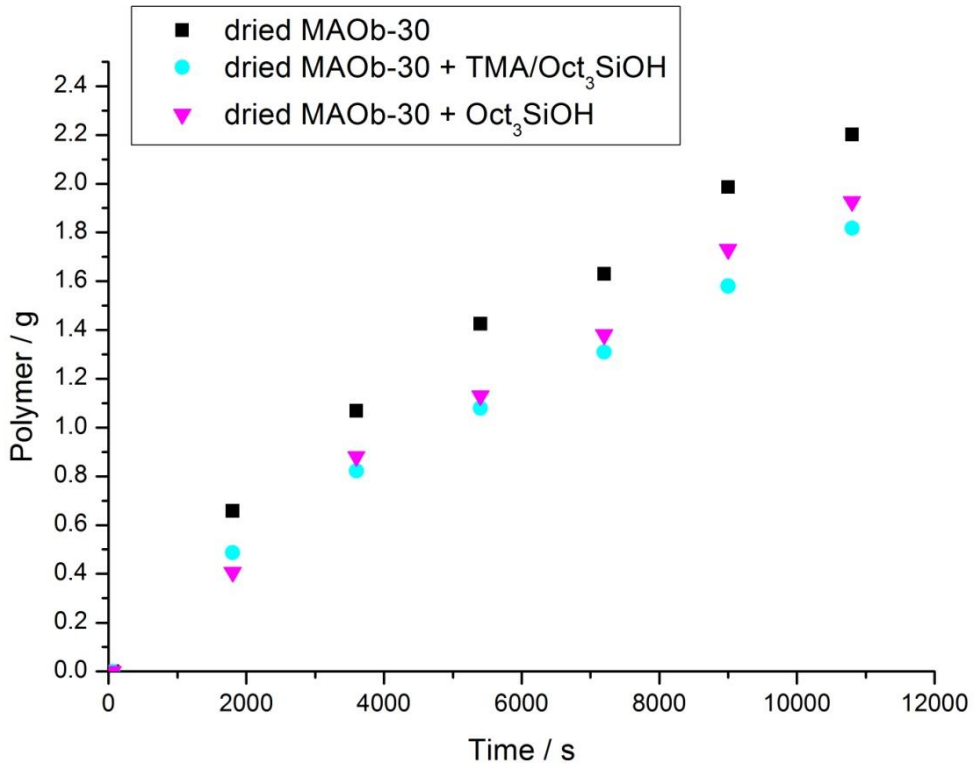

Figure 5.21: Productivity as a function of reaction time for modified MAO with TMA/Oct_3SiOH and Oct_3SiOH in heptane. A test polymerization with unmodified MAO is displayed for comparison.

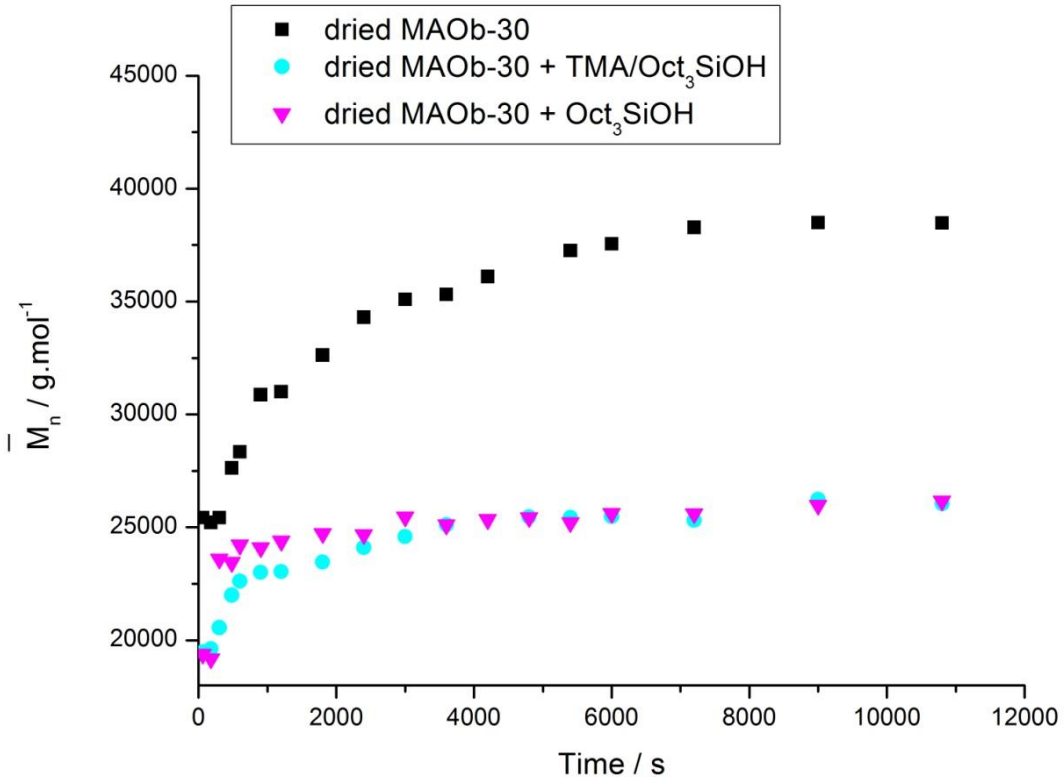

Figure 5.22: Time dependence of $\overline{M_n}$ for modified MAO with TMA/Oct_3SiOH and Oct_3SiOH in heptane. A test polymerization with unmodified MAO is displayed for comparison.

Table 5.14: Summary of the kinetic parameters for modified MAO with TMA/Oct_3SiOH and Oct_3SiOH in heptane. The MAO solution was pre-dried. The results from a test polymerization with unmodified MAO are also presented.

Aluminoxane	k_p ($L\ mol^{-1}s^{-1}$)	k_t ($10^{-3}s^{-1}$)	k_i ($L\ mol^{-1}s^{-1}$)	k_p^{app} ($L\ mol^{-1}s^{-1}$)	k_p^{app}/k_p
dried MAOb-30	1.33±0.08	4.89±0.35	3.8	0.17 ± (0.008)	0.13
+TMA/Oct_3SiOH	1.50±0.09	8.05±0.53	3.8	0.13 (± 0.005)	0.09
+Oct_3SiOH	2.35±0.19	12.58±1.06	3.8	0.14 (± 0.005)	0.06

5.2.5 Characterization of MAO

Reaction of MAO with Oct_3SiOH

When Oct_3SiOH is added to MAO the ^1H NMR signal attributed to Me_2Al^+ species, after addition of THF, decreases with increasing amounts of the silanol addition. The original MAO solution was pre-dried in order to remove any free TMA prior to reaction with the silanol. The so called 'bound' TMA is still present after the drying process, but it decreases with increasing amounts of the silanol. When the same Al/Si ratios are employed as in the polymerizations there is practically no Me_2Al^+ species or 'bound' TMA left (Table 5.15).

When TMA was added to the mixture, the Me_2Al^+ re-appears and seems to increase with higher TMA concentrations.

The same trend is observed for MAO-10 reacted with $^iPr_3SiOH$ in heptane or toluene, and for MAOb-30 after reaction with Oct_3SiOH and the reaction product of the TMA/Oct_3SiOH mixture in heptane or toluene: when the same Al/Si ratios are employed as in the respective polymerizations the Me_2Al^+ and 'bound' TMA signals disappear.

Table 5.15: Addition of increasing amounts of Oct_3SiOH to a pre-dried MAO 10 T solution re-dissolved in heptane

Ratio Al/Si	Cat/Al (n/n)	'bound' TMA (w/w%)
Si=0	0.016	0.57
Al/Si = 8.5	0.012	0.24
Al/Si=4.6	0.010	0.12
Al/Si=2.9	~ 0	~ 0

Similarly, when $^tBu_2Si(OH)_2$ was reacted with an MAO-30-I solution in toluene under the same conditions used in the modification of MAO for 1-hexene polymerizations in toluene, reduction of the % w/w TMA was observed, as well as reduction of the amount of Me_2Al^+ (Table 5.16).

Table 5.16: Addition of increasing amounts of $^tBu_2Si(OH)_2$ to an MAO-30-I solution in toluene

Ratio Al/Si	Cat/Al (n/n)	TMA (w/w%)
Si=0	0.021	3.9
Al/Si = 17.1	0.011	2.0
Al/Si=8.6	0.008	1.2

5.3 Conclusions

Modification of MAO with branched [Al(*i*-Bu)$_3$] or long chain [e.g. Al(Oct)$_3$] aluminium trialkyls, produce a modified methylaluminoxane that is soluble in aliphatic hydrocarbons such as n-heptane. Poly(1-hexene) with higher $\overline{M_n}$ values is obtained when MAOs modified with Al(*i*-Bu)$_3$ or Al(Oct)$_3$ are employed.

Conversely, the modification of MAO with long chain silanols like Oct$_3$SiOH produces a modified methylaluminoxane that, although soluble in aliphatic hydrocarbons, results in a polymer with a significantly lower $\overline{M_n}$. ^{1}H NMR spectroscopic studies revealed that the concentration of TMA, either 'free' or 'bound', decreases upon addition of a silanol to an MAO solution. A decrease of the concentration of Me_2Al^+ species that exists in MAO is also observed. However, when TMA is added back to the mixture these species seem to re-appear, which is interesting since it shows that the structures in MAO that are capable of generating potentially activating $AlMe_2^+$ cations are formed reversibly and are not irrecovably destroyed by the Si–OH reactions. Since TMA was added back to the mixture before addition of the catalyst in all polymerizations carried out in n-heptane, the decrease of $AlMe_2^+$ species due to silanol addition should not have been a problem.

One possible reason that could lead to lower molecular weights and lower productivities relative to unmodified MAO, could have been the formation of $R_3SiOAlMe_2$ or similar products which may act as poisoning agents. For example, it has been reported[11] that $PhCMe_2OAlMe_2$ acts as a poisoning agent in 1-hexene polymerization. Additionally, considering the results of the study on the reaction of TMA with certain silanols ($(C_8H_{17})_3SiOH$ and $^iPr_3SiOH$) which surprisingly led to the formation of several products, one might think that reaction of MAO with compounds containing Si–OH bonds might be more complicated than originally anticipated.

This study was successful in producing heptane-soluble MAOs after treatment with long-chain silanols, but the catalyst systems did not exhibit the required catalytic performance in 1-hexene polymerizations. This means that the MMAOs used in this study do not acquire the characteristics that make MAO-treated silica surfaces such good co-catalyst in heterogeneous polymerizations. Perhaps modification of MAO with different silanols that contain some very bulky groups in combination with some long alkyl chains could lead to different results: according to Brintzinger and his co-workers[34] the reaction of some very

bulky silanols with TMA gave a binuclear siloxalane with one siloxy and one methyl bridge, which react with L_2ZrCl_2 *via* Me/Cl exchange, and it was believed that they represent a closer model for the activation reaction of metallocenes on TMA-treated silica gel surfaces.

One important outcome of this research was the determination of the role of TMA on the catalytic activity of an MAO-activated catalyst system. It is the first time that the exact relationship between the TMA concentration and (a) polymer yield and (b) the number-average polymer molecular weight has been clearly established.

5.4 Additional Information

The tables below present the number average molecular weights and polydispersity values from all the polymerisations presented in this study.

Polymerizations in Toluene

Table 5.17a The M_w and PDI values of Polymerizations in toluene with addition of $^tBu_2Si(OH)_2$ and $C_{12}H_{25}Ph_2SiOH$ (A1 series of experiments). The results from a test polymerization with unmodified MAO are presented.

MAO-30			**MAO-30 + $(^tBu)_2Si(OH)_2$ (i)**			**MAO-30 + $(^tBu)_2Si(OH)_2$ (ii)**		
Time (s)	**M_w**	**PDI**	**Time (s)**	**M_w**	**PDI**	**Time (s)**	**M_w**	**PDI**
60	48300	1.9	60	43500	1.8			
180	56700	1.9	180	48700	2.0	180	49200	1.9
300	64400	1.9	300	53200	1.9	300	54100	1.9
480	69300	1.9	480	60300	1.9	480	60400	2.0
600	71400	1.9	600	62200	2.0	600	62500	2.0
900	79800	1.9	900	67400	2.3	900	68400	2.1
1200	85100	1.9	1200	65800	2.0	1200	72900	2.1
1500	89400	1.9	1800	78300	2.1	1800	76200	2.2
1800	94100	1.9	2400	82600	2.0	3000	79800	2.1
2400	100700	1.9	3000	85600	2.0	3600	87900	2.1
3000	107900	1.9	3600	86500	2.1	4200	91700	2.1
3600	110400	2.0	4200	89600	2.1	4800	88700	2.1
4200	117200	2.0	4800	90500	2.1	5400	92400	2.2
4800	117300	1.9	5400	90800	2.1	6000	93300	2.2
5400	120000	2.0	6000	92300	2.1	7200	94700	2.1
6000	122800	2.0	7200	92300	2.1	9000	94500	2.1
7200	126200	2.0	9000	92700	2.1	10800	93100	2.2
9000	130400	2.1	10800	92200	2.1			
10800	132900	2.0						

Table 5.17b Continuation of table 5.17a

MAO-30 + $(^tBu)_2Si(OH)_2$ (iii)			MAO-30 + $C_{12}H_{25}Ph_2SiOH$		
Time (s)	**M_w**	**PDI**	**Time (s)**	**M_w**	**PDI**
120	46700	1.9	90	39300	2.0
180	56000	2.2	180	42900	1.8
300	58000	2.1	300	46900	1.7
480	51700	2.0	480	51600	1.8
600	57800	2.0	600	54300	1.9
900	65100	2.1	900	57600	1.9
1200	68200	2.0	1200	60800	1.9
1500	69800	2.0	1500	63100	1.9
1800	74300	2.0	1800	65400	1.9
2400	76300	2.0	2400	68400	2.0
3000	81800	2.1	3000	70000	2.0
3600	83900	2.1	3600	73400	1.9
4200	86000	2.1	4200	73700	2.0
4800	90100	2.1	4800	74900	2.0
5400	88100	2.1	5400	76900	2.0
7200	94500	2.2	6000	77800	2.0
9000	97800	2.2	7200	76700	2.0
10800	97400	2.1	9000	78100	2.0

Table 5.18 The M_w and PDI values of the polymerizations in toluene with addition of TMA or 2,6-di-*tert*-butylphenol (DBP), (A2 series of experiments)

MAO-10			MAO-10 + DBP			MAO-30			MAO-30 + TMA		
Time (s)	**M_w**	**PDI**	**Time (s)**	**M_w**	**PDI**	**Time (s)**	**M_w**	**PDI**	**Time (s)**	**M_w**	**PDI**
30	41300	1.9				30	50900	2.1			
60	43900	1.9	60	61000	2.3	60	56000	2.2	**60**	43000	1.6
180	45800	1.7	300	78800	2.5	180	60000	2.0	180	58300	1.8
300	52200	1.7	600	99400	2.5	300	66800	2.0	300	52200	1.6
480	59500	1.8	1200	106300	2.4	480	74100	2.0	600	57200	1.6
600	69000	1.8	1800	111900	2.4	600	83900	2.1	900	62200	1.7
900	71500	1.8	2400	124400	2.4	900	92400	2.0	1200	66700	1.7
1200	73700	1.8	3000	129500	2.3	1200	93800	2.0	1800	73000	1.7
1500	78100	1.8	3600	136800	2.4	1500	103300	2.0	2400	75500	1.7
1800	81800	1.8	4800	141600	2.3	1800	108000	2.0	3000	77900	1.7
2100	84000	1.8	5400	143800	2.2	2100	108400	2.0	3600	80100	1.8
2400	85300	1.8	6000	146600	2.2	2400	112100	1.9	4500	80200	1.7
3000	87200	1.8	7200	147300	2.1	3000	123000	2.0	5400	82100	1.8
3600	88000	1.8	9000	157100	2.1	3600	126600	1.9	7200	84700	1.8
4200	90000	1.8	10800	161500	2.1	4200	126900	2.0	9000	86200	1.8
4800	90000	1.8				4800	129600	1.9	10800	86400	1.8
5400	92900	1.8				5400	131000	1.9			
6000	95100	1.9				6000	136500	1.9			
6600	96900	1.9				6600	137300	2.0			
7200	97200	1.9				7200	141000	2.0			
9000	98400	1.9				9000	145800	2.1			
10800	101200	1.9				10800	154500	2.2			

Table 5.19 The M_w and PDI values of the polymerizations in toluene with addition of Ph_3SiOH (A3 series of experiments)

MAO-10			MAO-10 + Ph_3SiOH		
Time (s)	**M_w**	**PDI**	**Time (s)**	**M_w**	**PDI**
60	39700	1.5			
180	46000	1.5	180	32900	1.5
300	50100	1.6	300	36700	1.5
480	53800	1.5	480	39700	1.5
600	55800	1.6	600	42900	1.5
900	60400	1.6	900	45000	1.5
1200	65500	1.6	1200	48400	1.6
1500	69800	1.5	1800	51600	1.6
1800	72300	1.6	2400	53000	1.6
2400	78200	1.6	3000	56300	1.5
3000	85300	1.6	3600	57900	1.6
3600	88300	1.6	4200	59900	1.6
4200	91500	1.7	4800	60500	1.6
4800	93600	1.7	5400	62700	1.5
5400	99400	1.7	6000	63300	1.5
6000	100200	1.7	7200	64900	1.6
7200	106400	1.7	9000	68800	1.6
9000	111400	1.7	10800	72000	1.6
10800	116300	1.8			

Polymerizations in Heptane

Table 5.20a The M_w and PDI values of the polymerizations in heptane with addition of AlR_3 (B1 series of experiments-Method A)

dried MAO-30 + $AlMe_3$ (A)			**dried MAO-30 + $Al(i\text{-}Bu)_3$ (A)**			**dried MAO-30 + $AlOct_3$ (A)**		
Time (s)	**M_w**	**PDI**	**Time (s)**	**M_w**	**PDI**	**Time (s)**	**M_w**	**PDI**
60	32300	1.7	60	38300	2.0	60	36800	1.6
180	33200	1.6	180	42200	1.7	180	40500	1.6
300	34400	1.7	300	45900	1.7	300	46500	1.7
480	37000	1.7	600	51500	1.7	480	47200	1.7
600	38100	1.6	900	59100	1.7	600	48600	1.7
900	41100	1.8	1200	65600	1.7	900	50300	1.7
1200	42100	1.8	1800	67500	1.7	1200	53600	1.7
1800	42700	1.8	2400	74700	1.7	1500	54000	1.7
2400	43500	1.8	3000	78500	1.8	1800	61700	1.8
3000	45700	1.9	3600	80200	1.8	2400	67500	1.8
3600	45800	1.8	4800	87500	1.8	3000	72000	1.9
4200	45900	1.8	6000	89200	1.8	3600	74700	1.9
4800	46200	1.9	7200	93700	1.9	4200	76900	1.9
5400	46400	1.9	9000	95300	1.9	4800	81900	1.9
6000	47100	1.9	10800	100100	2.0	5400	83700	1.9
7200	47400	1.9	10800	101100	2.0	6000	85000	1.9
9000	47900	1.9				7200	89000	1.9
10800	48000	1.8				9000	94500	2.0
						10800	97900	2.0

Table 5.20b The M_w and PDI values of the polymerizations in heptane with addition of AlR_3 (B1 series of experiments-Method C)

dried MAO-30 + $AlMe_3$ (C)			dried MAO-30 + Al(*i*-Bu)$_3$ (C)			dried MAO-30 + $AlOct_3$ (C)		
Time (s)	**M_w**	**PDI**	**Time (s)**	**M_w**		**Time (s)**	**M_w**	**PDI**
			60	51800	2.4			
180	44000	2.4	180	71300	2.6	180	41500	1.8
300	45400	2.5	300	82800	2.6	300	55000	2.2
600	49100	2.5	600	87500	2.7	600	56900	2.0
900	50100	2.6	900	98800	2.7	900	62600	2.1
1200	50400	2.6	1200	100900	2.7	1200	67400	2.2
1800	53300	2.6	1800	119800	2.7	1800	74200	2.2
2400	54800	2.7	2400	126300	2.7	2400	80200	2.3
3000	55000	2.7	3000	129700	2.7	3000	89700	2.4
3600	57400	2.7	3600	136900	2.7	3600	91000	2.3
4500	60400	2.7	4500	142600	2.6	4500	96000	2.4
5400	61600	2.7	5400	145700	2.6	5400	98600	2.3
7200	62100	2.7	7200	151700	2.6	7200	105500	2.4
9000	63700	2.7	9000	157200	2.7	9000	109000	2.4
10800	67700	2.8	10800	158600	2.6	10800	109700	2.2

Table 5.21 The M_w and PDI values of the polymerizations with addition of $C_{12}H_{25}Ph_2SiOH$ (B2 series of experiments)

MAOb-30			**MAOb-30 + $C_{12}H_{25}Ph_2SiOH$ (i)**			**MAOb-30 + $C_{12}H_{25}Ph_2SiOH$ (ii)**		
Time (s)	**M_w**	**PDI**	**Time (s)**	**M_w**		**Time (s)**	**M_w**	**PDI**
60	43300	1.7	60	34900	1.8	60	37300	1.7
180	45000	1.8	180	35800	1.8	180	38500	1.8
300	47800	1.9	300	38100	1.9	300	40900	1.9
480	51200	1.9	480	39200	1.9	480	44700	1.9
600	53400	1.9	600	40700	1.9	600	44700	1.9
900	56800	1.8	900	40800	1.9	900	45800	1.9
1200	60200	1.9	1200	42000	1.9	1200	52400	2.0
1800	62100	1.9	1500	43800	1.9	1500	50500	1.9
2400	66600	1.9	1800	44000	1.9	1800	53500	2.0
3000	68100	1.9	2400	44500	1.9	2400	54700	2.0
3600	69000	2.0	3000	45300	1.9	3000	55400	2.0
4200	70800	2.0	3600	48000	2.0	3600	55800	2.0
5400	72500	1.9	4200	48800	2.0	4200	55900	2.0
6000	72900	1.9	4800	49100	2.0	4800	56000	2.0
7200	73800	1.9	5400	49200	2.1	5400	57000	2.1
9000	74100	1.9	6000	49500	2.1	6000	56200	2.0
10800	75000	1.9	7200	49900	2.1	7200	56000	2.1
			9000	50100	2.1	10800	57300	2.1
			10800	50400	2.1			

Table 5.22 The M_w and PDI values of the polymerizations with addition of Oct_3SiOH (B3 series of experiements). The results of a test polymerisation are also presented.

MAO-10			MAO-10 + Oct_3SiOH (i)			MAO-10 + Oct_3SiOH (ii)			MAO-10 + Oct_3SiOH (iii)		
Time (s)	**M_w**	**PDI**	**Time (s)**	**M_w**	**PDI**	**Time (s)**	**M_w**	**PDI**	**Time (s)**	**M_w**	**PDI**
180	36200	1.7	60	17900	1.3	180	23900	1.4	180	22700	1.5
300	35100	1.6	180	20200	1.4	300	24500	1.4	300	23900	1.4
480	37100	1.6	300	21600	1.3	480	28600	1.4	480	25600	1.4
600	38300	1.6	480	22900	1.3	600	30000	1.5	600	36800	1.4
900	40700	1.6	600	26100	1.4	900	31200	1.5	900	28700	1.4
1200	41500	1.6	900	31100	1.6	1200	31400	1.5	1200	30500	1.5
1500	43600	1.6	1200	29800	1.5	1500	32200	1.5	1500	30800	1.5
1800	45200	1.6	1500	28100	1.4	1800	32200	1.5	1800	31300	1.5
2400	44200	1.6	1800	29800	1.4	2400	32200	1.5	2400	30900	1.5
3000	45400	1.6	2400	32200	1.5	3000	32300	1.5	3000	30600	1.4
3600	46300	1.6	3000	32500	1.5	3600	32300	1.5	3600	32100	1.5
4200	46400	1.6	3600	33000	1.5	4200	32300	1.5	4200	32000	1.5
4800	46700	1.6	4200	31900	1.4	4800	32500	1.5	4800	32200	1.5
5400	47000	1.6	4800	33300	1.5	5400	32700	1.5	5400	32300	1.5
6000	48300	1.7	5400	32800	1.5	6000	32700	1.5	7200	32500	1.5
7200	48900	1.6	6000	33300	1.5	7200	33100	1.5	9000	33100	1.5
9000	47700	1.6	7200	33300	1.5	9000	33600	1.5	10800	32400	1.5
10800	49200	1.6	9000	33600	1.5	10800	34600	1.6			
			10800	33700	1.5						

Table 5.23 The M_w and PDI values of the polymerizations with the product of the reaction of Oct_3SiOH + TMA (B4 series of experiments). The results of the test polymerization and a polymerization with addition of Oct_3SiOH are also presented.

MAOb-30			**+TMA/Oct_3SiOH**			**+Oct_3SiOH**		
Time (s)	**M_w**	**PDI**	**Time (s)**	**M_w**	**PDI**	**Time (s)**	**M_w**	**PDI**
60	38400	1.5	60	27600	1.4	60	28700	1.5
180	40100	1.6	180	28900	1.5	180	31000	1.6
300	42700	1.7	300	30700	1.5	300	38100	1.6
480	44000	1.6	480	33600	1.5	480	35400	1.5
600	44900	1.6	600	34000	1.5	600	37300	1.5
900	49200	1.6	900	35400	1.5	900	37500	1.6
1200	52000	1.7	1200	35900	1.6	1200	38100	1.6
1800	53500	1.6	1800	36500	1.6	1800	38800	1.6
2400	53300	1.6	2400	38600	1.6	2400	38900	1.6
3000	55800	1.6	3000	39000	1.6	3000	39600	1.6
3600	58800	1.7	3600	40100	1.6	3600	39900	1.6
4200	58800	1.6	4800	40300	1.6	4200	40200	1.6
5400	59700	1.6	5400	40400	1.6	4800	40200	1.6
6000	61900	1.6	6000	40600	1.6	5400	40300	1.6
7200	62100	1.6	7200	40900	1.6	6000	40700	1.6
9000	65700	1.7	9000	41500	1.6	7200	41000	1.6
10800	67400	1.8	10800	41700	1.6	9000	41200	1.6
						10800	41400	1.6

5.5 Experimental

5.5.1 General Procedures and Materials

All manipulations were conducted under inert atmosphere of dry Argon using standard Schlenk techniques. All reagents were used as purchased without further purification unless otherwise stated. The catalyst *rac*-Me_2Si(2-Me-Benz[e]Ind)$_2ZrCl_2$ was used as received (SABIC Europe) and stored in the glove box at room temperature. Methylaluminoxane (MAO) was provided as toluene solutions (Chemtura Organometallics GmbH) and stored at –20 °C (30 weight % solution) or at +4 °C (10 weight %). 'MAO 30T' or 'MAO 10T' describes toluene solutions containing 30g or 10g respectively of MAO plus TMA per 100 g of solution. The 'MAOb 30T' is used to describe a toluene solution containing 30 g of MAO plus TMA per 100 g of solution, synthesized via a different synthetic procedure than 'MAO 30T'. The age of the samples at the time of analysis is stated in each series of experiments. The specifications of the MAO grades are summarized in Table 5.24.

Table 5.24: Specifications of the MAO samples used in this study

Sample name	Al content (weight-%)	TMA content (weight%)	Amount used in polymerizations (mL)
MAO-30-I	13.58	3.9	2.2
MAO-30-II	13.56	2.4	2.2
MAO-10	4.82	3.9	6.3
MAOb-30	13.71	3.0	2.2

Solvents were dried over Na/benzophenone (tetrahydrofuran) or sodium (toluene) before use and purged with argon. 1-Hexene was dried over sodium. Anhydrous heptane (Acros) was degassed with a stream of argon and stored over activated 4 Å molecular sieves. Ph_3SiOH was purchased from Sigma-Aldrich (98% purity). $(^tBu)_2Si(OH)_2$[66], $C_{12}H_{25}Ph_2SiOH$[67-68], $^iPr_3SiOH$ and $(C_8H_{17})_3SiOH$[69] were prepared according to literature procedures. NMR spectra were recorded on a Bruker Avance DPX-300 spectrometer. ^1H NMR chemical shifts were referenced to the residual solvent peaks of an external standard of CD_2Cl_2. Signals were integrated against internal standards, using 1,3,5-tri-*tert*-butylbenzene or pentamethylbenzene (for the determination of the TMA content) or pentamethylbenzene (for monitoring the consumption of 1-hexene). A relaxation time (D_1) of 25 s and 16 scans

were used for ^{1}H NMR spectra. The number average molecular weight, $\overline{M_n}$, of poly(1-hexene) was measured using an integrated Varian PL-GPC-50Plus system described below.

5.5.2 Instrumentation for GPC Analysis

The instrumentation used to monitor the $\overline{M_n}$ of the poly(1-hexene) and PDI was an integrated Varian PL-GPC-50Plus system, supplied by Agilent, operating at 30 °C with filtered HPLC grade THF as eluant (1mL·min^{-1}, 7 min per sample) and equipped with a PLgel 10 μm guard column (50 x 7.5 mm), a PL-rapid L column (150 x 7.5 mm) and a refractive index detector. Polystyrene narrow standards (peak $\overline{M_w}$ = 580; 1,480; 3,950; 10,680; 31,420; 70,950; 170,800; 578,500 g·mol^{-1}) were used for calibration. All samples for GPC analysis were prepared in distilled THF and filtered using Acrodisc Syringe filters (0.2 μM PTFE membrane).

The initial plan was to create an automative sampling system which could allow the collection of samples directly from the reaction mixture at the required time intervals using an Agilent pump/dilution system. Teflon tubing was inserted into the polymerization vessel through a rubber septum and this sampled via a continuous stream of the reaction. The end of the tubing inside the reaction vessel was equipped with a filter. The pump system included two pumps: one pump operated to take samples from the reaction mixture and the second pump was transferring toluene to the dilution chamber where the two streams were mixed. Then the diluted sample was transferred via teflon tubing to the GPC system for analysis with toluene as eluent and the same conditions as described above. However, this method proved to be not practicable because aluminium hydroxide generated during the quenching of MAO-containing samples was being deposited on the very narrow tubes of the autosampler. This white deposit damaged the filters and finally the pump system leading to overpressure and blockages.

The best solution to this problem was to withdraw samples manually at precise time intervals and to use the GPC system alone with THF as solvent for dilution, detection and analysis instead of toluene, with manual injection of the samples after filtering them through an Acrodisc syringe filter. Samples were taken from the reaction mixture at regular intervals, using a stopwatch and a gas-tight syringe. The samples were injected into vials containing THF/MeOH/HCl (2 mL, 100:1:1 v/v) to quench the polymerization reaction, and they were left drying in air overnight and re-dissolved in THF (3 mL) before injection. Even when this

method was followed, the use of a pre-column (PLgel 10 μm guard column) proved to be necessary to avoid blockage of the main column (PL-rapid L column).

5.5.3 Synthesis of $^{t}Bu_2Si(OH)_2$[66]

Di(t-butyl)silyl bis(trifluoromethanesulfonate) (2.5 g, 5.67 mmol) was added dropwise to 150 mL deionised water at room temperature and the mixture was stirred for 30 min. The solid was filtered with a Büchner filter and washed with deionised water. The solid was recovered, transferred to a flask and kept under vacuum overnight to dry. ^{1}H NMR in toluene (300.1 MHz, 25 °C, CD_2Cl_2 capillary) δ 1.68 (s, 2H, OH), δ 1.06 (s, 18H, CH_3)

5.5.4 Synthesis of $C_{12}H_{25}Ph_2SiOH$[67-68]

Firstly, $C_{12}H_{15}Li$ was synthesized: Lithium particles (1.43 g, 0.206 mol) were added to 35 mL of Et_2O. n-$C_{12}H_{25}Br$ (14.33 mL, 0.083 mol) were placed in a dropping funnel. 1 mL was added slowly to the mixture at room temperature and stirred until the reaction started (the Li particles have a bright shiny appearance). Then the mixture was cooled to approximately −10 °C and the rest of the solution of n-$C_{12}H_{25}Br$ was added dropwise over a period of 1h while the temperature was kept at −10 °C. After addition of the halide, the mixture was warmed up to 10 °C and stirred for an additional hour. Then it was left to warm up to room temperature, stirred for another two hours and filtered. The solvent was removed in vacuo.

$C_{12}H_{25}Li$ in light petroleum ether was added to Ph_2SiCl_2 (1.25 equivalents) in light petroleum ether slowly. The exothermic reaction heats the mixture to reflux. The refluxing was kept for one hour. The mixture was filtered and the solvent was removed in vacuo. ^{1}H NMR (300.1 MHz, 25 °C, $CDCl_3$) δ 7.7 – 7.6 (m, 4H, Ph), 7.5 – 7.3 (m, 6H, Ph), 1.4 – 1.1 (m, 22H, CH_2), 0.9 – 0.8 (m, 3H, CH_3).

5.5.5 Synthesis of $^{i}Pr_3SiOH$ and $(C_8H_{17})_3SiOH$[69]

KOH (7.1 g, 127 mmol) was dissolved in EtOH (40 mL). $^{i}Pr_3SiH$ (5 g, 31.6 mmol) was added dropwise to the solution. The mixture was heated to reflux and left refluxing overnight. The next day the solution was yellow. After being left to cool down, HCl was added until neutral pH (determined by pH paper). The solution was extracted with 3x50 mL

hexane and dried under vacuum. A slightly yellow oil was obtained. . ^{1}H NMR (300.1 MHz, 25 °C, $CDCl_3$) δ 1.72 (s, 1H, OH), 1.1 – 0.8 [m, 21H, $CH(CH_3)_2$].

For the synthesis of $(C_8H_{17})_3SiOH$ the same synthetic procedure was followed as the one described above using the following amounts of KOH (3.1 g, 54.7 mmol) and Oct_3SiH (5g, 13.6 mmol). . ^{1}H NMR (300.1 MHz, 25 °C, $CDCl_3$) δ 1.54 (s, 1H, OH), 1.27 (m, 36H, CH_2), 0.9 (m, 9H, CH_3), 0.6 (m, 6H, CH_2).

5.5.6 Reaction of TMA with $^{t}Bu_2Si(OH)_2$

TMA (0.74 mL, 7.72 mmol) was added to 15 mL of toluene and the solution was cooled down to −78 °C. $^{t}Bu_2Si(OH)_2$ (0.67 g, 3.8 mmol) was dissolved in 15 mL of toluene and added dropwise via cannula to the solution while stirring. The ratio of Al/Si was 2/1 n/n. Some gas evolution was observed. The mixture was left to warm up slowly while stirring. The same procedure was repeated with addition of $^{t}Bu_2Si(OH)_2$ at −40 °C and at R.T.

The above procedure was repeated for a ratio of Al/Si = 1/1 n/n, with addition of $^{t}Bu_2Si(OH)_2$ at −78 °C , −40 °C and at R.T.

The same procedure was also repeated for ratios of Al/Si = 1/1 and 2/1 in THF. In each case the mixture was filtered, divided in different flasks, dried under vacuum and re-dissolved in suitable solvents for crystallization (e.g. toluene, toluene/light petroleum, DCM/light petroleum, diethyl ether). Their ^{1}H NMR spectra were recorded in toluene and THF for reactions in toluene and THF respectively.

5.5.7 Reaction of TMA with Ph_3SiOH, $(C_8H_{17})_3SiOH$ and $^{i}Pr_3SiOH$ [10, 32]

TMA (0.37 mL, 3.86 mmol) was added to 15 mL toluene and the solution was cooled down to −78 °C. Ph_3SiOH (1.05 g, 3.8 mmol) was dissolved in 15 mL of toluene and added dropwise via cannula to the solution while stirring. Some gas evolution was observed. The mixture was left to warm up slowly while stirring, and then kept stirring at R.T. overnight (~ 12 h). The same procedure was repeated with addition of the Ph_3SiOH at −15 °C and at R.T. The compound synthesized with addition of the Ph_3SiOH at −15 °C was filtered, re-dissolved in toluene and placed in the freezer (−28 °C) for crystallization (see section 5.2.8).

The above procedure was followed for reaction of TMA with $(C_8H_{17})_3SiOH$ and i-Pr_3SiOH with addition of the silanols to the solution at −78 °C. (The reaction of TMA with $^{i}Pr_3SiOH$ was also performed at −15 °C.)

5.5.8 Characterization of $[Me_2Al(\mu\text{-}OSiPh_3)]_2$ by X-Ray Crystallography

A suitable crystal of the sample $[Me_2Al(\mu\text{-}OSiPh_3)]_2$ (the reaction product of TMA and Ph_3SiOH) wascoated in an inert perfluorinated polyether oil, mounted on a glass fibre and fixed in the cold nitrogen stream of an Oxford Diffraction Xcalibur-3/Sapphire3-CCD diffractometer, equipped with Mo-Kα radiation and graphite monochromator. The diffraction intensities for the compound were recorded at 140(2)K and data collection was carried out using the CrystAlisPro-CCD and –RED software.[70]

The data were processed by Dr. Dragos Rosca using CrystalClear-SM Expert 3.1 b21 (Rigaku, 20112) programs. The structure of the sample was determined by direct methods in the SHELXS program and refined by full-matrix least-squares methods on F^2 in SHELXL.[71] Non-hydrogen atoms were refined with anisotropic thermal parameters. Hydrogen atoms were included in idealised positions. No missed symmetry was reported by PLATON.[72] Computer programs used in this analysis were run through WinGX.[73] Scattering factors for neutral atoms were taken from reference 74. The crystal data and structure refinement parameters for $[Me_2Al(\mu\text{-}OSiPh_3)]_2$ are presented on Table 5.25.

Table 5.25: Crystal data and structure refinement for X-Ray characterization of $[Me_2Al(\mu\text{-}OSiPh_3)]_2$

Empirical formula	C40 H42 Al2 O2 Si2
Formula weight	664.88
Temperature	293(2) K
Wavelength	0.71073 Å
Unit cell dimensions	a = 8.814(4) Å
	b = 9.563(2) Å
	c = 12.758(4) Å
Volume	898.2(5) $Å^3$
Z	1
Density (calculated)	1.229 Mg/m^3

Absorption coefficient	0.181 mm^{-1}
F(000)	352
Theta range for data collection	3.32 to 27.48°.
Index ranges	-11<=h<=11, -12<=k<=12, -16<=l<=16
Reflections collected	14131
Independent reflections	4118 [R(int) = 0.0741]
Completeness to theta = 27.48°	99.8 %
Refinement method	Full-matrix least-squares on F^2
Data / restraints / parameters	4118 / 0 / 208
Goodness-of-fit on F^2	1.167
Final R indices [I>2sigma(I)]	R1 = 0.0675, wR2 = 0.1702
R indices (all data)	R1 = 0.0882, wR2 = 0.1870
Largest diff. peak and hole	0.755 and -0.454 $e.Å^{-3}$

5.5.9 Polymerizations in Toluene

5.5.9.1 General Procedure

The catalyst *rac*-Me_2Si(2-Me-Benz[e]Ind)$_2ZrCl_2$ (5.8 mg, 0.01 mmol) was dissolved to a minimal amount of toluene (5 mL) and added to a toluene solution of MAO or modified MAO (~10 mmol Al) at 30 °C (The total volume was 40 mL). The yellow solution turned orange. The solution was kept stirring at 30 °C before addition of 1-hexene (10 mL, 81 mmol). After addition of 1-hexene the solution slowly turned dark violet and the polymerization reaction was kept stirring for 3 h at 30 °C while samples were taken at regular intervals, using a stopwatch and a gas-tight syringe. The samples were injected into vials containing THF/MeOH/HCl (2 mL, 100:1:1 v/v) and pentamethylbenzene (35 g, 0.24 mmol). Samples for NMR analysis were filtered using glass wool and analysed immediately, while samples for GPC measures were left drying in air overnight and redissolved in THF (3 mL) before injection.

5.5.9.2 Polymerizations in Toluene with Addition of $^{t}Bu_2Si(OH)_2$ (A1 series of experiments)

$^{t}Bu_2Si(OH)_2$ (0.53 mmol, 1.06 mmol and 2.12 mmol) was dissolved in 32.8 mL of toluene. MAO 30T (I) (2.2 mL, 9.1 mmol Al as MAO, 1.1 mmol Al as TMA) was added to the solution which was cooled down to 0 °C. The mixture was warmed up to 30 °C and stirred for 1 h. Then, the catalyst was added, followed by standard polymerization procedures as described above. The 'MAO-30-I' was 9-10 months old at the time of the analysis; its specifications are presented in Table 5.1.

A test polymerization was performed without addition of $^{t}Bu_2Si(OH)_2$, following the general procedure as described above.

5.5.9.3 Polymerizations in Toluene with Addition of $C_{12}H_{25}Ph_2SiOH$ (A1 series of experiments)

MAO 30 T (2.2 mL, 9.1 mmol Al as MAO, 1.1 mmol Al as TMA) was transferred to a flask, toluene (20 mL) and a toluene solution of $C_{12}H_{25}Ph_2SiOH$ (0.53 mmol) were added to the mixture, at room temperature and stirred for two hours at 30 °C. Then, the catalyst was added, followed by standard polymerization procedures as described above. The 'MAO-30-I' was 9 – 10 months old at the time of the analysis; its specifications are presented in Table 5.1.

5.5.9.4 Polymerizations in toluene with the addition of TMA or 2,6-di-*tert*-butylphenol (DBP) (A2 series of experiments)

The required quantity of TMA or DBP was reacted with the MAO sample (10 – 10.1 mmol Al) and toluene (overall volume = 40 mL). The solution was left stirring for 1 h at 30 °C. Then the catalyst was added, followed by standard polymerization procedures. MAO 10T (6.3 mL, 7.05 mmol Al as MAO, 3.07 mmol Al as TMA) and MAO 30T (2.2 mL, 9.49 mmol Al as MAO, 0.67 mmol Al as TMA) were used in this study. The MAO samples were 2 months old at the time of analysis, and the MAO 30T comes from a new batch described as: MAO-30-II. The specifications of the samples are presented in Table 5.1.

Test polymerizations with MAO-10 and MAO-30-II were performed without addition of TMA or DBP.

5.5.9.5 Polymerizations in Toluene with Addition of Ph_3SiOH (A3 series of experiments)

MAO 10 T (6.3 mL, 7.05 mmol Al as MAO, 3.07 mmol Al as TMA; 8 months old at the time of the analysis) was dried overnight under vacuum to remove toluene and free TMA. The solid MAO was redissolved in toluene (25 mL) and Ph_3SiOH (0.59 g, 2.14 mmol) dissolved in toluene (10 mL) was added to the solution. The mixture was left stirring at 45 °C for 2 h before addition of the TMA (0.11 mL, 1.15 mmol), followed by stirring for 1 h. Then, standard polymerization procedures were followed.

A test polymerization was performed, following the same procedures, without addition of the silanol for comparison.

5.5.10 Polymerizations in Heptane

5.5.10.1 General Procedure

The MAO solution was dried overnight under vacuum to remove toluene. The white solid was suspended in heptane followed by addition of the modifier (which will be described in detail for each case) apart from the 'test polymerizations' in heptane where unmodified MAO was used. In each case the total volume of heptane was 35 mL. TMA was added (unless stated otherwise) and the mixture was stirred for 1 h. The catalyst *rac*-Me_2Si(2-Me-Benz[e]Ind)$_2ZrCl_2$ (5.8 mg, 0.01 mmol) was dissolved to a minimal amount of toluene (5 mL) and added to the MAO or modified MAO solution at 30 °C (total volume = 40 mL). The yellow solution turned slowly orange. The solution was kept stirring at 30 °C before addition of 1-hexene (10 mL, 81 mmol). After addition of 1-hexene the solution slowly turned dark violet or light violet in some cases and the polymerization reaction was kept stirring for 3 h at 30 °C while samples for NMR and GPC analysis were taken as above.

5.5.10.2 Polymerization in Heptane with Addition of $AlMe_3$, Al^iBu_3 or $Al(Oct)_3$ (B1 series of experiments)[18]

For the polymerizations in heptane with addition of AlR_3 (R = Me, ^{i}Bu or Oct) three methods were followed.

Method A follows the general synthetic procedure as described above. MAO-30-II (2.2 mL, 9.49 mmol Al as MAO, 0.67 mmol Al as TMA, 2 months old) was dried under

vacuum overnight. The white solid was suspended in heptane (35 mL). AlR_3 (1.58 mmol Al) was added and the mixture was left stirring at 30 °C for 1 h. Then standard polymerization procedures were followed.

Method B and C differ from the general procedure described in 5.2.9.1. Method B: To a toluene solution of MAO (10 mmol Al, MAO-30-II), was added toluene (10 mL) and then the catalyst dissolved in toluene (5 mL). The catalyst was allowed to react with the MAO at 30 °C for 1 h and then the volatiles were removed under vacuum overnight. Method C follows the same procedure with the difference that the catalyst is allowed to react for 10 min at 30 °C and then the mixture is left under vacuum only for 1 h to remove the volatiles. In both methods, the solid residue was suspended in heptane (40 mL) and AlR_3 (R = Me, *i*-Bu or Oct; 1.58 mmol Al) was added. The resulting mixture was left stirring for 1 h at 30 °C. Then standard polymerization procedures were followed.

5.5.10.3 Polymerization in Heptane with Modified MAO with $^{t}Bu_2Si(OH)_2$

MAO-30-II (2.2 mL, 9.49 mmol Al as MAO, 0.67 mmol Al as TMA, 4 months old) was dried overnight under vacuum to remove toluene and free TMA. The solid MAO was suspended in heptane (20 mL) and the silanol (0.53 mmol) dissolved in heptane (14.9 mL) was added to the mixture. The mixture was left stirring overnight at room temperature but no enhancement of the solubility was observed. TMA was added back to the mixture (0.11 – 0.2 mL, 1.15 – 2.09 mmol), followed by 1 h stirring. Then, standard polymerization procedures were followed. Addition of 1-hexene did not cause the usual colour change. The colour turned slowly to light pink.

5.5.10.4 Polymerization in Heptane with Modified MAO with $C_{12}H_{25}Ph_2SiOH$ (B2 series of experiments)

MAOb-30 (2.2 mL, 9.23 mmol Al as MAO, 0.82 mmol Al as TMA, 4 months old) was dried overnight under vacuum to remove toluene and free TMA. The solid MAO was suspended in heptane (20 mL) and a suspension of $C_{12}H_{25}Ph_2SiOH$ (0.53 mmol or 1.06 mmol), in heptane (14.89 mL) was added to the mixture. The mixture was left stirring overnight at room temperature but no enhancement of the solubility was observed. TMA was added back to the mixture (0.2 mL, 2.09 mmol), followed by 1 h stirring. Then, standard polymerization procedures were followed.

A test polymerization was performed, following the same procedures, without addition of the silanol for comparison.

5.5.10.5 Polymerization in Heptane with Modified MAO with $(C_8H_{17})_3SiOH$ (B3 series of experiments)

MAO 10 T (6.3 mL, 7.05 mmol Al as MAO, 3.07 mmol Al as TMA, 9 months old) was dried overnight under vacuum to remove toluene and free TMA. The solid MAO was suspended in heptane and a solution of the silanol (2.8 mmol), in heptane was added to the mixture. The mixture was left stirring for 2 h at 45 °C, until a clear solution was obtained. TMA was added back to the mixture (1.15 mmol, 2.09 mmol, 4.36 mmol), followed by 1 h stirring. The total volume of the mixture was 40 mL. Addition of the TMA resulted to a pale solution. Then, standard polymerization procedures were followed.

A test polymerization was performed, following the same procedures, without addition of the silanol for comparison.

5.5.10.6 Polymerization in Heptane with Modified MAO with the Reaction Product of TMA plus $(C_8H_{17})_3SiOH$ (B4 series of experiments)

MAOb-30 (2.2 mL, 9.23 mmol Al as MAO, 0.82 mmol Al as TMA, 4 months old) was dried overnight under vacuum to remove toluene and free TMA. The solid MAO was suspended in heptane and a solution of the reaction product TMA + Oct_3SiOH (2.4 mmol), in heptane was added to the mixture. The mixture was left stirring for 3 h at 45 °C, but no enhancement of the solubility was observed. Another 1.6 mmol of the reaction product of TMA + Oct_3SiOH were added and the mixture was left stirring overnight at 30 °C. The next day the solution was clear. TMA was added back to the mixture (0.2 mL, 2.09 mmol), followed by 1 h stirring. The total volume of the mixture was 35 mL. Addition of the TMA resulted to a pale solution. Then, standard polymerization procedures were followed.

A test polymerization was performed, following the same procedures, without any additives, for comparison as well as a polymerization with Oct_3SiOH. Specific details are given on the tables listed on the results part.

5.5.11 Characterization of MAO after addition of silanols or Oct_3SiOH/TMA: Quantification of $AlMe_3$ and $[AlMe_2]^+$ content[62]

MAO 10T (6.3 mL, 7.05 mmol Al as MAO, 3.07 mmol Al as TMA) was dried overnight under vacuum to remove all volatiles. The solid MAO was suspended in heptane and a solution of $(C_8H_{17})_3SiOH$ (0.81 mmol – 2.4 mmol) in heptane was added to the mixture. The total volume of the mixture was 35 mL. The mixture was left stirring for 2 h at 45 ◦C. THF (3.3 mL; Al/THF (n/n) = 1 : 4) was added to the mixture, which was stirred for another 15 min at R.T. An aliquot of the resulting solution was transferred to an NMR tube with a CD_2Cl2 capillary and pentamethylbenzene (10 μL, 0.97 M in toluene) and ^1H NMR spectra were recorded.

The same procedure was followed for MAO-10 and $^iPr_3SiOH$ in heptane and toluene, and for MAOb-30 and Oct_3SiOH, and the reaction product TMA+Oct_3SiOH in heptane and toluene. The same conditions (concentration of the reactants, reaction time and temperature) used in the respective polymerizations were used here.

$^tBu_2Si(OH)_2$ (0.53 mmol, 1.06 mmol) was dissolved in 32.8 mL of toluene. MAO 30T (I) (2.2 mL, 9.1 mmol Al as MAO, 1.1 mmol Al as TMA) was added to the solution which was cooled down to 0 °C. The mixture was warmed up to 30 °C and stirred for one hour. THF (3.3-6.6 mL; Al/THF (n/n) = 1/4 – 1/8) was added to the mixture, which was stirred for another 15 min at R.T. An aliquot of the resulting solution was transferred to an NMR tube with a CD_2Cl2 capillary and 1,3,5-tri-*tert*-butylbenzene (20 μL, 0.52 M in toluene) and ^1H NMR spectra were recorded.

References

1. J.-N. Pédeutour, K. Radhakrishnan, H. Cramail, A. Deffieux, *Macromol. Rapid Commun.*, **2001**, *22*, 1095.
2. J. R. Severn, J. C. Chadwick, R. Duchateau, N. Friederichs, *Chem. Rev.*, **2005**, *105*, 4073.
3. Abstracts of Papers, 221st ACS National Meeting, San Diego, CA, United States, April 1-5, 2001 Horton, Andrew yr:2001

4. V. N. Panchenko, L. G. Echevkaya, V. A. Zakharov, M. A. Matsko, *Appl. Catal. A: Gen.*, **2011**, *404*, 47.
5. S. A. Sangokoya, M. S. Howie, L. A. Dunaway, US Pat. Appl., 5,157,008, 1992 (Ethyl Corporation)
6. S. A. Sangokoya, M. S. Howie, T. A. Trumbo, US Pat. Appl., 5,066,631, 1991 (Ethyl Corporation).
7. D. B. Malpass, S. W. Palmaka, G. M. Smith, J. S. Rogers, Pat. Appl. WO 98/18801, 1998 (Akzo Nobel)
8. E. Y.-X. Chen, T. J. Marks, *Chem. Rev.*, **2000**, *100*, 1391.
9. C. C. Crapo, D. B. Malpass, US Pat. Appl. 5,041,584, 1991 (Texas Alkyls, Inc.)
10. S. J. Obrey, A. R. Barron, *J. Chem. Soc., Dalton Transactions*, **2001**, 2456.
11. T. Dalet, H. Cramail, A. Deffieux, *Macromol. Chem. Phys.*, **2004**, *205*, 1394.
12. G. M. Smith, S. W. Palmaka, J. S. Rogers, D. B. Malpass, U.S. Pat. Appl. 5,831,109, 1998 (Akzo Nobel nv)
13. R. L. Geerts, T. G. Hill, U.S. Pat. Appl. 5,414,180, 1995 (Phillips Petroleum Company)
14. Y. V. Kissin, U.S. Pat. Appl. 5,258,475, 1993 (Mobil Oil Corporation)
15. D. B. Malpass, S. W. Palmaka, G. M. Smith, J. S. Rogers, Pat. Appl. WO 98/18801, 1998 (Akzo Nobel)
16. H. Kurokawa, T. Sugano, *Macromol. Symp.*, **1995**, *97*, 143.
17. P. A. Charpentier, S. Zhu, A. E. Hamielec, M. A. Brook, *Polymer*, **1998**, *39*, 6501.
18. F. Ghiotto, C. Pateraki, J. R. Severn, N. Friederichs, M. Bochmann, *Dalton Transactions*, **2013**, *42*, 25.
19. M. O. Kristen, *Topics in Catalysis*, **1999**, *7*, 89.
20. V. N. Panchenko, N. V. Semikolenova, I. G. Danilova, E. A. Paukshits, V. A. Zakharov, *J. Mol. Catal. A*, **1999**, *142*, 27.
21. E. P. Talsi, N. V. Semikolenova, V. N. Panchenko, A. P. Sobolev, D. E. Babushkin, A. A. Shubin, V. A. Zakharov, *J. Mol. Catal. A*, **1999**, *139*, 131.
22. M. E. Bartram, T. A. Michalske, J. W. Rogers, *J. Phys. Chem.*, **1991**, *95*, 4453.
23. K. Soga, M. Kaminaka, *Makromol. Chem.*, **1993**, *194*, 1745.
24. M. C. Haag, C. Krug, J. Dupont, G. B. de Galland, J. H. Zimnoch dos Santos, T. Uozumi, T. Sano, K. Soga, *J. Mol. Catal. A: Chem.*, **2001**, *169*, 275.
25. S. Scott, T. L. Church, D. H. Nguyen, E. A. Mader, J. Moran, *Top. Catal.*, **2005**, *34*, 109.

26. W. Kaminsky, C. Strübel, *J. Mol. Catal. A: Chem*., **1998**, *128*, 191.
27. M. Bochmann, *Top. Catal*., **1999**, *7*, 9.
28. J. Li, J. A. Diverdi, G. E. Maciel, *J. Am. Chem. Soc*., **2006**, *128*, 17093.
29. M. D. Skowronska-Ptasinska, R. Duchateau, R. A. van Santen, G. P. A. Yap, *Organometallics*, **2001**, *20*, 3519.
30. A. W. Apblett, A. C. Warren, A. R. Barron, *Can. J. Chem*., **1992**, *70*, 771.
31. S. J. Obrey, S. G. Bott, A. R. Barron, *Organometallics*, **2001**, *20*, 5119.
32. O. Wrobel, F. Schaper, U. Wieser, H. Gregorius, H. H. Brintzinger, *Organometallics*, **2003**, *22*, 1320.
33. K. Soga, H. J. Kim, T. Shiono, *Makromol. Chem., Rapid Commun*., **1993**, *14*, 765.
34. O. Wrobel, F. Schaper, H. H. Brintzinger, *Organometallics*, **2004**, *23*, 900.
35. S. J. Obrey, S. Bott, A. R. Barron, *Organometallics*, **1990**, *9*, 2137.
36. R. Mülhaupt, J. Calabrese, S. D. Ittel, *Organometallics*, **1991**, *10*, 3403.
37. G. M. Smith, D. B. Malpass, S. W. Palmaka, Pat. Appl. EP 0818456 A2, 1998 [Priority US 67902896 A, 1996] (Akzo Nobel NV)
38. S. A. Sangokoya, US Pat. Appl. 5,731,253, 1998 (Albemarle Corporation)
39. A. M. Piotrowski, E. I. Band, US Pat. Appl. 4,945,076, 1990 (Akzo America Inc.)
40. S. A. Sangokoya, S. P. Diefenbach, C. Daly, L. S. Simeral, Pat. Appl. WO2007/005400 A3, 2007 (Albemarle Corporation)
41. S. A. Sangokoya, B. L. Goodall, L. S. Simeral, Pat. Appl. WO 03/082879 A1, 2003 (Albemarle Corporation)
42. S. A. Sangokoya, X. Wu, S. P. Diefenbach, B. Kneale, Pat. Appl. WO 2009/029857 A1, 2009, (Albemarle Corporation)
43. P. A. Wilson, PhD Thesis 'Mechanistic Aspects of Polymerization Catalysts, University of East Anglia, 2008.
44. M. Bochmann, *J. Organomet. Chem*., **2004**, *689*, 3982.
45. U. Stehling, J. Diebold, R. Kirsten, W. Röll, H.-H. Brintzinger, S. Jüngling, R. Mülhaupt, F. Langhauser, *Organometallics*, **1994**, *13*, 964.
46. J. C. W. Chien, *J. Am. Chem. Soc*., **1959**, *81*, 86.
47. F. Song, R. D. Cannon and M. Bochmann, *J. Am. Chem*., **2003**, *125*, 7641.
48. F. Song, R. D. Cannon, S. J. Lancaster, M. Bochmann, *J. Mol. Catal*., **2004**, *218*, 21.
49. F. Song, M. D. Hannant, R. D. Cannon, M. Bochmann, *Macromol. Symp*., **2004**, *213*, 173.
50. J. C. W. Chien and B. P. Wang, *J. Polym. Sci., Part A: Polym. Chem*., **1988**, *26*, 3089.

51. J. C. W. Chien and B. P. Wang, *J. Polym. Sci., Part A: Polym. Chem.*, **1989**, *27*, 1539.
52. Z. Liu, E. Somsook, C. R. Landis, *J. Am. Chem. Soc.*, **2001**, *123*, 2915.
53. Chapter 4, Section 4.2.2
54. D. W. Imhoff, L. S. Simeral, S. A. Sangokoya, J. H. Peel, *Organometallics*, **1998**, *17*, 1941.
55. F. Ghiotto, C. Pateraki, J. Tanskanen, J. R. Severn, N. Lühmann, A. Kusmin, J. Stellbrink, M. Linnolahti, M. Bochmann, *Organometallics*, **2013**, *32*, 3354.
56. F. Song, R. D. Cannon, M. Bochmann, *Chem. Commun.*, **2004**, 542.
57. V. Busico, R. Cipullo, F. Cutillo, N. Friederichs, S. Ronca, B. Wang, *J. Am. Chem. Soc.*, **2003**, *125*, 12402.
58. M. D. Healy, D. A. Wierda, A. R. Barron, *Organometallics*, **1988**, *7*, 2543.
59. A. Tynys, J. L. Eilertsen, J. V. Seppala, E. Rytter, *J. Polym. Sci., Part A: Polym. Chem.*, **2007**, *45*, 1364.
60. V. Busico, R. Cipullo, V. Esposito, *Macromol. Rapid Commun.*, **1999**, *20*, 116.
61. R. Brüll, H. Pasch, H. G. Raubenheimer, R. Sanderson, U. M. Wahner, *J. Polym. Sci., Part A: Polym. Chem.*, **2000**, *38*, 2333.
62. Review: M. Bochmann, *Organometallics*, **2010**, *29*, 4711.
63. M. Bochmann, S. J. Lancaster, *Angew. Chem., Int. Ed. Engl.*, **1994**, *33*, 1634.
64. M. Bochmann, S. J. Lancaster, *J. Organomet. Chem.*, **1995**, *497*, 55.
65. P. A. Wilson, M. H. Hannant, J. A. Wright, R. D. Cannon, M. Bochmann, *Macromol. Symp.*, **2006**, *236*, 100.
66. C. von Hänisch, S. Traut, S. Stahl, *Z. Anorg. Allg. Chem.*, **2007**, *633*, 2199.
67. C. Tamborski, G. J. Chen, D. R. Anderson, Jr. E. Carl, *Ind. Eng. Chem. Prod. Res. Dev.*, **1983**, *22*, 2, 172.
68. M. Nadvornik, K. Handlir, J. Holecek, J. Klikorka, A. Lycka, *Z. Chem.*, **1980**, *20*, 9, 343.
69. A. R. Chadeayne, P. T. Wolczanski, E. B. Lobkovsky, *Inorg. Chem.*, **2004**, *43*, 11, 3421.
70. *Programs CrysAlisPro*, Oxford Diffraction Ltd., Abingdon, UK (2010)
71. G. M, Sheldrick *Acta Cryst.* **2008**, *A64*, 112.
72. A. L. Spek (2006) PLATON – A Multipurpose Crystallographic Tool, Utrecht University, Utrecht, The Netherlands. A. L. Spek, *Acta Cryst.*, **1990**, *A46*, C34
73. Farrugia, L. J. *J. Appl. Crystallogr.*, **1999**, *32*, 837.

74. ‘*International Tables for X-ray Crystallography’*, Kluwer Academic Publishers, Dordrecht (1992). Vol. C, pp. 500, 219 and 193.

Chapter 6

Ethyl-*iso*-butylaluminoxane

6.1 Introduction

While methylaluminoxane (MAO) has been the 'centre of attention' for many research groups since it was proven to be such an efficient catalyst activator, the activation ability of other aluminoxanes with different structures has been less scrutinised. Several studies have shown that different aluminoxanes, even methylaluminoxanes with different preparative histories[1], may demonstrate similar or completely different catalytic behaviour. This huge variation in the performance of different catalyst systems (combination of different aluminoxanes with different catalysts) could only be explained by the differences in the structures of the aluminoxanes which may reflect differences in their alkylation ability, the stability of the active species and tightness of the ion pair.[2, 3]

Ethyl-*iso*-butylaluminoxane (EBAO) is a promising aluminoxane due to the low cost of its production and its high solubility in saturated hydrocarbons. It can generally be made *via* the hydrolysis of a mixture of triethylaluminium (TEA) and triisobutylaluminium (TIBA). TEA and TIBA are cheaper starting materials than the trimethylaluminium (TMA), which is required for the synthesis of MAO. The alkyl molar ratio may vary, as well as the H_2O/Al ratio. It has been reported[4] (see Table 1) that the best results are obtained for an Et/^{i}Bu molar ratio of 4/1, and most studies on EBAO were focused in a H_2O/Al ratio of 0.9/1 or 1/1. More specifically, Wang *et al.*[5-6] synthesised EBAO by the direct addition of water (dropwise) to a mixture of TEA/TIBA at –20 °C (H_2O/Al ratio of 1/1), the mixture was allowed to reach room temperature slowly, where it was stirred for 3 hours, followed by reflux for 15 minutes. Later on, Wang and his co-workers[4] published a modified synthetic procedure which included direct addition of water at –78 °C (H_2O/Al ratio of 0.9/1) and the mixture was not refluxed after the 3 hour-period stirring at R.T.

Table 6.1[4]: Propylene Polymerization by (2,4,7-$Me_3Ind)_2ZrCl_2$/Different Aluminoxanes

Aluminoxane[b]	Ethyl (mol %[c])	Activity 10^6 (gPP/molZr·H)	M_n[d] (*10^4)
MAO	–	2.50	4.7
EBAO55	10	3.59	9.3
EBAO64	15	3.70	8.2
EBAO73	45	3.89	8.0
EBAO82	57	4.12	10.8
EBAO91	70	4.00	9.9

[a]General polymerization conditions [Zr] = $2.0 \cdot 10^{-5}$M, Al/Zr = 3000, T_p = 0 °C, and t = 60 min.

[b]Various EBAOs were numbered according to the TEA/TIBA ratio in a hydrolysis reaction. For example, EBAO82 was prepared by hydrolysis of mixed alkylaluminium solution with an TEA/TIBA molar ratio of 8/2.

[c]Ethyl mol % is the molar percentage of Et/(Et + *i*-Bu) of EBAO. It was determined by GC.

[d]Measured by GPC.

When the catalytic activity of EBAO is compared with MAO, the results vary depending on the catalyst system and conditions used each time. Most studies have shown that EBAO is inferior to MAO in terms of reactivity in ethylene homo- and co-polymerizations with catalysts such as Cp_2ZrCl_2 [5,7], *rac*-Et$(Ind)_2ZrCl_2$[8], $Me_2SiCp_2ZrCl_2$[6] or nickel-based complexes[9]. EBAO made by Wang *et al.*[4] using a slightly different synthetic procedure (as described above) than in their previously published studies[5-8], was the first EBAO example to demonstrate a performance superior to MAO in propylene polymerization, when non-bridging metallocenes such as (2,4,7-$Me_3Ind)_2ZrCl_2$ were employed and in ethylene polymerization with (*n*- $BuCp)_2ZrCl_2$ and (2,4,7-$Me_3Ind)_2ZrCl_2$. Conversely, when a bridged metallocene like *rac*-Et$(Ind)_2ZrCl_2$ was employed, poor activity was observed in propylene polymerization. EBAO/*rac*-Et$(Ind)_2ZrCl_2$ or Cp_2ZrCl_2 systems were active in ethylene polymerization, but worse than the analogous MAO systems. Although EBAO could

not always compete with the cocatalytic activity of MAO, it has always demonstrated a much better performance than ethylaluminoxane (EAO) or iso-butylaluminoxane (*i*-BAO)[5]. Many attempts were made to explain this behaviour by gathering information that would allow an insight to the structural characteristics of EBAO.

Coordination number of Al sites and Lewis acidity of ethylisobutylaluminoxane

^{27}Al-NMR spectroscopic studies have shown that 4-coordinate Al sites are the most common in methylaluminoxane solutions, while they also verified the existence of 3-coordinated Al sites (see Chapter 1) in various alkylaluminiums and aluminoxanes. The existence of the latter is of great interest with respect to the activation efficiency of these aluminoxanes, and in particular in the case of ethylisobutylaluminoxane, because 3-coordinate Al atoms have a higher Lewis acidity, and they could be essential for the formation of a coordination site for alkene insertion, either through extraction of an alkide or by breaking a bridging alkyl bond. [10-15]

Sugano and his co-workers[11] studied the structure of MAO, EAO and *i*-BAO by using ^{27}Al-NMR spectroscopy: they claimed that as TMA and TEA have a structure with 4-coordinate Al sites, MAO and EAO have also a structure with 4-coordinate Al sites and that one plausible structure could include two C–Al bonds and two O–Al bonds (Figure 6.1). They suggest that their association possibly comes from C–Al dative bonds. In the case of *i*-BAO, which comes from 3-coordinate monomeric TIBA, there were some differences attributed to the steric hindrance afforded by the isobutyl group, which could prevent coordination of an Al atom to a second isobutyl group. They suggest that the bonding in *i*-BAO could consist of three O–Al bonds and only one C–Al bond, with the association coming from an O–Al dative bond; forming an Al–O–Al bridge (Figure 6.1). This means that coordination of the Al sites in *i*-BAO to more O atoms could cause a decrease in the Lewis acidity of the aluminoxane, and affect its ability to generate active species and complex anions. [5, 11, 16]

The structures (Figure 6.1) of aluminoxanes that were suggested by Sugano[11] are only simplified models of the aluminoxanes and possibly unrealistic. The aim was to compare the possible differences between the structures of MAO or EAO and *i*-BAO, but the actual structure of the aluminoxanes is far more complex and presence of Al–Me–Al bridges has

never been reported in MAO structures. (More details and references on the MAO structure can be found on Chapter 1, Section 1.2.)

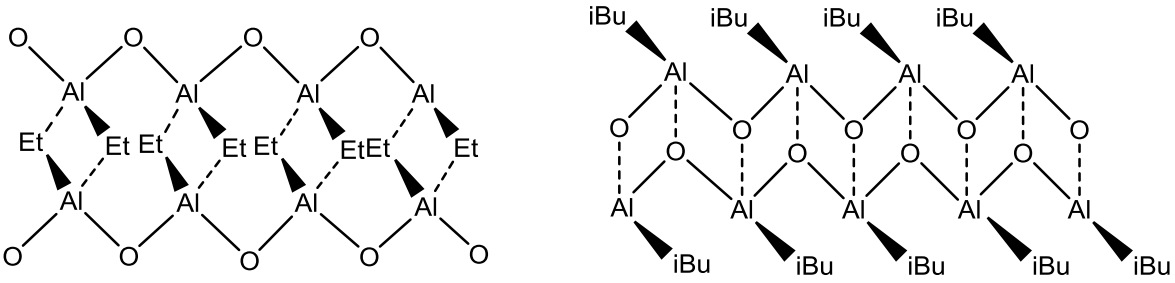

Figure 6.1: Possible structure of EAO and *i*-BAO as proposed by Sugano *et al*.[11]

Heating the dimeric $(^{i}Bu_2AlOAl^{i}Bu_2)_2$, which was made by partial hydrolysis of TIBA with an Al/H_2O molar ratio of 2/1, at ~80 °C for 6 hours, led to the synthesis and isolation of crystals of $Al_{10}O_6{}^{i}Bu_{16}(\mu\text{-}H)_2$ [12] (Figure 6.2).

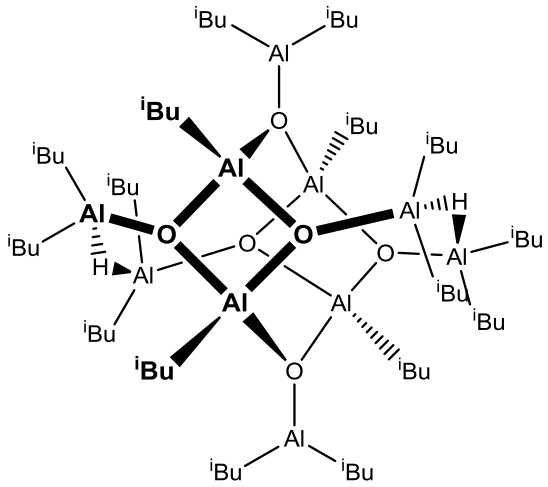

Figure 6.2: Structure of $Al_{10}O_6{}^{i}Bu_{16}(\mu\text{-}H)_2$

This isobutylaluminoxane (TIBAO) structure was formed due to a disproportionation reaction, as shown in reaction (6.1) which occurred due to β-hydride elimination from an isobutyl group, leading to the generation of $Al^{i}Bu_3$ and formation of an Al–H–Al bridge. The presence of a hydride was verified by ^{1}H NMR spectroscopy (a broad resonance at 3.80 ppm), and the crystal structure of the compound revealed the existence of 3-coordinate Al sites. Although the isobutylaluminoxane (*i*-BAO) cage contains Lewis acidic 3-coordinating Al atoms, it was found not to be catalytically active when combined with a number of metallocenes. This was attributed to the fact that the bulky isobutyl groups obstruct interaction of the metallocene with the 3- coordinate Al sites, reducing their reactivity.

$$(^{i}Bu_2AlOAl^{i}Bu_2)_2 \xrightarrow{\Delta} Al(^{i}Bu)_3 + Al_{10}O_6R_{16}(\mu\text{–}H)_2 + \text{others} \qquad (6.1)$$

A similar result by Barron *et al.*[17-18], led researchers to question the role and importance in catalytic activity of the presence of 3-coordinate Al sites in aluminoxanes. Specifically for $[(^{t}Bu)_2Al\{\mu\text{-}OAl(^{t}Bu)_2\}]_2$ made by partial hydrolysis of $Al(^{t}Bu)_3$ as shown in reaction (6.2), which contained two 3-coordinate Al atoms did not show any catalytic activity with Cp_2ZrMe_2.

$$2\ Al(^{t}Bu)_3 + H_2O \longrightarrow 1/2\ [(^{t}Bu)_2Al\{\mu\text{-}OAl(^{t}Bu)_2\}]_2 + 2\ ^{t}BuH \qquad (6.2)$$

On the other hand, $[(^{t}Bu)Al(\mu_3\text{-}O)]_6$, which contains only 4-coordinate Al atoms, gave an active ethylene polymerization catalyst. The clusters $[(^{t}Bu)AlO]_n$ (n = 6, 7, 8, 9, 12) were made by low temperature hydrolysis of $Al(^{t}Bu)_3$, followed by mild thermolysis as shown in reactions (6.3) and (6.4).

$$Al(^{t}Bu)_3 + H_2O \longrightarrow 1/3\ [(^{t}Bu)_2Al(OH)]_3 + ^{t}BuH \qquad (6.3)$$

$$1/3\ [(^{t}Bu)_2Al(OH)]_3 \xrightarrow{\Delta} 1/n\ [(^{t}Bu)AlO]_n + ^{t}BuH \qquad (6.4)$$

^{1}H NMR spectroscopic evidence showed the formation of the complex $[Cp_2ZrMe][(^{t}Bu)_6Al_6O_6Me]$ (**I**) after reaction of $[(^{t}Bu)Al(\mu_3\text{-}O)]_6$ with Cp_2ZrMe_2. The structure of **I**, proposed by Barron, is shown in Figure 6.3. The *tert*-butylaluminoxanes $[(^{t}Bu)Al(\mu_3\text{-}O)]_7$ and $[(^{t}Bu)Al(\mu_3\text{-}O)]_9$ were also active, although no evidence showed the formation of a similar complex. In order to explain the catalytic activity of saturated and unsaturated Al sites in aluminoxanes, Barron introduced the concept of 'latent Lewis acidity'. According to this theory, a 4-coordinate Al site could possess some latent Lewis acidity because of the ring strain within the cluster.

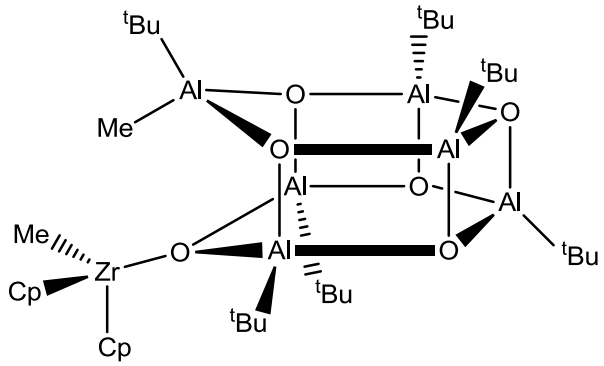

Figure 6.3: The complex $[Cp_2ZrMe][(^tBu)_6Al_6O_6Me]$ (**I**) after reaction of $[(^tBu)Al(\mu_3\text{-}O)]_6$ with Cp_2ZrMe_2

Although there is some ambiguity when the cocatalytic activity of MAO and EBAO are compared, EBAO is indisputably a much better cocatalyst than either *i*-BAO or EAO. At this point, the structural differences of the mixed aluminoxane should be considered. The condensation reaction when $Al(Et)_3$ and $Al(i\text{-}Bu)_3$ are hydrolysed would lead to a random distribution of the ethyl and isobutyl groups within the three dimensional cages of EBAO and cause some defects in its cluster structure. These irregularities in the structure of the aluminoxane could be the main reason that EBAO contains a higher number of 3-coordinate Al sites, as was found by Electron Spin Resonance (ESR) spin method.[7] Wang *et al.* assumed that the higher number of 3-coordinate Al sites could probably lead to a higher number of Lewis acidic sites and aid to the stabilization of the counterion by complexing anions like X^-, CH_3^- or ^-OR, explaining this way the superiority of EBAO compared to the homo-aluminoxanes.[5,7]

The structure of isobutylmethylaluminoxane (MBAO) was investigated by Sugano[19], who claims the existence of 3-coordinate Al sites in MBAO, supported by ^{27}Al-NMR investigations of the reaction product of isobutylaluminoxane with *tert*-butyl chloride, and proposed the structure in Figure 6.4 for MBAO.

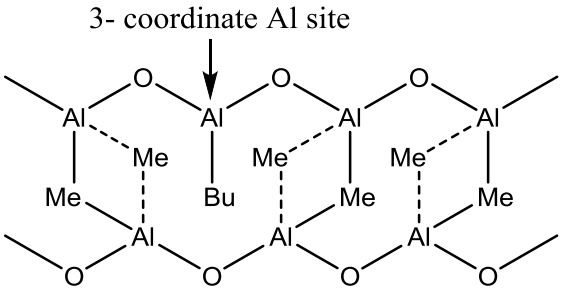

Figure 6.4: Structure of Isobutylmethylaluminoxane as proposed by Sugano[19].

If the latent Lewis acidity of EBAO is taken into consideration, this mixed and random distribution of ethyl and isobutyl groups should increase it, enhancing the overall latent Lewis acidity of the aluminoxane cluster and improving its cocatalytic activity.

Ion-Pair Formation

Another factor that could greatly affect the cocatalytic activity of EBAO, and is also dependent on the alkyl groups present in the aluminoxane, is the tightness of the ion pair formed when a metallocene reacts with the aluminoxane.[20-30]

Wang *et al.*[4] used UV-Visible spectroscopy to study the interactions between (2,4,7-$Me_3Ind)_2ZrCl_2$ and EBAO, and compared it with the UV-visible studies on (2,4,7-$Me_3Ind)_2ZrCl_2$/MAO by Chen and co-workers [29-30]. It was found that for the same Al/Zr ratio, the absorption band of the EBAO system had a higher bathochromic shift than the MAO system, which could reveal the difference in the tightness of the ion-pair; with the EBAO system being associated with a looser ion-pair. A similar conclusion was drawn when Wang *et al.*[7] studied the transformation of *rac*-Et$(Ind)_2ZrCl_2$ into cationic species in the presence of EBAO using UV-visible spectroscopy, and compared their findings with the results of Coevoet *et al.*[26] who studied the *rac*-Et$(Ind)_2ZrCl_2$/MAO system. Again, the EBAO system had a higher bathochromic shift, which could imply that the formation of the dissociated ionic species is faster and more complete.

The reaction of (2,4,7-$Me_3Ind)_2ZrCl_2$ with *i*-BAO was also studied in order to gather more information about the tightness of the ion-pair of different aluminoxanes with a metallocene, and compare their reactivity patterns. *i*-BAO is able to form the ion-pair species only when a very high Al/Zr ratio is employed (ca. 3000/1). Additionally, when the ion pair is formed its concentration decreases with time showing that it is not stable. *I*-BAO's low ability to form and stabilize its ion-pairs could explain its poor cocatalytic activity. The steric

hindrance that the *i*-Bu groups provide is probably the main reason that *i*-BAO produces such a loose ion-pair, resulting in the negative effect on its reactivity.[8]

Wang *et al.*[6] support their hypothesis that EBAO forms a looser ion-pair with the metallocene through their studies on the copolymerization of ethylene and norbornene. Wang and his co-workers argued that EBAO's bulkier alkyl groups should inhibit very close interaction of the cationic species formed and the counterion, allowing a higher insertion rate of norbornene units. They explained the fact that more norbornene was incorporated within the polymer when more Al(*i*-Bu)$_3$ was employed in the feed.

The steric effect of the *i*-Bu and partly Et groups of EBAO on the formation of a loose ion-pair may also inhibit any side reactions such as transfer to aluminium, that would cause the formation of inactive species, between the active species and the aluminoxane.[4] A similar observation was made by De Souza and co-workers[31,] who studied the polymerization of ethylene by a nickel catalyst and (a) TMA and (b) TIBA. The TIBA system achieved higher productivity and molecular weight, due to the looser ion-pair formed inhibiting chain transfer reactions.[32] A lower polymer molecular weight distribution (M_w/M_n) was observed for the TIBA system.

Wang *et al.*[5], who studied the polymerization of ethylene with Cp_2ZrCl_2 and EAO, *i*-BAO and EBAO, found out that the molecular weight distribution (MWD) of the polymer produced was wider than in MAO polymerizations. On the other hand, H. Yang *et al.*[33] reported narrower MWD values for ethylene polymerization with iron based catalysts/EBAO compared to the MAO analogues, suggesting formation of a simple active site or that few side reactions occurred. However, it is difficult to compare and interpret with certainty results coming from different authors, as many factors have to be considered that may not be reported in their published work (e.g. amount of free AlR_3).

Reactions between aluminoxanes and metallocenes

As it has already been mentioned, and observed by several studies [4-9] on different metallocene/aluminoxane systems, the combination of a particular metallocene with a particular aluminoxane is a crucial factor in determining the cocatalytic activity of the system. The choice of the ligands of the metallocene determines the electron density available

to the metal centre, which may affect the efficiency of each system in a positive, or a negative way [34-39].

Galimberti *et al.*[40] examined the reactions between branched β-alkyl-substituted aluminoxanes, such as tetraisobutylaluminoxane (TIBAO) and tetraisooctylaluminoxane (TIOAO), made *via* hydrolysis of their parent aluminium alkyls with an Al/H_2O ratio of 2/1, and *rac*-ethylenebis(tetrahydroindenyl)zirconium dichloride (*r*-EBTHIZrCl_2) performing ethylene/propylene copolymerizations. It was found that the MAO system results in higher productivities than the TIBAO or TIOAO system. The copolymer characteristics were also investigated, linking the microstructure of the copolymer with the metallocene rather than the cocatalyst used each time. Tritto *et al.*[34] continued the studies on β-alkyl substituted aluminoxanes by examining the reactions between TIBAO and TIOAO and Cp_2ZrCl_2 and $(Me_5Cp)_2ZrCl_2$ and testing their catalytic activities in ethylene polymerization. TIBAO did not demonstrate any catalytic activity with Cp_2ZrCl_2, while TIOAO showed minor activity. On the other hand, they both demonstrated high activities with $(Me_5Cp)_2ZrCl_2$. When a bridged metallocene was employed, *rac*-ethylenebis(4,7-dimethyl-1-indenyl)zirconium dichloride (*rac*-EBDMIZrCl_2), with two electron donating methyl substituents, good activities were achieved by all aluminoxanes. TIBAO and Cp_2ZrCl_2 demonstrated some catalytic activity in ethylene polymerization in a previous study by Reddy[41], but only when higher concentrations of Cp_2ZrCl_2 were employed. Although the TIBAO system was less active than the analogous MAO system, it remained active for a longer period.

^{13}C NMR studies showed that when the Cp_2ZrCl_2 was reacted with the β-alkyl-substituted aluminoxanes, they began to decompose as soon as the alkylated species were formed, generating several types of decomposition products. The decomposition process was less prominent with the aluminoxanes than their parent alkylaluminiums. At 313 K, no Cp_2ZrCl_2 is left after reaction with TIBA, triisooctylaluminum (TIOA) or even with TIBAO. Reaction with TIBA or TIOA yields one decomposition product which is a neutral dihydride[42], and probably inactive towards polymerization. Only reaction with TIOAO leaves a small percentage of alkylated species behind (~16%) (Scheme 6.2).

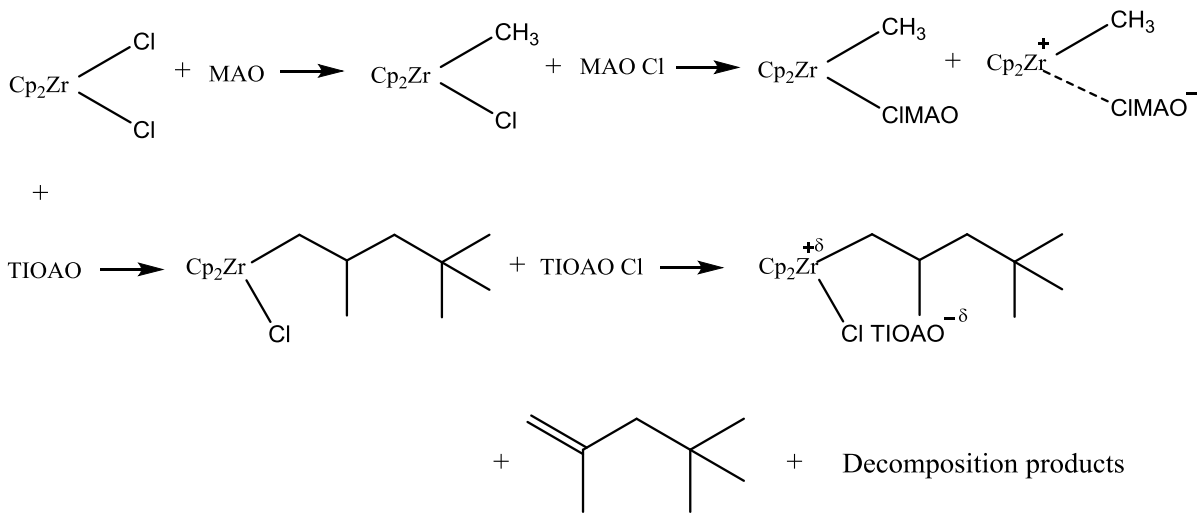

Scheme 6.2: As proposed by Tritto *et al.*

Götz *et al*.[35] who studied the reaction between Cp_2ZrCl_2 and TIBA through ^1H NMR spectroscopy, found that for ratios of Al/Zr >10/1, only one product is detected (Scheme 6.3): a dimeric metallocene complex with Zr–H–Zr and Zr–H–Al bridges. It has been claimed that some of the isobutene observed, is produced *via* the self-decomposition equilibrium of TIBA to diisobutylaluminium hydride and isobutene (Scheme 6.4).

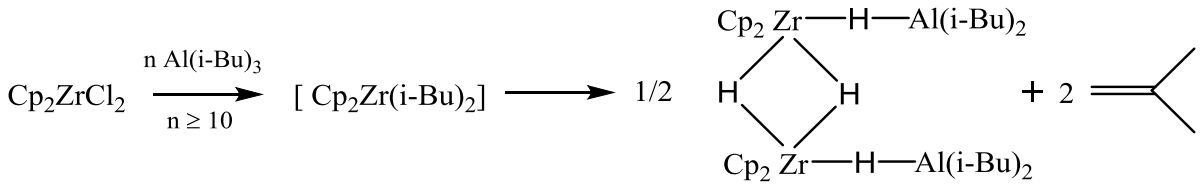

Scheme 6.3: The reaction between Cp_2ZrCl_2 and TIBA. Formation of $Cp_2ZrH_2{\cdot}Al(i\text{-}Bu)_3$ at Al/Zr>10/1

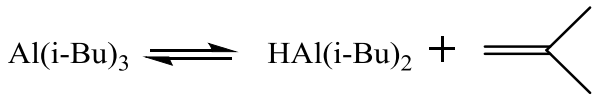

Scheme 6.4: Self-decomposition equilibrium of TIBA to diisobutylaluminium hydride and isobutene.

Beck and Brintzinger[36] observed irreversible decomposition products even at an Al/Zr ratio of 1/1, by uptake of two alkyl groups. Reaction of the zirconocene with TEA at a 1/1 ratio yields the monoethyl complex $Cp_2Zr(CH_2CH_3)Cl$, and is accompanied by evolution of

ethane and formation of an ethene complex $Cp_2Zr(C_2H_4)$ when higher Al/Zr ratios are employed.

The steric hindrance provided by the methylated Cp ligands of $(Me_5Cp)_2ZrCl_2$ and the increased electron density at the metal centre, reduce the reactivity of the metallocene. At 256 K only 19% of the complex is alkylated by MAO or TMA, 4% by TIBAO and none by TIBA; TIOAO is the best alkylating agent at this temperature. However, it seems like the remaining zirconocene is ionized when TIBA, TIBAO, TIOA and TIOAO are used. At 313 K TIBAO has a much better alkylating ability (4 times higher). At this point, it is worth noting that no decomposition products were observed and reported. The steric and electronic effects of the zirconocene ligands inhibit β-hydrogen elimination and decomposition of the alkylated species (Scheme 6.5).[34]

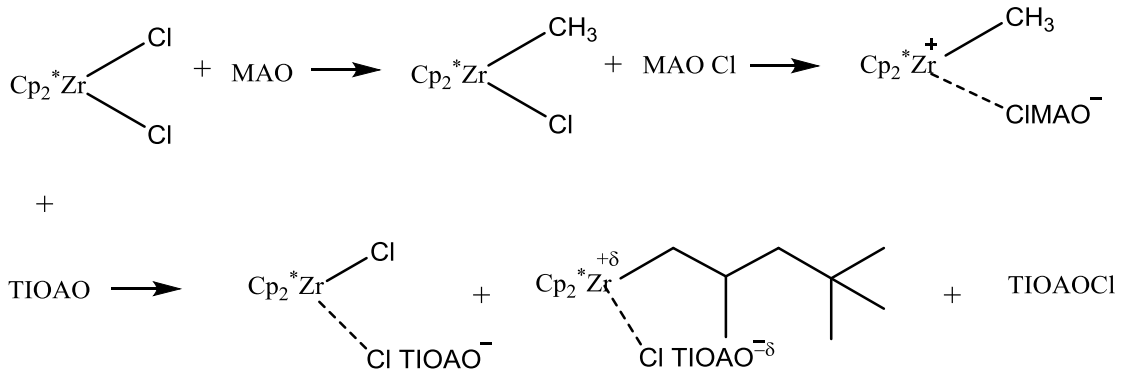

Scheme 6.5: As proposed by Tritto *et al.*

At the same time, Götz *et al.*[35] studied the reaction of TIBA with an *ansa*-metallocene, $Ph_2C(CpFlu)ZrCl_2$, which leads to the formation of the monoalkylated complex $Ph_2C(CpFlu)ZrClBu^i$; even with a 50-fold excess of TIBA.

Wang and his co-workers[4,8-9] also discuss the alkylation ability of EBAO compared to MAO. They support that since the steric hindrance of the alkyl group increases in the order Me < Et < *i*-Bu, the reactivity of the R–Al bond decreases in the order Me–Al > Et –Al > *i*-Bu–Al, meaning that one disadvantage of using ethyl and isobutyl groups rather than methyl groups in the synthesis of aluminoxanes, could possibly be the lower alkylation ability of the aluminoxane.

Since the most recent studies of Wang *et al.*[4] on EBAO with certain catalyst systems showed comparable or better activities than the analogous MAO systems in propylene or ethylene polymerizations, it was decided to investigate further the polymerization performance of EBAO in heptane polymerization using the catalyst system and polymerization conditions that were used in our MAO studies (see Chapter 5) in order to be able to compare the two systems directly. It was believed that the use of ethyl and isobutyl groups instead of methyl groups would provide an aluminoxane soluble in saturated hydrocarbons, which is a valuable advantage for industrial applications.

6.2 Results and Discussion

6.2.1 Polymerizations in Heptane using 'homemade' EBAO instead of MAO

The first target of this study was the synthesis of EBAO in toluene, prepared by direct addition of water to a toluene solution of triethylaluminium and triisobutylaluminium, following the main synthetic procedures described in the literature[4-5] (see *Route 1*), and test its catalytic performance in 1-hexene polymerization in heptane, using the same conditions used in the previous studies of this project on the polymerization performance of various MAO samples in heptane. The aim was to compare the catalytic efficiency of EBAO and MAO in heptane, using the same concentrations of catalyst and monomer, the same Al/Zr ratio and the same polymerization temperature and reaction time, and test the theory that EBAO should be soluble in saturated hydrocarbons like heptane, and for this reason would compete with MAO.

Based on the findings of previous studies on EBAO polymerization systems[4-5] which demonstrate that EBAO prepared with an initial feed of 8:2 molar ratio of TEA and TIBA shows the best activity in ethylene and propylene polymerizations, the same ratio was employed. All samples prepared using this molar ratio, are named as 'EBAO82'.

The EBAO samples used in the polymerizations in heptane named as 'EBAO82-1a', 'EBAO82-2a', 'EBAO82-1b', 'EBAO82-2b' and 'EBAO82-4b' were all synthesized in toluene, and for this reason they were dried under vacuum prior using them in any polymerization studies. The drying process was brief (maximum of ten minutes), aiming to

the removal of the solvent. During drying it was expected that some of the volatile components (ethane, isobutane, free TEA and TIBA) would also be removed. Soluble aluminoxanes in heptane were obtained due to the presence of ethyl and iso-butyl groups, as it was expected. When heptane was added to a solid (pre-dried) EBAO sample the solid was dissolved resulting a clear solution.

The samples 'EBAO82-1a' and 'EBAO82-2a' were prepared by direct addition of water in the mixed alkylaluminium toluene solution at −78 °C and −20 °C respectively (see *Route 1*), while the samples 'EBAO82-1b', 'EBAO82-2b' and 'EBAO82-4b' were prepared by addition of a mixed alkylaluminium toluene solution to a pre-cooled toluene/ water mixture at −78 °C (see *Route 2*). All samples were allowed to reach R.T. slowly, and kept at R.T. for 3 h.

The reason that led to the development of a different procedure for the EBAO synthesis than the ones reported in literature was the fact that EBAO prepared via *Route 1* showed some inconsistency in the reproducibility of the polymerization results. Specifically, some of the attempts to synthesize EBAO following this way led to an inactive alumoxane. On the other hand, following *Route 2* led to a 100% success rate and reproducible results. In detail, more than 10 different batches of EBAO were synthesized and tested, and they all showed similar results. In order to prove the reproducibility of results, the productivity and growth of number-average molecular weight $\overline{M_n}$ as a function of reaction time were measured for three EBAOs which come from three different batches synthesized following the same procedure. Additionally, 'EBAO82-4b' is a sample which comes from a larger batch, prepared by using an overhead stirrer for efficient stirring.

At this point, it should be pointed out that following the polymerization procedure used in the previous MAO studies where the catalyst, rac-Me_2Si(2-Me-Benz[e]Ind)$_2ZrCl_2$, was dissolved in a minimal amount of toluene followed by activation with the aluminoxane in heptane (or toluene) prior to the addition of the monomer, was unsuccessful. When the catalyst was left to react with the EBAO in a heptane or toluene solution, without the presence of the monomer, the catalyst was deactivated after a few minutes. More specifically, after 10 minutes the catalyst was 'dead' which was confirmed by failure of demonstrating any catalytic activity when the monomer was added to the system. The deactivation of the

catalyst was also obvious by the loss of the deep yellow colour of the solution over time. Addition of the catalyst and the monomer in quick succession was attempted but the results were difficult to reproduce. These observations led to the development of a different methodology, changing the succession of addition of the components. In particular, addition of the monomer prior to addition of the catalyst led to a successful initiation and continuation of the polymerization and to reproducible results.

The deactivation of the catalyst when it was allowed to react with EBAO in the absence of the monomer, could be explained by reduction of Zr (IV) to Zr (II) via β-hydride elimination[43-44], after alkylation of the zirconocene, as displayed in Scheme 6.6. The scheme demonstrates the β-hydride elimination of an iso-butyl group. Ethyl groups could undergo similar β-hydrogen elimination, and release of ethene and ethane. The $L_2Zr^{(II)}$ could coordinate with the alkene (iso-butene or ethene) and undergo further cyclisation. Otherwise, possible formation of a neutral dihydride complex $[L_2ZrH_2{\cdot}AlR_3]_2$, as it was described earlier in Scheme 6.3, could explain the decomposition of the catalyst and lack of reactivity.

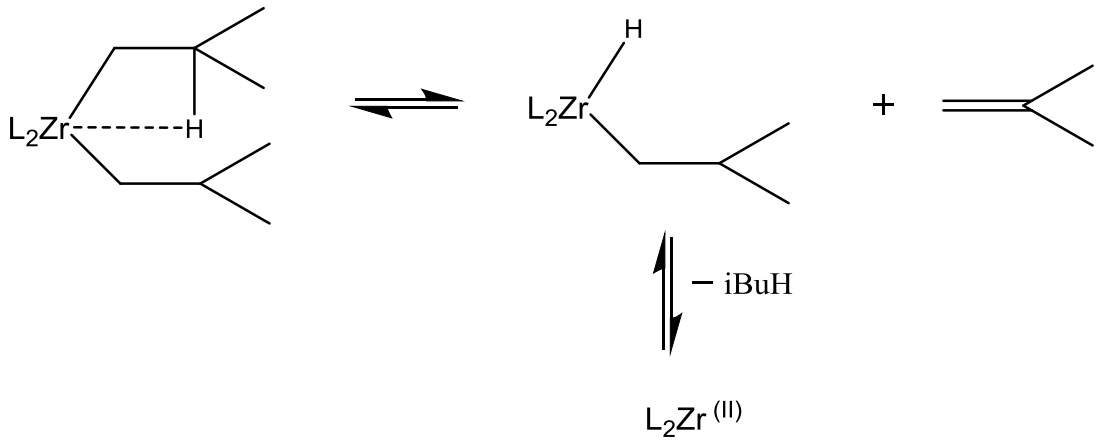

Scheme 6.6: One possible explanation for the decomposition of the zirconocene

The performance of the catalyst system generated with the EBAOs mentioned earlier was tested in heptane, by manually taking samples for NMR and GPC analysis at regular intervals, which were quenched in vials containing THF-MeOH-HCl. The 1-hexene conversion was followed by using quantitative NMR spectroscopy (Figure 6.5). The use of an internal standard (pentamethylbenzene) allowed the quantification of the polymer produced over the period of 3 hours that the polymerization was monitored. Seven samples were collected for NMR analysis, one every 30 minutes. The number average molecular weight $\overline{M_n}$ was determined by gel permeation chromatography (GPC) techniques (Figure 6.6). The

samples were left to dry overnight, and analysed on the GPC instrument as THF solutions the next day. Samples were collected more frequently during the first 30 minutes.

The productivity of the polymerizations with 'EBAO82-1a', 'EBAO82-2a', 'EBAO82-1b', 'EBAO82-2b' and 'EBAO82-4b' as a function of reaction time is given in Figure 6.5. A standard polymerization with a 10% MAO solution in toluene (which had been pre-dried) in heptane is also displayed on the same graph for comparison. All polymerizations with the different EBAOs have similar productivities. The productivity obtained by EBAO as an activator is close to the productivity of a typical 'MAO-10' activator. Specifically, as it can be seen on Table 6.3 the polymer obtained by each polymerization with an 'EBAO82' sample was between 1.6 to 1.9 g, with the total % conversion of 1-hexene to poly-(1-hexene) lying between 23 to 28%. These values are close to the 1.6 g of polymer obtained by a typical polymerization with 'MAO-10' with a 24% conversion rate.

The time dependence of the $\overline{M_n}$ of the polymer produced in the polymerizations where the aforementioned EBAOs were used is also shown, in Figure 6.6. The $\overline{M_n}$ versus reaction time of a typical polymerization with 'MAO-10' is also displayed. It can be seen that the different EBAOs produce polymer with close $\overline{M_n}$ values, within the range of 37000 to 45200 (see Table 6.3) relatively higher to the 'MAO-10' ($\overline{M_n}$ = 30400).

As it has been shown for polymerizations with MAO in the previous chapter, initial monomer consumption proceeds linearly with time[45] (Equation 6.1). Deviation from linearity in the latter stages of the reaction reflects monomer depletion.[1, 46]

$$Rate = -\frac{d[M]}{dt} = k\,[C]_T[M] \qquad (6.1)$$

The NMR data were fitted according to Equation 6.2, as previously reported:

$$Slope = m_M \cdot [M]_0 \cdot C^0 \cdot k_p^{app} \qquad (6.2)$$

where $[M]_0$ is the initial monomer concentration, C^0 is the concentration of total catalyst precursor and k_p^{app} is the apparent propagation rate. The parameters k_p and k_t were determined, as for the MAO polymerization studies in Chapter 5, by curve fitting of the $\overline{M_n}$ data versus time using the Equation (6.3) which describes the rate of growth of the polymer chain, irrespective of the number of metal centres involved. The parameter k_i was kept the

same as in the MAO kinetic studies. Here, as well, varying the k_i over a wide range of values had a small effect on the curve fitting and estimation of the k_p and k_t values.

$$\langle n \rangle = \frac{\frac{(k_p[M]_0 + k_t)t}{k_t} + \frac{k_p[M]_0 + k_t - k_i[M]_0}{k_i[M]_0(k_t - k_i[M]_0)}\left(e^{-k_i[M]_0 t} - 1\right) - \frac{(k_p[M]_0\, k_i[M]_0}{{k_t}^2\,(k_t - k_i[M]_0)}\left(e^{-k_t t} - 1\right)}{t + \frac{1}{k_i[M]_0}\, e^{-k_i[M]_0 t} - \frac{1}{k_i[M]_0}} \quad (6.3)$$

where $\langle n \rangle = \overline{M_n}/m_M$ is the degree of polymerization (m_M is the relative molar mass of the monomer), $[M]_0$ is the monomer concentration at t = 0, k_i is the initiation rate constant, k_t the termination rate constant, k_p the propagation rate constant, and t the reaction time.

The curve fitting gave acceptable estimates of the k_p and k_t. The k_p^{app}/k_p ratio gives an estimate of the active species concentration involved in chain growth at any one time. As it can be seen at Table 6.2, all the EBAO82 compositions gave similar k_p^{app} values varying from 0.11 to 0.14 L mol^{-1}s^{-1} . The associated errors with each value are also reported on the table. The k_p^{app}values are not very different from the one obtained for 'MAO-10', which was 0.11 L mol^{-1}s^{-1}. All the EBAO's with an initial feed of Et/i-Bu = 8/2 molar ratio exhibit lower $k_p$values, in the range of 0.77 to 0.61 L mol^{-1}s^{-1}, compared to 'MAO-10' polymerization which has a $k_p = 1.07$ L mol^{-1}s^{-1}. Also, the k_t values associated with the EBAOs are lower (2.60 to 2.03$\times 10^{-3} s^{-1}$) than that of the 'MAO-10' ($4.84 \times 10^{-3} s^{-1}$ which explains the relatively higher polymer molecular weights. Finally, the active species count with EBAO polymerizations is relatively higher (0.19 - 0.16) than that of 'MAO-10' (0.10).

When a minimal amount of $AlEt_3$ (1.8 and 1 mmol) or Al(i-Bu)$_3$ (1.6 and 1 mmol) was added to the EBAO solution in heptane, prior to addition of the monomer, activation of the catalyst system did not occur. The colour of the solution did not change to purple and no monomer consumption was observed. Free $AlEt_3$ or Al(*i*-Bu)$_3$ seemed to have a 'poison' effect on the catalytic activity of the system. Additionally, the presence of free $AlEt_3$ seems to cause some 'disturbance' of the EBAO structure which is responsible for a small amount of precipitation. They could also be responsible for the formation of decomposition products and deactivation of the catalyst. As it was discussed earlier, reaction of the zirconocene with

$Al(i\text{-}Bu)_3$ could lead to the formation of inactive dihydride complexes, reduction of the zirconium in the case of free $AlEt_3$ or $Al(i\text{-}Bu)_3$ or formation of an alkene complex.

When Bravaya *et al.*[47] synthesized isobutylaluminoxanes with a high Al/H_2O ratio, they observed that the molecular weight of the polymer increases with removal of excess $Al(i\text{-}Bu)_3$. Excess $Al(i\text{-}Bu)_3$ participates in chain transfer reactions and causes a decrease of the molecular weight of the polymer.

Since this study was aiming towards the synthesis of an aluminoxane which would have been soluble in hydrocarbons, it was found interesting to investigate the synthesis of EBAO in heptane. From an industrial point of view, it would have been cost efficient to avoid the step of having to remove toluene from the aluminoxane. Unfortunately synthesis of EBAO in heptane in the present study was unsuccessful. When EBAO was synthesized in heptane precipitation occurred. EBAO synthesized in heptane demonstrated no or minimal catalytic activity. Many different procedures where used in order to test fully the possibility of creating an active catalyst system. In a number of polymerizations EBAO was used as it was and without drying it prior to polymerization. In other cases EBAO was dried prior to polymerization to ascertain the fact that the presence of free $AlEt_3$ or $Al(i\text{-}Bu)_3$ would not affect the activation of the catalyst or 'poison' the system, as it was seen earlier. Also, some EBAO samples synthesized is heptane were filtered or heated up to reflux. None of them, though, exhibit any significant catalytic activity. It seems like synthesis in heptane causes some differences in the EBAO framework that play a crucial role concerning its reactivity. It should be reminded here, that any structural differences in the aluminoxane might cause a different ring strain and thus, possess a different latent Lewis acidity.

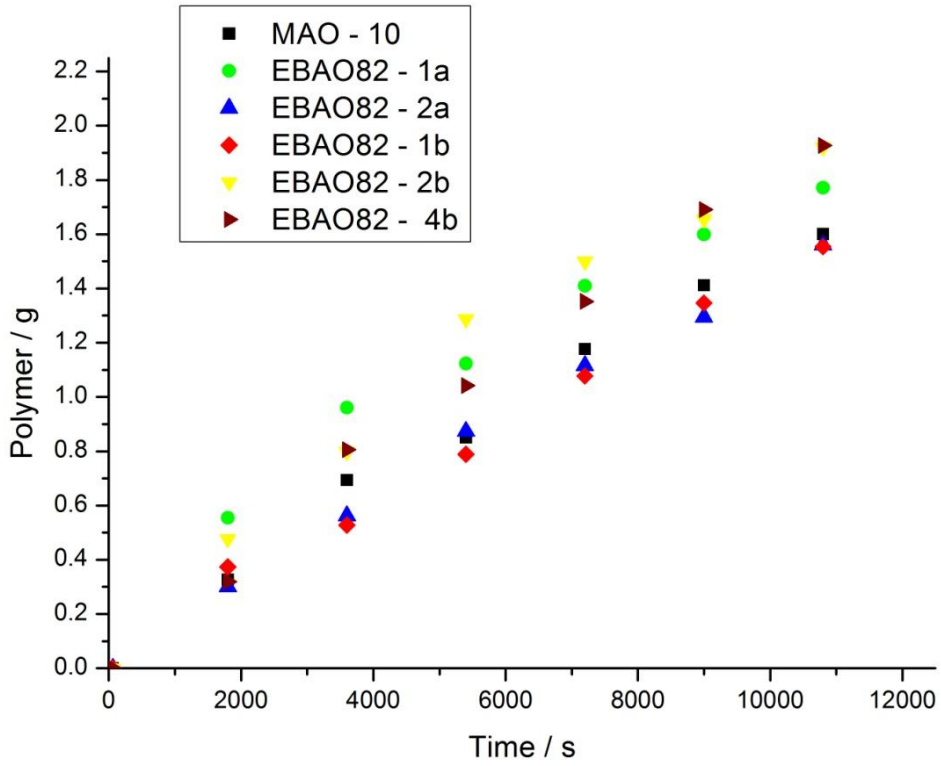

Figure 6.5: Productivity as a function of reaction time for various 'homemade' EBAO samples prepared by hydrolysis of mixed alkylaluminium solution with an 8/2 molar ratio of $AlEt_3/Al(i\text{-}Bu)_3$ in the feed, using *Route 1* or *Route 2.* A polymerization with an MAO 10% solution is displayed for immediate comparison.

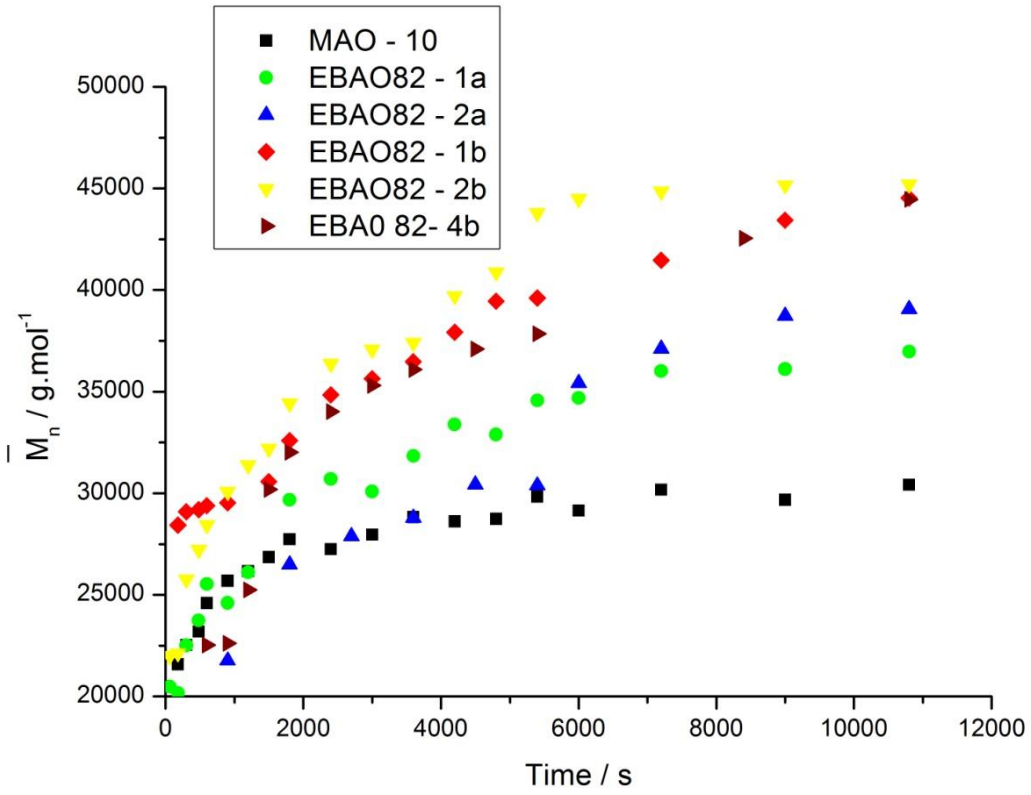

Figure 6.6: Time dependence of M_n for various 'homemade' EBAO samples prepared by hydrolysis of mixed alkylaluminium solution with an 8/2 molar ratio of $AlEt_3/Al(i\text{-}Bu)_3$ in the feed, using *Route 1* or *Route 2.* A polymerization with an MAO 10% solution is displayed for immediate comparison.

Table 6.2: Summary of the kinetic parameters obtained from fitting NMR and GPC data for various 'homemade' EBAO samples prepared by hydrolysis of mixed alkylaluminum solution with an 8/2 molar ratio of $AlEt_3/Al(i\text{-}Bu)_3$ in the feed, using *Route 1* or *Route 2.* The parameters obtained for polymerization with an MAO 10% solution, are displayed for comparison. All polymerizations were performed in heptane.

Aluminoxane	k_p $(L\,mol^{-1}s^{-1})$	k_t $(10^{-3}s^{-1})$	k_i $(L\,mol^{-1}s^{-1})$	k_p^{app} $(L\,mol^{-1}s^{-1})$	k_p^{app}/k_p
MAO-10	1.07 ± 0.06	4.84 ± 0.30	3.8	0.11 (± 0.003)	0.10
EBAO82-1a	0.71 ± 0.02	2.60 ± 0.11	3.8	0.13 ±0.01	0.18
EBAO82-2a	0.61 ± 0.05	2.20 ± 0.26	3.8	0.11 (± 0.002)	0.18
EBAO82-1b	0.67 ± 0.03	2.03 ± 0.1	3.8	0.11 (± 0.002)	0.16
EBAO82-2b	0.77 ± 0.04	2.29 ± 0.14	3.8	0.14 ± 0.01	0.18
EBAO82-4b	0.72 ± 0.02	2.29 ± 0.12	3.8	0.14 (± 0.003)	0.19

6.2.2 Polymerizations in Heptane using 'homemade' EBAO with Different Et/*i*-Bu Ratio in the Initial Feed

Since the synthesis of EBAO82 in toluene following the '*Route 2*', with addition of the mixture of alkylaluminium in a pre-cooled to –78 °C mixture of toluene and ice proved to be successful, and produced an aluminoxane which could compete MAO in polymerization of 1-hexene in heptane, it was considered significant to synthesize EBAOs with a different ethyl to *iso*-butyl molar ratios for comparison of polymerization performance and composition. That led to the synthesis of an EBAO solution in toluene with an initial feed of Et/*i*-Bu of 7/3 molar ratio, which is named 'EBAO73-1c', and the synthesis of an EBAO solution with a feed of 1/1 molar ratio of Et/*i*-Bu, which is named 'EBAO11-2c'. The same polymerization procedure was employed as for EBAO82.

The productivity of the polymerizations with the above EBAO samples as a function of reaction time is given in Figure 6.7. The polymerization with 'EBAO82-4b' is also displayed on the graph for comparison. The polymer produced during the polymerization with 'EBAO73-1c' (1.4 g) and with 'EBAO11-2c' (1.7 g) is very similar to the amount of polymer produced by the EBAO82 series of samples (Table 6.4). Figure 6.8 shows the time dependence of number average molecular weight of all three EBAOs; the $\overline{M_n}$ values are very close, apart from 'EBAO73-1c', which shows relatively higher $\overline{M_n}$. This comes in agreement with the relatively lower k_t value ($1.69 \times 10^{-3} s^{-1}$). 'EBAO73-1c' has also a relatively lower active species count, but, in general all three EBAO compositions demonstrate a similar behaviour in 1-hexene polymerization in heptane (Table 6.3). The polydispersities of all EBAOs reported above were ≈ 1.6 – 1.7, the same value (1.6) was obtained for the heptane polymerization with 'MAO-10', verifying that the catalyst system retains its single-site character.

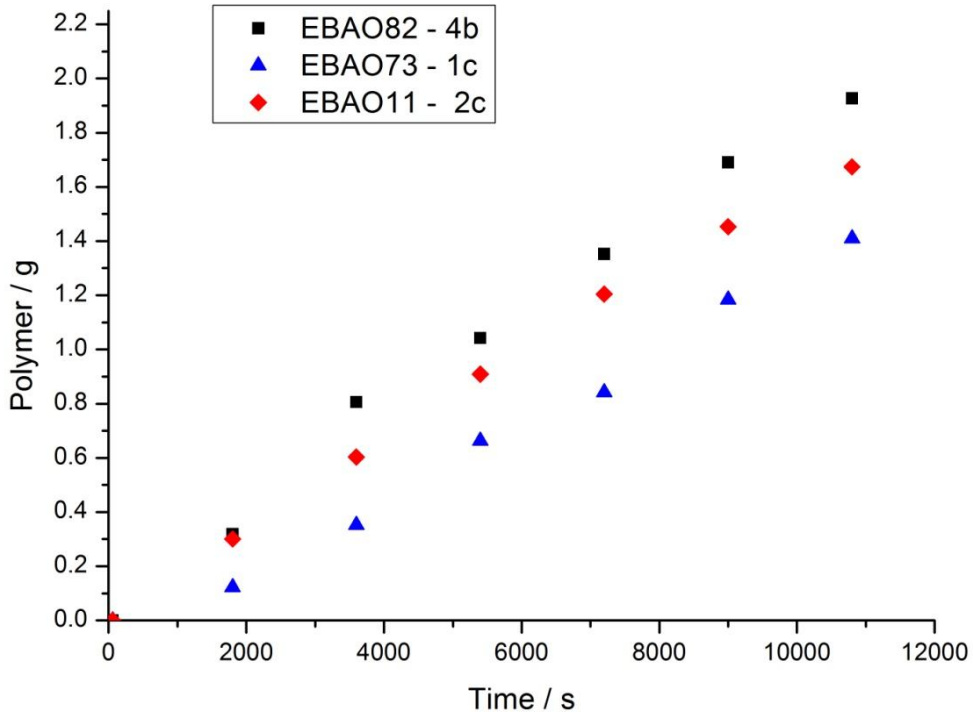

Figure 6.7: Productivity as a function of reaction time for various 'homemade' EBAO samples prepared by hydrolysis of mixed alkylaluminium solutions with 8/2, 7/3, 1/1 molar ratios of $AlEt_3/Al(i\text{-}Bu)_3$ in the feed, for EBAO82, EBAO73 and EBAO11, respectively.

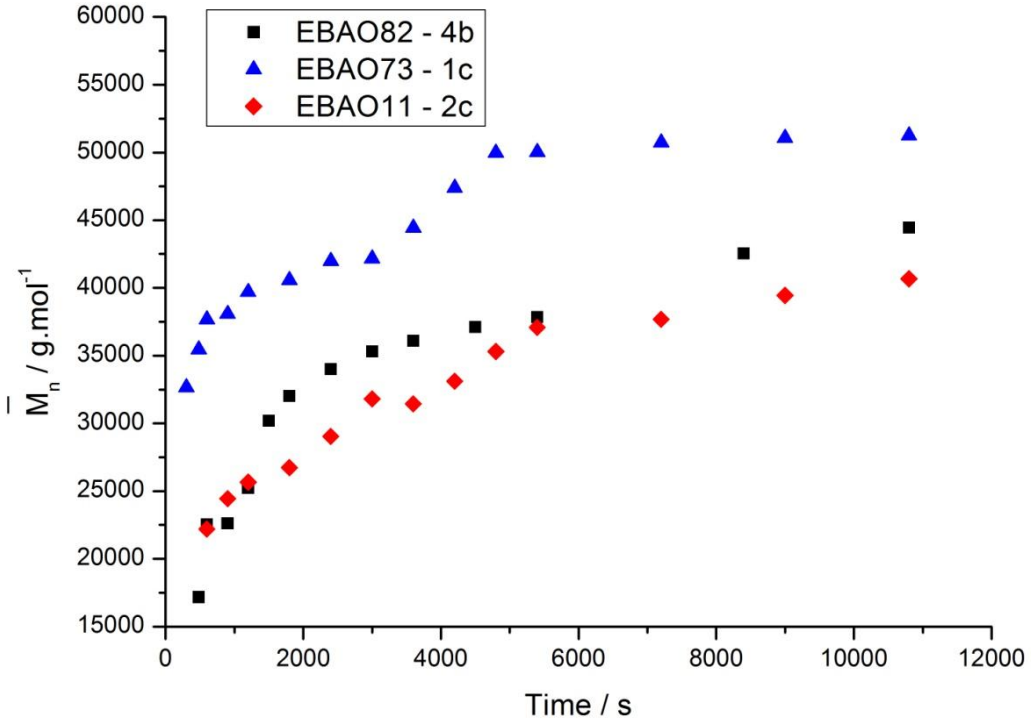

Figure 6.8: Time dependence of M_n for various 'homemade' EBAO samples prepared by hydrolysis of mixed alkylaluminium solution with 8/2, 7/3, 1/1 molar ratios of $AlEt_3$/ $Al(i\text{-}Bu)_3$ in the feed, for EBAO82-4b, EBAO73-1c and EBAO11-2c, respectively.

Table 6.3: Summary of the kinetic parameters obtained from fitting NMR and GPC data for various 'homemade' EBAO samples prepared by hydrolysis of mixed alkylaluminium solution with 8/2, 7/3, 1/1 molar ratios of $AlEt_3/Al(i\text{-}Bu)_3$ in the feed, for EBAO82-4b, EBAO73-1c and EBAO11-2c, respectively. All polymerizations were performed in heptane.

Aluminoxane	k_p $(L\,mol^{-1}s^{-1})$	k_t $(10^{-3}s^{-1})$	k_i $(L\,mol^{-1}s^{-1})$	k_p^{app} $(L\,mol^{-1}s^{-1})$	k_p^{app}/k_p
EBAO82-4b	0.72 ± 0.02	2.29 ± 0.12	3.8	0.14 (± 0.003)	0.19
EBAO73-1c	0.68 ± 0.03	1.69 ± 0.11	3.8	0.09 (± 0.003)	0.13
EBAO11-2c	0.72 ± 0.05	2.59 ± 0.22	3.8	0.12 (± 0.002)	0.17

Table 6.4: Final productivity and $\overline{M_n}$ of heptane polymerization with the various EBAOs

Aluminoxane	Polymer (g)	Conversion (%)	Final $\overline{M_n}$ *
MAO-10	1.6	24	30400
EBAO82-1a	1.8	26	37000
EBAO82-2a	1.6	23	39100
EBAO82-1b	1.6	23	44500
EBAO82-2b	1.9	28	45200
EBAO82-4b	1.9	28	44500
EBAO73-1c	1.4	21	51200
EBAO11-2c	1.7	25	40700

*Rounded to the nearest hundred

6.2.3 Characterization of the 'homemade' EBAO samples

The structure of EBAO, as the structure of MAO is not known. Though, certain methods were employed and developed in order to gain a further insight into the composition and main characteristics of the EBAO that was produced. Aluminium titration was performed, allowing the estimation of the amount of Al needed in its polymerization. The % Al yield is listed in Table 6.4 for the samples 'EBAO82-4b', 'EBAO73-1c', 'EBAO11-2c'. A sample of each was also dried, re-diluted in toluene and titrated, to determine the Al loss, since the EBAO used in heptane polymerizations was dried prior to use. Approximately 10 % of Al is lost after a short drying period. Loss of Al could have been expected as any free or loosely bonded within the EBAO framework $AlEt_3$ or Al(*i*-Bu)$_3$ could have been removed after drying. The standard deviation for each measurement was between the range of 1.5 - 0.8. The Al titration method was tested against a known amount of a toluene solution of $AlEt_3$ (2.19 mmol Al), and the titration results (2.22 mmol Al) were within a 1.7% difference of the theoretical value.

It was crucial to find a way to determine the Et/i-Bu ratio of EBAOs, and since an appropriate GC instrument was not available, a quantitative NMR method was developed. The reaction of trialkylaluminiums with halogens has been studied many years ago[2], and it has been found that the general reaction scheme is:

$$R_3Al + 3\ Br_2 \longrightarrow 3\ RBr + AlBr_3 \qquad (6.5)$$

So, EBAO was allowed to react with excess Br_2 in diethyl ether with the belief that it will follow a similar reaction scheme:

$$(R_{x,y}Al_zO_m)_n + (x + y)\,Br_2 \longrightarrow x\,EtBr + y\,i\text{-}BuBr + (Br_{x+y}Al_zO_m)_n \quad (6.6)$$

where $(R_{x,y}Al_zO_m)_n$ represents an EBAO unit, R_x is the number of Et groups in this unit and R_y the number of *i*-Bu groups.

The use of diethyl ether, a polar solvent, proved to be crucial for successful cleavage of the Br-Br bond to Br^+ and Br^-. The ^1H NMR spectrum of a mixture of commercial EtBr and i-BuBr in Et_2O/toluene was recorded for comparison, and supports the existence of EtBr and i-BuBr in the reaction mixture of EBAO with Br_2. Both ^1H NMR spectra are shown in Figure 6.10. The ^1H NMR spectrum of a 'homemade' EBAO82 is also presented in Figure 6.9. As it can be seen, it is very hard to extract any useful information about the EBAO structure since its spectrum consists of two very broad signals for the methyl and methylene protons at δ 1.3 and 0.5, respectively, indicating the formation of oligomeric products and exchange of the alkyl groups. The doublet at δ 0.91 and the multiplet at δ 1.7 prove the existence of some isobutane (CH_3 and CH respectively), and the singlet at δ 0.86 could be due to the presence of ethane.

The spectrum of the commercial EtBr and *i*-BuBr, in Figure 6.10, in Et_2O/toluene is the spectrum at the bottom. The EtBr can be identified by the signals of the CH_3 group at δ 2.0 ppm (t, J_{HH} = 7.4 Hz) and the CH_2 at δ 3.8 (q, J_{HH} = 7.3 Hz), and the i-BuBr by the signals of the CH_3 at δ 1.5 (d, J_{HH} = 6.6 Hz), CH at δ 2.4 (m) and the CH_2 at δ 3.7 (d, J_{HH} = 6 Hz). The spectrum on the top shows the spectrum of the EBAO after reaction with excess Br_2, and the identification of the proton signals of EtBr and *i*-BuBr is obvious. There is a shift of the signals to the right, because a slightly different Et_2O/toluene ratio was employed. The use of a solution of 1,3,5-trioxane in toluene as an external standard, in a capillary, allows quantification of the Et and *i*-Bu groups present. The signal of the 1,3,5-trioxane is a singlet at δ 4.7. The triplet of the CH_3 protons of the EtBr was integrated (area A) against the standard. However, as it can be seen, there is some overlap of the signals of the CH_3 protons of the *i*-BuBr with the signal of the ^{13}C satellites of the CH_3 of diethyl ether. For this reason, in order to determine the area of integration of the signal, the triplet of the carbon satellites on the left hand side of the main peak for the CH_3 of diethyl ether was integrated (area B), and

subtracted from the area C. The signals of the toluene have been omitted from the spectra for clarity.

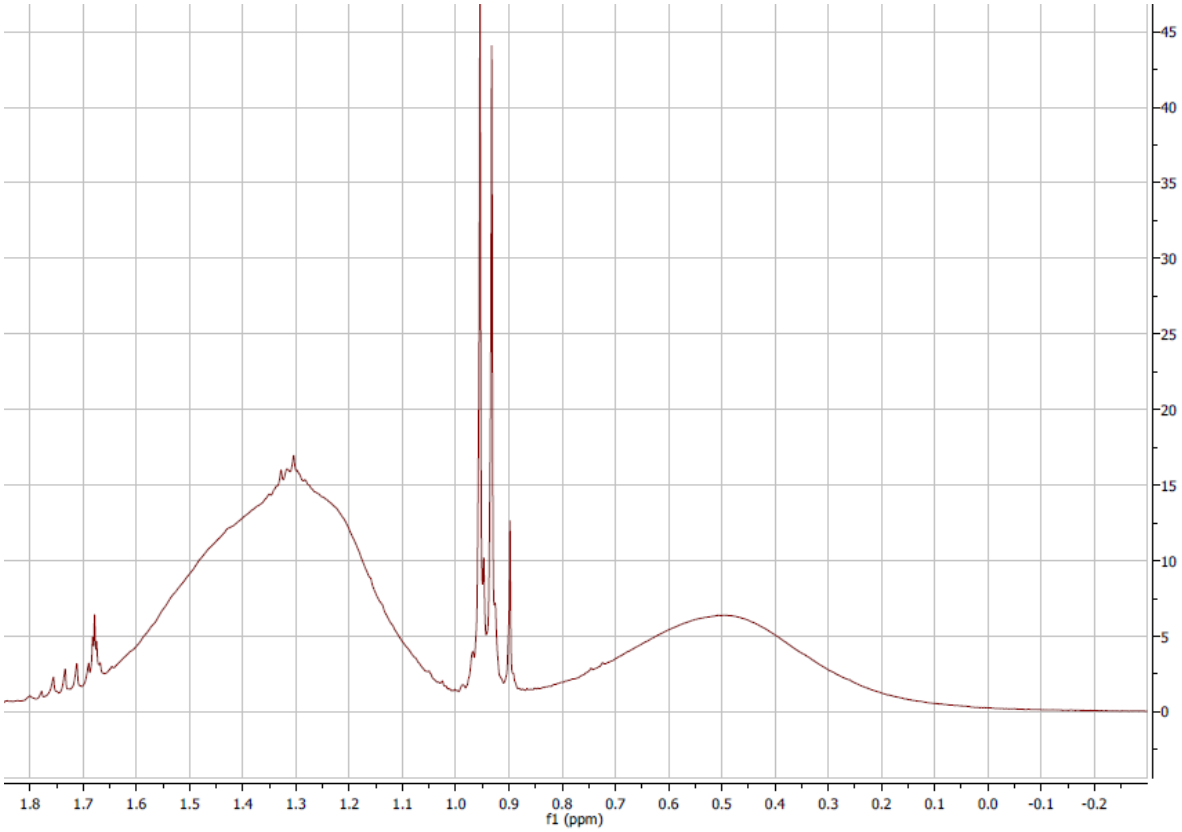

Figure 6.9: Fragment of the ^{1}H NMR spectrum of isobutylaluminoxane in toluene solution obtained by hydrolysis of a mixture of $AlEt_3/Al(i\text{-}Bu)_3$, in a 8/2 molar ratio in the feed, at H_2O/Al =0.9.

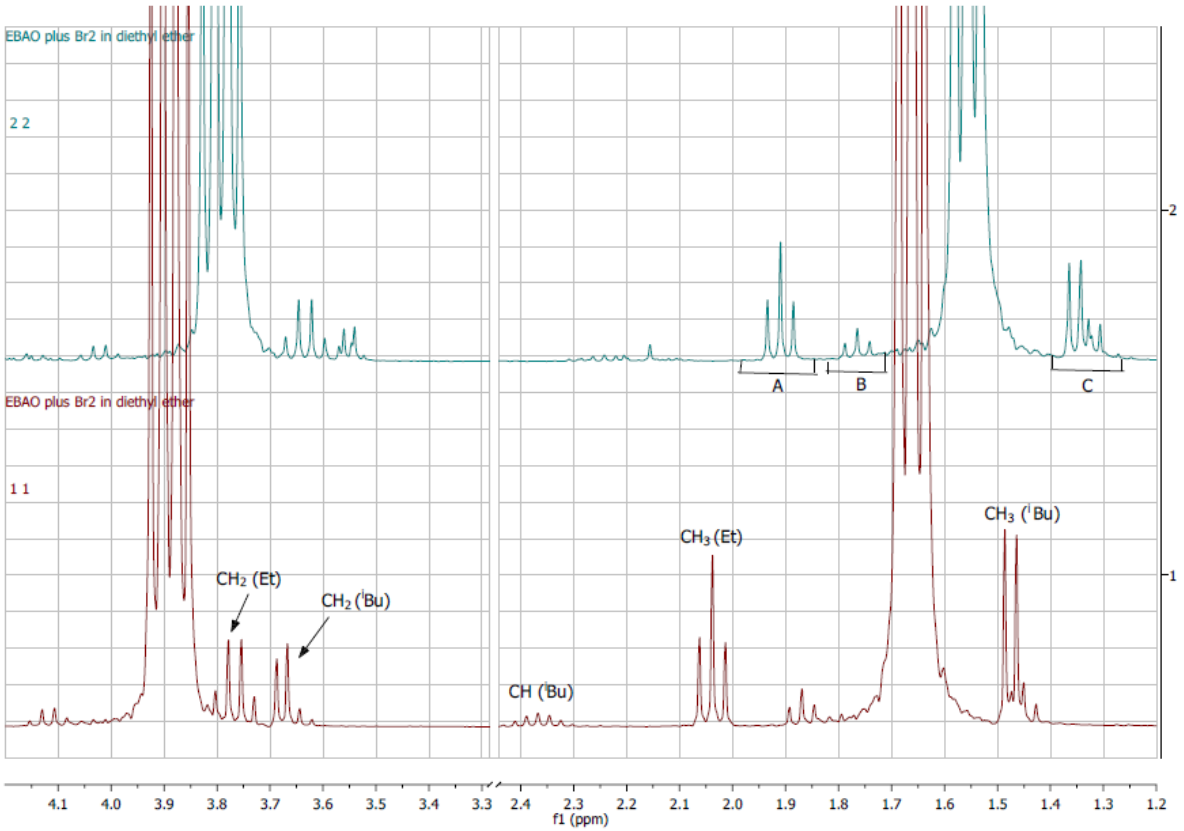

Figure 6.10: Sections of the ^{1}H NMR spectra of commercial EtBr and *i*-BuBr in Et_2O/toluene (bottom spectrum) and the reaction products of the reaction of 'homemade' EBAO82 with excess Br_2 in a Et_2O/toluene solution.

When an initial feed of 80% of $AlEt_3$ was employed in 'EBAO82-4b', the end product had only 54.5 % of ethyl groups left. A similar reduction in the percentage of ethyl groups from the initial feed to the final product was observed for 'EBAO73-1c' and 'EBAO11-2c', from 70% to 45.9% and from 50% to 21.3%, respectively. These values are close to the values reported by Wang *et al.*: 57, 45 and 10% of ethyl groups for EBAO 8/2, 7/3 and 1/1 Et/i-Bu molar ratios in the feed. This was expected as $AlEt_3$ is more active than $Al(i\text{-}Bu)_3$. It has been reported[48] that when $AlEt_3$ and $Al(i\text{-}Bu)_3$ are mixed in a 1/1 ratio the alkyl groups will exchange to form $AlEt_2(^{i}Bu)$ and $AlEt(^{i}Bu)_2$ in an equilibrium. If the mixture is hydrolysed with an Al/H_2O ratio of 2, then it is claimed that at −78 °C the Et–Al bond is more reactive, and it will be the only one that takes part in the hydrolysis forming a tetralkylaluminoxane (TAAO), and resulting in a more *i*-Bu rich aluminoxane, as shown in Scheme 6.7.

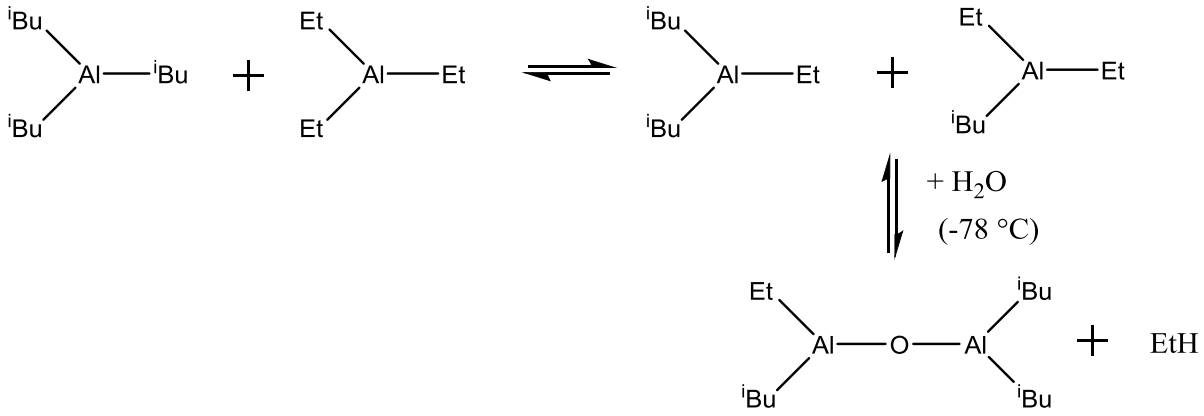

Scheme 6.7: Synthesis of TAAO, as proposed by Wang and Li.[48]

On the other hand, when drying takes place it seems likely there is higher % loss of iso-butyl groups instead of ethyl. EBAO has as higher percentage of ethyl groups than before drying (see Table 6.5). Apparently monomeric Al(*i*-Bu)$_3$ is lost preferentially.

Studies[2] on the structure of MAO, EAO and BAO have shown that while the Al atoms of MAO and EAO are able to coordinate with other alkyl groups forming Me bridges between Al atoms, the Al atoms of BAO because of the steric hindrance that the *i*-Bu groups provide are unable to do this. The possible structures, proposed by Sugano have been shown in Figure 6.1. This phenomenon would probably mean, that in the case of EBAO, where both Et and *i*-Bu groups participate , the Et groups would form Al – Et – Al bridges while the *i*-Bu groups due to their steric effect would not coordinate with other Al atoms, and thus might be easier to remove while drying. Additionally, the monomeric Al(*i*-Bu)$_3$ is more volatile than the dimeric $AlEt_3$, which may be present as free AlR_3, so Al(*i*-Bu)$_3$ will be removed faster.

After looking more closely the quantitative data on Table 6.4, it is noticeable that there is a greater alkyl loss than it would have been expected compared to the Al loss, after drying. Specifically, for 'EBAO82-4b', 4.6 mol of Al and 15.8 mmol of alkyl groups were lost after drying. If the Al is lost in the form of the volatile AlR_3, a loss of 13.8 mmol of R (3×4.6) would have been expected. Similarly, in the case of 'EBAO73-1c' 16.5 mmol of R are lost instead of the expected 13.5 mmol, and in the case of 'EBAO11-2c' 17.7 mmol are lost instead of 12 mmol. These results would indicate that the drying process may cause some changes in the structure of EBAO that would favour and justify the extra loss of *i*-Bu groups. One possible explanation could be the coordination of a β-hydrogen of an *i*-Bu group

attached to a Lewis acidic 3-coordinate Al site that could lead to the removal of isobutene during pumping off the solvent and formation of an Al–H bond. Presence of isobutene in the system, either because it was not completely removed during the drying process or because of the equilibrium reaction that was presented in Scheme 6.4 would lead to the formation of 1,2-dibromo-2-methyl-propane $(CH_3)_2CBrCH_2Br$. The proton signals of $(CH_3)_2CBrCH_2Br$ appear at $\delta \sim 1.9$ (s, CH_3) and 3.9 ppm (s, CH_2) in chloroform-d. A small singlet at δ 2.2 ppm in the reaction spectrum (Fig. 6.10, spectrum on top) is not identified and it could have been attributed to the methyl signal of $(CH_3)_2CBrCH_2Br$. The shift could be explained by the solvent effect. The area ~4 ppm is all masked by the big proton signals of the methylene groups of Et_2O.

Of course, the accuracy and precision of the methods (titration and quantitative NMR) should be taken into account. The standard deviation values related to the NMR measurements for 'EBAO82-4b' are reported below the Table 6.5.

Table 6.5: Specifications of the main EBAO samples synthesized in this study, determined by Al titration and NMR methods.

Aluminoxane	Al yield %	Ethyl % (n/n)	Et (mmol)	*i*-Bu (mmol)	Al (mmol)	R / Al
EBAO82-4b	97.0	54.5	26.5	22.1	38.8	1.3
EBAO82-4b dried	87.3	72.0	23.7	9.2	33.9	1.0
EBAO73-1c	95.8	45.9	20.5	24.1	38.3	1.2
EBAO73-1c dried	83.4	48.8	13.7	14.4	33.3	0.8
EBAO11-2c	96.3	21.3	11.8	43.5	38.5	1.4
EBAO11-2c dried	86.3	30.6	11.5	26.1	34.5	1.1

*The highest standard deviations for the alkyl content measurements were observed for 'EBAO82-4b'. For example: Et = 54.5 ± 0.8%, Et = 26.5±0.1 mmol, ^{i}Bu = 22.1 ± 0.5 mmol and R = 48.6 ± 0.6 mmol.

6.2.4 Commercial EBAO Samples

Six samples of EBAO, which were synthesized by Chemtura, were received and tested in 1-hexene polymerization in heptane. These EBAOs were synthesized by addition of neat water with a syringe pump at 0 °C to a mixture of $AlEt_3$/Al(*i*-Bu)$_3$ in heptane. The resulting mixture was put under reduced pressure to eliminate volatiles (ethane and butane) and filtered. The feed of $AlEt_3$/Al(*i*-Bu)$_3$ varied in each sample: 7/3, 3/2, 1/1, 5/1, 4/1 and 3/1 molar ratios were employed. The samples were named as 'EBAO73', 'EBAO32', 'EBAO11', 'EBAO51', 'EBAO41' and 'EBAO31', respectively.

When 'EBAO73', 'EBAO32', and 'EBAO11' were employed in the polymerization of 1-hexene, they showed some catalytic activity, although this was significantly lower that the 'homemade' EBAOs in toluene. The productivity of the polymerizations with the above EBAO samples as a function of reaction time is given in Figure 6.11. The polymerization with 'EBAO82-4b' is also displayed on the graph for comparison. It can be seen that deactivation of the catalyst starts to take place after 2 hours, in most cases. The mass of polymer produced is significantly lower (1.1 g) with a conversion of 17 to 16%, for the different EBAOs. The exact values are displayed in Table 6.7.

The time dependence of the $\overline{M_n}$ of the polymer produced in the polymerizations where the aforementioned EBAOs were used is also shown, in Figure 6.12. Again, the $\overline{M_n}$ versus reaction time of a polymerization with 'EBAO82-4b' is displayed. It can be seen that the different commercial EBAOs produce polymer with lower $\overline{M_n}$ values, within the range of 20100 to 32100 (Table 6.7). The 'EBAO73' produces the polymer with the lowest $\overline{M_n}$ value. The polydispersities of the commercial EBAOs that were catalytically active were the same as those with 'homemade' EBAOs $\approx$ 1.6-1.7.

The polymerization kinetics was studied following the same protocol as earlier, and the kinetic parameters are reported in Table 6.6. The kinetic parameters of the 'homemade EBAO82-4b' are listed for comparison. Commercial EBAOs show low activity, i.e. low k_p^{app}values (from 0.09 to 0.07 $\mathrm{L\,mol^{-1}s^{-1}}$), and a lower active species count (from 0.13 to 0.11). Also, the lower $\overline{M_n}$ values could be associated with the relatively higher k_t values, ranging between 4.30 to 3.29 $\times$ $10^{-3}\mathrm{s^{-1}}$.

When these samples were dried and re-dissolved in heptane they exhibited no catalytic activity. This would imply that drying the samples resulted in structural changes that affect the ability of EBAO to activate the catalyst.

At this point, it should be mentioned that, even though these six samples were all synthesized following the same procedures, and only changing the feed of Et/i-Bu for each sample, some of them appeared to be catalytically active and some not. The different alkyl ratios would not explain the reason why this happened. Given that, 'homemade' EBAO generated in heptane appeared to be inactive in the polymerization of 1-hexene and precipitation was observed, and the synthetic procedure of the commercial EBAO in heptane has certain differences and little detail is given by the industry it could only be assumed that the reaction products or intermediates of the hydrolysis reaction of $AlEt_3/Al(i\text{-}Bu)_3$ are not fully soluble in heptane, precipitation takes place which has a great influence in the final EBAO composition and structure. Also, delivery of water was probably more efficient using an industrial syringe pump and a better stirring system. As it has been proven with the *Route 1*, synthesis of EBAO is very sensitive to the mode of water addition; especially when heptane is involved instead of toluene, where there are some solubility problems, the hydrolysis reaction is a harder issue to handle.

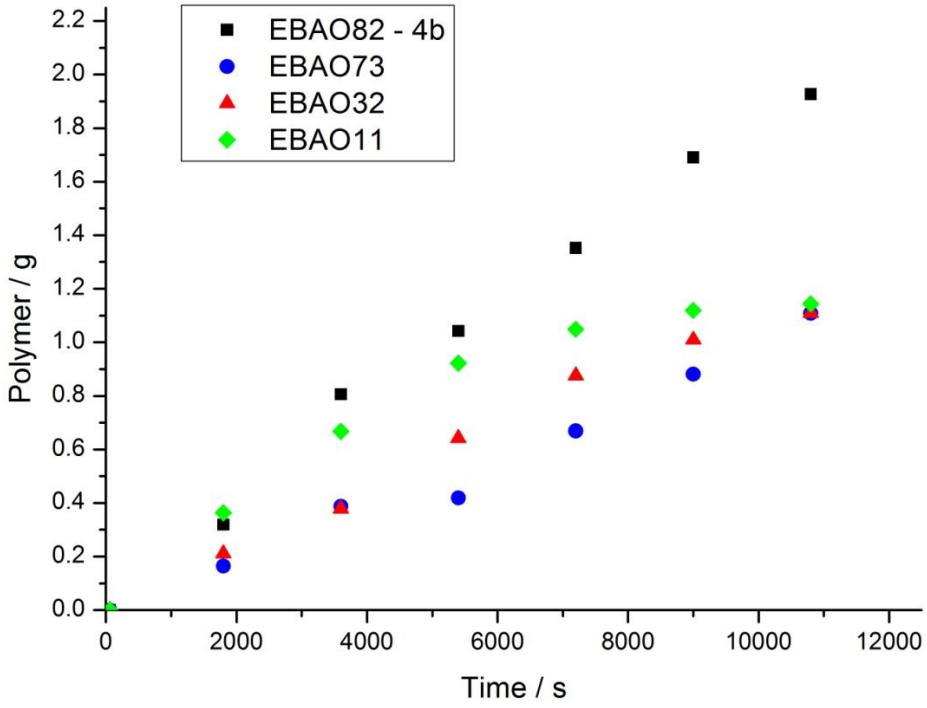

Figure 6.11: Productivity as a function of reaction time for various commercial EBAO samples prepared by hydrolysis of mixed alkylaluminium solutions with different molar ratios of $AlEt_3/Al(i\text{-}Bu)_3$ in the feed. For example, 'EBAO73' was prepared by hydrolysis of an $AlEt_3/Al(i\text{-}Bu)_3$ solution of a 7/3 molar ratio. A polymerization with a 'homemade' EBAO solution 'EBAO82 – 4b' is displayed for comparison.

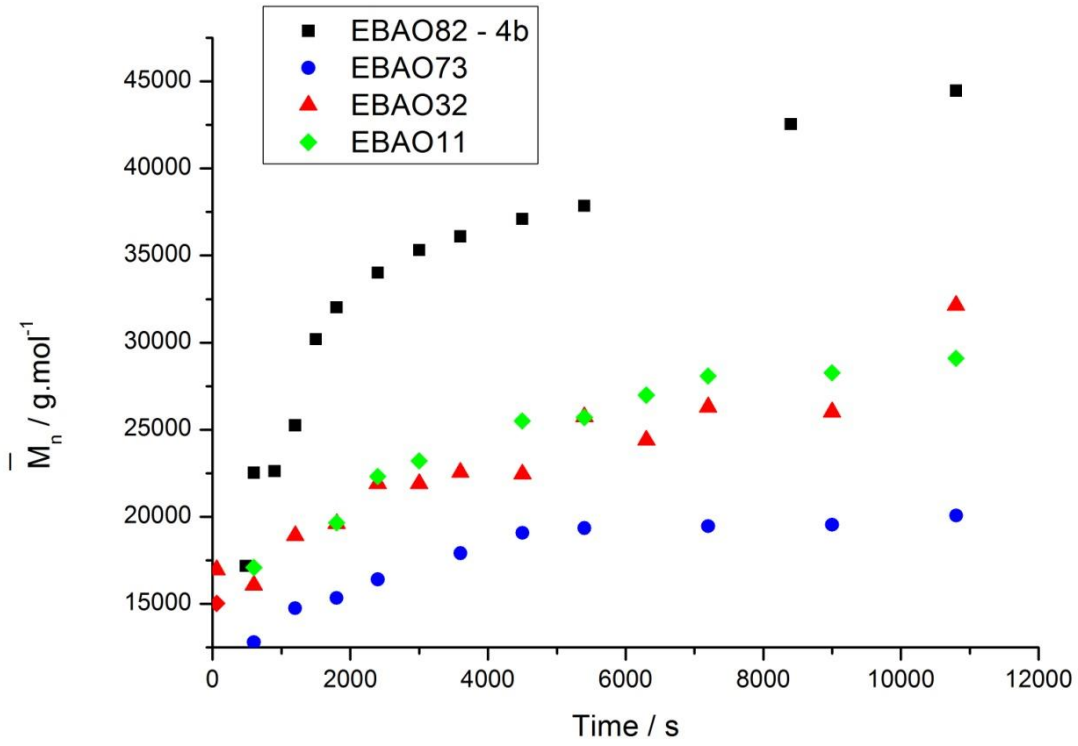

Figure 6.12: Time dependence of M_n for various commercial EBAO samples prepared by hydrolysis of mixed alkylaluminium solutions with different molar ratios of $AlEt_3/Al(i\text{-}Bu)_3$ in the feed. For example, 'EBAO73' was prepared by hydrolysis of an $AlEt_3/Al(i\text{-}Bu)_3$ solution of a 7/3 molar ratio. A polymerization with a 'homemade' EBAO solution 'EBAO82 – 4b' is displayed for comparison.

Table 6.6: Summary of the kinetic parameters obtained from fitting NMR and GPC data for various commercial EBAO samples prepared by hydrolysis of mixed alkylaluminum solutions with different molar $AlEt_3/Al(i\text{-}Bu)_3$ feed ratios. For example, 'EBAO73' was prepared by hydrolysis of an $AlEt_3/Al(i\text{-}Bu)_3$ solution of an 7/3 molar ratio. A polymerization with a 'homemade' EBAO solution 'EBAO82 – 4b' is displayed for comparison. All polymerizations were performed in heptane.

Sample	k_p $(L\,mol^{-1}s^{-1})$	k_t $(10^{-3}s^{-1})$	k_i $(L\,mol^{-1}s^{-1})$	k_p^{app} $(L\,mol^{-1}s^{-1})$	k_p^{app}/k_p
EBAO82-4b	0.72 ± 0.02	2.29 ± 0.12	3.8	0.14 (± 0.003)	0.19
EBAO73	0.62 ± 0.04	4.30 ± 0.33	3.8	0.07 (± 0.002)	0.11
EBAO32	0.64 ± 0.07	3.29 ± 0.44	3.8	0.08 (± 0.002)	0.13
EBAO11	0.68 ± 0.06	3.31 ± 0.38	3.8	0.09 ± 0.01	0.13

Table 6.7: Final Productivity and $\overline{M_n}$ of heptane polymerization with the various EBAOs synthesized by Chemtura.

Aluminoxane	Polymer (g)	Conversion (%)	Final $\overline{M_n}$ *
EBAO73	1.1	16	20100
EBAO32	1.1	16	32100
EBAO11	1.1	17	29100
EBAO51	-	-	-
EBAO41	-	-	-
EBAO31	-	-	-

*Rounded to the nearest hundred

Table 6.8: Specifications of the commercial EBAO samples, as they were determined by Chemtura.

Aluminoxane	Al.-cont. (wt.-%)	% free Al	Ethane % n/n	Iso-Butane	R / Al (n/n)
EBAO73	6.70	15.70	59.74	39.48	1.38
EBAO32	7.00	11.70	50.69	48.55	1.27
EBAO11	7.00	13.80	37.87	60.98	1.37
EBAO51	6.49	12.94	78.88	18.49	1.43
EBAO41	6.61	14.52	74.28	23.05	1.43
EBAO31	6.52	13.34	68.70	28.62	1.40

6.3 Conclusions

This is believed to be the first study in which EBAO is successfully used in 1-hexene polymerization in heptane as a soluble component, and leads to comparable or even higher productivities and higher number average molecular weights compared to the MAO catalytic systems. It should also be noted that a bridged metallocene catalyst was used, and EBAO demonstrated a good catalytic activity. Wang *et al.*[4], had previously claimed that EBAO gave a poor performance when ansa-metallocenes were used in propylene polymerization.

At this point it should be highlighted that the combination of a specific metallocene with a specific aluminoxane is extremely important when the performance of the system is concerned. The steric and electronic effects of the ligands of the metallocene could greatly affect its cocatalytic activity.

The bulkiness of the *i*-Bu groups could affect the tightness of the ion pair, leading towards the formation of a less tight ion pair, and possibly eliminate any side reactions such as chain transfer to Al, resulting in a relatively higher number average molecular weight as has been observed.

Additionally, studies have shown[7] that there are more 3-coordinate Al sites in EBAO than MAO because of the defects that are formed in the aluminoxane structure by the random distribution of the mixture of ethyl and isobutyl groups. It has also been supported that this random distribution of the alkyl groups could enhance the latent Lewis acidity of EBAO that could lead to an increase in the active species count compared to the 'MAO10' (Tables 6.2, 6.3) and stabilize the counterion.

6.4 Future work

The EBAO that was synthesized in this study demonstrated good catalytic performance and it was soluble in saturated hydrocarbons, making it a promising cocatalytic activator in polymerization of olefins. The cheaper, easier and less risky production process of EBAO could be a great advantage in the industrial world. As its structure is not defined, it would have been useful to gather more information about its structural characteristics like the cluster size, the exact ratios of Al/R/O groups, the existence of acidic sites within an EBAO cluster that could lead to a better understanding of the activation mechanisms during the polymerization. As this study proved, it is also necessary to look more carefully on the effects of the drying process on EBAO's structure.

The kinetic studies on the catalytic performance of EBAO were focused on its combination with one metallocene catalyst. In order to be able to draw certain conclusions on the cocatalytic behaviour of EBAO it would be necessary to expand these studies to a larger number of catalysts that are commonly used in industry. Also, in industrial processes most polymerizations take place using catalysts supported silica gel. The next logical step is therefore to check EBAO's performance on silica supported systems.

Finally, this research focused in 1-hexene polymerizations since it is easier to control the polymerization conditions and monitor the monomer conversion since the final polymer remains soluble. However, it will be a necessity to investigate EBAO's cocatalytic activity in

ethylene and propylene polymerizations, as they are the most important monomers from an industrial point of view.

Since EBAO is successfully used in 1-hexene polymerization in heptane and leads to comparable or even higher productivities and higher number average molecular weights compared to the MAO catalytic systems, a similar performance could be expected in ethylene or propylene polymerisations. Of course, the use of a different catalyst might affect the catalytic performance of the system.

6.5 Additional Information

The tables below present the number average molecular weights and polydispersity values from all the polymerisations presented in this study.

Table 6.9a Polymerisations in heptane using 'homemade' EBAO instead of MAO; M_w and PDI values for various 'homemade' EBAO samples prepared by hydrolysis of mixed alkylaluminum solution with an 8/2 molar ratio of $AlEt_3/Al(i\text{-}Bu)_3$ in the feed, using *Route 1* or *Route 2*.

MAO-10			**EBAO82-1a**			**EBAO82-2a**		
Time (s)	**M_w**	**PDI**	**Time (s)**	**M_w**	**PDI**	**Time (s)**	**M_w**	**PDI**
			60	28200	1.4			
180	36200	1.7	180	31300	1.6			
300	35100	1.6	300	34700	1.5			
480	37100	1.6	480	37200	1.6			
600	38300	1.6	600	39000	1.5			
900	40700	1.6	900	39500	1.6	900	30300	1.4
1200	41500	1.6	1200	40700	1.6	1800	37200	1.4
1500	42600	1.6	1800	47600	1.6	2700	39400	1.4
1800	45200	1.6	2400	49800	1.6	3600	40100	1.4
2400	44200	1.6	3000	49800	1.7	4500	44100	1.5
3000	45400	1.6	3600	51600	1.6	5400	44300	1.5
3600	46300	1.6	4200	53700	1.6	6000	53500	1.5
4200	46400	1.6	4800	55100	1.7	7200	58200	1.6
4800	46700	1.6	5400	56900	1.6	9000	60600	1.6
5400	48400	1.6	6000	57400	1.7	10800	62700	1.6
6000	47000	1.6	7200	59300	1.6			

7200	48900	1.6	9000	60400	1.7
9000	47700	1.6	10800	62300	1.7
10800	49200	1.6			

Table 6.9b: Continuation of Table 6.9a

EBAO82-1b			**EBAO82-2b**			**EBAO82-4b**		
Time (s)	**M_w**	**PDI**	**Time (s)**	**M_w**	**PDI**	**Time (s)**	**M_w**	**PDI**
			60	31300	1.4			
180	33000	1.2	180	35300	1.6			
300	38400	1.3	300	39500	1.5			
480	40500	1.4	480	43200	1.6	480	24300	1.4
600	42000	1.4	600	45000	1.6	600	37200	1.7
900	43900	1.5	900	48600	1.6	900	37500	1.7
1500	48700	1.6	1200	52200	1.7	1200	41600	1.6
1800	51000	1.6	1500	54800	1.7	1500	47600	1.6
2400	53800	1.5	1800	57400	1.7	1800	51400	1.6
3000	54400	1.5	2400	60400	1.7	2400	55100	1.6
3600	57600	1.6	3000	62900	1.7	3000	57000	1.6
4200	60500	1.6	3600	64200	1.7	3600	59000	1.6
4800	60000	1.5	4200	66300	1.7	4500	61000	1.6
5400	64300	1.6	4800	71300	1.7	5400	63800	1.7
7200	67800	1.6	5400	73300	1.7	8400	71200	1.7
9000	72900	1.7	6000	76300	1.7	10800	76400	1.7
10800	72300	1.6	7200	79500	1.8			
			9000	80100	1.8			
			10800	81600	1.8			

Table 6.10 Polymerisations in heptane using 'homemade' EBAO with different Et/*i*-Bu ratio in the initial feed; M_w and PDI values for various 'homemade' EBAO samples prepared by hydrolysis of mixed alkylaluminium solution with 8/2, 7/3, 1/1 molar ratios of $AlEt_3/Al(i\text{-}Bu)_3$ in the feed, for EBAO82-4b, EBAO73-1c and EBAO11-2c, respectively.

EBAO82-4b			**EBAO73-1c**			**EBAO11-2c**		
Time (s)	**M_w**	**PDI**	**Time (s)**	**M_w**	**PDI**	**Time (s)**	**M_w**	**PDI**
			300	51400	1.6			
480	24300	1.4	480	56200	1.6			
600	37100	1.6	600	60300	1.6	600	34300	1.5
900	37500	1.7	900	62700	1.6	900	36100	1.5
1200	41600	1.6	1200	64800	1.6	1200	38900	1.5
1500	47600	1.6	1800	66600	1.6	1800	43300	1.6
1800	51400	1.6	2400	68300	1.6	2400	46500	1.6
2400	55100	1.6	3000	70200	1.7	3000	53800	1.7
3000	57000	1.6	3600	72500	1.6	3600	48500	1.5
3600	59000	1.6	4200	76400	1.6	4200	54200	1.6
4500	61000	1.6	4800	80000	1.6	4800	59800	1.7
5400	63800	1.7	5400	83000	1.7	5400	64400	1.7
8400	71200	1.7	7200	87300	1.7	7200	62900	1.7
10800	76400	1.7	9000	89100	1.7	9000	68100	1.7
			10800	94300	1.8	10800	71500	1.8

Table 6.11 Commercial EBAO samples; M_w and PDI values for heptane polymerization with the various EBAOs synthesized by Chemtura

EBAO82-4b			EBAO73			EBAO32			EBAO11		
Time (s)	**M_w**	**PDI**	**Time (s)**	**M_w**	**PDI**	**Time (s)**	**M_w**	**PDI**	**Time (s)**	**M_w**	**PDI**
			60	26400	1.5	60	24900	1.5	60	25700	1.7
480	24300	1.4	900	30700	1.6	600	28100	1.7	600	26400	1.5
600	37200	1.7	1800	30500	1.6	1200	29900	1.6	1800	31100	1.6
900	37500	1.7	2700	32300	1.6	1800	31800	1.6	2400	36000	1.6
1200	41600	1.6	3600	33800	1.7	2400	35000	1.6	3000	37200	1.6
1500	47600	1.6	4500	34700	1.6	3000	35500	1.6	4500	43700	1.7
1800	51400	1.6	5400	34300	1.6	3600	35100	1.6	5400	43600	1.7
2400	55100	1.6	7200	34400	1.6	4500	36800	1.6	6300	44800	1.7
3000	57000	1.6	9000	34000	1.6	5400	40100	1.6	7200	47600	1.7
3600	59000	1.6	10800	35400	1.6	6300	41800	1.6	9000	47700	1.7
4500	61000	1.6				7200	42200	1.6	10800	49100	1.7
5400	63800	1.7				9000	43700	1.7			
8400	71200	1.7				10800	47200	1.5			
10800	76400	1.7									

6.6 Experimental

6.6.1 General Procedures

All manipulations were conducted under inert atmosphere of dry argon using standard Schlenk techniques. All reagents were used as purchased without further purification unless otherwise stated. The catalyst rac-Me_2Si(2-Me-Benz[e]Ind)$_2ZrCl_2$ was used as received (SABIC Europe) and stored in the glove box at room temperature. The commercial EBAO samples were provided as heptane solutions (Chemtura Organometallics GmbH) and stored at +4 °C.

Solvents were dried over Na/benzophenone (tetrahydrofuran, diethyl ether), or sodium (toluene) before use and purged with argon. 1-Hexene was dried over sodium. Anhydrous heptane (Acros) was degassed with a stream of argon and stored over activated 4 Å molecular sieves. NMR spectra were recorded on a Bruker Avance DPX-300 spectrometer. ^{1}H NMR chemical shifts were referenced to the residual solvent peaks of an external standard of CD_2Cl_2. Signals were integrated against internal standards, using 1,3,5-trioxane (for determining the alkyl content of EBAO, after Br_2 reaction) or pentamethylbenzene (for monitoring the consumption of 1-hexene). A relaxation time (D_1) of 25 s and 16 scans were used for ^{1}H NMR spectra. The number average molecular weight, $\overline{M_n}$, of poly(1-hexene) was measured using an integrated Varian PL-GPC-50Plus operating at 30 °C with filtered HPLC grade THF as eluant (1mL·min^{-1}, 7 min per sample) and equipped with a PLgel 10 μm guard column (50 x 7.5 mm), a PL-rapid L column (150 x 7.5 mm) and a refractive index detector. Polysterene narrow standards (peak M_w = 580; 1,480; 3,950; 10,680; 31,420; 70,950; 170,800; 578,500 g·mol^{-1}) were used for calibration. All samples for GPC analysis were prepared in distilled THF and filtered using Acrodisc Syringe filters (0.2 μM PTFE membrane).

6.6.2 Synthesis of Ethyl-*iso*-butylaluminoxane (EBAO)

Route 1

EBAO was prepared by partial hydrolysis of a mixture of triethylaluminium and triiso-butylaluminium in toluene via direct addition of water. Specifically, Al(Et)$_3$ (4.37 mL, 0.032 mol) and Al(*i*-Bu)$_3$ (2.02 mL, 0.008 mol) were added to toluene (40 mL) in a pear

shaped Schlenk flask equipped with a cross-shaped stirrer bar. The mixture was stirred for 15 minutes, and cooled down to −78 °C with a dry-ice/acetone bath. Distilled water (0.65 mL, 0.036 mol) was added dropwise, over a time period of 15 minutes, to the solution which was rapidly stirred. The temperature was increased slowly until the mixture reached room temperature (R.T.). Then it was stirred for an additional 3 hours and 30 min at R.T. After this, the resulting mixture was stored at 4 °C under an argon atmosphere.[4, 49]

Alterations

i. The above procedure was repeated changing the addition temperature from −78 °C to −20 °C. [5]
ii. EBAO was prepared following the procedure described above, in (i), followed by 15 min refluxing. The resulting mixture was allowed to cool down to R.T. [5]
iii. The procedure described in *Route 1* was repeated, using heptane instead of toluene, as a solvent.
iv. The procedure described in (iv) was repeated, changing the addition temperature from −78 °C to −20 °C. The resulting mixture, after the 3 hours of stirring at R.T. was refluxed for 15 min and then allowed to cool down to R.T. before storing it.

Changing the addition temperature to −20 °C increased the precipitation, even in toluene. Some precipitation occurred in EBAO prepared in toluene at −78 °C.

It was noticeable that when heptane was used as a solvent, a substantial amount of precipitate was formed. The EBAO mixture was filtered through a filter cannula.

Route 2

EBAO was prepared by partial hydrolysis of a mixture of triethylaluminium and iso-butylaluminium in toluene. Specifically, distilled water (0.65 mL, 0.036 mol) was added dropwise to a pre-cooled toluene solution (27 mL) at −78 °C, in a pear shaped Schlenk flask equipped with a cross-shaped stirrer bar (flask A). The mixture was kept at −78 °C with a dry-ice/acetone bath and a mixture of $Al(Et)_3$ (4.37 mL, 0.032 mol) and $Al(i\text{-}Bu)_3$ (2.02 mL, 0.008 mol) in 13 mL of toluene were cannula transferred dropwise to the flask A. The addition was completed within 20 minutes. The mixture was allowed to slowly warm up to R.T. and kept at R.T. for 3 hours and 30 min. After this, ‘EBAO82’ was stored at 4 °C under an argon atmosphere.[16]

Alterations

i. The procedure described in *Route 2* was repeated, scaling up the amounts used, by a factor of three using an overhead stirrer for sufficient stirring; equipped with quickfit ground sleeve stirrer glands. A cup shaped lubricant reservoir surrounds sleeve in order to minimise any risks of oxygen insertion.

ii. The procedure described in *Route 2* was repeated, using heptane instead of toluene as a solvent.

iii. The procedure described in *Route 2* was repeated, employing different ratios of Et/*i*-Bu groups. Specifically, EBAO11 was prepared using a 1/1 molar ratio of Et/*i*-Bu groups (0.05 mol of $Al(Et)_3$ and 0.05 mol of $Al(i\text{-}Bu)_3$), and EBAO73 was prepared with a 7/3 molar ratio of Et/i-Bu (using of 0.028 mol of $Al(Et)_3$ and 0.012 mol of $Al(i\text{-}Bu)_3$).

EBAO prepared following the *Route 2* showed only small signs of precipitation. When the solvent was changed to heptane, a substantial amount of precipitate was observed. The EBAO mixture was filtered through a filter cannula.

6.6.3 Al Titration of EBAO[50-52]

The Al content of EBAO was determined by back-titration. An aliquot of EBAO solution (2 mL) was transferred by a 2.5 mL high precision Hamilton gastight syringe to a buffer solution of sodium acetate/acetic acid of a pH ~4.8 in an Erlenmeyer flask, where it was hydrolysed. The stock solution of the buffer was prepared by diluting 53 g (0.65 mol) of CH_3COONa and 36 g (0.6 mol) of CH_3COOH to 300 mL of deionised water, before diluting up to 1 L with deionised water. The amount of EBAO added allowed the use of at least 10 mL of 0.1 mol/L Zn^{2+} solution. 30 mL of 0.1 M Na_2EDTA solution were added via a Mohr pipette. The flask walls were washed with deionised water. The mixture was heated to 100 $^{\circ}C$ for approximately 20 min to allow the quantitative formation of the Al-EDTA complex, and then it was allowed to cool down to R.T. After addition of 4-5 drops of an aqueous solution of xylenol orange tetrasodium salt as an indicator, the excess EDTA was back titrated with 0.1 M Zn^{2+} solution. The Zn^{2+} stock solution was prepared by addition of a 37% HCl solution (at least 41.8 mL, 0.5 mol) on Zinc granules (1.63 g, 0.025 mol), in ~20 mL deionised water. When zinc had reacted the solution was diluted up to 250 mL with deionised water. The Zn^{2+}

solution was standardised by a titration with 0.1 M EDTA-Na_2 solution. The addition of Zn^{2+} solution stopped when a colour change from yellow to pink was observed. Xylenol orange is yellow in acidic conditions and its metal complexes are red[53]. The titration procedure was repeated at least three times for each sample.

A solution of EBAO was transferred to a Schlenk flask and dried under vacuum. The dried EBAO was dissolved in a small volume of toluene, and the above procedure for Al titration was followed.

Prior to proceeding with Al titration of EBAO solutions, a 'test' titration of an aluminium alkyl solution was performed, following the same titration procedure, by using a known amount of $AlEt_3$ (0.3 mL, 2.19 mmol) instead of EBAO.

6.6.4 Determination of Et/*i*-Bu Ratio

A solution of EBAO (4 mL, 3.7 – 3.8 mmol Al depending on the EBAO sample) was transferred to a Schlenk flask containing 3 mL of diethyl ether, equipped with a magnetic stirrer bar. The solution was stirred and cooled down to –25 °C. A mixture of bromine/diethyl ether (~0.3 mL, 11.7 mmol Br_2 in 3 mL of Et_2O) was added slowly to the solution, while stirring [2]*. The mixture was allowed to warm up slowly to R.T. After ~30 min, 0.5 mL of the mixture were transferred to an NMR tube, equipped with a capillary of CD_2Cl_2 used as an NMR standard and a capillary of a solution of 1,3,5-trioxane in toluene (0.09 mmol in 65 μL of toluene) as an internal standard for quantitative NMR purposes. The capillary of the internal standard was filled up by a stock solution of 1,3,5-trioxane in toluene using a high precision Hamilton gastight microsyringe (100 μL). At least three NMR measurements were taken for each EBAO sample.

A solution of EBAO was dried under vacuum, and re-dissolved in toluene. The procedure described above was repeated.

*Modified literature procedure for the reaction of Al(*i*-Bu)$_3$ with Br_2

6.6.5 Polymerization

The EBAO solution (10 mmol Al) was dried under vacuum until most of the solvent was removed. A sticky solid was left behind, and dissolved in heptane (35 mL). The solution

was heated to 30 °C while stirring. The monomer, 1-hexene (0.81 mmol, 10 mL), was added to the solution followed by stirring at 30 °C for an additional 30 min before addition of the catalyst. The catalyst, rac-Me_2Si(2-Me-Benz[e]Ind)$_2ZrCl_2$ (0.01 mmol), was dissolved to a minimal amount of toluene (5 mL) and added to the solution, to start the polymerization. The colour of the solution turned to red/violet. The polymerization reaction was kept stirring for 3 hours at 30 °C while samples for NMR and GPC analysis were taken at regular intervals, using a stopwatch and a gas-tight syringe. The samples were injected into vials containing THF/MeOH/HCl (2 mL, 100:1:1 v/v) and pentamethylbenzene (35 g, 0.24 mmol). Samples for NMR analysis were filtered using glass wool and analysed immediately, while samples for GPC measures were left drying in air overnight and redissolved in THF (3 mL) before injection.[54]

Alterations

i. For EBAO samples prepared in heptane apart from the above procedure, the EBAO samples were also used without being dried. In both cases the total volume of heptane was 35 mL.

ii. For EBAO samples prepared in toluene, in some cases, a small amount of $Al(Et)_3$ (1.8 and 1 mmol) was added to the solution before addition of 1-hexene, and the solution was kept at 30 °C stirring for an additional hour. The total amount of Al was adjusted to 10 mmol taking into consideration the amount of $AlEt_3$ added to the system. Then the standard polymerization procedure was followed.

iii. The same procedure described in (ii) was followed, employing Al(*i*-Bu)$_3$ (1.6 and 1 mmol) instead of $AlEt_3$.

References

1. F. Ghiotto, C. Pateraki, J. R. Severn, N. Friederichs, M. Bochmann, *Dalton Trans.*, **2013**, *42*, 9040.
2. L. I. Zakharkin, V. V. Gavrilenko, *Bulletin of the Academy of Sciences of the USSR, Division of chemical science*, **1959**, *8*, 1, 151.
3. Q. Wang, H. Yang, Z. Fan, *Macromol. Rapid Commun.*, **2002**, *23*, 639.

4. Q. Wang, J. Hong, Z. Fan, R. Tao, *J. Polym. Sci., Part A: Polym. Chem.*, **2003**, *41*, 998.
5. Q. Wang, J. Weng, Z. Fan, L. Feng, *Eur. Polym. J.*, **2000**, *36*, 1265.
6. Q. Wang, J. Weng, Z. Fan, L. Feng, *Macromol. Rapid Commun*., **1997**, *18*, 1101.
7. Q. Wang, Y. Zhao, L. Song, Z. Fan, L. Feng, *Macromol. Chem. Phys*., **2001**, *202*, 448.
8. Q. Wang, L. Song, Y. Zhao, L. Feng, *Macromol. Rapid Commun*., **2001**, *22*, 1030.
9. H. Yang, Q. Wang, Z. Fan, W. Lou, L. Feng, *Eur. Polym. J*., **2003**, *39*, 275.
10. N. N. Korneev, I. M. Khrapova, A. V. Polonskii, N. I. Ivanova, A. V. Kisin, V. S. Kolesov, *Russ. Chem. Bull.*, **1993**, *42*, 8, 1390.
11. T. Sugano, K. Matsubara, T. Fijita, T. Takahashi, *J. Mol. Catal*., **1993**, *82*, 93.
12. F. J. Wu, L. S. Simeral, A. A. Mrse, J. L. Eilertsen, L. Negureanu, Z. Gan, F. R. Fronczek, R. W. Hall, L. G. Butler, *Inorg. Chem*., **2007**, *46*, 1, 44.
13. D. E. Babushkin, N. V. Semikolenova, V. N. Panchenko, A. P. Sobolev, V. A. Zakharov, E. P. Talsi, *Macromol. Chem. Phys.*, **1997**, *198*, 3845.
14. C. J. Harlan, M. R. Mason, A. R. Barron, *Organometallics*, **1994**, *13*, 2957.
15. P. L. Bryant, C. R. Harwell, A. A. Mrse, E. F. Emery, Z. Gan, T. Caldwell, A. P. Reyes, P. Kuhns, D. W. Hoyt, L. S. Simeral, R. W. Hall, L. G. Butler, *J. Am. Soc*., **2001**, *123*, 12009.
16. M. Boleslawski, *J. Organomet. Chem*., **1983**, *254*, 159.
17. C. J. Harlan, S. G. Bott, A. R. Barron, *J. Am. Chem. Soc*., **1995**, *117*, 6465.
18. A. R. Barron, *Macromol. Symp.*, **1995**, *97*, 15.
19. H. Kurokawa, T. Sugano, *Macromol. Symp*., **1995**, *97*, 143.
20. D. Cam, U. Giannini, *Makromol. Chem*., **1992**, *193*, 1049.
21. D. E. Babushkin, C. Naundorf, H. H. Brintzinger, *Dalton Trans*., **2006**, 4539.
22. I. Tritto, S. X. Li, M. C. Sacchi, G. Zannoni, *Macromolecules*, **1993**, *26*, 7111.
23. I. Tritto, S. X. Li, M. C. Sacchi, P. Locatelli, *Macromolecules*, **1995**, *28*, 5358.
24. I. Tritto, R. Donnetti, M. C. Sacchi, P. Locatelli, G. Zannoni, *Macromolecules*, **1997**, *30*, 1247.
25. I. Tritto, R. Donnetti, M. C. Sacchi, P. Locatelli, G. Zannoni, *Macromolecules*, **1999**, *32*, 264.
26. D. Coevoet, H. Cramail, A. Deffieux, *Macromol. Chem. Phys*., **1998**, *199*, 1451.
27. E. Giannetti, G. M. Nicoletti, R. Mazzocchi, *J. Polym. Sci., Polym. Chem. Ed*., **1985**, *23*, 2117.

28. E. Y. X. Chen, *Chem. Rev.*, **2000**, *100*, 1391.
29. Y. X. Chen, C. L. Stern, S. Yang, T. J. Marks, *J. Am. Chem. Soc*., **1996**, *118*, 12451.
30. Y. X. Chen, M. V. Metz, L. Li, C. L. Stern, T. J. Marks, *J. Am. Chem. Soc*., **1998**, *120*, 6287.
31. L. C. Simon, R. S. Mauler, R. F. De Souza, *J. Polym. Sci., Part A: Polym. Chem.*, **1999**, *37*, 4656.
32. L. Resconi, S. Bossi, L. Abis, *Macromolecules*, **1990**, *23*, 4489.
33. H. Yang, Q. Wang, Z. Fan, H. Xu, *Polym. Int.*, **2004**, *53*, 37.
34. I. Tritto, D. Zucchi, M. Destro, M. C. Sacchi, T. Dall'Occo, M. Galimberti, *J. Mol. Catal. A: Chem*., **2000**, *160*, 107.
35. C. Götz, A. Rau, G. Luft, *J. Mol. Catal*., **2002**, *184*, 95.
36. S. Beck, H. H. Brintzinger, *Inorg. Chim. Acta*, **1998**, *270*, 376.
37. A. R. Siedle, W. M. Lamanna, R. A. Newmark, *Makromol. Chem., Macromol. Symp.*, **1993**, *66*, 215.
38. N. Piccolrovazzi, P. Pino, G. Consiglio, A. Sironi, M. Moret, *Organometallics*, **1990**, *9*, 3098.
39. R. Fusco, L. Longo, F. Masi, F. Garbassi, *Macromol. Rapid Commun*., **1997**, *18*, 433.
40. M. Galimberti, M. Destro, O. Fusco, F. Piemontesi, I. Camurati, *Macromolecules*, **1999**, *32*, 258.
41. S. S. Reddy, *Polymer Bulletin*, **1996**, *36*, 317.
42. L. I. Shoer, K. I. Gell, J. Schwartz, *J. Organomet. Chem*., **1977**, *136*, C19.
43. P. J. Chirik, J. E. Bercaw, *Organometallics*, **2005**, *24*, 5407.
44. J. A. Pool, E. Lobkovsky, P. J. Chirik, *Organometallics*, **2003**, *22*, 2797.
45. J. C. W. Chien, *J. Am. Chem. Soc*., **1959**, *81*, 86.
46. F. Song, R. D. Cannon, M. Bochmann, *Chem. Commun*., **2004**, 542.
47. N. M. Bravaya, E. E. Faingol'd, O. N. Babkina, S. L. Saratovskikh, A. N. Panin, I. V. Zharkov, E. A. Fushman, *Russ. Chem. Bull., Int. Ed*., **2013**, *62*, 2, 560.
48. Q. Wang, L. Li, *Polym. Int.*, **2004**, *53*, 1473.
49. Q. Wang, H. Yang, Z. Fan, H. Xu, *J. Polym. Sci., Part A: Polym. Chem*., **2004**, *42*, 1093.
50. *Determination of the content of aluminium in aluminium alkyls (EDTA titration),* Test Method , non-controlled copy, Chemtura Organometallics GmbH.
51. N. Kayal, N. Singh, *Chem. Cent. J.*, **2007**, 1:24.
52. O. P. Bhargava, *Talanta*, **1979**, *26*, 146.

53. G. Schwarzenbach, H. Flaschka, (1969), *Complexometrix Titrations*, 2nd English Ed., London, Methuen.
54. Modified polymerization procedure as in Chapter 6

Chapter 7

Overview

MAO is an important co-catalyst used in industrial scale olefin polymerisation. However, despite the efforts of many scientists over the last few decades the exact structure of MAO remains unknown. The need for the industrial world to produce a 'superior' MAO with better catalytic activity, solubility in aliphatic hydrocarbons or a longer storage life, has fed many studies trying to investigate or change the structural features of MAO. Even a small improvement in the synthesis of MAO could potentially lead to a huge industrial advantage.

For this reason, the work presented in Chapters 2-4 focused on the structural characterisation of MAO. Chapters 2 and 3 focused upon the formation of MAO by studying the hydrolysis reaction of TMA, with a greater interest in the initial reaction steps of TMA with H_2O. This was attempted by using ^{1}H VT NMR spectroscopy and by combining infrared spectroscopy with the matrix isolation technique. Low temperature NMR experiments successfully led to the identification of the $AlMe_3 \cdot H_2O$ adduct as the first intermediate, followed by formation of Me_2AlOH, when THF was employed as a solvent. The results of these studies were shared with our collaborative partners, and especially the industry that produces MAO, which was aiming for the synthesis of a 'superior' MAO.

Various MAO samples, as well as the characterised 'beyond-the-state' MAO (a MAO produced in a different way), were given to us and our other collaborative partners by our industrial partners for analysis. Chapter 4 focused on the characterization of some of those MAO samples, showing the development of a fast and reliable method for quantification of the TMA content of commercial MAO solutions via ^{1}H-NMR spectroscopy, with addition of donors. This is very important since the TMA concentration plays an important role in the catalytic activity of a MAO system, as was also revealed by the studies presented in Chapter 5, and it is vital to be able to determine it easily with precision at any time (especially if we take into consideration that the TMA concentration of an MAO sample might change over time).

This research also showed that MAO contains a small amount of certain structures, which upon addition of THF or pyridine can lead to the formation of the cationic species

$[AlMe_2L_2]^+$. These Lewis acidic sites might have an important role in the activation process of metallocene catalysts by MAO in olefin polymerization. Their discovery and quantification, apart from the determination of the TMA content, is another important step to a better understanding of the performance of MAO as a catalyst activator.

The samples analysed and presented in Chapter 4 are not the ones used later on, in Chapter 5, but the same procedures were followed for the new samples in order to determine their TMA content and cationic species before using them.

After all this research in order to gain a further insight in the synthesis of MAO and its main structural features, it was decided to proceed by studying its performance in 1-hexene polymerization, with the aim of enhancing MAO's catalytic efficiency. The kinetic studies on 1-hexene polymerizations enabled the determination of the exact relationship between the TMA concentration and (a) polymer yield and (b) the number-average polymer molecular weight.

One of the main targets in Chapter 5 was to produce MAO that was soluble in aliphatic hydrocarbons by addition of branched or long chain aluminium trialkyls, which proved to be effective solubilizing agents, and by modification of MAO with long chain silanols. Modification of MAO with branched [$Al(i\text{-}Bu)_3$] or long chain [e.g. $Al(Oct)_3$] aluminium trialkyls, produced a modified methylaluminoxane that is soluble in aliphatic hydrocarbons such as n-heptane. Poly(1-hexene) with higher $\overline{M_n}$ values is obtained when MAOs modified with $Al(i\text{-}Bu)_3$ or $Al(Oct)_3$ are employed.

Addition of silanols on the other hand, led to polymers with lower $\overline{M_n}$. Differences in productivity, polymer molecular weight and number of active species were shown to be primarily a linear function of the TMA concentration. The methods developed in Chapter 4 for the determination of TMA content and cationic sites were useful here as well. Although heptane-soluble MAO was produced after treatment with long-chain silanols, the catalyst system did not exhibit the required catalytic performance in 1-hexene polymerizations. This means that the MMAOs used in this study do not acquire the characteristics that make MAO-treated silica surfaces such good co-catalysts in heterogeneous polymerizations. Perhaps modification of MAO with silanols that contain some very bulky groups in combination with some long alkyl chains could lead to different results.

The studies that focused on the production of a heptane-soluble MAO by treatment with silanols were not fruitful, since this modification had a negative influence on the catalytic performance of the system, and so the final part of this research focused on the production of a different aluminoxane that will be soluble in aliphatic hydrocarbons but also compete with MAO in terms of catalytic efficiency. For this reason, the work presented in Chapter 6 was devoted to the development of a synthetic route towards ethyl-iso-butylaluminoxane (EBAO) and its use in 1-hexene polymerization. This is the first study where EBAO is successfully used as a soluble component in 1-hexene polymerization in heptane and leads to comparable or even higher productivities and higher number average molecular weights than the MAO catalytic systems.